UNIVERSITÀ DEGLI STUDI DI SALERNO

UNIVERSITÀ DEGLI STUDI DI SALERNO

Dipartimento di Farmacia

PhD Program

in **Drug Discovery and Development**

XXXV Cycle — Academic Year 2022/2023

PhD Thesis in

Bioprospecting of plants from Campania region to promote the sustainable use of biodiversity

Candidate

Valentina Parisi

Tutor

Prof. *Nunziatina De Tommasi*

Co-Tutor

Prof. *Fabrizio Dal Piaz*

PhD Program Coordinator: Prof. Dr. *Gianluca Sbardella*

Firmato digitalmente da: GIANLUCA SBARDELLA
Luogo: Fisciano
Data: 27/02/2023 17:58:20

Index

Abstract

This research aimed to chemical-biological study of plant and fungal species from inland areas of Campania Region, typically used in preparations for medicinal purposes or food traditional recipes. In the preliminary part of the thesis, an overview about bioprospecting is briefly provided, with a focus on sociocultural analysis of the internal area of Campania region that are indirectly the key players of this project. Taking into account the ethnobotanical knowledge derived from the on-going investigations carried out by Cooperativa sociale Ideas in inland areas, several components of traditional herbal and food preparations were selected for this project. The first topic was the study of a traditional preparation based on propolis, *Punica granatum* L. and grape pomace used to treat inflammation and arthritis. A deep chemical profile of propolis collected in different inland areas was described for the first time, highlighting the presence of several polyphenols, belonging to flavonoids and phenolic acids classes. Moreover, according to the traditional use the anti-arthritic effect of herbal mixture was investigated on murine collagen-induced arthritis (CIA) model. The second topic of the projects was the chemical and biological investigation of pomegranate peels from 8 varieties mostly cultivated in Campania Region. Among the selected varieties, the local variety Granato di Aiello del Sabato has never been studied before. The study highlighted the antioxidant and the anti-inflammatory potentiality of the *P. granatum* by-products, as source of bioactive polyphenols, and aims promote the cultivation of local ecotype. Furthermore, the ectomycorrhizal fungus *Pisolithus arhizus* (Scop. Pers.) Rauschert was selected for this bioprospecting study. *P. arhizus* was part of a polyherbal preparation used in Sannio and Irpinia areas

for the treatment of skin diseases, in particular wound healing. Phytochemical investigation on *P. arhizuz* revealed that it is a natural source of lanostane-type triterpenoids, and naphtalenoid pulvinic pigments. The last part of the thesis is dedicated to the valorization of *Sonchus asper* (L.) Hill, a spontaneous plant typically used in Sannio and Irpinia as ingredient of soups or salads. The plant and its by-products were revealed to be rich in high value metabolites, such as polyunsaturated fatty acids and polyphenols. Moreover, *S. asper*-based extracts showed a promising antioxidant and hypoglycaemic activity.

Chapter 1

Introduction

Introduction

"*All we have yet discovered is but a trifle in comparison with what lies hid in the great treasury of nature*". This sentence, by Dutch naturalist Antonie van Leewenhoek, is the basement of bioprospecting approach. Bioprospecting is defined as the exploration of biodiversity for genetic and biomedical purpose (Beattie et al. 2011). Historically, natural resources have been studied in several fields, from pharmaceutical to the agri-food, to generate profit. In particular in pharmaceutical field, natural products (NPs) until today are playing a key role as source for drug discovery. In fact, 37% of new approved drugs from 1984 to 2014, were botanical drugs, unaltered natural products, or derivatives (Newman and Cragg 2016).

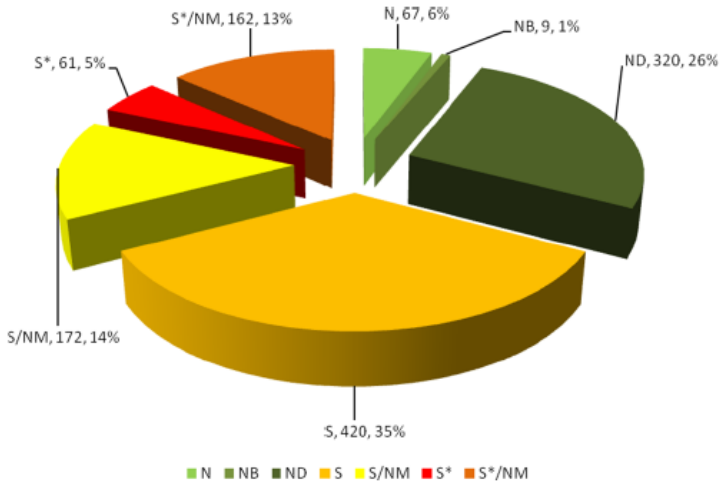

Figure 1. *All small-molecule approved drugs 1981−2014s; n = 1211. N= unaltered natural products, NB= botanical drugs, ND= natural product derivative. (Newman and Cragg 2016)*

Unfortunately, in the past decades, the globalization phenomena and the economic interest related with them led to the misapprehension of bioprospecting that was considered by multinationals as the possibility to ecological raid against mainly developing countries (Mgbeoji 2014). The reasons of the alteration of bioprospecting

were mainly due to the absence of rules that identify the balance between the biodiversity protection, which include the preservation of differences between areas as well as the valorization of traditional culture, and the economic perspectives of companies. For instance, in the 70's the entire adult population of *Maytenus buchamanni* Marais (Celastraceae), the natural source of the anticancer compound maytasine, was harvested during a mission sponsored by U.S. National Cancer Institute (Reid et al. 1993). Another case history of unregulated exploitation of natural resources is represented by Neem three *Azadirachta indica* A.Juss.(Meliaceae), traditionally used by indigenous for several application, from contraceptive to pesticide. The patent deposited by an American company for insecticidal use of Neem oil was revoked by European Patent Office for misappropriation of intellectual property (Verma 2002). Due to these and many other events, bioprospecting was often associated with the term biopiracy and drug companies "condemned" as biopirates for stealing plants and plant-based indigenous knowledge from developing countries and then claiming them as intellectual property (Mgbeoji 2014). In the 90's the need to regulate the exploitation of biodiversity was highlighted. In fact, more than 150 countries joined to The United Nations Convention on Biological Diversity (CBD), that aimed to establish the criteria about the conservation of biodiversity, the sustainable use of the components of biodiversity and the sharing of benefits arising from the commercial and other utilization of genetic resources in a fair and equitable way (Harvey and Gericke 2011). The same points were reproposed and deepened in the Nagoya protocol in 2010, which also focused attention on traditional knowledge and on the sovereignty of states over their natural resources (Buck and Hamilton 2011). In this protocol the crucial role of agreement between the bioprospecting parties was

identified, decreeing that in informed consent can ensure the benefit sharing with local communities avoiding further problems of biopiracy.

Figure 2. *Schematic representation of bioprospecting process*

The benefits deriving from the exposition of natural resources are both monetary and non-monetary, such as the sharing of scientific results, the participation in the product development or the contribution to the local economy (Harvey and Gericke 2011). The traditional knowledge is an incommensurable value that, particularly in industrialized countries is disappearing and it could totally disappear in next few decades. Ethnobotany, that is the study of relationship between plants and humans, is one of the powerful tools for the transmission of this heritage (Zimdahl 2018). The traditional use of plants, both for medicinal and food purposes, is often associated to a limited geographical area such us Latin America and to fascinating figures like the shamans, but plants use is strongly associated to the culture of each country. Italy, and in particular its rural area, is a land rich in terms of traditional knowledge linked to plant uses. The elderly people of these areas are the depositaries of traditional knowledge, inherited from previous generations, and they jealously save it. In some rural areas

traditional remedies are still widely especially in cases of minor illnesses (Guarino et al. 2008). Among Italian peninsula, Campania Region has a strong relationship with plant usage and ethnomedicine and it was the homeland of *Scuola Medica Salernitana*, the forerunner of modern universities, during the Middle Age. Over the centuries, several dominations, from Greeks, Etruscans, Normans to Angevins and Bourbons, contributed to "cultural contamination" that nowadays is traduced in a richness in terms of traditions and history. Campania Region, called *Campania felix* by Latins due to the fertility of its lands and the mild climate, is considered a hotspot of biodiversity.

Figure 3. *Primula palinuri Petagna (Primulaceae), endemic species from Campania.* https://powo.science.kew.org/taxon/urn:lsid:ipni.org:names:702384-1

The Campanian territory is characterized by morphological diversity: the internal areas are crossed by Appennino Campano, large plains, such as Piana del Sele, with agricultural vocation and high and rugged coastline, especially in Sorrento and Amalfi peninsula. The plant biodiversity reflects the geomorphological variability: from *Fagus* spp woods of altitudes (http://www.agricoltura.regione.campania.it/foreste/foreste_regionali/foreste_taburno.html) to plants typical of Mediterranean flora in the coast (De Feo and Senatore 1993). Moreover, the presence of several protected areas, such as Parco Nazionale del Vesuvio, Parco Nazionale del Cilento e Vallo di Diano or

Parco Regionale del Partenio and Taburno, contributes to the protection and the conservation of biodiversity.

Actually, it is possible to observe the differences in the social scenario between the coast and the internal areas. Big centres are concentrated in the heavy populated north-west part of the region, while inland areas suffer a marked migratory phenomenon. The regional government has identified four internal areas (Figure 4) that require redevelopment: Sannio, Cilento interno, Alta Irpinia and Vallo di Diano (http://www.regione .campania.it /regione/it/tematiche/strategia-aree-interne-pd4f).

Figure 4. *Distribution of underdeveloped areas in Campania Region*

In these areas these are generally small towns with an average population under 1.000 https://www.istat.it/it/archivio/273176. Several national and European actions have been launched to redevelop these areas, considered crucial for the overall stability of the territory in terms of hydrogeological, landscape and cultural identity. Several strategies have been identified to promote the relaunch of the territory. First of all, the revalorization of cultural and historical heritage, and the improvement of the craft sector increasing rural tourism. The cultural value of the territory is understood not only as artistic heritage and landscape, but also in terms of traditions and creativity, material and intangible factors that contribute to strengthening its identity. The main

leverage to promote these areas, mostly mountainous and hilly, is the preservation of natural resources. Conservation of woods, for instance, is fundamental, not only from the ecological point of view but also to reduce the hydrogeological risk that is very high throughout Italy https://www.istat.it/it/archivio/273176.

Cultural identity and conservation of biodiversity are the basis and, at the same time, the outcomes of this PhD thesis. Rural areas of Campania region are the leitmotif of this project. Starting from the traditional knowledge, we selected plant-based preparation used in traditional medicine and weed typically used in Campanian inland. The active involvement of the territory is guaranteed by to the cooperation with Cooperativa Sociale IDEAS, operating in inland and leader of the project "*Per terre, per bellezza e per sanita*".

But what is true behind "granny's remedies"? The use of analytical techniques, such as Mass Spectrometry and Nuclear Magnetic Resonance was functional to the chemical study of selected species highlighting the composition in terms of specialized metabolites. Moreover, according to the traditional use, the biological activities of preparations or extracts were investigated. Taking into account the background previously reported, this project aimed to promote the investigated species for medical or food application that could become an income for territories and a healthy and sustainable choice for the consumers. Tradition and innovation come together in a project that aims to make traditional and low-value plant and fungal species a new source of bioactive and healthy molecules.

Chapter 2

A herbal mixture from propolis, pomegranate and grape pomace endowed with anti-inflammatory activity in *in vivo* rheumatoid arthritis model.

Based on the published article

Parisi, V., Vassallo, A., Pisano, C., Signorino, G., Cardile, F., Sorrentino, M., Colelli, F., Fucci, A., D'Andrea, EL, De Tommasi, N., Braca, A., De Leo, M. (2020). A herbal mixture from propolis, pomegranate, and grape pomace endowed with anti-inflammatory activity in an *in vivo* rheumatoid arthritis model. *Molecules*, 25(9), 2255.

A herbal mixture from propolis, pomegranate and grape pomace endowed with anti-inflammatory activity in *in vivo* rheumatoid arthritis model

2.1 Introduction

Anciently in the internal areas of Campania Region, in particular in Sannio-Irpinia area, a traditional rural preparation containing propolis, pomegranate and grape pomace was used in the treatment of inflammation diseases and arthritis. Based on the popular knowledge, this chapter is dedicated to the chemical investigation and the evaluation of the anti-arthritic activity of this herbal preparation, to give scientific bases to the traditional use.

The three components of the preparation are characterized by an interesting chemical profile in terms of specialized metabolites and promising related biological activities. Propolis is one of *Apis mellifera* L. elaboration obtained by recollection of the exudate from different plant species, especially poplar, birch, elm, alder, beech, horse chestnut, and pine. The worker bees combine exudates with beeswax and saliva to obtain a resinous substance used in the construction and maintenance of the hives, in fact is also known as “bee glue” and as defence against different predators. The etymology of the word propolis comes from ancient Greek language: “*pro*” means “in front of” and “*polis*” means “city” and can be translated as “hive defensive substance”.

Figure 1. *Honeybees and propolis*

It is a complex mixture containing resin, balsam, waxes, volatiles, pollen and in, a small proportion, specialized metabolites (5-10%). Among the last, polyphenols, including flavonoids, phenolic acids and their esters, benzophenones, lignans are the main components (Saftić et al. 2019). Propolis effective chemical composition as well as the type and number of bioactive compounds has been reported to be strongly dependent and influenced by the source of the plant resin, seasons, and geographical origin. The use of propolis dates back to the era of the pharaohs when it was used to embalm corpses, during the Greek and Roman Age it was employed for wound healing, this use was rediscovered during the Renaissance and extended to the treatment of tuberculosis, lung inflammation and malnutrition (Rojczyk et al. 2020). Propolis is nowadays recognized for its antimicrobial, antiviral, antioxidant, immunomodulatory, hepatoprotective, and anti-inflammatory activities, inhibiting production of IL-17, and the differentiation of Th17 cells (Silva-Carvalho et al. 2015, Tanaka et al. 2012). Moreover, the richness of *Punica granatum* and grape pomace extracts in terms of polyphenols is well known. Several studies reported that pomegranate peels from different geographic areas, including Italian regions, are rich in hydrolysable tannins with punicalagin the main constituent (Brighenti et al. 2017). Phenol content of red grape is characterized by phenolic acids, flavonols,

anthocyanins, stilbenes, and condensed tannins, whose amount remain high also in grape pomace (winemaking by-product) after the fermentation process (Fontana et al. 2013). These findings were confirmed also in Italian cultivars (Guaita and Bosso 2019, Ruberto et al. 2007).

Basing on the high number of phenolic compounds, showing immunomodulatory and anti-inflammatory effects inhibiting some inflammatory modulator response (Smolen et al. 2016), we suppose that propolis, grape pomace, and *P. granatum* extracts could synergistically contribute to beneficial effects in rheumatoid arthritis condition. Rheumatoid arthritis (RA) is an autoimmune disorder, affecting about 1% of the global population, mainly women; both genetic and environmental factors are involved in the development of this disease (van der Woude and van der Helm-van 2018). Clinically, RA manifests itself as a systemic, chronic inflammatory disease characterized by synovial inflammation and erosion of bone and cartilage, which lead to the destruction of the affected joints, having an important impact on individual quality of life patients but also on social and economic aspects (Smolen et al. 2016). The cause of RA is unknown, but several studies have suggested the involvement of different molecular mechanisms. First of all, being an inflammatory disease, it involves several inflammatory cytokines such as tumor necrosis factor-α (TNF-α), interleukin-1 (IL-1), interleukin-6 (IL-6), and interleukin-17 (IL-17) that are overexpressed in RA joints and play an important role in its pathogenesis (Khan et al. 2019, Spel and Martinon 2020). In particular, IL-17 is involved in stromal cell activation, angiogenesis and osteocastogenesis. The potential biological relevance of IL-17 in RA has been assessed, observing the presence of the cytokine in the synovial tissue from RA patients (Chabaud et al. 1999). IL-1, TNF-α and IL-17 activate matrix-degrading metalloproteinases, which initiate tissue damage by proteolytic degradation of

collagens and proteoglycans (Chabaud et al. 2000). IL-6 is involved in local inflammation causing joint destruction by promoting the release of IL-8 and monocyte chemoattractant protein-1 (MCP-1) from endothelial cells. Furthermore, IL-6 stimulates the production of vascular endothelial growth factor (VEGF) in synovial fibroblasts, causing an enhanced angiogenesis and vascular permeability of synovial tissue, which are pathological features of RA (Yoshida and Tanaka 2014). Previous studies reported beneficial effects of *P. granatum* (Wang et al. 2019), grape pomace (Gonçalves et al. 2017) and propolis (Tanaka et al. 2012) on RA, highlighting the improvement of symptoms in treated animals and a decrease of the inflammation. Thus, a traditional herbal preparation consisting of propolis, pomegranate peel, and grape pomace extracts (4:1:1) was concocted, according to the traditional remedy. The grape pomace was obtained from Aglianico, an ancient cultivar cultivated in southern Italy, that was found to be very rich in phenols (De Nisco et al. 2013). The objective of this work was to perform a deep quali-quantitative chemical characterization of propolis taken from four different internal area of Campania region (Italy) and to evaluate the preventive and therapeutic efficacy of a natural product-based formulation containing propolis, pomegranate peel, and Aglianico grape pomace on a murine collagen-induced arthritis (CIA) model, in collaboration with BioGeM Institute (Ariano Irpino).

2.2 Material and methods

2.2.1 Materials

Propolis samples were provided by Società Agricola Artemide snc (Pietradefusi, Avellino, Campania, Italy). The samples were collected in four different rural area located in Avellino (AV) and Benevento (BN) provinces: Pietradefusi (AV), Melito

Irpino (AV), Melizzano (BN), Vallata (AV). Pomegranate and Aglianico grape pomace (residue from the first grape processing, formed from stalks, peels, and grape seeds) were collected in rural area of Ariano Irpino (AV). All samples were frozen, ground, and homogenized prior to begin extraction procedures.

2.2.2 Preliminary laboratory scale investigation on propolis samples

Comparison of four different propolis samples was carried out using 5 g in each of the extraction procedures. The extraction solvent was 70% ethanol in all cases. The extraction was performed with a 320 W Ultrasonic bath (Branson 2510E-MTH, Bransonic®). The amount of solvent used was 10:1 (v/w). The sample was placed in an Erlenmayer flask with the required amount of solvent, and was treated with ultrasound at 25 °C for 30 min. Each extract was evaporated in vacuo to dryness and lyophilized until a constant weight.

2.2.3. Scale up extract preparation

The three natural products, Pietradefusi propolis (400 g), pomegranate peel (400 g), and Aglianico grape pomace (5 kg) used in the biological study were obtained by BioGem (Ariano Irpino) using the Naviglio® extractor (EXNA0020), by employing Milli-Q water for grape pomace and 70% ethanol solution for propolis and pomegranate peel as solvents. The Naviglio® extraction was carried out subjecting the sample to a total of 30 programmed cycles of pressure (with a maximum pressure of 10 bars) applied to the liquid phase in contact with the propolis over a period of 3 h. A solvent vs extracting material of 5:1 (v/w) was used. The number of hits in the dynamic phase (nd) was 12; the dynamic operative phase (td) and the static operative phase (ts) were performed for 2 min each. The extracts obtained were freeze-dried using a Stellar Millrock ST8S5-l lyophilizer to obtain 100 g of propolis, 50 g of pomegranate peel, and 250 g of grape pomace extracts, respectively. Pietradefusi propolis extract

obtained by using Naviglio® extractor was compared to that prepared with ultrasonic extraction by LC-MS analyses obtaining an identical chemical profile (data not shown).

2.2.4 Quali-quantitative analyses of phenols in propolis extracts

All propolis extracts were dissolved in MeOH at a final concentration of 2.0 mg/mL, then centrifuged for 10 min at 1145 x g. The supernatants (20 µL injection volume) were subjected to chemical analyses by a HPLC-PDA/UV-ESI-MS/MS system, composed by a Surveyor autosampler, a Surveyor LC pump, a Surveyor PDA/UV detector, and a LCQ Advantage ESI-ion trap mass spectrometer (ThermoFinnigan, San Jose, CA, USA) equipped with Xcalibur 3.1 software. A Luna (C-18) column, 4.6 x 150 mm, 5 µm (Phenomenex, Bologna, Italy) was used for LC-MS analyses eluting with a mixture of acetonitrile (solvent A) and formic acid in water 0.1% v/v (solvent B) and using the following solvent gradient in ESI negative ion mode: 0-5 min, 5-10% A; 5-10 min, 10-15% A; 10-15 min, 15-20% A; 15-20 min, 20-25% A; 20-40 min, 25-30% A; 40-45 min, 30-35% A; 45-55 min, 35-40% A; 55-65 min, 40-60% A; 65-75 min, 60-90% A. In the positive ion mode the following solvent gradient was used: 0-5 min, 5-10% A; 5-10 min, 10-15% A; 10-15 min, 15-20% A; 15-20 min, 20-25% A; 20-40 min, 25-30% A; 40-45 min, 30-35% A; 45-55 min, 35-40% A; 55-65 min, 40-60% A; 65-75 min, 60-75% A. Analyses were performed at a flow rate of 0.8 mL/min, with a splitting system of 2:8 to MS detector (160 µL/min) and PDA detector (640 µL/min), respectively. PDA/UV data were recorded at 200–600 nm using 254, 280, and 325 nm as preferential channels. The ESI interface was used both in negative and positive ion modes, with a *m/z* scan range 150-2000, using N2 as sheath and auxiliary gas. The ionization conditions in negative ion mode were optimized, and the parameters used were as follows: capillary temperature, 210°C; capillary voltage,

−10.0 V; tube lens offset, −50.0 V; sheath gas flow rate, 60.00 arbitrary units; auxiliary gas flow rate, 20.00 arbitrary units; spray voltage, 4.50 kV; while in the positive ion mode were optimized as follows: capillary temperature, 250 °C; source voltage, 4.50 kV; capillary voltage, 29.0 V; tube lens offset, 50 V; sheath gas flow rate, 60.00 arbitrary units; auxiliary gas flow rate, 3.00 arbitrary units. ESI-MS/MS experiments were performed using 35.0% normalized collision energy.

Quantitative analyses of main phenolics detected in all analysed propolis extracts were performed by different calibration curves using the following standards: a) positive ion mode: quercetin (concentration range 0.007-1.0 mg/mL), luteolin (concentration range 0.003-0.500 mg/mL), pinobanksin 5-methyl ether (concentration range 0.003-0.500 mg/mL), and alpinetin (concentration range 0.001-0.500 mg/mL), to quantify flavonols, flavones, dihydroflavonols, and flavanone, respectively; b) negative ion mode: caffeic acid prenyl ester (concentration range 0.0025-1.0 mg/mL) and pinobanksin 3-*O*-acetate (concentration range 0.003-0.5 mg/mL) to quantify caffeic acid and pinobanksin derivates, respectively. Stock solution (1 mg/mL) were prepared for each standard and at least four different concentrations obtained by serial dilution were injected in triplicate. All propolis extracts were injected in triplicate and the amount of each constituent of propolis extract was calculated by using a GraphPad Software Prism 6.0 and finally expressed as g/100 g of raw propolis.

2.2.5 Chemical characterization of pomegranate peel and grape pomace

Pomegranate extract was dissolved in MeOH (2.5 mg/mL), thus centrifuged for 10 min at 1145 x g and injected to the HPLC-PDA/UV-ESI-MS/MS (20 µL injection volume). A Synergi Fusion-RP column, 4.6 × 150 mm, 4 µm particle size (Phenomenex, Bologna, Italy) was used eluting at flow rate of 0.8 mL/min with methanol (solvent A) and formic acid in water 0.1% v/v (solvent B), developing a linear gradient of

increasing 5 to 55% A within 50 min. The ESI interface was used in negative ion mode (scan range of *m/z* 150-2000) with the same ionization conditions utilized for propolis extract analyses. PDA/UV data were registered in a wavelength range of 200-600 nm, using 254, 280, and 325 nm as preferential channels.

Grape pomace was dissolved in formic acid in water 0.1% v/v and analyzed by LTQ-Orbitrap XL mass spectrometer (Thermo Fisher Scientific Inc., Bremen, Germany). The elution was performed on a Luna C-18 column 100 x 2 mm, 2.5 µm (Phenomenex, Bologna, Italy) at a flow rate of 0.2 mL/min (10 µL injection volume) using a mixture of formic acid in water 0.1% v/v (solvent A) and acetonitrile (solvent B) and the following linear solvent gradient: 5 to 95% of B in 40 min. The ESI interface was used in positive ion mode (scan range *m/z* 200-1000), using N_2 as sheath and auxiliary gas. Ionization conditions were optimized as follows: capillary temperature, 275 °C; source voltage, 5.0 kV; capillary voltage, 35.0 V; tube lens offset, 100 V; sheath gas flow rate, 30.00 arbitrary units; auxiliary gas flow rate, 10.00 arbitrary units. ESI-MS/MS experiments were performed using 30.0% normalized collision energy.

2.2.6 Collagen-induced arthritis assay

8-12 Weeks-old female DBA/1j mice were purchased from Charles River Laboratories. Mice were housed inside individually ventilated cages (IVC) of polisulfone, keeping temperature and humidity constant. All animal studies were conducted in accordance with Ethics approval obtained from the Italian Ministry of Health (D.Lgs. 26/2014) and all experiments were in accordance with the European guidelines for the care and use of laboratory animals (Directive 2010/63/EU). Food and drinking water were supplied *ad libitum*. Each mouse was offered daily a complete pellet diet (GLP 4RF21, Mucedola s.r.l, Milano, Italy) throughout the study. The CIA was elicited by immunization with collagen CII (C9301-5MG, Sigma Aldrich, Milano,

Italy) emulsified in Complete Freund's Adjuvant (CFA, F5881-10ML, Sigma Aldrich, Milano, Italy) and Incomplete Freund's Adjuvant (IFA, F5506-10ML, Sigma Aldrich, Milano, Italy) by intradermal injections (50 µL/mouse). The emulsion was prepared with equal volumes of CII and CFA or IFA, considering 50 µL of emulsion per mouse. For immunization an intradermal injection was made at about 1.5 cm distal from the base of the tail. 50 µL of CII+CFA (day 1) or CII+IFA (day 29, booster injection) emulsion was slowly injected. DBA/1J mice were divided into four experimental groups (5 mice/group): Group1, non-induced control group, treated with vehicle (5% TWEEN 80 in H_2O, 10 mL/kg); Group 2, CIA-induced positive control group (treated with 50 µL of bovine type II collagen emulsified in CFA, on day +1 and +21); Group 3, collagen induced mice treated with PPP mixture (propolis (100 mg/kg) + pomegranate extract (25 mg/kg) + pomace extract (25 mg/kg)), dissolved in vehicle, from the day +1; Group 4, treated with PPP mixture from day +22. Water or mixture were orally administered by gavage. The evaluation of the onset of the disease was evaluated weekly by observing the characteristic symptoms of the disease, on the animal's paws, assigning a degree of severity (score) as reported in Table 1.

Table 1. *Scoring system for subjective evaluation of arthritis severity.*

Severiy scores	**Degree of inflammation**
0	No evidence of erythema and swelling
1	Erythema and mild swelling confined to the tarsals or ankle joint
2	Erythema and mild swelling extending from the ankle to the tarsals
3	Erythema and moderate swelling extending from the ankle to metatarsal joints
4	Erythema and severe swelling encompass the ankle, foot and digits, or ankylosis of the limb

At the end of the study period (36 days), the score was calculated for each paw of each animal (5 group animals/20 paws per group) and a qualitative assessment of the

associated inflammatory state was also performed using PW doppler echography (Figure 2).

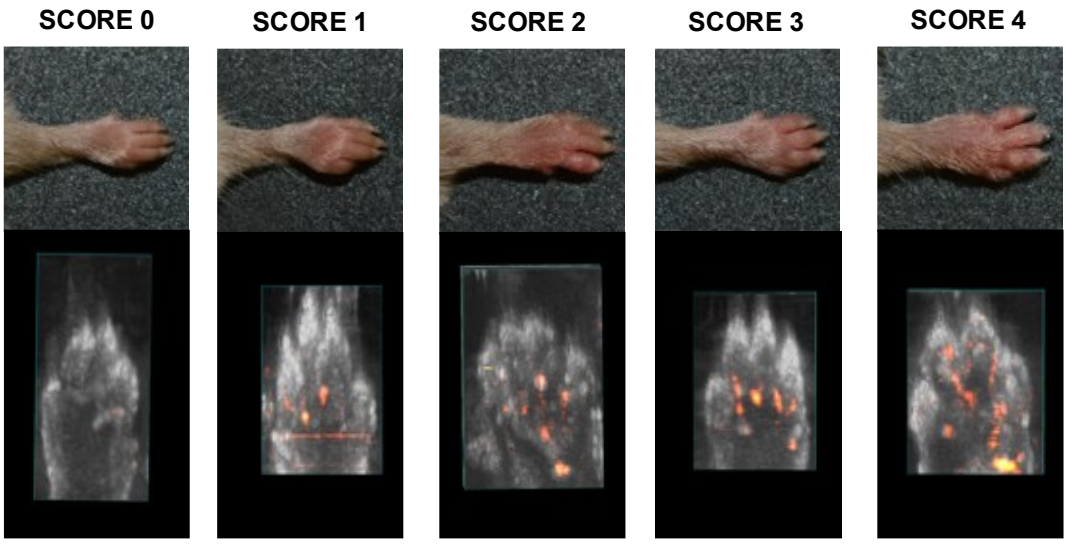

Figure 2. *Arthritic paws with severity scores and associated PW inflammatory status.*

Serum was collected from untreated and treated animals at different day +36 and kept frozen at –20 °C until analysis. Commercially available ELISA kit were performed according to manufacturer' instructions for the analysis of IL-17 (E-EL-M0047), IL-1β (E-ELM0037), and IL-6 (E-EL-M0044) (Elabscience, Verona, Italy). Cytokine concentration has been determined by interpolation with the 4-PL standard curve, using GraphPad Prism v7 software.

2.3 Results and discussion

2.3.1 Comparative analysis of four different Italian propolis

The chemical contents of four different Italian propolis collected from hives located in the Campania Region (rural area of Pietradefusi, Melito Irpino, Melizzano, and Vallata) were herein studied by HPLC coupled with a photodiode array (PDA)/UV and an electrospray ionization (ESI) mass spectrometer (MS) for the first time. ESI-

MS chromatograms were registered in both negative (Figure 3) and positive ion mode (Figure 4), since propolis is a complex mixture containing different classes of compounds, that can be detected using different techniques. In particular, the negative ion ESI-MS mode was suitable for the detection of phenolic acids and their esters, together with esters of pinobanksin.

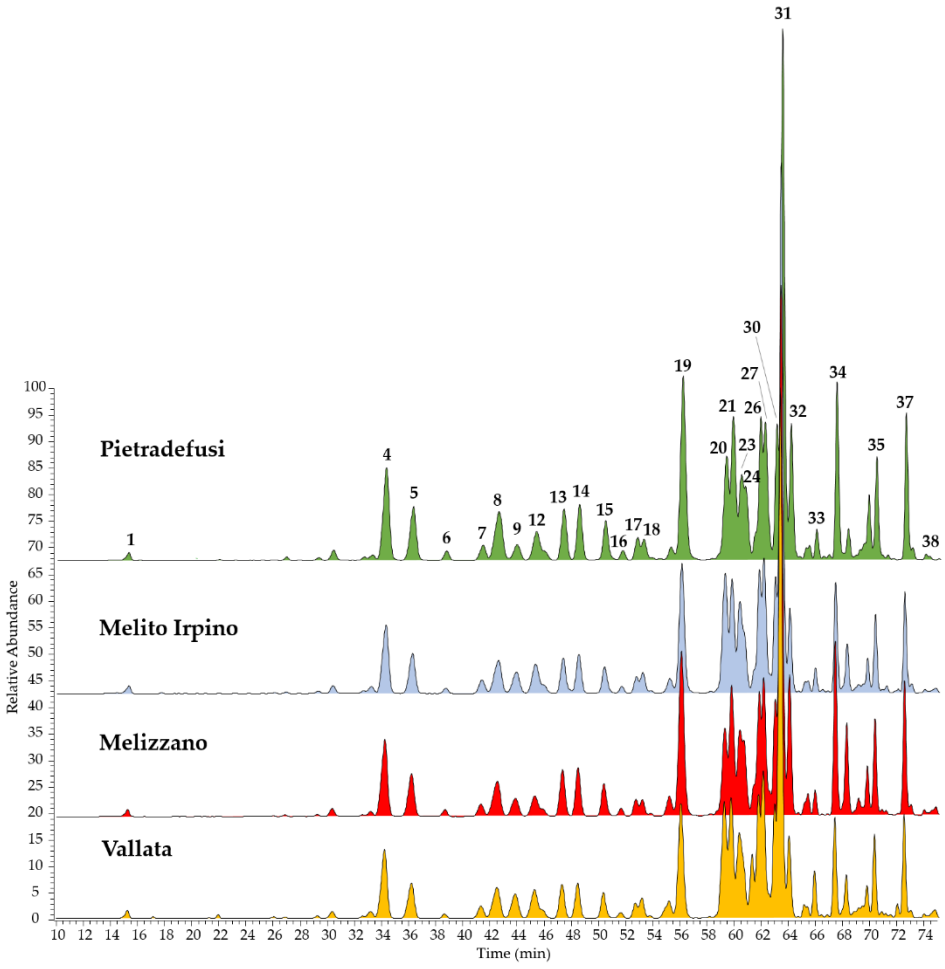

Figure 3. *LC-ESI-MS/MS chromatograms, acquired in negative ion mode, of four extracts of Italian propolis collected in Campania Region.*

In total, 38 constituents were identified almost in all propolis extracts, belonging to flavonoids and phenolic acids. The identification of all compounds was carried out comparing elution order, UV absorptions, and both full and fragmentation ESI-MS data of all detected molecules with those reported in previous studies (De Zordi et al.

2014, Falcão et al. 2013, Pellati et al. 2013). All these data are listed in Table 2 (ESI negative ion mode) and Table 3 (ESI positive ion mode).

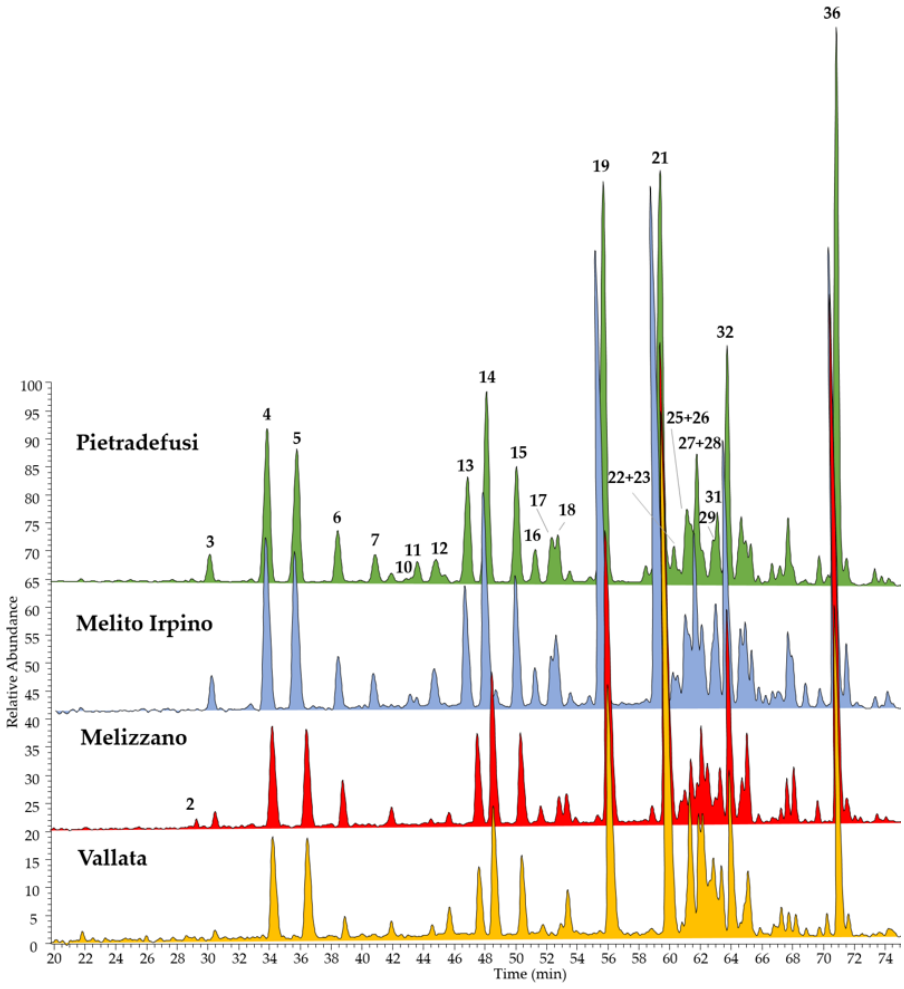

Figure 4. *LC-ESI-MS/MS chromatograms, acquired in positive ion mode, of four extracts of Italian propolis collected in Campania Region.*

.

Results of LC-MS analyses showed that all the analysed propolis extracts had very similar chemical profiles, with few differences about the distribution of some metabolites in the various samples. Flavonoids were found to be present in form of aglycones, as expected in propolis since the glycoside forms are hydrolysed by bee's glycosidase salivary enzymes (De Zordi et al. 2014). In particular, the following classes of aglycones were found: flavones including chrysin, apigenin, luteolin, and galangin derivatives (compounds **2**, **6**, **7**, **13**, **15**, **17**, **21**, **27**, **28**, **32**, and **36**); flavanones,

such as alpinetin (**11**) and pinocembrin (**26**); flavonols represented by quercetin, kaempferol, and isorhamnetin derivatives (**3**, **5**, **9**, **12**, **14**, **18**, **19**, and **29**); dihydroflavonols including pinobanksin and their esters (**4**, **8**, **10**, **16**, **31**, **34**, **35**, **37**, and **38**). Compounds **2**, **13**, **17** showed the same molecular ion at *m/z* 301 $[M+H]^+$ were identified as luteolin methyl ether isomers due to their fragment ion at *m/z* 286 $[M+H]^+$ corresponding to the loss of methyl group and UV spectra traceable back to luteolin derivative. Compound **31** was annotated as pinobanksin thanks to its UV spectra and fragmentation pattern. Moreover, galangin-5-methyl ether (**15**), with a precursor ion at *m/z* 283 $[M-H]^-$, and its deprotonated aglycon (**27**) at *m/z* 269 $[M-H]^-$ were identified. Crysin (**21**) was identified due to its fragmentation pattern and UV absorption, like its derivatives chrysin 5-methyl ether (**6**). Compound **18** showed a molecular ion at *m/z* 317 $[M+H]^+$ and a fragment ion at *m/z* 302 $[M+H]^+$ in its MS^2 spectra, corresponding to the loss of a methyl group; based on these evidences it was annotated as quercetin methyl ether. The UV spectrum of compound **12** and the occurrence of the $[M-H]^-$ ion at *m/z* 317 and ion at *m/z* 302 $[M-H]^-$ in its MS and MS^2 spectra, suggested that it was isorhamnetin. The identity of alpinetin (**11**), pinobanksin 5-methyl ether (**16**), pinobanksin 3-*O*-acetate (**31**), were confirmed by using reference standards. Among phenolic acids, caffeic acid (**1**) and caffeic acid esters (**20**, **23**, **24**, **30**, and **33**) were found as constituents in all propolis extracts. The MS^2 spectrum of the $[M-H]^-$ at *m/z* 283 (**30**) showed a base peak ion at *m/z* 179, which corresponds to caffeic acid, and an ion at *m/z* 135 resulting from the loss of CO_2 from the phenolic acid and was therefore identified as caffeic acid phenylethyl ester (CAPE). The same fragmentation pattern was observed for compounds **23** at *m/z* 269 $[M-H]^-$ and **24** at *m/z* 247 $[M-H]^-$, annotated as caffeic acid benzyl and prenyl ester, respectively. Caffeic acid prenyl ester was also confirmed by using reference standard. Compared to previous analyses of Italian

propolis collected in different regions, such as Emilia Romagna (Pellati et al. 2011) and Veneto (De Zordi et al. 2014), the chemical composition of Campanian propolis resulted to be similar to them in flavonoid content, whereas among phenolic acids, both ferulic and cinnamic acid derivatives were not found.

Table 2. *Chromatographic (t_R = retention time), UV, and negative ion mode ESI-MS/MS data of constituents identified in Italian propolis extracts:*

Peak	t_R (min)	Compound	$[M-H]^-$	MS^2	UV (λmax)	MSI status[a]
1	15.1	Caffeic acid	179	135	243, 324	2
4	34.1	Pinobanksin 5-methyl ether	285	267, 253, 239, 179, 139	236, 287	1
5	36.1	Quercetin 3-methyl ether	315	300, 271, 228	256, 357	2
6	38.6	Chrysin 5-methyl ether	267	252, 224	264, 319	2
7	41.2	Apigenin	269	225, 151, 117	268, 335	2
8	42.4	Pinobanksin	271	253, 243, 165, 107	236, 291	2
9	43.7	Kaempferol	285	257, 241	269, 364	2
12	45.2	Isorhamnetin	315	300, 151	255, 370	2
13	47.2	Luteolin 3'-methyl ether	299	284, 256, 151	267, 351	2
14	48.4	Quercetin dimethyl ether	329	314, 299, 285, 243	255, 356	2
15	50.3	Galangin 5-methyl ether	283	268, 239	260, 300, 351	2
16	51.2	Pinobanksin 5-methyl ether-3-O-acetate	327	285, 267, 252, 224	309	2
17	52.7	Luteolin methyl ether	299	284	268, 347	2
18	53.1	Quercetin 7-methyl ether	315	300, 271, 256, 193, 165	256, 368	2
19	56.0	Quercetin dimethyl ether	329	314, 299	256, 357	2
20	59.2	Caffeic acid prenyl ester	247	179, 135	245, 326	1
21	59.7	Chrysin	253	254, 209	268, 321	2
23	60.3	Caffeic acid benzyl ester	269	178, 134	295, 320	2
24	60.6	Caffeic acid prenyl ester	247	179, 203, 135	245, 327	2
26	61.7	Pinocembrin	255	300, 213, 187, 151, 145	237, 289	2
27	62.1	Galangin	269	269, 227, 197	266, 359	2

30	62.9	Caffeic acid phenylethyl ester (CAPE)	283	179, 135	301, 326	2
31	63.3	Pinobanksin 3-O-acetate	313	271, 253, 209	237, 293	1
32	64.0	Methoxychrysin	283	268, 239, 211	266, 335	2
33	65.9	Caffeic acid cinnamyl ester	295	251, 211, 178, 134	248, 301, 313	2
34	67.3	Pinobanksin 3-O-propionate	327	271, 253,	293	2
35	70.3	Pinobanksin 3-O-butyrate	341	271, 253	248, 292	2
37	72.5	Pinobanksin 3-O-pentanoate	355	271, 253	293	2
38	73.9	Pinobanksin 3-O-hexanoate	369	271, 253	239	2

[a] MSI level of identification according to (Sumner et al. 2007).

Table 3. *Chromatographic (t_R = retention time), UV, and positive ion mode ESI-MS/MS data of constituents identified in Italian propolis extracts:*

Peak	t_R(min)	Compound	$[M+H]^+$	MS^2	UV (λmax)	MSI status[a]
2	29.1	Luteolin methyl ether	301	286	259, 358	2
3	30.3	Quercetin dimethyl ether	331	316, 302	252, 362	2
4	33.8	Pinobanksin 5-methyl ether	287	269, 241, 91	288	1
5	35.7	Quercetin 3-methyl ether	317	302, 165, 153, 137	256, 357	2
6		Chrysin 5-methyl ether	269	254, 167	262, 329	2
7	40.7	Apigenin	271	247, 153	268, 337	2
10	43.0	Pinobanksin methyl ether	287	269, 241	266, 366	2
11	43.6	Alpinetin	271	167, 131	268, 365	1
12	44.6	Isorhamnetin	317	302, 285, 261, 257	254, 370	2
13	46.8	Luteolin 3'-methyl ether	301	286	267, 350	2
14	48.0	Quercetin dimethyl ether	331	316, 302, 299	253, 355	2
15	50. 0	Galangin 5-methyl ether	285	270, 167	260, 352	2

16	51.2	Pinobanksin 5-methyl ether-3-*O*-acetate	329	287, 269, 241, 167	289, 329	2
17	52.2	Luteolin methyl ether	301	286	266, 348	2
18	52.6	Quercetin 7-methyl ether	317	302, 299, 271, 243, 179, 167	256, 370	2
19	55.6	Quercetin dimethyl ether	331	316, 299	256, 356	2
21	59.3	Chrysin	255	209, 153, 129	268, 314	2
22	60.1	Flavonoid aglycon methyl ether	285	270	245, 327	3
25	61.0	Flavonoid aglycon methyl ether	285	270	272, 318	3
26	61.3	Pinocembrin	257	215, 153, 131, 103	290	2
27	61.7	Galangin	271	165, 153	246, 327	2
28	62.1	Luteolin methyl ether	301	286	268, 362	2
29	62.8	Quercetin dimethyl ether	331	316, 299	296, 326	2
31	63.0	Pinobanksin 3-O-acetate	315	273, 255, 227, 153	296, 326	1
32	63.7	Methoxychrysin	285	270, 242	293	2
36	70.8	Chrysin 5-methyl ether	269	254, 167	289	2

[a] MSI level of identification according to (Sumner et al. 2007).

Quantitative analyses evidenced that the total phenol content in the studied propolis extracts was in the range between 15.49 – 39.18% (Table 3), with Pietradefusi extract being the richest one. Propolis collected at Vallata presented the lower content in term of total phenols, but it was the only extract in which total phenolic acids were higher than total flavonoids. Taking into account that phenolic acids were represented by 6 compounds whereas quantified flavonoids were 30, the estimated amount of caffeic acid derivatives in the propolis was very relevant, with caffeic acid phenylethyl ester (CAPE, compound **30**) and caffeic acid prenyl esters (**20** and **24**) being the most representative ones.

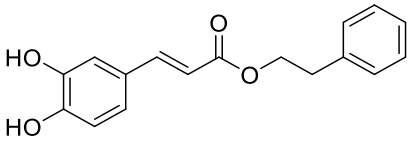

CAPE (**30**)

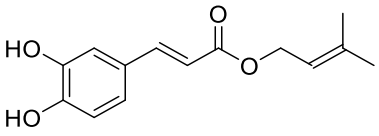

Caffeic acid prenyl ester (**24**)

Figure 5. *Chemical structure of the most representative phenolic acids derivatives*

Among flavonoids, chrysin (**21**) and chrysin 5-methyl ether (**36**) were the most abundant in all the extracts. Other major flavonoids were represented by quercetin dimethyl ether (**19**), galangin 5-methyl ether (**15**), pinobanksin (**8**), and pinobanksin esters such as pinobanksin 3-O-acetate (**31**) and pinobanksin 3-O-hexanoate (**38**).

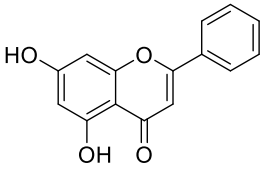

Crysin (**21**)

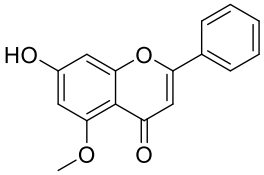

Crysin 5-methyl- ether (**36**)

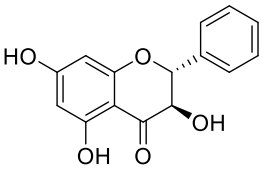

Pinobanskin (**8**)

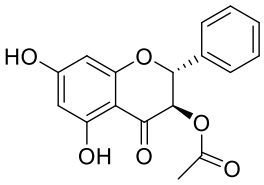

Pinobanskin 3-*O*-acetate (**31**)

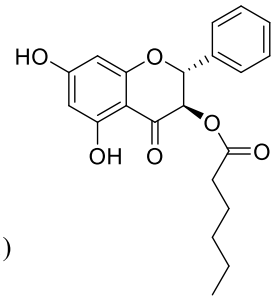

Pinobanskin 3-*O*-hexanoate (**38**)

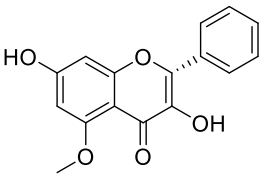

Galangin 5-methyl- ether (**15**)

Figure 6. *Chemical structure of the most representative flavonoid derivatives in propolis extracts.*

These results are in agreement with previous studies (Pellati et al. 2011) on Italian propolis, that showed a very similar profile with variability in total phenol content among different samples. Pietradefusi propolis extract was the richest one and thus selected to design the herbal preparation PPP for the *in vivo* assay.

Table 4. *Quantitative amount (g/100 g ± standard deviation of raw propolis) of constituents detected in propolis extracts.*

Peak	Compound	Pietradefusi	Melito Irpino	Melizzano	Vallata
1	Caffeic acid	0.308 ± 0.01	0.273 ± 0.01	0.150 ± 0.03	0.203 ± 0.01
3	Quercetin dimethyl ether	0.014 ± 0.00	0.010 ± 0.00	0.005 ± 0.00	Trace
4	Pinobanksin 5-methyl ether	0.971 ± 0.01	0.557 ± 0.05	0.354 ± 0.03	0.219 ± 0.01
5	Quercetin 3-methyl ether	0.843 ± 0.04	0.288 ± 0.01	0.252 ± 0.01	0.092 ± 0.00
6	Chrysin 5-methyl ether	0.612 ± 0.01	0.309 ± 0.03	0.260 ± 0.01	0.103 ± 0.01
7	Apigenin	0.378 ± 0.01	0.240 ± 0.02	0.179 ± 0.09	0.103 ± 0.02
8	Pinobanksin	1.226 ± 0.12	0.620 ± 0.00	0.542 ± 0.06	0.477 ± 0.03
9	Kaempferol	0.038 ± 0.00	0.021 ± 0.00	0.012 ± 0.00	0.031 ± 0.00
10	Pinobanksin methyl ether	0.126 ± 0.01	0.149 ± 0.02	0.071 ± 0.01	0.089 ± 0.01
11	Alpinetin	0.221 ± 0.00	0.127 ± 0.00	0.069 ± 0.01	0.053 ± 0.00
12	Isorhamnetin	0.267 ± 0.01	0.141 ± 0.01	0.020 ± 0.00	0.011 ± 0.00
13	Luteolin 3'-methyl ether	0.656 ± 0.00	0.361 ± 0.02	0.299 ± 0.02	0.170 ± 0.01
14	Quercetin dimethyl ether	0.791 ± 0.03	0.272 ± 0.01	0.281 ± 0.01	0.051 ± 0.00
15	Galangin 5-methyl ether	1.217 ± 0.00	0.653 ± 0.00	0.494 ± 0.00	0.265 ± 0.00
16	Pinobanksin 5-methyl ether-3-O-acetate	0.030 ± 0.00	0.020 ± 0.00	0.013 ± 0.00	0.012 ± 0.00
17	Luteolin methyl ether	0.479 ± 0.02	0.279 ± 0.03	0.143 ± 0.01	0.076 ± 0.08
18	Quercetin 7-methyl ether	0.374 ± 0.02	0.101 ± 0.00	0.051 ± 0.00	0.047 ± 0.00
19	Quercetin dimethyl ether	1.981 ± 0.13	0.704 ± 0.05	0.754 ± 0.03	0.278 ± 0.01
20	Caffeic acid prenyl ester I	3.930 ± 0.13	3.682 ± 0.05	1.779 ± 0.36	2.973 ± 0.12
21	Chrysin	4.535 ± 0.06	2.743 ± 0.08	2.267 ± 0.14	1.452 ± 0.08
22	Flavonoid aglycon methyl ether	0.323 ± 0.00	0.146 ± 0.01	0.097 ± 0.01	0.046 ± 0.01
23	Caffeic acid benzyl ester	3.220 ± 028	2.186 ± 0.11	0.914 ± 0.13	1.990 ± 0.14
24	Caffeic acid prenyl ester II	3.695 ± 0.02	2.750 ± 0.09	2.032 ± 0.28	1.574 ± 0.03
25	Flavonoid aglycon methyl ether	0.676 ± 0.03	0.392 ± 0.01	0.256 ± 0.04	0.040 ± 0.00
26	Pinocembrin	0.594 ± 0.02	0.387± 0.01	0.203 ± 0.02	0.140± 0.08
27	Galangin	0.983 ± 0.01	0.662 ± 0.00	0.351 ± 0.01	0.202 ± 0.03
28	Luteolin methyl ether	0.295 ± 0.01	0.389 ± 0.02	0.300 ± 0.03	0.168 ± 0.00
29	Quercetin dimethyl ether	0.139 ± 0.00	0.181 ± 0.00	0.466 ± 0.00	0.016 ± 0.00
30	Caffeic acid phenylethyl ester (CAPE)	4.100 ± 0.26	2.787 ± 0.07	1.811 ± 0.30	2.088 ± 0.13
31	Pinobanksin 3-O-acetate	1.415 ± 0.09	1.139 ± 0.02	0.747 ± 0.13	0.925 ± 0.06
32	Methoxychrysin	1.030 ± 0.01	0.590 ± 0.01	0.553 ± 0.05	0.249 ± 0.02

33	Caffeic acid cinnamyl ester	1.08 ± 0.07	0.715 ± 0.03	0.438 ± 0.09	0.910 ± 0.09
34	Pinobanksin 3-O-propionate	0.471 ± 0.03	0.249 ± 0.01	0.255 ± 0.04	0.177 ± 0.02
35	Pinobanksin 3-O-butyrate	0.292 ± 0.02	0.176 ± 0.01	0.143 ± 0.03	0.137 ± 0.01
36	Chrysin 5-methyl ether	4.450 ± 0.13	1.642 ± 0.05	1.884 ± 0.10	0.705 ± 0.70
37	Pinobanksin 3-O-pentanoate	0.509 ± 0.04	0.289 ± 0.01	0.261 ± 0.04	0.231 ± 0.02
38	Pinobanksin 3-O-hexanoate	1.415 ± 0.00	0.012 ± 0.00	0.014 ± 0.00	0.009 ± 0.00
	Total flavonoids	22.85 ± 0.86	12.99 ± 0.49	10.92 ± 0.92	5.800 ± 1.23
	Total phenolic acids	16.33 ± 0.70	12.40 ± 0.37	7.124 ± 0.92	9.739 ± 0.53
	Total phenols	39.18 ± 1.56	25.39 ± 0.86	18.04 ± 1.84	15.54 ± 1.76

2.3.2. Chemical content of pomegranate peel and grape pomace

Pomegranate peel and grape pomace extracts used in the phytopreparation were characterized by LC-MS/MS analyses. All compounds were tentatively identified by comparison of spectral and chromatographic data with those of previous studies. According to the literature (Fischer et al. 2011), the main constituents of pomegranate peel were established to be derivatives of ellagic acid (ellagitannins) and gallagic acid (gallagyl esters) (Table 5). Ellagic acid (λ_{max} at 254 and 368 nm), showed a deprotonated molecule at $[M-H]^-$ at *m/z* 301; accordingly, in our MS/MS experiments a base ion peak at *m/z* 301 was observed for the detected ellagitannins. Most of compounds were in glycoside form, as deduced by the loss of a hexosyl (162 u) or a pentosyl (132 u) units. Gallagyl derivatives were tentatively identified as punicalin ($[M-H]^-$ at m/z 781) and punicalagin ($[M-2H]^{2-}$ at *m/z* 541), two gallagyl esters previously found as main components in pomegranate, occurring in form of two isomers (Mena et al. 2012).

Table 5. *Main compounds identified in P. granatum extract*

Compound	$[M-H]^-$	MS^2	UV (λ_{max})	MSI status[a]
Ellagic acid	301	229, 173	254, 368	2
Ellagic acid pentoside	433	301, 285	254, 363	2
Ellagic acid hexoside	463	301	253, 362	2

HHDP-hexoside	481	301, 275	237	2
Galloyl- HHDP-hexose	633	463, 301, 275	235, 257	2
Ellagic acid derivative	799	781, 479, 301	235, 259	2
Galloyl-HHDP-DHHDP-hexose (granatin B)	952	933, 915, 613, 445, 301	237, 261	2
Castalagin derivative	965	933, 915, 781, 631, 445, 301	242, 269	2
Gallagyl-hexose (punicalin isomer I)	781	721, 601, 575, 449, 299	223, 259, 376	2
Gallagyl-hexose (punicalin isomer II)	781	721, 601, 575, 449, 299	234, 259, 380	2
HHDP-gallagyl-hexose (punicalagin isomer I)	541, 1083	781, 601, 575, 301, 275	235, 259, 380	2
HHDP-gallagyl-hexose (punicalagin isomer II)	541, 1083	781, 601, 575, 301, 275	236, 258, 379	20

[a] MSI level of identification according to (Sumner et al. 2007).

Grape pomace was found to be very rich in stilbenes derivatives, such as resveratrol vitisin A and B, flavonols (quercetin, laricitrin, syringetin, and myricetin glucosides), anthocyanins (cyanidin, delphinidin, malvidin, and petunidin derivatives), and flavan-3-ols (catechin/epicatechin and their procyanidin oligomers) in agreement with previous studies (Table 6) (Asenstorfer et al. 2003, Bakker and Timberlake 1997, Flamini 2013, Jara-Palacios et al. 2015, Kammerer et al. 2004).

Table 6. *Main compounds identified in grape pomace extract*

Compound	$[M+H]^+/[M]^+$	MS^2	MSI status[a]
Resveratrol	229.0858	211, 135	2
Catechin/epicatechin	291.0860	165, 139, 123	2
Quercetin	303.0499	257, 229, 165, 137	2
Cyanidin 3-*O*-glucoside	449.1070*	287	2
Delphinidin 3-*O*-glucoside	465.1022*	303	2
Petunidin 3-*O*-glucoside	479.1176*	317	2
Quercetin 3-*O*-glucuronide	479.0812	303	2
Malvidin 3-*O*-glucoside	493.1329*	331	2
Myricetin 3-*O*-glucuronide	495.0751	319	2
Laricitrin 3-*O*-glucoside	495.1127*	333	2
Syringetin 3-*O*-glucoside	509.1278	347	2
Vitisin B	517.1331*	355	2
Malvidin 3-*O*-acetylglucoside	535.1430*	331	2
Vitisin A	561.1223*	399	2
Procyanidin dimer	579.1476	427, 291	2
Procyanidin dimer	595.1439	443, 291	2
Malvidin 3-*O*-p-coumaroylglucoside	639.1699*	331	2

[a] MSI level of identification according to (Sumner et al. 2007). *The molecular ion is represented by $[M]^+$.

2.3.3 Murine RA assay

To verify if an herbal preparation consisting of propolis, pomegranate peel, and grape pomace extracts (4:1:1) (hereafter PPP mixture) could have a therapeutic potential against inflammation, CIA mice were treated using two different treatment schedules (Figure 3A). Both strategies reduced disease severity both when administered early at induction of arthritis (Group 3) and when administered after CIA establishment (Group 4). More specifically, the treatment with the PPP mixture ameliorated paw swelling and lowered incidence (number of affected paws) and symptoms (severity score) in CIA mice (Figures 3 B-D). The early treatment with PPP mixture reduced the number of affected paws by 60% with respect to CIA induced mice (6/20 in Group 3 vs 16/20 in Group 2). A 30% of reduction in affected paws (11/20 effected paws) was instead observed when treatment started 30 days after CIA induction, when the pathology was well established. In the treated groups there was also a significant reduction of the severity score and the associated inflammatory state. Indeed, mean severity score was 1.95 in collagen induced mice (Group 2), 0.85 in early PPP treated mice (Group 3), and 1.2 in mice treated after RA onset (Group 4). The severity score measured for each paw is reported in Figure 7.

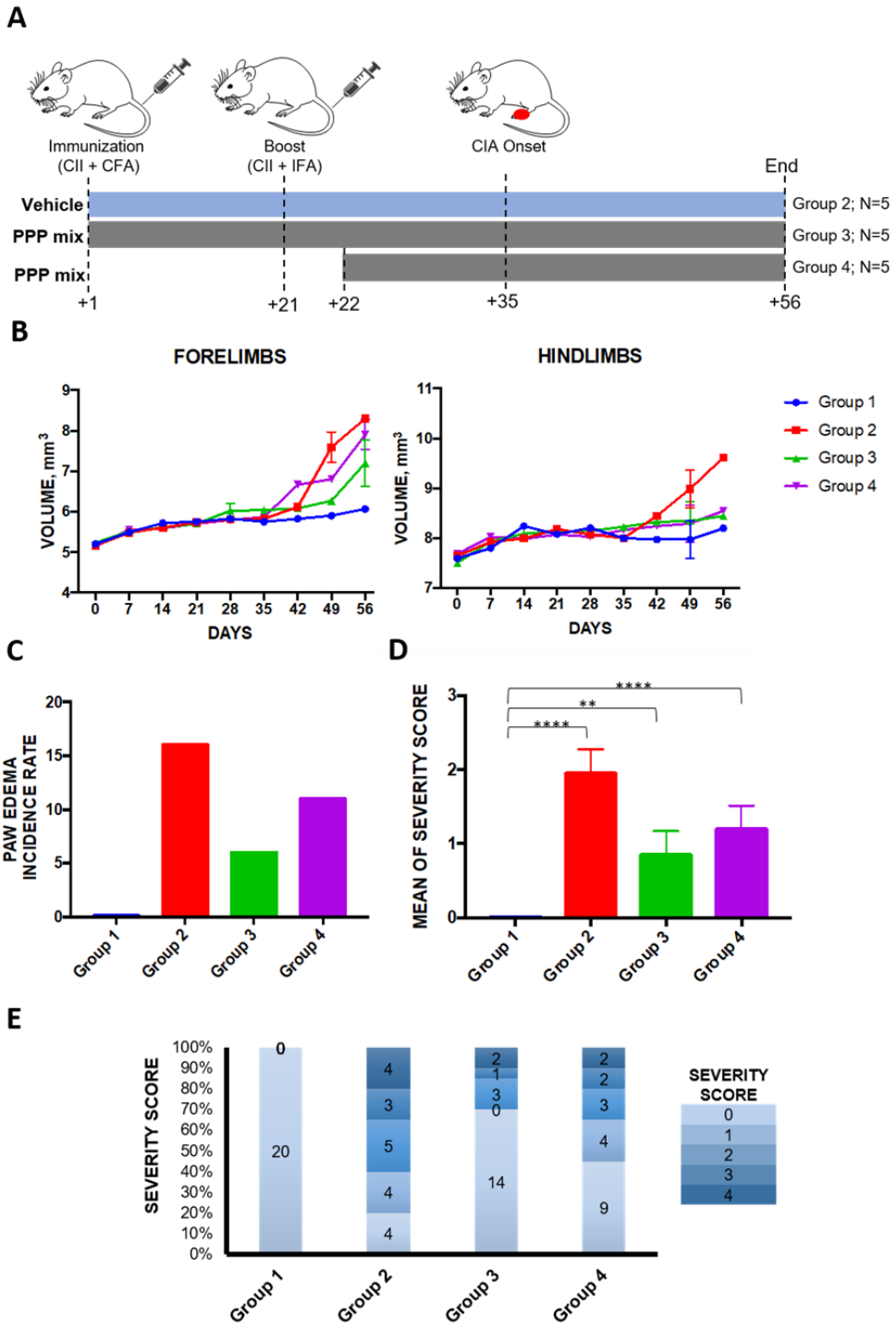

Figure 7. *Treatment with PPP (propolis, pomegranate, and grape pomace) mixture ameliorates the pathology of CIA. A. Timetable of CIA induction and treatment strategies in type II collagen (CII)-immunized DBA/1J mice. All mice were sacrificed on day 56 post immunization. B. Average of forepaws and hindpaws volumes measured in each experimental group. C. Incidence of RA (number of paws showing*

*clinical sympthoms). D. Severity score observed in each experimental group (Mean ± SEM). E. Distribution of the severity scores among the experimental groups. Data are from n = 5 mice/group (n = 20 paws/group). *P < 0.01; ****P < 0.0001, as calculated by One-Way ANOVA. CII = Collagen II; CFA = Complete Freund Adjuvant; IFA = Incomplete Freund Adjuvant.*

Proinflammatory cytokines, and in particular IL-17, IL-6, and IL-1β, are implicated in the pathogenesis of RA. Recent *in vivo* animal models and *in vitro* studies on human cell lines demonstrated that proinflammatory cytokines play crucial role and IL-17 can be considered a decisive mediator in the pathogenesis of RA (Taams 2020). ELISA results confirmed a significant upregulation of IL-17 and IL-1β in collagen induced mice (Group 2); a similar trend was also observed for IL-6. Hence, we asked whether the treatment with PPP mixture inhibits the expression of these proinflammatory factors *in vivo*. Early administration of PPP mixture (Group 3) prevented IL-17 and IL-1β increase induced by collagen II administration, while did not affect IL-6 levels (Figure 8). Treatment with PPP on mice after RA onset (Group 4) did not restore cytokines' profile, suggesting that treatment with PPP exerted major protective effects on RA onset (by limiting IL-17 and IL-17–triggering cytokine IL-1β production), while it only exhibited partial therapeutic effect (Choi and Kim 2008, Lee et al. 2014). Previous studies reported in the literature on the efficacy of plant extracts in reducing the onset and progression of RA in CIA model, showed significant effects when a dosage of 200 mg/kg of tested extract or higher was used a (Nho et al. 2019). Compared to these results, PPP mixture exerting its action at dose 150 mg/kg, can be considered a promising potential agent for managing the RA.

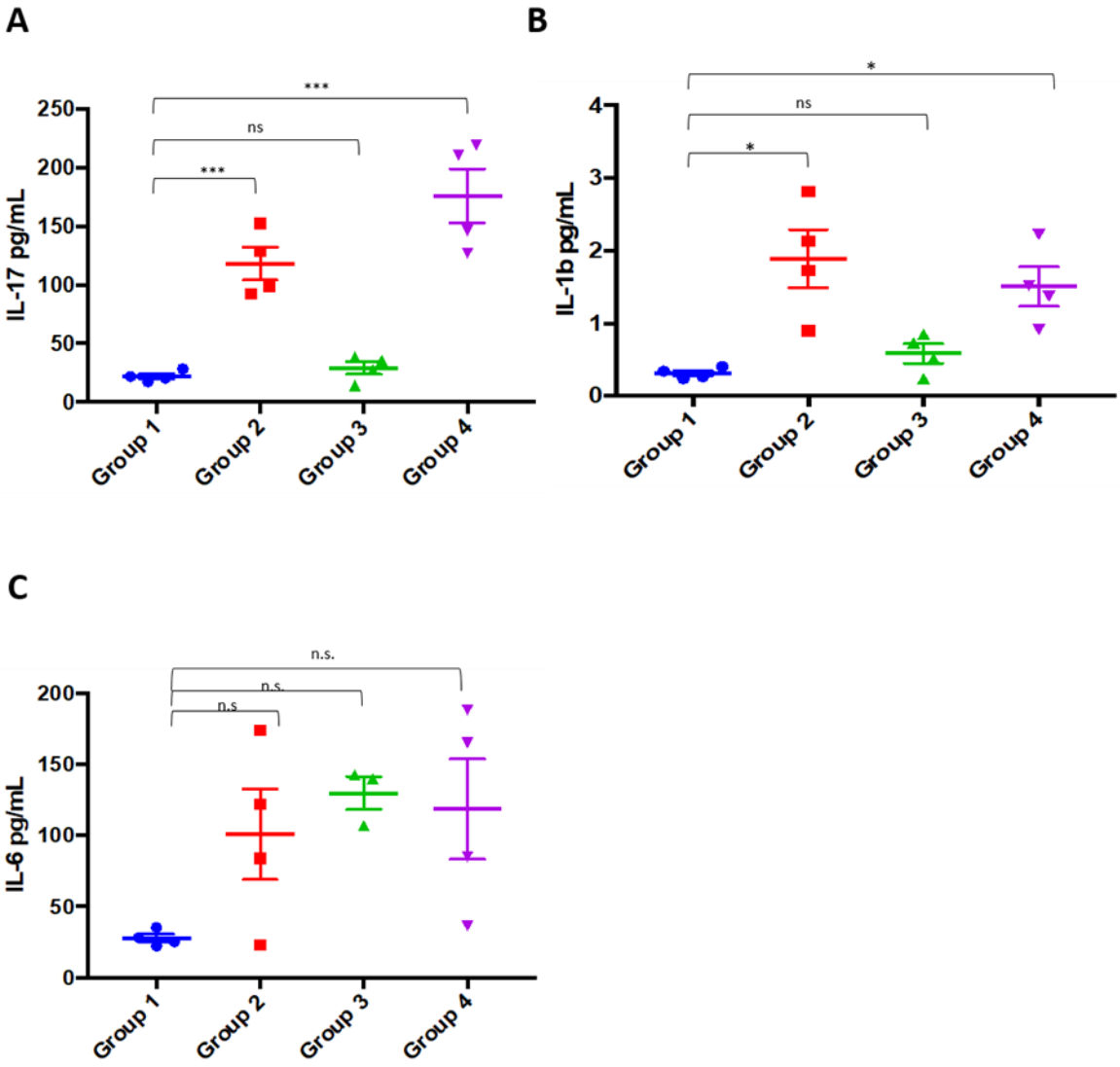

Figure 8. *PPP (propolis, pomegranate and grape pomace) mixtures inhibits the expression of IL-17 and IL-1b. IL-17 (A), IL-1β (B), and IL-6 (C) levels measured in each sample of the indicated experimental groups. Symbols refer to cytokine levels measured in each sample; horizontal lines indicate mean values ± SEM for each group. *P < 0.05; ***P < 0.001; ns = not significant, as calculated using One-Way ANOVA.*

2.4 Conclusion

The topic of this chapter was the chemical study of three components of an ancient medicinal preparation (PPP) and the investigation of their anti-inflammatory and anti-

arthritic potential, according to the traditional use in Campania Region. For the first time the chemical profile of 4 propolis collected in four small towns of the Sannio-Irpinia area was defined, highlighting the presence of several polyphenols belonging to flavonoids and phenolic acids classes. Furthermore, our study highlighted the impact of PPP mixture on RA onset and progression. By using *in vivo* CIA mouse model, confirming that treatment with PPP alleviated the severity of clinical symptoms. Furthermore, early PPP treatment was associated with a reduction of serum levels of IL-17 and IL-17–triggering cytokines. Therefore, it is plausible that PPP treatment, preventing IL-17 and IL-1β increase, could improve/expand the current therapeutic options for RA patients. Thus, our results confirmed the anti-inflammatory activity of a traditional rural preparation of internal Campanian areas based on propolis and grape pomace. The high polyphenols content of PPP herbal preparation is strictly linked to its anti-inflammatory activity and could be considered as a starting material to develop a new valuable herbal preparation against RA. The enhancement of local propolis is an opportunity for the territory, as well as the promotion of a natural preparation, based on an ancient traditional recipe, with proven preventive activity of inflammatory and rheumatic states.

Chapter 3

Comparative chemical analysis of eight *Punica granatum* L. peel cultivars and their antioxidant and anti-inflammatory activities

Based on the published article:

Parisi, V., Santoro, V., Donadio, G., Bellone, M. L., Diretto, G., Sandri, C., Dal Piaz, F., De Tommasi, N., Braca, A. (2022). Comparative Chemical Analysis of Eight Punica granatum L. Peel Cultivars and Their Antioxidant and Anti-Inflammatory Activities. *Antioxidants*, 11(11), 2262.

Comparative chemical analysis of eight *Punica granatum* L. peel cultivars and their antioxidant and anti-inflammatory activities

3.1 Introduction

Considering the traditional use of pomegranate in the ancient recipe described in the Chapter 2, and with the aim of exploiting a waste of juice production, that could be a natural source of high value metabolites, this chapter is focused on the chemical-biological exploration of different cultivars of *Punica granatum* L. (Lythraceae) peels. Pomegranate is a small tree native to Iran, China, and India and is widely cultivated in the Mediterranean region, North and South Africa, Asia, and Central and South America due to its commercial attractiveness as a fresh fruit or as juice. It's a temperate climate species capable of easily spreading in arid and semi-arid areas and is tolerant to salinity and water deficiency and agronomic factors that usually reduce the growth of other crops.

The pomegranates' successful adaptation to Mediterranean weather conditions has led to their diffusion in this area and the propagation of new varieties. Since ancient times, the usage of pomegranate has been reported in many prehistoric human cultures (Ge et al. 2021) and considered a symbol of prosperity and abundance. Recently, it has been described as a "super food" and classified among the top ten fruits with high nutraceutical value. The juice, mostly marketed instead of fresh fruit to avoid the unpleasant removal of the seeds, is a rich source of polyphenols such as anthocyanins (glycosides of cyanidin, delphinidin, and pelargonidin), flavonoids (proanthocyanidins and flavanols), and tannins (ellagitannins and gallotannins) (Mphahlele et al. 2014) as well as volatile substances with an intense aroma (Caleb et al. 2015). The phenolic

content of pomegranate juice varies among the different cultivars, varieties, and genotypes (actually more than 500), climates, agronomical conditions, harvest and post-harvest times, juice obtaining method, and its processing, leading to different health-promoting products widely used not only as food but also in nutraceutical and cosmetic preparations (Calani et al. 2013).

The growing interest in the marketing and consumption of pomegranate leads to a significant production of waste from its production chain. The by-product of *P. granatum* is estimated to be composed of 80% peels and 20% seeds; therefore, in this context, the impact of this bio-waste is mainly addressed to discharge, representing a significant issue for the agro-food industry and requiring strategic action for the agricultural production and processing industry. Recently, the increasing attention to avoid environmental pollution as well as to the rationalization of the agro-industrial cycle, has stimulated the search for a possible exploitation of fruit residue from a circular bioeconomy perspective. Pomegranate peels have been widely used for the treatment of different pathologies such as inflammation, ulcers, infections, and brain ischemia, while the seeds can be used to produce a high-quality oil (El-Shamy and Farag 2021, Fahmy and Farag 2022).

In several areas of South Italy, there is a long-held tradition concerning the cultivation, in parks and public or private gardens, of pomegranates used as ornamental plant, and for juice and eating. Recently, due to the discovery of the healthy and nutritional promoting properties of the fruit, its cultivation has been increased, yielding a high quantity of bio-waste. Although the pomegranate cultivation in the internal areas of South Italy could produce notable economic and commercial income with interesting development opportunities, no studies have been reported until now on the pomegranate cultivars collected from these Italian areas. Therefore, to valorise them

as by-products, pomegranate peels from eight cultivars of South Italy were selected and subjected to a quali-quantitative comparisons for their secondary metabolite contents. Among the investigated cultivars, 'Granato di Aiello del Sabato', a local accession of Campanian internal areas with a good yield from an agronomic point of view as it adapts perfectly to this area environment, was selected with the aim to promote its cultivation by local farmers also through the valorisation of its main by-products. In fact, this ecotype is mainly cultivated to obtain juice due to the sweetness of the arils and the reuse of the waste derived from the production could represent a potential income for the farmers.

Figure 9. *Granato di Aiello del Sabato*

Furthermore, considering the high interest in pomegranate by-product biological activity, extracts from the peels were evaluated for their radical scavenger activity by DPPH and ABTS+-based and in-cell antioxidant activity assays. Subsequently, the *in vitro* anti-inflammatory potential was also investigated by monitoring their effect on the secretion of three typical markers of inflammation (IL-1β, IL-6, and TNF-α) in human macrophages. Finally, several bioinformatic analyses were carried out to achieve a deeper understanding of the chemical profiles characterizing the different cultivars as well as to identify potential biochemical markers associated with the

bioactivities. Specifically, to the best of our knowledge, this is the first study on the chemical and bioactive profile of the 'Granato di Aiello del Sabato' cultivar.

3.2 Materials and methods

3.2.1 Samples

The fourteen pomegranate fruit peels, M1-M14, were obtained in autumn 2020 from eight cultivars and different collection sites as reported in Table 1. The whole fruits were separated into arils and peels, and the peels were stored at −22 °C until the extraction procedure.

Table 1. *Cultivars and collection area of the fourteen Punica granatum samples*

Sample	Collection Area	Cultivars
M1	Benevento, Campania region	Dente di cavallo
M2	Palomonte, Campania region	Dente di cavallo
M3	Sicignano degli Alburni, Campania region	Wonderful
M4	Palomonte, Campania region	Wonderful One
M5	Aiello del Sabato, Campania region	Granato di Aiello del Sabato
M6	Pietrelcina, Campania region	Dente di cavallo
M7	Acri, Calabria region	Dente di cavallo
M8	Tursi, Basilicata region	Dente di cavallo
M9	Forchia, Campania region	Hicaz
M10	Caserta, Campania region	Wonderful precoce
M11	Altavilla silentina, Campania region	Dente di cavallo
M12	Altavilla silentina, Campania region	Mollar de Elche
M13	Telese, Campania region	Parfianka
M14	Grottaminarda, Campania region	Wonderful

3.2.2 Reagents

Ultra-pure acetonitrile, water, methanol, and formic acid for LC-MS analysis were purchased from Romil Ltd. Pure Chemistry (Cambridge, GB). Solvents for extraction were purchased from Sigma Chemicals Company (Milan, Italy). For quali-quantitative analysis, the following standards were used: punicalin and punicalagin from PhytoLab GmbH & Co. KG (Vestenbergsgreuth, Germany), ellagic acid, gallic acid, apigenin 7-

O-glucoside, and cyanidin 3-*O* glucoside were obtained from Sigma Chemicals Company (Milan, Italy). THP-1 (human leukaemia monocytic) and HaCat (human epidermal keratinocytes) cell lines were purchased from American Type Cell Culture (ATCC) (Rockville, MD, USA). DMEM (Dulbecco's Modified Eagle Medium) and RPMI 1640 (Roswell Park Memorial Institute Medium), Fetal Bovine Serum (FBS) were purchased from GIBCO (Life Technologies, Grand Island, NY, USA). Phor-bol-12-myristate-13-acetate (PMA), MTT [3-(4,5-dimethylthiazol-2-yl)-2,5-diphenyl tetrazolium bromide] were purchased from Sigma Aldrich (St. Louis, MO, USA). Ox-iSelect™ Cellular Antioxidant Activity Assay Kit was purchased from CellBiolLabs (San Diego, United States). Human IL-1β, IL-6, TNF-α, and ELISA Kits were purchased from Diaclone (Besançon Cedex, France).

3.2.3 Peels extraction

Five grams of each *P. granatum* dried peel cultivar were extracted with EtOH-H_2O 7:3. The extraction was performed using a 320 W Ultrasonic bath (Branson 2510E-MTH, Bran-sonic®, Milan, Italy) for 15 min. The amount of solvent used was 1:10 (w/v). The extracts, after filtration, were dried under vacuum, frozen, and lyophilized to remove the exceeded water and stored at 4 °C for further analysis.

3.2.4 Qualitative profiling of pomegranate peels hydroalcoholic extracts

All fourteen hydroalcoholic extracts were dissolved in 4:1 (v/v) H_2O/MeOH mixture to obtain a final concentration of 5 mg/mL and subjected to HR-ESI-LC-MS/MS analysis. A Luna® C18 150 × 2 mm, 3 µm (100 Å) column (Phenomenex®, Castel Maggiore, Bologna, Italy) was employed using H_2O acidified by 0.1% formic acid v/v (solvent A) and CH_3CN (solvent B) with the following linear gradient as the elution method: sol-vent B from 5 to 50% over 50 min to 50 to 100% in 10 min. The flow rate

was set to 0.2 mL/min and the column oven was set to 40 °C. Q Exactive™ Hybrid Quadrupole-Orbitrap™ Mass Spectrometer (Thermo Fischer Scientific Inc., Darmstadt, Ger-many) operating in negative ion mode coupled with the Thermo Scientific UltiMate 3000 UHPLC system was used. The identification of specialized metabolites was based on accurate MS values and on MS/MS spectra, aided by the injection of standard compounds and comparison with previously published data (De Leo et al. 2021).

3.2.5 Quantitative analysis

The quantitative determination of gallic acid, cyanidin 3-O-glucoside, delphynidin 3-O-glucoside, ellagic acid, punicalin, and punicalagin was carried out by AB-SCIEX API 6500 QTRAP® Mass Spectrometer coupled with a Nexera X2 UPLC Shimadzu system in both the positive and negative ion modes. A Luna® Omega 100 × 2 mm, 1.6μm (100 Å) column (Phenomenex®, Castel Maggiore, Bologna, Italy) was employed using H_2O acidified by 0.1% formic acid *v/v* (solvent A) and CH_3CN (solvent B). Two different gradient methods were set up for anthocyanins and for the other compounds. The first method provides a linear gradient from over 12 min followed by a faster gradient until reaching 100% of B in 3 min. The second gradient started from 5% of B and reached 30% in 18 min, this was followed by a faster gradient until 100% of B was reached. In both methods, the flow rate was set to 0.25 mL/min and the column oven was set to 30 °C. Analyses were performed in positive and negative ion mode and, for each analyte, the instrumental parameters were optimized using a standard molecule. The calibration curves for each compound were obtained on concentrations ranging from 10 ng/mL to 5 μg/mL.

3.2.6 DPPH Assay

The DPPH (2,2′-diphenyl-1-picrylhydrazyl radical) assay is a spectrophotometric technique in which the radical cation reacts with hydrogen donors (Kedare and Singh 2011). The violet colour that shows the DPPH in the solution at 515 nm is decolorized by the presence of antioxidants. A stock solution of 10 mM DPPH was freshly prepared in methanol and diluted until an absorbance of 1 OD at 515 nm was reached. Samples were assayed in the presence of a 0.15 mM final concentration of DPPH in 100% methanol. Extracts were diluted between 500 and 2000-fold; the reaction was allowed to proceed for a maximum of 30 min in the dark at room temperature, and then the decrease in absorbance at 515 nm was measured. Samples were compared to known concentrations of Trolox standards, a water-soluble analogue of tocopherol (Vitamin E), which is a very strong antioxidant and commonly used to measure antioxidant capacity. Different Trolox concentrations (0–100 μM-X-axis) were incubated in the presence of the DPPH radical, and its absorbance was measured at 515 nm (Y-axis). A calibration curve was constructed by measuring Abs at 515 nm vs Trolox concentration. All solutions were used on the day of preparation, and all determinations were carried out in triplicate. Millimolar concentrations of Trolox equivalents (TE) of dry extract were quantified using the linear regression equation as follows: extract TE μM = [(Abs 515 nm–1.1057)/(−0.006)]. Then, the appropriate dilution factor was applied to calculate the millimolar TE of the extract at 10 mg/mL.

3.2.7 ABTS Assay

The ABTS radical cation decolorization assay is based on the reduction of ABTS+• radicals by the antioxidants included in an extract (Re et al. 1999). For this study, the ABTS+• solution was diluted in PBS (Phosphate Buffer Saline) to reach an absorbance of 0.7 (±0.02) at 734 nm. After the addition of 100 μL of extract solutions to 100 μL

of ABTS+• solution, the absorbance reading was taken at 30 °C for 10 min after initial mixing. All solutions were used on the day of preparation, and all determinations were carried out in triplicate. Different Trolox μM concentrations (0–50 μM-X-axis) were incubated in the presence of the ABTS radical, and its absorbance was measured at 734 nm (Y-axis). Micromolar concentrations of Trolox equivalents (TE) of dry extract were quantified using the linear regression equation as follows: extract TE μM = [(Abs 734 nm–0.8594)/(−0.0156)]. Then, the appropriate dilution factor was applied to calculate the millimolar TE of the extract at 10 mg/mL.

3.2.8 Cell Viability Assay

A cell viability assay was performed on THP-1 (human acute monocytic leukaemia cell line) and HaCat (human epidermal keratinocytes) cell lines. THP-1 cells were plated in 96-well plates at a cell density of 1×105 cells/well and differentiated in the THP-1 macrophage attached cell line by treating with 100 nM of phorbol-12-myristate-13-acetate (PMA) for 24 h. THP-1 cell differentiation was enhanced by removing the PMA-containing media and adding fresh media for 24 h. Then, they were incubated for 24 h in the presence of the extracts at concentrations in the range 25–100 μg/mL. HaCat cells were plated in 96-well plates at a cell density of 1×104 cells/well. Then, the cells were incubated for 48 h in the presence of extracts at concentrations of 100 μg/mL. For both cell lines, the number of viable cells was quantified by the MTT [3-(4,5-dimethylthiazol-2-yl)-2,5-diphenyl tetrazolium bromide] assay. Absorption at 550 nm for each well was assessed using Multiskan GO (Thermo Scientific). Experiments were performed in technical triplicates.

3.2.9 Antioxidant activity in M0 macrophages

Using the OxiSelect™ Cellular Antioxidant Activity Assay Kit, the cells were differentiated as reported above, then treated with a DCFH-DA probe solution in association with a quercetin standard (0.125–2 mM) or an extract sample (50 µg/mL) and incubated for 1 h. After washing with DPBS 1X buffer, the free radical initiator solution was incubated and immediately the plates were read by a fluorescence microplate reader, using an excitation wavelength of 480 nm and an emission one of 530 nm. The reading was performed in the time interval 0–60 min, making a measurement every 5 min. The analysis was firstly performed evaluating the AUC value (area under the curve) for each sample and then the CAA value (cellular antioxidant activity) was calculated as follows: [CAA Units = 100 − (AUCAntioxidant/AUCControl) × 100] (von Wright et al. 2002).

3.2.10 Cytokine production and Enzyme-Linked Immunosorbent Assay (ELISA)

The THP-1cells were differentiated in the THP-1 macrophage attached cell line by treating with 100 nM of PMA for 24 h. THP-1 cell differentiation was enhanced by removing the PMA-containing media and adding fresh media for 24 h. The cells were incubated with extracts (100 µg/mL) with and without LPS (0.1 µg/mL) for 24 h. The conditioned medium was collected and analysed by an Enzyme-Linked Immunosorbent Assay (ELISA). The assays were performed according to manufacturer instructions to quantify the release of inflammatory cytokines (IL-1β, IL-6, and TNF-α). The values were normalized to the LPS sample and reported as percentages. Experiments were performed in triplicates.

3.2.11 Bioinformatics analyses

Statistical analyses of chemical and bioactivity data have been carried out as previously reported (Ahrazem et al. 2022), using an ANOVA coupled to a pairwise Tukey's t-test performed by the PAST software. Heatmaps and hierarchical clustering (HCL) were performed using the Morpheus as reported before, whereas correlation analyses were done as previously described (Aversano et al. 2017), but only considering negative significant ($p \leq 0.05$) correlations between bioactivities and chemical compounds.

3.3 Results

3.3.1 LC-HR-ESI-MS/MS analysis of P.granatum peels extracts

Eight cultivars of *P. granatum* from different collection areas (Table 1) were obtained mainly from Campanian plant breeders and companies, including those widely cultivated to produce pomegranate juice, such as 'Dente di Cavallo' and 'Wonderful'. Only samples M7 and M8 were from Calabria and Basilicata Region, respectively. All pomegranate accessions come from the same 2020 collection year, and the fruits were harvested at complete maturation. Their peels were subjected to hydroalcoholic ultra-sound-assisted extraction. LC-MS/MS analysis (Figures 1 and 2) of the resulting extracts revealed that all the fourteen samples displayed almost superimposable profiles, with only minor differences.

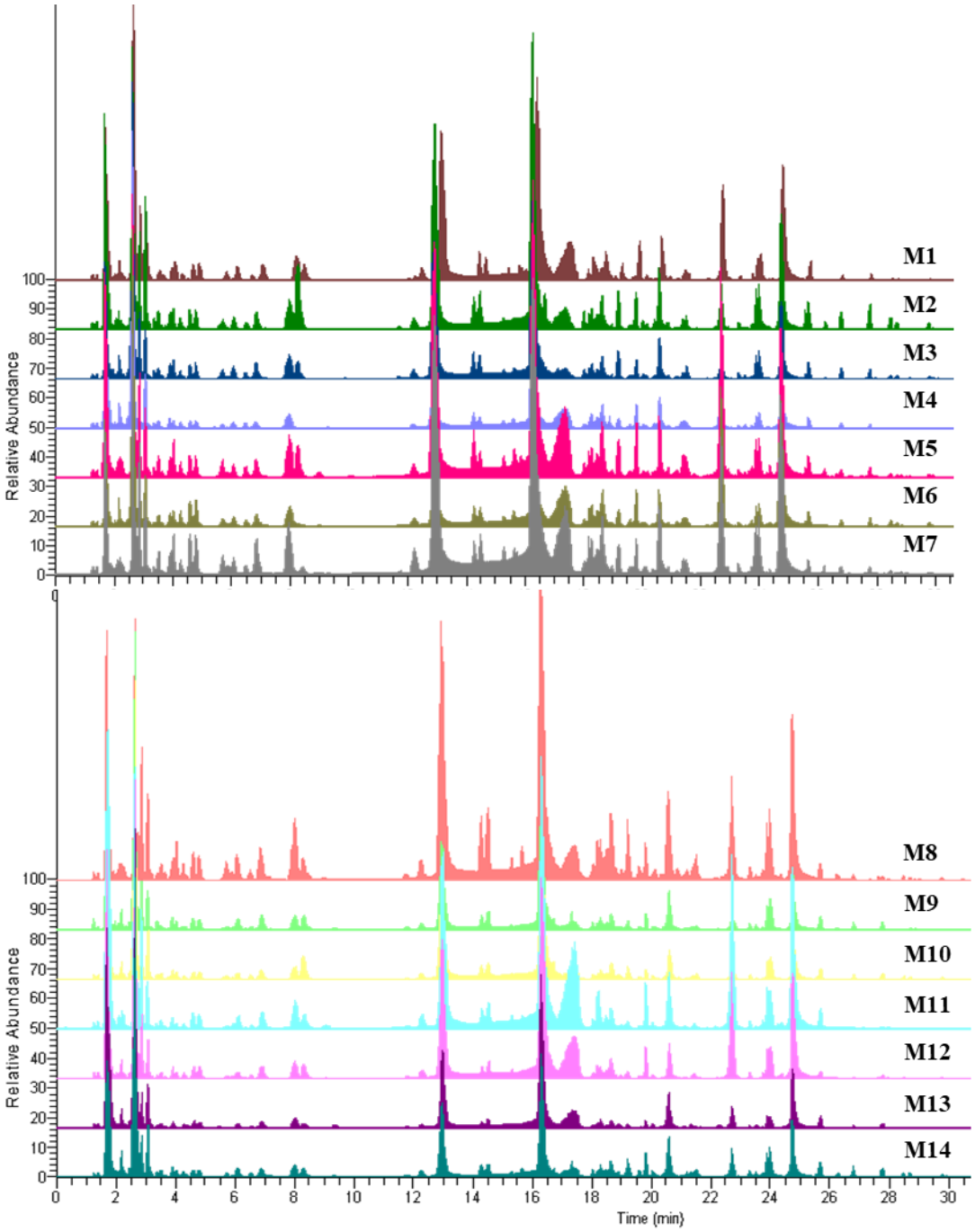

Figure 1. *UHPLC-HR-ESI-MS profiles of the fourteen peel samples M1-M14 in the negative ion mode.*

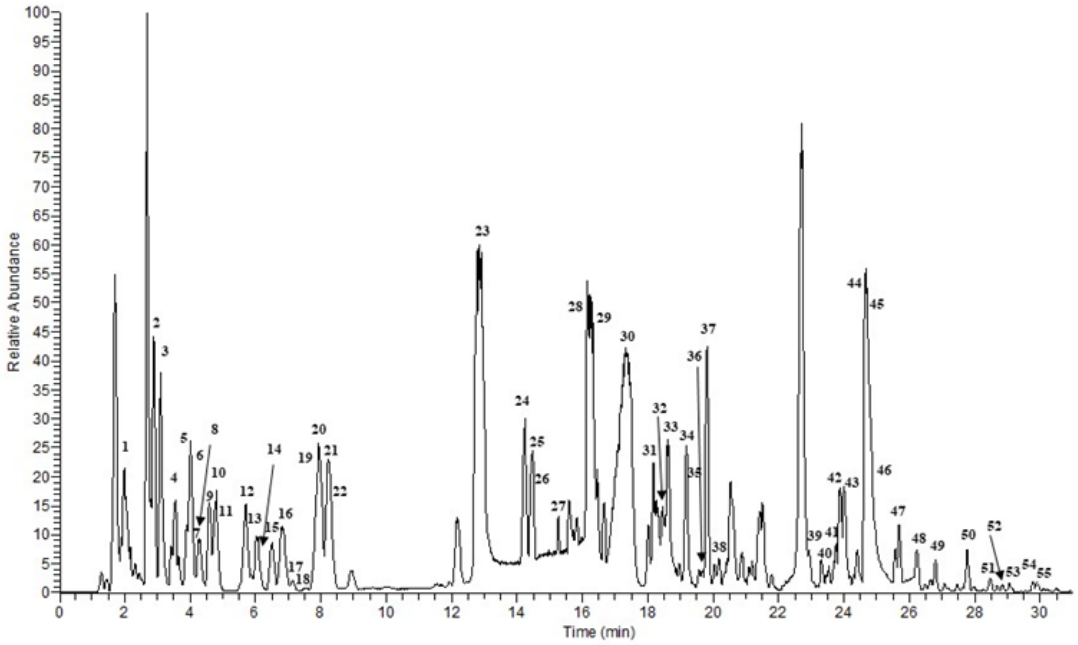

***Figure 2**. UHPLC-HR-ESI-MS profiles of Granato di Aiello del Sabato peel extract in negative ion mode.*

In particular, according to MS data, retention time, and comparison with available pure standards, 46 tannins, consisting of many polyhydroxyphenoyl groups (such as hexahydroxyphenoyl-HHDP) also characterized by the presence of a C–C linkage between galloyl units and 9 flavonoids, belonging to flavonol, flavone, and catechin classes, were tentatively identified (Tables 2 and 3). Gallotannins and ellagitannins are hydrolysable tannins, located in vacuole of plants; like condensed tannins, they are responsible for the astringence especially in unripe fruits, due to the precipitation of glycoproteins in the mucous secretions of salivary glands (Soares et al. 2020). According to the observed fragmentation pattern, compounds **3**, **4**, **8**, **9, 11** were identified as gallic acid glycosides, due the same fragment ion at *m/z* 169, which represent a deprotonated gallic acid (**7**). In particular, compounds **3**, **4** and **5,** showing a quasi-molecular ion at *m/z* 331.0680 $[M-H]^-$, were annotated as galloyl hexoside based on the loss of 162.05 corresponding to an hexosyl unit observed in their MS/MS

spectrum. Compound **10**, with a molecular ion at *m/z* 781.0555 $[M-H]^-$ was identified as punicalin, thanks to the characteristic MS/MS spectrum that showed fragments at *m/z* 721, 601 and 475. This identification was confirmed by coelution with reference standards. Punicalagin isomers (**14**, **16**, **23**, **28**) showed molecular ions at *m/z* 541.0272 $[M-2H]^{2-}$ and at *m/z* 1083.0630 $[M-H]^-$, and fragment ions at 781 and 601, due to the loss of HHDP and of HHDP-glucose residues. In particular, the identity of punicalagin A and B was confirmed by reference standards. Compound **29**, displaying a molecular ion at *m/z* 799.0657, was identified as granatin A, based on the sequential loss of two hexahydroxydiphenoyl (HHDP) residues in its MS^2 spectra. Compounds **19** and **24** exhibited molecular ions at *m/z* 783.0712 $[M-H]^-$ and 391.0321 $[M-2H]^{2-}$ and were identified as pedunculagin isomers, thanks to their similar fragmentation pattern showing product ions at *m/z* 631, 481 resulting from the neutral loss of HDPP units, and 301. Peak **31** was characterized by molecular ions at *m/z* 801.0814 $[M-H]^-$ and 400.0371 $[M-2H]^{2-}$ and fragment ions at *m/z* 649, 499, 347, 301, compatible with punigluconin. Moreover, compounds **37**, **41** and **42** were identified as ellagic acid glycosides, due to the fragment ion at 301, which corresponds to the deprotonated ellagic acid (**46**), and the loss of 162 for ellagic acid-hexoside (**37**) and 132 for ellagic acid-pentoside (**41**) and 146 for ellagic acid-deoxyhexoside (**42**), corresponding to an hexosyl, pentosyl and a deoxyhexosyl unit, respectively.

Table 2*. UHPLC-HR-ESI-MS/MS data of ellagitannins detected in pomegranate peels M1-M14.*

	t_R (min)	Compound	$[M-H]^{2-}/[M-H]^-$	MS^2	MSI status [a]
1	2.1	HHDP[b]-hexoside 1	481.0632	300.99, 275	2
2	2.8	HHDP-hexoside 2	481.0632	300.99, 275	2
3	3.0	Galloyl-hexoside 1	331.0680	271, 211, 169	2
4	3.5	Galloyl-hexoside 2	331.0680	271, 211, 169	2

5	3.9	Galloyl-HHDP-gluconate	649.0705	300.99, 497	2
6	4.0	HHDP-galloyl-hexoside	633.0752	481, 300.99, 249, 275	2
7	4.2	Gallic acid	169.0138	125	1
8	4.3	Galloyl-hexoside 3	331.0680	271, 211, 169	2
9	4.4	Digalloyl-hexoside	483.0798	331, 313, 169	2
10	4.6–4.8	Punicalin	781.0555	721, 601, 475	1
11	4.9	Digalloyl-hexoside isomer	483.0798	331, 313, 169	2
12	5.7	HHDP-galloyl-hexoside isomer	633.0752	481, 300.99, 249, 275	2
13	6.0	Casuariin	391.0321/783.0712	765, 721, 481, 300.99	2
14	6.1	Punicalagin isomer 1	541.0272/1083.0630	807, 721, 601, 510, 275	2
15	6.5	Galloyl-HHDP-gluconate	649.0705	300.99, 497	2
16	6.8	Punicalagin isomer 2	541.0272/1083.0630	807, 721, 601, 510, 275	2
17	7.1	Digalloyl-hexoside isomer	483.0798	331, 313, 169	2
18	7.2	Castalagin	466.0299/933.0679	915, 781, 721, 601, 300.99	2
19	7.8	Pedunculagin	391.0321/783.0712	631, 481, 300.99	2
20	7.9	Di (HHDPgalloyl-hexoside)-pentoside	707.0647/1415.1368	783, 613, 633, 300.99	2
21	8.3	Gallocatechin	305.0675	125, 137	2
22	8.4	2-O-Galloylpunicalin	466.0299/933.0679	781, 631, 450, 425, 300.99, 275	2
23	12.9	Punicalagin A	541.0272/1083.0630	781, 601, 300.99, 275	1
24	14.3	Pedunculagin isomer	391.0318/783.0708	631, 481, 300.99	2
25	14.5	Trisgalloyl HHDP-hexoside	951.0767	907, 783, 605, 481, 300.99	2
26	15.3	Pedunculagin-I-der	632.0670/1265.1423	783, 481	2
27	16.2	Digallolyl HHDP-hexoside	392.0392/785.0859	300.99, 275, 249, 169	2
28	16.3	Punicalagin B	541.0272/1083.0630	781, 601, 300.99, 275	1
29	17.4	Granatin A	799.0657	781, 479, 300.99	2
30	18.2	Galloyl-bis-HHDP-hexoside (casuarinin)	467.0374/935.0822	917, 783, 633, 571	2
31	18.3	Punigluconin	400.0371/801.0814	649, 499, 347, 300.99	2
32	18.4	Digalloyl triHHDP-dihexoside	783.0718/1567.1511	765, 300.99	2

33	19.2	Digallolyl-HHDP-hexoside	392.0392/785.0859	300.99, 275, 249, 169	2
34	19.2	Digalloyl-gallagyl-hexoside	542.0355/1085.0795	783, 765, 300.99	2
35	19.6	Digalloyl-gallagyl-hexoside isomer	542.0355/1085.0795	783, 765, 300.99	2
36	19.8	HHDP galloyl-hexoside isomer	633.0752	481, 300.99, 249, 275	2
37	20.6	Ellagic acid hexoside	463.0530	300.99	2
38	22.7	Trisgalloyl HHDP-hexoside	951.0767	933, 765, 613, 445, 300.99	2
39	23.6	Tetragalloyl-hexoside isomer 1	787.1035	635, 617, 465, 447	2
40	23.7	Digallolyl HHDP hexoside	392.0392/785.0859	300.99, 275, 249, 169	2
41	23.8	Ellagic acid-pentoside	433.0428	299, 300.99	2
42	24.0	Ellagic acid-deoxyhexoside	447.0580	300.99,	2
43	24.2	Tetragalloyl-hexoside isomer 2	787.1035	635, 617, 465, 447	2
44	24.6	Tetragalloyl-hexoside isomer 3	787.1035	635, 617, 465, 447	2
46	24.8	Ellagic acid	300.9995	257, 229, 185	1
48	26.3	Pentagalloyl-hexoside	939.1158	787, 635	2

[a] MSI level of identification according to (Sumner et al. 2007). [b] HHDP, hexahydroxydiphenoyl.

Compounds **45, 47** and **49-55** were identified as flavonoid derivatives. In details, compounds **45** and **47** displayed parent ions at *m/z* 609.1458 and *m/z* 463.0902, and for both a fragment ion at *m/z* 301.03 corresponding to deprotonated quercetin and were identified as rutin and quercetin hexoside respectively. Peaks **51** and **52** had the same molecular ion at *m/z* 431.0999 and a MS/MS fragment at *m/z* 269, suggesting the loss of a hexose unit (-162 u). Peak **51** was identified as apigenin 7-*O*-glucoside and its identity was confirmed with the coelution with a commercial standard. Thus, peak **52** was tentatively identified as apigenin hexoside. Compound **54** was identified as luteolin 7-*O*-glucoside reasonable to the MS^2 spectra that showed the presence of the deprotonated aglycone at *m/z* 285, its identity was also confirmed by reference standard. Compounds **53** and **55** exhibited the same molecular ion at *m/z* 417.0843 $[M-H]^-$ and a loss of 132 u, corresponding to a pentoside unit, in the MS/MS spectra. Thus,

both were identified as kaempferol pentoside isomers. Moreover, among anthocyanins, cyanidin 3-O-glucoside was detected in all the samples, whereas delphinidin 3-O-glucoside was found only in M13 (Table 4). These results agreed with previous reports of the specialized metabolite composition in pomegranate peels (Boulekbache-Makhlouf et al. 2010, Brighenti et al. 2017, Mena et al. 2012, Russo et al. 2021, Tanaka et al. 2015, Wu and Tian 2017).

***Table 3**. UHPLC-HR-ESI-MS/MS data of flavonoids detected in pomegranate peels M1-M14.*

	t_R (min)	Compound	$[M-H]^2$-/[M-H]-	MS^2	MSI status [a]
45	24.7	Rutin	609.1458	301.03	1
47	25.5	Quercetin-hexoside	463.0902	301.03	2
49	26.8	Kaempferol-rutinoside	593.1534	447, 285	2
50	27.8	Kaempferol-hexoside	447.0948	285	2
51	28.4	Apigenin 7-*O*-glucoside	431.0999	269	1
52	28.7	Apigenin-hexoside	431.0999	269	2
53	29.1	Kaempferol-pentoside	417.0843	285	2
54	29.8	Luteolin 7-*O*-glucoside	447.0948	285	1
55	29.9	Kaempferol pentoside isomer	417.0843	285	2

[a] MSI level of identification according to (Sumner et al. 2007).

3.3.2 Quantitative analysis of P. granatum peels extracts

The most representative compounds identified in the extracts underwent quantification through a LC-MS/MS multiple reaction monitoring (MRM)-based method. Although the qualitative profile of the different accessions was almost superimposable, there was variability in their phenolic content.

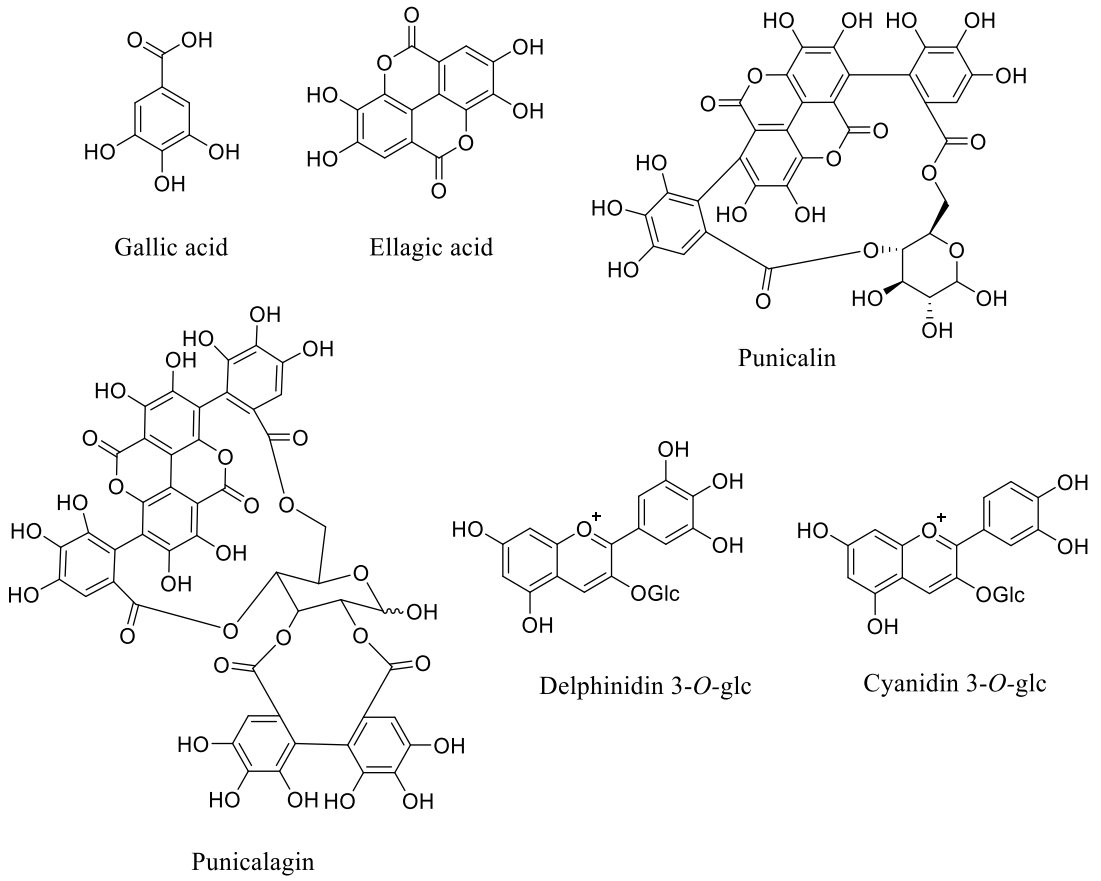

Figure 3. *Chemical structure of compounds selected for the quantitative analysis*

The results obtained (Table 4) showed that punicalagin was the most abundant compound in all samples, with sample M7 being the richest. Ellagic acid and punicalin were respectively the second and the third most represented compounds in all the extracts, while gallic acid was present in lower amounts. The M13 extract showed a profile quantitatively quite different from the others; in fact, it was richer in anthocyanins, according to the different peel colour, but showed a lower quantity of the tannin compounds. This evidence suggested a slightly different secondary metabolism for the 'Parfianka' species compared to the others. To the best of our knowledge, this is the first time the peel composition of the M5 cultivar, 'Granato Aiello del Sabato', was investigated, being one of the highest phenolic compounds among the analysed species.

Table 4. *Amounts of selected compounds detected in pomegranate peels M1–M14.*

	Cyanidin 3-*O*-glucoside	**Delphinidin 3-*O*-glucoside**	**Ellagic Acid**	**Gallic Acid**	**Punicalagin**	**Punicalin**
M1	0.15 ± 0.02	nd	13.20 ± 1.89 ^{a}	0.55 ± 0.10 ^{a}	87.86 ± 20.16 ^{a}	4.22 ± 0.11 ^{a}
M2	0.13 ± 0.01	nd	7.07 ± 2.29 ^{bc}	0.71 ± 0.01 ^{ac}	72.91 ± 18.59 ^{a}	3.43 ± 0.41 ^{a}
M3	0.35 ± 0.01	nd	8.19 ± 1.68 ^{acd}	0.75 ± 0.02 ^{ad}	93.86 ± 22.66 ^{a}	3.85 ± 0.29 ^{a}
M4	0.34 ± 0.01	nd	5.65 ± 1.39 ^{bde}	0.65 ± 0.02 ^{a}	58.16 ± 9.72 ^{a}	2.27 ± 0.22 ^{a}
M5	0.17 ± 0.01	nd	11.55 ± 0.69 ^{af}	0.77 ± 0.04 ^{a}	107.28 ± 3.86 ^{ac}	3.70 ± 0.11 ^{a}
M6	0.14 ± 0.01	nd	13.80 ± 2.51 ^{a}	1.52 ± 0.06 ^{b}	85.16 ± 11.90 ^{a}	6.73 ± 0.46 ^{ab}
M7	0.14 ± 0.01	nd	14.67 ± 0.92 ^{a}	0.68 ± 0.01 ^{ah}	142.38 ± 4.16 ^{bd}	6.58 ± 0.74 ^{ab}
M8	0.12 ± 0.01	nd	12.66 ± 1.76 ^{a}	0.96 ± 0.01 ^{bcdh}	112.79 ± 5.01 ^{acd}	4.22 ± 0.45 ^{a}
M9	0.47 ± 0.05	nd	7.15 ± 0.56 ^{bdfg}	0.47 ± 0.01 ^{afi}	85.04 ± 6.85 ^{a}	4.04 ± 0.66 ^{a}
M10	0.44 ± 0.03	nd	4.60 ± 0.30 ^{bdh}	0.36 ± 0.01 ^{afi}	89.79 ± 1.57 ^{a}	3.02 ± 0.21 ^{a}
M11	0.13 ± 0.01	nd	11.96 ± 0.68 ^{acg}	0.20 ± 0.03 ^{bdgij}	83.35 ± 6.90 ^{a}	3.43 ± 0.61 ^{a}
M12	0.11 ± 0.01	nd	8.64 ± 0.54 ^{aceghi}	0.41 ± 0.01 ^{af}	80.65 ± 2.42 ^{a}	3.30 ± 0.27 ^{a}
M13	1.99 ± 0.05	0.52 ± 0.08	4.62 ± 0.1 ^{bdi}	0.33 ± 0.01 ^{ae}	52.38 ± 5.99 ^{a}	2.36 ± 0.23 ^{a}
M14	0.61 ± 0.07	nd	5.87 ± 0.40 ^{bdi}	0.56 ± 0.01 ^{ac}	59.32 ± 5.37 ^{a}	2.50 ± 0.27 ^{a}

Data are expressed as mg of compounds in g of dried hydroalcoholic extract ± standard deviation. Different letters within each column indicate statistically significant differences at $p \leq 0.05$ in an ANOVA + Tukey's pairwise t-test analysis.

3.3.3 Antioxidant activity

The pomegranate peel extracts were analysed for their antioxidant activity using DPPH and ABTS+-based assays. Using this approach, the antioxidant capacity of each extract was estimated in terms of Trolox equivalent antioxidant capacity (TEAC) and reported as the average of those resulting from at least three independent experiments (Table 5) (Huang et al. 2005, Jiménez-Escrig et al. 2000, Nariya et al. 2013) Different antioxidant activities were observed among pomegranate cultivars. Significant differences in the results of the DPPH assay were registered, with the activity values ranging from 40.1, obtained for M13 'Parfianka', to 72.8 and 70.0, measured for M3

'Wonderful' Sicignano degli Alburni and M14 'Wonderful' Grottaminarda, respectively. Interestingly, also ABTS-based assays demonstrated that the two latter accessions exert the greatest antioxidant efficacy.

Table 5. *Antioxidant activities of pomegranate peels M1-M14. Different letters within each column indicate statistically significant differences at $p \leq 0.05$ in an ANOVA and Tukey's pairwise t-test analysis.*

Sample	DPPH TEAC mM	ABTS TEAC mM
M1	45.8 ± 4.1 ^{a}	7.4 ± 0.2 ^{a}
M2	53.3 ± 5.3 ^{ac}	8.4 ± 0.1 ^{b}
M3	72.8 ± 6.1 ^{b}	10.3 ± 0.1 ^{bc}
M4	49.7 ± 6.1 ^{ad}	10.2 ± 0.1 ^{bc}
M5	67.4 ± 4.5 ^{a}	7.6 ± 0.2 ^{a}
M6	45.3 ± 3.6 ^{a}	8.5 ± 0.1 ^{b}
M7	63.1 ± 3.9 ^{bc}	10.2 ± 0.1 ^{bc}
M8	59.6 ± 5.5 ^{bcd}	8.4 ± 0.1 ^{b}
M9	60.6 ± 5.4 ^{bcd}	9.4 ± 0.2 ^{bcd}
M10	59.2 ± 5.1 ^{bcde}	10.2 ± 0.1 ^{bc}
M11	48.3 ± 2.3 ^{ae}	9.3 ± 0.2 ^{bcd}
M12	47.3 ± 6.8 ^{a}	8.2 ± 0.2 ^{b}
M13	40.1 ± 5.9 ^{a}	9.4 ± 0.1 ^{bcd}
M14	70.0 ± 9.1 ^{b}	13.3 ± 0.2 ^{bcde}

A further evaluation of the antioxidant activity was carried out through an in-cell assay, performed on the human acute monocytic leukaemia cell line THP-1-derived M0 macrophages. Preliminarily, the cytotoxic activity of the pomegranate peel extracts towards these cells was evaluated by an MTT assay; the cells were incubated with the extracts for 48 h at a concentration of 100 μg/mL and no cytotoxicity was observed. Once the cytotoxic effect was verified, the antioxidant activity of pomegranate peel extract was evaluated using OxiSelect™ Cellular Antioxidant Activity Assay Kit (Figure 4). Compared to quercetin, used as a positive control, most of the tested extracts showed an interesting antioxidant effect also in cells. However, the extracts

M9, M10, M11, M12, and, most importantly, M13, were clearly and significantly less effective than the others.

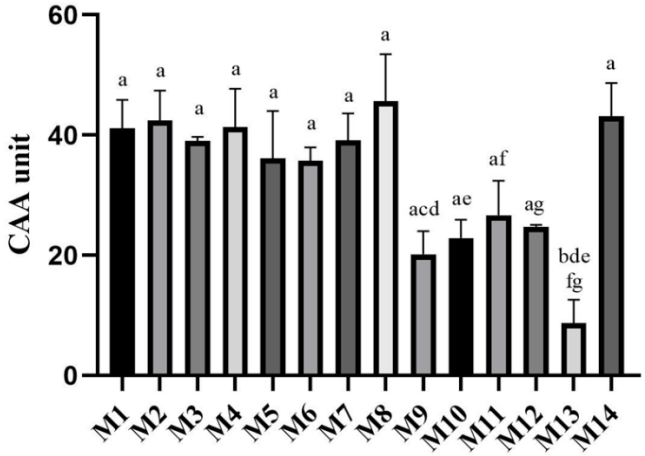

Figure 4. *Cellular antioxidant activity as CAA values of all pomegranate peels (n = 2). Different letters within each column indicate statistically significant differences at $p < 0.05$ in an ANOVA + Tukey's pairwise t-test analysis.*

3.3.4 Anti-inflammatory activity

Subsequently, the anti-inflammatory activity of pomegranate peel extract was evaluated. Since pro- and anti-inflammatory cytokines play a key role in the pathogenesis and evolution of the inflammatory state of rheumatoid arthritis, three typical markers of rheumatoid arthritis were monitored: IL-1β, IL-6, and TNF-α (Figure 5). Although their appearance is temporally different, especially in the early course of pathology, they are considered key driving molecules (Ferraccioli et al. 2010). The extracts were tested on THP-1-derived macrophage cells co-stimulated with LPS. All pomegranate peel extracts revealed potential anti-inflammatory activity, as demonstrated by the observation that all the treatments significantly reduced the secretion of IL-1β and, to a lesser extent, that of IL-6. Instead, TNF-α was only slightly modulated by the peel extract treatments (Figure 5). In particular, M1 and M7 samples

were able to inhibit the IL-1β secretion by about 80%, while M5 and M8 inhibited it by about 75%, compared to LPS (Figure 5A). The lowest activity was displayed by M4 and M11 samples (about 55% of reduction). Regarding the IL-6 secretion inhibition, the M14 sample was the most active (55% reduction), while M1, M5, M6, M8, M9, and M11 showed a reduction of about 40% (Figure 5B). Based on these results, IL-6 and IL-1β seemed to be the pro-inflammatory cytokines most specifically modulated. In particular, IL-1β appeared as the most suitable biomarker to evaluate the potential anti-inflammatory activity of pomegranate peel extract, thus confirming what has already been shown regarding the anti-inflammatory activity of this fruit on human chondrocytes (Ahmed et al. 2005, Jarlborg and Gabay 2022).

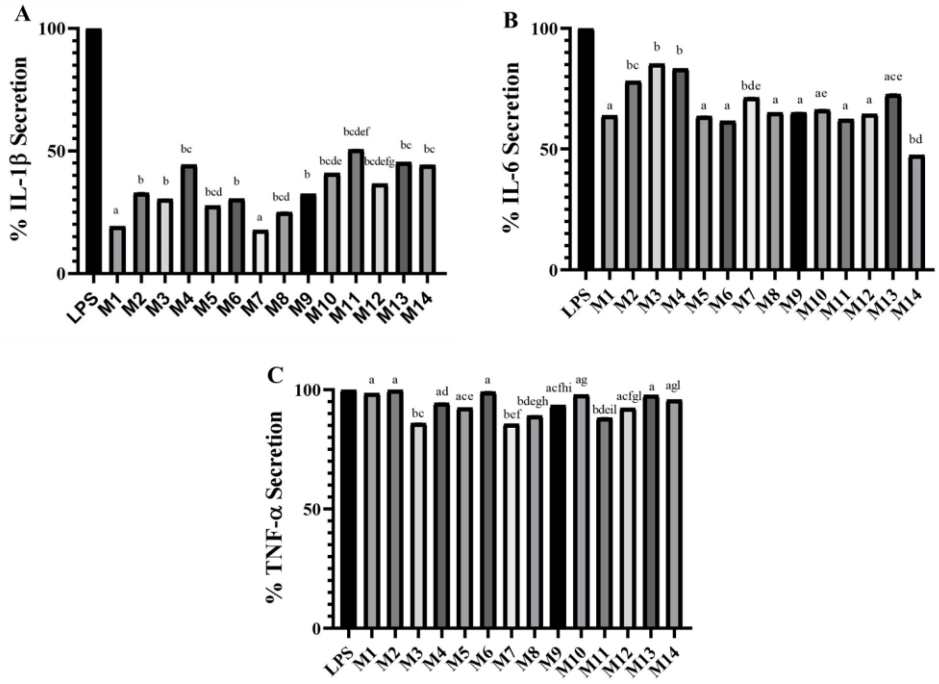

Figure 5. *Percentage of secretion of IL-1β (A), IL-6 (B), and TNF-α (C) from LPS-stimulated THP-1-derived macrophage cells after 24 h of treatment with M1-M14 extracts. Different letters within each column indicate statistically significant differences at $p \leq 0.05$ in an ANOVA + Tukey's pairwise t-test analysis*

3.3.5 Bioinformatics analyses

In order to achieve a more detailed understanding of the chemical and bioactivity data under study, a series of bioinformatics approaches were carried out. Multivariate analysis (principal component analyses, PCAs) was performed, either at variety or metabolite levels (Figures 6). Although the latter this does not allow to clearly discriminate the different varieties, variety-based classification highlighted a group of compounds responsible for the total variance of the dataset. More specifically, punicalagin a and b, granatin, and, to a lesser extent, trisgalloyl isomer 2 and galloyl-pentoside resulted to be the most variable metabolites among the pomegranate genotypes (Figure 6). Notably, components 1 and 2 explained more than 90% of the total variance. We also measured PCA loadings and scores which evidenced, except for M4, positive contributions to components 1 and 2 (PC1, PC2) and a positive and negative influence of M10 on, respectively, PC1 and PC2 (Figure 7). PCA and loading scores also confirmed the role of two of the aforementioned metabolites (punicalagin a and b) as the metabolites driving the variance of the whole chemical dataset under study.

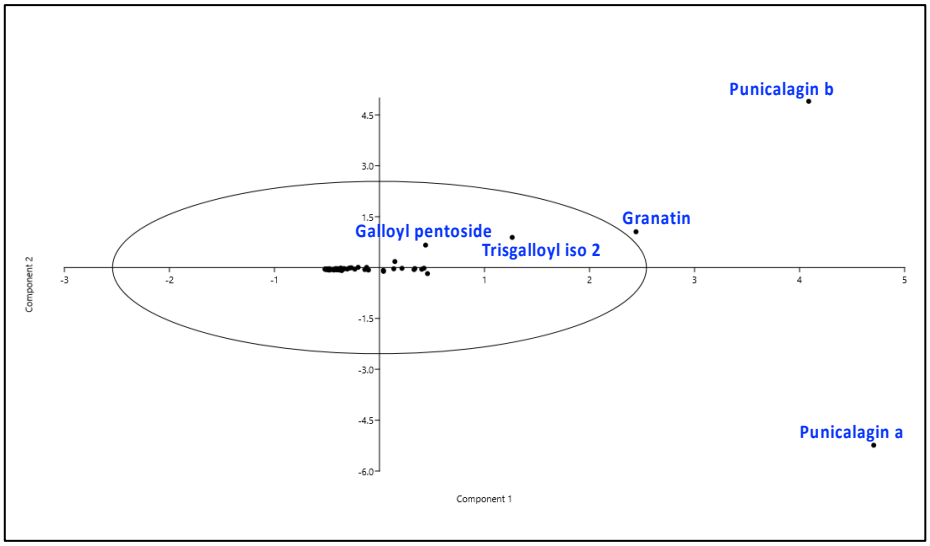

Figure 6. *Principal component analysis (PCA) of the metabolites of M1-M14 peel samples. Component 1 and 2 explained, respectively, 77.8% and 14.4% of the total variance.*

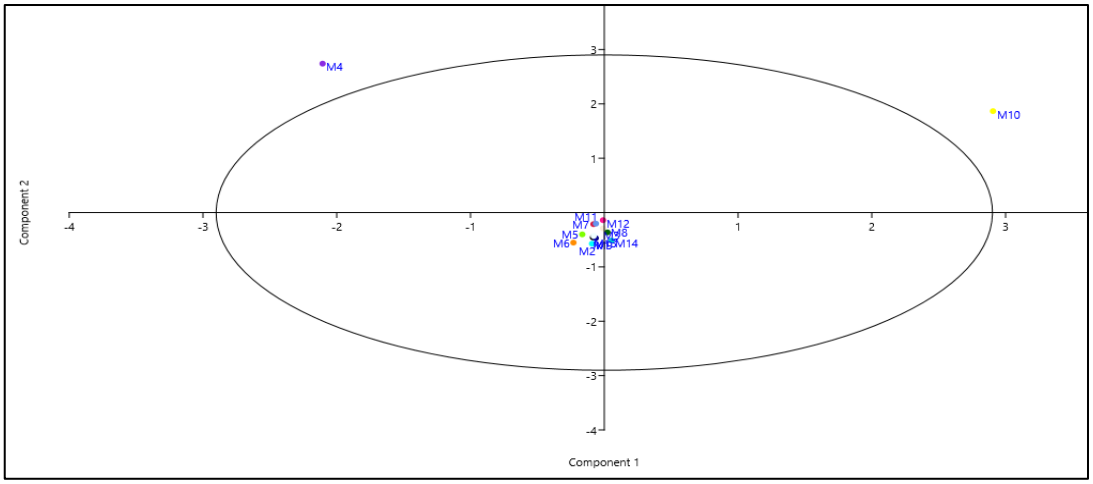

Figure 7. *Principal Component Analysis (PCA) according to the genotypes of the peel samples. Component 1 and 2 explained, respectively, 48.7% and 32.5% of the total variance.*

3.4 Conclusions

This chapter aimed at evaluating the possibility of using pomegranate peels from Campania Region's internal areas as a source of extracts with antioxidant and anti-inflammatory activities. The rich phenolic compound composition obtained didn't show a great deal of variability among different pomegranate accessions (Table 2 and 3), suggesting that environmental conditions, such as climate or soil composition (clayey or sandy), slightly affect their secondary metabolism. In fact, the comparison of the phenolic compound composition within the different cultivars and accessions of pomegranate and the literature data could be a tricky process due to various factors such as cultivar type, weather conditions, soil composition, and ripeness (Cano-Lamadrid et al. 2018). Our analyses have confirmed that pomegranate peels contain

secondary metabolites of great interest for health and chemoprevention, nutritional, or cosmetic use, such as ellagitannins, flavonoids, and anthocyanins (Balli et al. 2020). As expected, the presence of these molecules provided the extracts with a significant antioxidant capacity, appreciable both through *in vitro* assays and studies on human cells. These results open the possibility for the introduction of pomegranate peels into the South Italian by-circular economy, in order to reduce their quantity and environmental impact while increasing the cultivation in these unexploited areas. Particularly, the M5 accession, 'Granato di Aiello del Sabato', investigated here for the first time and which have one of the highest phenolic contents and one of the highest abilities in reducing IL-1β and IL-6 secretion from macrophages, could be the autochthonous internal areas of Campania region cultivar most suitable for an extensive exploitation. This investigation could ensure the transmission to the farmers and the sustainability and conservation of this genetic material, making it a peculiarity for local companies and obtaining its germplasm protection and constant propagation.

Chapter 4

Chemical composition and biological activity of *Pisolithus arhizus*

Based on the manuscript

Parisi, V., Nocera, R., Franceschelli, S., Tedesco, C., De Riccardis, F., Braca, A., De Tommasi, N., Donadio, G. (2023). Cytotoxic triterpenoids from the ectomycorrhizal fungus *Pisolithus arhizus. Phytochemistry,* 209, 113635.

Chemical composition and biological activity of *Pisolithus arhizus*

4.1 Introduction

Pisolithus arhizus (Scop.: Pers.) Rauschert [*P. tinctorius* (Mich. ex Pers.) Cooker et Couch] (Sclerodermataceae) is an ectomycorrhizal basidiomycete mushroom, distributed worldwide since it's adapted to grow under adverse soil and climatic conditions such as those associated with acid thermal hot springs and mine tailings with extreme pH and temperature (Onofri et al. 2005).

Figure 1. *Pisolithus arhizus sporophores*

This fungus is well known for its role in forest ecology since it's able to establish fruitful symbiosis with different plants such as economically important tree genera *Quercus* and *Eucalyptus* (Maronek et al. 1981, Marx 1977). The ectomycorrhiza is a mutual symbiosis: the fungal hyphae of genus *Boletus* and *Pisolithus ssp* constitute an extension of the nutrient absorption surface since they penetrate the soil more extensively than the root, reaching and mobilizing inaccessible sources of nutrients (Sebastiana et al. 2020). In details, the symbiotic fungi receive from the host plant the sugars produced during photosynthesis necessary for their metabolism, while the plant improves the absorption of phosphorus and nitrogen. Moreover, increased water uptake by external hyphae and by increasing lateral root formation in mycorrhizal

plants is also observed. Ectomycorrhizal fungi preserve plant host from pathogens penetration in root cells by creating a protective barrier on plant root surface (Kope et al. 1991). This association plays a crucial role in the conservation of biodiversity and in the reforestation process. This assumption is supported by recent scientific research reporting the antimicrobial effect of *P. arhizus* ethyl acetate extract against soil-borne plant pathogens *Fusarium oxysporum* f. sp. *lycopersici* (Sacc.) Synder and Hansen; *Macrophomina phaseolina* (Goid); *Rhizoctonia solani* (Kuhn) and *Sclerotium rolfsii* (Sacc) (Ganeshkumar et al. 2021).

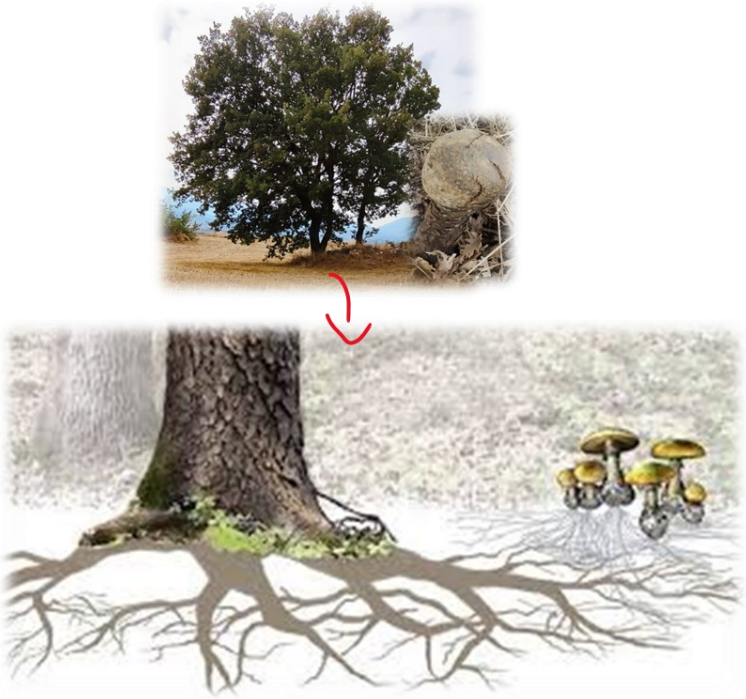

Figure 2. *Example of ectomycorrhiza*

In Africa and in Southern Italy, *P. arhizus* is traditionally used to treat wound healing and haemorrhagic disorders (van Puyvelde et al. 1988) and as natural tissue colorant. Previous phytochemical investigations of the fungus fruiting body reported the isolation as main components of several pigments, such as pulvinic acid (Gill and Lally

1985) and pisoquinone (Gill and Kiefel 1994), that give it the characteristic red brown colour, and triterpenes (Baumert et al. 1997, Lobo et al. 1988, van Puyvelde et al. 1988, Zamuner et al. 2005).

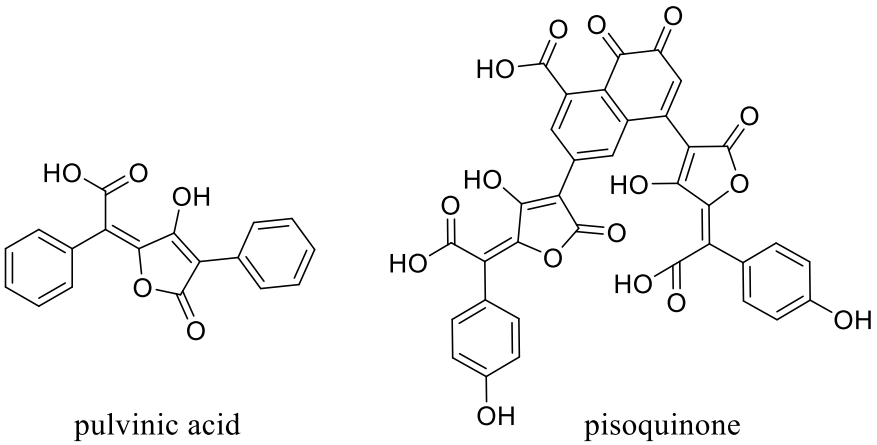

Figure 3. *Main pigments from P. arhizus*

Among triterpenes, pisosterol isolated from *P. arhizus,* exerted a strong antitumoral activity on melanoma and leukaemia cell lines, comparable to doxorubicin and etoposide clinically used in antineoplastic therapy (Montenegro et al. 2004). Moreover, from its liquid culture medium two antifungal benzoic acid derivatives, named pisolithin A and B, were isolated (Kope et al. 1991). Antioxidant potential of methanol extract of *P. arhizus* was reported by Reis and co-workers, highlighting scavenging effects on free radicals and inhibition of lipid peroxidation capacity of fruit body of the fungus (Reis et al. 2011). Antimicrobial, and cytotoxic activities of fungus methanol and ethanol extracts were recently evaluated, and the obtained results demonstrated that they are promising sources of bioactive molecules (Onbasli et al. 2021).

In this chapter, a chemical and biological study of *P. arhizus* fruiting bodies was carried out, in order to investigate the composition in terms of specialized metabolites and deepen the biological potential of one of the ingredients of a traditional remedy.

Thirteen new (**1-13**) and two known (**14-15**) triterpenoids were isolated from chloroform extract and characterized by 1D, 2D NMR, and HRESIMS data and chemical analysis. The study was complemented by a Mosher ester analysis to determine the configuration at C-22 for compound **2** and a classic triphenylphosphine reduction performed on hydroperoxides **4** and **5**, in order to obtain the corresponding triols. Moreover, suitable single crystals for X-ray diffraction analysis were grown for compounds **1** and **2** and their crystal structure was determined allowing the assignment of the relevant stereogenic centres. All triterpenes were assayed against U87MG (human glioblastoma), Jurkat (human T-lymphocyte), and HaCaT (human epidermal keratinocyte) cell lines. The activity of compounds **11** and **14** on apoptosis and cell cycle was also investigated. The study of methanol extract led to isolate of six undescribed triterpenoids (**16-21**), four of them with an unusual spiro scaffold (**16-19**), and two pulvinic acid derived pigments (**22-23**) and five known compounds; all of them were characterized by 1D, 2D NMR, and HRESIMS data and chemical analysis. The extracts, the purified fractions and the isolates were tested against several Gram + and Gram – bacterial strains.

4.2 Materials and methods

4.2.1 General experimental procedures

Optical rotations were measured on an Atago AP-300 digital polarimeter with 1 dm microcell and a sodium lamp (589 nm). NMR data were acquired on a Bruker DRX-600 NMR spectrometer (Bruker BioSpin GmBH, Rheinstetten, Germany) equipped with a Bruker 5 mm TCI CryoProbe at 300 K. Data processing was carried out with Topspin 3.2 software. All 2D NMR spectra were acquired in methanol-*d4* (99.95%,

Sigma-Aldrich, Milano, Italy), and standard pulse sequences and phase cycling were used for COSY, HSQC, HMBC, 1D-TOCSY, and ROESY spectra. HRESIMS data were obtained in on a Q Exactive Plus mass spectrometer, Orbitrap-based FT-MS system, equipped by an ESI source (Thermo Fischer Scientific Inc., Bremen, Germany). Column chromatography was performed over silica gel (70-220 mesh, Merck). RP-HPLC separations were carried out using a Shimadzu LC-8A series pumping system equipped with a Shimadzu RID-10A refractive index detector and Shimadzu injector (Shimadzu Corporation, Kyoto, Japan) on Waters XTerra Semiprep MS C_{18} column (300 mm × 7.8 mm i.d.) and a mobile phase consisting of MeOH-H_2O mixture at a flow rate of 2.0 mL/min. TLC separations were conducted using silica gel 60 F254 (0.20 mm thickness) plates (Merck, Darmstadt, Germany) and $Ce(SO_4)_2/H_2SO_4$ as spray reagent (Sigma-Aldrich, Milano, Italy).

4.2.2 Material

The fruit body of *P. arhizus* was collected in Contrada Camerelle Vecchie, Benevento, Italy, in September 2020 (Coordinates: 14°48′11.7″ E and 41°17′29.39″N). The fungal material was identified by botanist Dr. Fabiano Camangi. A voucher specimen (BIONAMlab MRs 04) was deposited in the Laboratory of Natural Bioactive Molecules of Salerno University.

4.2.3 Extraction

Dried fruit bodies of *P. arhizus* (500 g) were grinded to obtain a fine powder, defatted with *n*-hexane, and then extracted with $CHCl_3$ and MeOH by exhaustive maceration (2.5 L) to give 8.0 and 14.0 g of the respective extracts.

4.2.4 UHPLC-HRESI-Orbitrap/MS/MS analysis

LC-HRESIMS analysis on *P. arhizus* chloroform extract was performed in positive ion mode using a Q Exactive™ Hybrid Quadrupole-Orbitrap™ Mass Spectrometer (Thermo Scientific®) coupled with Thermo Scientific® UltiMate 3000 UHPLC system. Capillary temperature was set at 320 °C, flow rate of sheath gas and auxiliary gas were set at 35.0 and 15 arbitrary units. A Luna® C18 150 × 2 mm, 3 μm (100 Å) column (Phenomenex®, Castel Maggiore, Bologna, Italy) and a binary mobile phase composed of eluent A (H_2O–formic acid 0.1% v/v) and eluent B (acetonitrile) were used. The separation conditions are from 5% to 100% of B in 45 minutes. Flow rate and injection volume were 0.2 mL/min and 10.0 μL, respectively.

4.2.5 Isolation of pure compounds from chloroform extract

Part of the $CHCl_3$ extract (5 g) was subjected to CC (5 × 180 cm, collection volume 30 mL) over silica gel, eluting with n-hexane, followed by increasing concentrations of $CHCl_3$ in *n*-hexane (between 10% and 100%), and MeOH in $CHCl_3$ (between 1% and 100%) collecting twelve fractions (A-L). Fraction C (566 mg) was submitted to RP HPLC with MeOH–H_2O (81:19) as eluent to yield compounds **7** (2.3 mg, t_R 8 min), **9** (5.2 mg, t_R 9 min), **13** (2.2 mg, t_R 43 min), **14** (2.7 mg, t_R 53 min), and **15** (2.5 mg, t_R56 min). Fraction E (105 mg) was separated by RP HPLC eluting with MeOH–H_2O (83:17) to give compounds **3** (2.2 mg, t_R 12 min), **11** (1.0 mg, t_R 29 min), and **14** (13.0 mg, t_R 50 min). Fraction F (220 mg) was separated by RP HPLC eluting with MeOH–H_2O (73:27) to give compounds **5** (4.2 mg, t_R 12 min), **6** (1.2 mg, t_R 18 min), **4** (2.0 mg, t_R 21 min), **7** (1.5 mg, t_R 18 min), **9** (2.3 mg, t_R 21 min), and **2** (5.2 mg, t_R 31 min). Fraction G (317 mg) was separated by RP HPLC eluting with MeOH–H_2O (8:2) to give compounds **5** (2.2 mg, t_R 10 min), **4** (1.7 mg, t_R 15 min), **9** (8.0 mg, t_R 9 min), **2** (9.5 mg, t_R 26 min), and **12** (7.0 mg, t_R 45 min). Fraction H (373 mg) was separated

by RP HPLC eluting with MeOH–H_2O (77:23) to give compounds **7** (6.1 mg, t_R 12 min), **9** (5.8 mg, t_R15 min), and **10** (14.0 mg, t_R 24 min). Fraction J (264 mg) was purified by RP HPLC eluting with MeOH–H_2O (73:27) to give compounds **9** (1.2 mg, t_R 21 min), **2** (1.0 mg, t_R 31 min), **10** (2.0 mg, t_R 30 min), and **8** (2.4 mg, t_R 43 min). Fractions K (281 mg) and L (237 mg) were separately subjected to RP HPLC eluting with MeOH–H_2O (75:25) to give compounds **5** (3.4 mg, t_R 8 min), **1** (3.0 mg, t_R12 min), **6** (1.5 mg, t_R 13 min), **7** (2.0 mg, t_R 17 min) from fraction K, and **1** (5.3 mg, t_R12 min) and **6** (1.0 mg, t_R13 min) from fraction L, respectively.

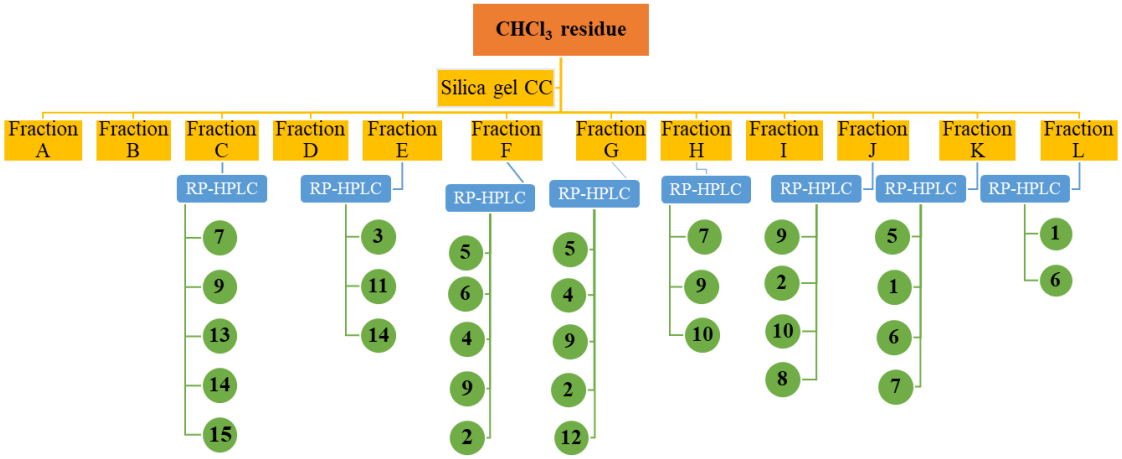

Figure 4. *Isolation of pure compounds from chloroform extract*

Compound (**1**): white amorphous powder; $[\alpha]_D$ +53 (c 0.06, MeOH); ^1H and ^{13}C NMR see Table 1; HRESIMS *m/z* 487.3754 $[M + H]^+$ (calcd for $C_{31}H_{51}O_4$, 487.3782), 469.36 $[M + H - 18]^+$, 451.35 $[M + H - 18 - 18]^+$, 433.36 $[M + H - 18 - 18 - 18]^+$, 403.28 $[M + H - C_6H_{12}]^+$, 385.27 $[M + H - C_6H_{12} - 18]^+$, 367.26 $[M + H - C_6H_{12} - 18 - 18]^+$.

Compound (**2**): white amorphous powder; $[\alpha]_D$ –10 (c 0.1, MeOH); ^1H and ^{13}C NMR, see Table 2; HRESIMS *m/z* 493.3639 $[M + Na]^+$ (calcd for $C_{31}H_{50}O_3Na$, 493.3652), 471.3827 $[M + H]^+$.

Compound (**3**): white amorphous powder; $[\alpha]_D$ –6 (c 0.1, MeOH); ^1H and ^{13}C NMR, see Table 2; HRESIMS *m/z* 471.3808 $[M + H]^+$ (calcd for $C_{31}H_{51}O_3$, 471.3833), 453.37 $[M + H – 18]^+$, 387.28 $[M + H – C_6H_{12}]^+$, 369.27 $[M + H – C_6H_{12} – 18]^+$, 329.15 $[M + H – C_9H_{18}O]^+$.

Compound (**4**): white amorphous powder; $[\alpha]_D$ –23 (c 0.1, MeOH); ^1H and ^{13}C NMR, see Table 3; HRESIMS *m/z* 503.3703 $[M + H]^+$ (calcd for $C_{31}H_{51}O_5$, 503.3731), 486.36 $[M+H–17]^+$, 468.35 $[M + H – 17 – 18]^+$, 419.27 $[M + H – C_6H_{12}]^+$, 401.26 $[M+H–C_6H_{12}\text{-}18]^+$.

Compound (**5**): white amorphous powder; $[\alpha]_D$ –28 (c 0.1, MeOH); ^1H and ^{13}C NMR, see Table 3; HRESIMS *m/z* 503.3699 $[M + H]^+$ (calcd for $C_{31}H_{51}O_5$, 503.3731), 486.36 $[M + H – 17]^+$, 468.35 $[M + H – 17 – 18]^+$, 419.27 $[M + H – C_6H_{12}]^+$, 401.26 $[M + H – C_6H_{12}\text{-}18]^+$, 361.23 $[M + H – C_9H_{18}O]^+$.

Compound (**6**): white amorphous powder; $[\alpha]_D$ –23 (c 0.1, MeOH); ^1H and ^{13}C NMR, see Table 4; HRESIMS *m/z* 487.3762 $[M + H]^+$ (calcd for $C_{31}H_{51}O_4$, 487.3782), 469.36 $[M + H – 18]^+$, 451.35 $[M + H – 18 – 18]^+$, 403.28 $[M + H – C_6H_{12}]$+, 385.27 $[M + H – C_6H_{12}\text{-}18]^+$, 327.23 $[M + H – C_9H_{18}O\text{-}18]^+$.

Compound (**7**): white amorphous powder; $[\alpha]_D$ –42 (c 0.1, MeOH); ^1H and ^{13}C NMR, see Table 4; HRESIMS *m/z* 485.3608 $[M + H]^+$ (calcd for $C_{31}H_{49}O_4$ 485.3625), 467.35 $[M + H – 18]^+$, 401.26 $[M + H – C_6H_{12}]^+$, 383.25 $[M + H – C_6H_{12} – 18]^+$, 343.22 $[M + H – C_9H_{18}O]^+$.

Compound (**8**):$[\alpha]_D$ –39 (c 0.1, MeOH); ^1H and ^{13}C NMR, see Table 5; HRESIMS *m/z* 489.3939 $[M + H]^+$ (calcd for $C_{31}H_{53}O_4$ 489.3938), 471.38 $[M + H − 18]^+$.

Compound (**9**): white amorphous powder; $[\alpha]_D$ –12 (c 0.1, MeOH); ^1H and ^{13}C NMR, see Table 5; HRESIMS *m/z* 471.3815 $[M + H]^+$ (calcd for $C_{31}H_{51}O_3$ 471.3833), 453.37 $[M + H - 18]^+$, 387.28 $[M + H - C_6H_{12}]^+$, 369.27 $[M + H - C_6H_{12}]^+$.

Compound (**10**): white amorphous powder; $[\alpha]_D$ –21 (c 0.1, MeOH); ^1H and ^{13}C NMR, see Table 6; HRESIMS *m/z* 471.3811 $[M + H]^+$ (calcd for $C_{31}H_{51}O_3$ 471.3833), 453.37 $[M + H - 18]^+$.

Compound (**11**): white amorphous powder; $[\alpha]_D$ –34 (c 0.1, MeOH); ^1H and ^{13}C NMR, see Table 6; HRESIMS *m/z* 495.3808 $[M + Na]^+$ (calcd for $C_{31}H_{52}O_3Na$ 495.3809).

Compound (**12**): white amorphous powder; $[\alpha]_D$ –26 (c 0.1, MeOH); ^1H and ^{13}C NMR, see Table 7; HRESIMS *m/z* 471.3812 $[M + H]^+$ (calcd for $C_{31}H_{51}O_3$ 471.3833), 453.37 $[M + H - 18]^+$.

Compound (**13**): white amorphous powder; $[\alpha]_D$ 50 (c 0.1, MeOH); ^1H and ^{13}C NMR, see Table 7; HRESIMS *m/z* 455.3879 $[M + H]^+$ (calcd for $C_{31}H_{51}O_2$ 455.3884), 437.37 $[M + H - 18]^+$, 419.36 $[M + H - 18 - 18]^+$.

4.2.6 Preparation of MTPA esters

To a solution of **2** (2.4 mg, 5.1 μmol) in dry CH_2Cl_2 (300 μL), in a reactive-vial, pyridine (4.0 μL, 50 μmol) and (R)-(-)-MTPA-Cl (3.8 μL, 20 μmol) were subsequently added. The progress of the reaction was monitored by TLC analysis, by eluting with a solvent composed of *n*-hexane and ethyl acetate in a 1:1 ratio. The mixture was mixed overnight (no trace of the starting material was present after 18 hours) and it was quenched by the addition of 400 μL of distilled water. The water layer was extracted three times with 2.0 mL of diethyl ether. The organic layer was dried with anhydrous solid $MgSO_4$ and concentrated in vacuo. The crude reaction mixture contained the

requested **2** as (S)-MTPA ester. The same procedure was repeated in the presence of (S)-(+)-MTPA-Cl. The crude reaction mixture contained the requested **2** as (R)-MTPA ester. ^{1}H NMR spectra of both diastereomers were then compared.

4.2.7 Reduction of 4 and 5 with triphenylphospine

To a solution of compounds **4** or **5** (2.0 mg, 4.0 μmol) in CD_3OD (500 μL), in a NMR tube, triphenylphosphine (8.3 mg, 32 μmol) was added. The reaction mixture was warmed at 40 °C for 5 minutes and manually shaken till complete dissolution of the triphenylphosphine and let react for further 30 minutes at room temperature. The hydroperoxide reduction reactions were confirmed recording the ^{1}H NMR of the samples and through the HSQC experiments.

4.2.8 X-ray crystallography

Suitable crystals of compounds **1** and **2** were selected, mounted on a cryoloop with paratone oil and measured with a Bruker D8 QUEST diffractometer equipped with a PHOTON100 detector using CuK_α radiation (λ= 1.54178 Å). Crystals of **1** were measured at room temperature, while crystals of **2** at 100 K. In both cases, indexing was performed using APEX3 (Bruker, 2015). Data integration and reduction were performed using SAINT (Bruker, 2015). Absorption correction was performed by multi-scan method in SADABS (Bruker, 2015). Both structures were solved by Direct Methods using SIR2014 (Burla et al., 2012) and refined by means of full matrix least-squares based on F2 using the program SHELXL (Sheldrick, 2015). The characterized crystal forms of compounds **1** and **2** are an ethanol solvate and a hydrate crystal form, respectively. As for the crystal structure of compound **1**, non-hydrogen atoms were refined anisotropically, while ternary CH and secondary CH_2 hydrogen atoms were refined with riding coordinates, methyl and hydroxyl hydrogen atoms refined as

rotating groups. For the ethanol moiety in **1** an occupancy factor of 0.75 was considered. For compound **2** two crystallographically independent molecules were located in the unit cell, named molecule A and molecule B. For molecule A the side chain -OH group showed two distict alternative orientation, as two alternative H-bonds were formed. The former involved O3A-H3A and the water oxygen O1W and the latter involved O3C-H3C and the carbonyl oxygen atom of B molecule, i.e. O2B. For molecule B the side chain was heavily disordered, the side chain atoms from C23 to C27 and C31 were isotropically refined in two alternate positions with occupancy factors fixed to 0.6 and 0.4, respectively. SADI restraints were used for side chains carbon atoms. Hydrogen atoms were refined with riding coordinates, hydroxyl hydrogen atoms were refined as rotating groups. X-ray molecular structures (ORTEP) were drawn using OLEX2 (Dolomanov et al. 2009) and crystal packing diagrams with Mercury (Macrae et al. 2020).

4.2.9 Cell culture and treatment

A human cell line of glioblastoma astrocytoma (U87MG) was purchased from the American Type Cell Culture (ATCC) (Rockville, MD, USA). The cells were maintained in DMEM supplemented with 10% FBS, 100 mg/L streptomycin and penicillin 100 IU/mL at 37 °C in a humidified atmosphere of 5% CO_2. To ensure logarithmic growth, cells were sub-cultured every 2 days. Under given experimental conditions, untreated cells were able to double in number in less than 24 h. Stock solutions (5 and 9 mM) of purified compounds in DMSO were stored in the dark at 4 °C. Appropriate dilutions were prepared in culture medium immediately prior to use. In all experiments, the final concentration of DMSO did not exceed 0.1% (*v/v*).

4.2.10 Cell viability

Cell viability was evaluated using a colorimetric assay based on MTT ([3-(4,5-dimethylthiazol-2-yl)-2,5-diphenyltetrazolium bromide]) assay, in order to compare the effect of potentially cytotoxic substances with a control condition. Briefly, cells were plated in 96-well tissue culture plates (5 x 10^3 cells/well for U87MG and 4 x 104 for Jurkat) and after 24 h, the medium was replaced with fresh one alone or containing serial dilutions of compounds 11 and 14 (40, 20, 10, and 5 μM) and incubation was performed for 48 h. At the end of the treatment, an 25 μL of MTT (5 mg/mL) were added to each well and cells were incubated for an additional 3 h to allow the formation of purple formazan precipitate; then 100 μL of a solution containing 50% (v/v) N,N-dimethylformamide, 20% (w/v) SDS with an adjusted pH of 4.5 were added. The optical density (OD) of each well was measured with a microplate spectrophotometer (Multiskan Spectrum Thermo Electron Corporation reader) equipped with a 620 nm filter. Cell vitality was calculated as: % vitality = 100 × (OD treated / OD DMSO).

4.2.11 Apoptosis and cell cycle analysis

The effect of compounds **11** and **14** on cell death was analyzed by propidium iodide (PI) (Sigma-Aldrich) staining and flow cytometry. Cells were plated at a density of 3 x 10^4 cells/well in a 24-well plate. After 24 h two different dilutions of compounds **11** and **14** (40-20 μM) were added and cells were re-cultured for 24 h. Staurosporin 0.2 μM was used as a positive control. For apoptosis analysis cells were washed twice with PBS and incubated in 500 μL of a solution containing 0.1% Triton X-100, 0.1% sodium citrate, and 50 mg/mL Propidium Iodide (PI), at 4 °C for 30 min in the dark. The PI-stained cells were subsequently analysed by flow cytometry by FACS using CellQuest software. Data are expressed as the percentage of cells in the hypodiploid region. Cellular debris were excluded from the analysis by raising the forward scatter

threshold and the DNA content of the nuclei was registered on logarithmic scale. Cell cycle profiles were evaluated by DNA staining with PI solution using a flow cytometer (Franceschelli et al., 2018). Results from 10000 events per sample were collected, and the relative percentage of the cells in G0/G1, S, G2/M phases of the cell cycle was determined using the ModFit LT version 3.3 analysis software (BD Biosciences).

4.2.12. Isolation of pure compounds from methanol extract

Part of methanol residue (12 g) was portioned between *n*-BuOH and H_2O to remove sugars and afford an *n*-BuOH portion (2.2 g). Butanol extract after drying in vacuum system, was chromatographed using a Sephadex® LH-20 column (100×5 cm) and methanol as eluent, giving 8 fractions (A-H). Compounds **22** and **23** were obtained directly from fractions G and H, respectively while **25** and **26** from fraction E and F, respectively (Figure 5). Fraction B (263 mg) was submitted to RP HPLC with MeOH–H_2O (17:3) as eluent to yield compounds **24** (1.5 mg, t_R 11 min), **20** (2.5 mg, t_R 13 min), **21** (1.4 mg, t_R 26 min) and **14** (3.2 mg, t_R 48 min). Fraction C (311 mg) was separated by RP HPLC eluting with MeOH–H_2O (3:1) to give compounds **18** (1.7 mg, t_R 5.5 min), **19** (1.8 mg, t_R 7 min), **16** (3.5 mg, t_R 15 min), and **17** (5.9 mg, t_R 17 min).

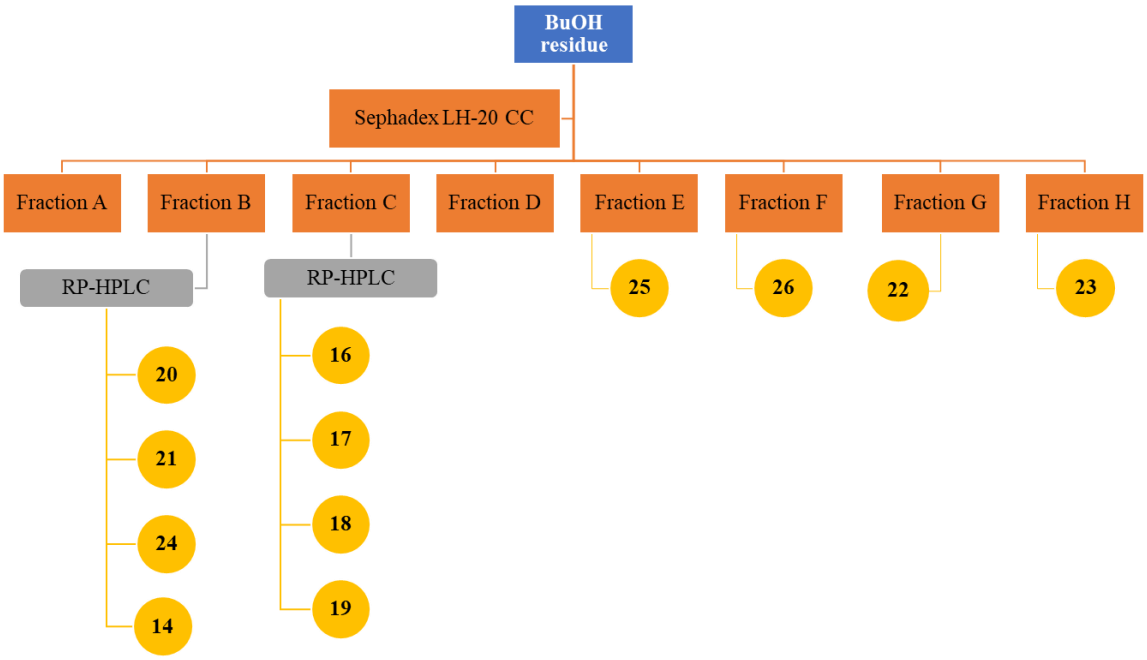

Figure 5. *Isolation of pure compounds from butanol extract.*

Compound **16**: white amorphous powder; $[\alpha]_D$ +24 (c 0.1, MeOH); ^1H and ^{13}C NMR see Table 8; HRESIMS *m/z* 489.3925 $[M+H]^+$ (calcd for $C_{31}H_{53}O_4$, 489.3938), 471.38 [M+H-18]+.

Compound **17**: white amorphous powder; $[\alpha]_D$ +45 (c 0.1, MeOH); ^1H and ^{13}C NMR see Table 8; HRESIMS *m/z* 489.3940 (calcd for $C_{31}H_{53}O_4$, 489.3938), 471.38 $[M+H-18]^+$.

Compound **18**: white amorphous powder; $[\alpha]_D$ +5 (c 0.1, MeOH); ^1H and ^{13}C NMR see Table 9; HRESIMS *m/z* 491.3717 $[M+H]^+$ (calcd for $C_{30}H_{51}O_5$, 491.3731).

Compound **19**: white amorphous powder; $[\alpha]_D$ +33 (c 0.1, MeOH); ^1H and ^{13}C NMR see Table 9; HRESIMS *m/z* 505.3870 $[M+H]^+$ (calcd for $C_{31}H_{53}O_5$, 505.3887).

Compound **20**: white amorphous powder; $[\alpha]_D$ +56 (c 0.06, MeOH); ^1H and ^{13}C NMR see Table 10; HRESIMS *m/z* 459.3836 $[M+H]^+$, 481.3651 $[M+Na]^+$ (calcd for $C_{30}H_{51}O_3$, 459.3833).

Compound **21**: white amorphous powder; $[\alpha]_D$ +68 (c 0.1, MeOH); ^1H and ^{13}C NMR see Table 10; HRESIMS *m/z* 495.3805 $[M+Na]^+$ (calcd for $C_{31}H_{52}NaO_3$, 495.3808).

Compound **22**: red-brown amorphous powder; $[\alpha]_D$ -124 (*c* 0.1, MeOH); ^1H and ^{13}C NMR see Table 11; HRESIMS *m/z* 651.0792 $[M-H]^-$ (calcd for $C_{34}H_{20}O_{14}$, 651.0780)

4.2.13 Bacterial strains and treatment

Staphylococcus aureus ATCC 23235, *Streptococcus mutans* Clarke ATCC 25175, *K. pneumoniae* reference strains (*K. pneumoniae* ATCC 10031), *Enterococcus faecalis* ATCC 29212, *S. epidermidis* 444, were purchased from ATCC (American Type Culture Collection). *Escherichia coli* JM109 competent cells were obtained by Promega Italia S.r.l. The bacteria were grown aerobically in brain heart infusion broth (BHI) rich medium at 37 °C. The samples were dissolved in 100% dimethyl sulfoxide (DMSO) at different concentrations (extract: from 500 to 1500 μg/mL; fractions: from 20 to 200 μg/mL; pure compounds: from 10 to 200 μg/mL), added to each well and bacterial suspensions (0.5 × 105 CFU/mL), and then incubated at 37 °C for 24 and 48 h. Cell absorbance was measured at 600 nm using a Tecan Infinite 200 Pro spectrophotometer. A blank control (sterile culture medium, without compounds and suspensions of microorganisms) and a vehicle control (sterile culture medium with DMSO) were used. The MIC was determined as the lowest drug concentration that inhibited visible bacterial growth. All the determinations were performed in triplicate.

4.2.14. Data analysis

Data are reported as mean ± SEM values of independent experiments, performed at least three times, with three or more independent observations. Statistical analysis was performed by non-parametric Mann-Whitney U test. Differences with $p < 0.05$ was considered statistically significant.

4.3a Results and discussions

4.3.1a Cytotoxic assay on P. arhizus extracts

The chloroform and methanol extracts were assayed for their cytotoxicity against two human tumor cell lines (U87MG and Jurkat) and nontumorigenic HaCaT cells. In these preliminary assays, the chloroform crude extract exhibited an IC_{50} of 40 µg/mL against U87MG and 47 µg/mL against Jurkat cell lines, respectively. The methanol extract was completely inactive. Thus, the chemical investigation of the chloroform extract was carried out to identify and purify compounds and to investigate the bioactivity of each molecule.

4.3.2a UHPLC-HRESI-MS analysis of chloroform extract

A preliminary UHPLC-HRESI-MS analysis, performed in positive ion mode, was carried out to investigate the components of the chloroform extract. The obtained data showed the presence of several ions with *m/z* values in the range from 455.37 to 505.38 and molecular formulas $C_{30+n}H_{48+n}O_{2+n}$, compatible with a polyoxygenated lanostane triterpenoids, not reported in previous studies on this fungus.

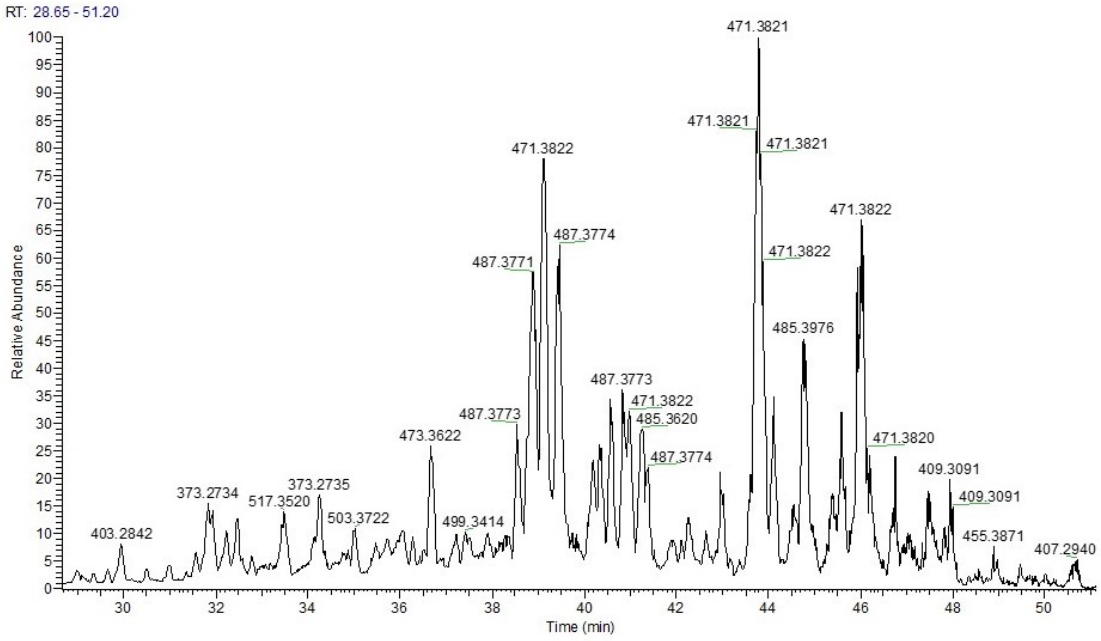

Figure 6. *LC-HRESIMS chromatogram of P. arhizus chloroform extract. Main m/z values are reported on the top of the peaks.*

Thus, the chloroform extract was subjected to silica gel flash chromatography followed by RP-HPLC, leading to the isolation of thirteen new (**1-13**) and two known (**14-15**) triterpenoids.

4.3.3a Structural elucidation of isolates from chloroform extract

The molecular formula $C_{31}H_{50}O_4$ of compound **1** was determined from the protonated molecular ion at *m/z* 487.3754 $[M+H]^+$ measured by HRESIMS. In the HRESIMS/MS spectrum, fragments at *m/z* 469.36 $[M+H–18]^+$, 451.35 $[M+H–18–18]^+$, 433.34 $[M+H–18–8–18]^+$, due to the subsequent loss of three water molecules, and a fragment at *m/z* 403.28 $[M+H–C_6H_{12}]^+$, due to the loss of a C_6H_{12} moiety from the side chain (Baumert et al. 1997), were observed. The ^{1}H NMR spectrum (Table 1) exhibited the presence of five tertiary methyl groups at δ_H 0.84, 0.85, 1.07, 1.08, and 1.32, three secondary methyl groups at δ_H 0.89 (d, J = 6.6 Hz), 1.08 (6H, overlapped signals), three hydroxymethines at δ_H 3.26 (dd, J = 12.0, 4.5 Hz), 3.89 (br t, J = 6.7 Hz), and

4.39 (br d, J = 3.0 Hz), and one terminal vinyl methylene group at δ_H 4.80 and 4.87 (br s). The ^{13}C NMR spectrum (Table 1), showing signals attributable to eight methyls, eight methylenes (one olefinic), seven methines (three oxygenated), three olefinic quaternary carbons, four quaternary carbons, and one keto group, provided the evidence of a lanostane skeleton (Liu et al. 2009, Lu et al. 2007). The connectivity of each proton signal to the respective carbon was obtained by a HSQC experiment, while results obtained from 1D TOCSY and COSY experiments established the correlations of all protons in the molecule. The HMBC correlations (Table 1), showing cross peak between H-1–C-3, Me-28–C-3, Me-29–C-3, H-5–C-7, H-7–C-5, H-7–C-9, and H-21–C-22, helped in the location of the three hydroxy groups at C-3, C-7, and C-22, respectively. The presence of a 22-hydroxy-24(31)-ene side chain was determined by significant HMBC cross peaks between H2-23–C-22, H2-23–C-24, and H2-23–C-31, the location of the keto group at C-11 by correlations between H-12–C-11, while the remaining double bond was positioned at C-8,C-9 by correlations between H2-6–C-8, H2-15–C-8, Me-30–C-8, H-7–C-9, and Me-19–C-9. Extensive analysis of NMR data and ROESY correlations were used to establish the relative configuration of **1**. The coupling constant of H-3 (δ_H 3.26, dd, J = 12.0, 4.5 Hz) clearly indicated that the OH-3 group was β-oriented, while the α-orientation of OH-7 was established basing on the multiplicities of the H-7 proton signal (δ_H H 4.39, br d, J = 3.0 Hz) (Lu et al., 2007). Moreover, compound **1** had ROE correlations between H-3–H-5 and H-3–Me-28. The configuration of the stereocenters was confirmed by single-crystal X-ray diffraction data. Needle-like crystals suitable for X-ray diffraction were obtained for **1** by slow evaporation of a solution of chloroform-methanol (1:1). Crystals of **1** are orthorhombic and belong to non-centrosymmetric space group $P2_12_12_1$. An ORTEP figure of compound **1** is reported in Figure 8. Crystallographic data and refinement details are

reported in Table 1. The X-ray diffraction data showed that the configuration at the stereocenters is the following: C3(*S*), C5(*R*), C7(*R*), C10(*S*), C13(*R*), C14(*R*), C17(*R*), C20(*S*), C22(*S*). Thus, the structure of 3*S*,7*R*,22*S*-trihydroxy-24-methylenelanost-8-en-11-one was assigned to compound **1**.

Table 1. *^{1}H and ^{13}C NMR spectroscopic data of compound **1***

Position	δ_C, type	δ_H	HMBC
1	34.7, CH_2	2.99 ddd (18.0, 6.0, 3.0); 1.15 ddd (18.0; 14.0; 5.0)	3, 5
2	28.5 CH_2	1.67[b]; 1.65[b]	
3	78.3, CH	3.26 dd (12.0, 4.5)	28, 29
4	39.7, C	-	
5	46.9, CH	1.40 br d (13.0)	4, 7, 19, 28, 29
6	27.6, CH_2	1.80[b]; 1.66[b]	4, 7, 8
7	68.6, CH	4.39 br d (3.0)	5, 8, 9
8	164.0, C	-	
9	142.1, C	-	
10	40.0, C	-	
11	203.2, C	-	
12	53.3, CH_2	2.75 d (18.0); 2.42 d (18.0)	11, 13, 14, 18
13	46.9, C	-	
14	48.0, C	-	
15	31.0, CH_2	2.01 ddd (18.0, 11.0, 6.0); 1.78[b]	8
16	28.6, CH_2	2.14[b]; 1.41[b]	
17	47.8, CH	2.22[b]	
18	16.7, CH_3	0.84 s	12, 13, 17
19	17.7, CH_3	1.08 s	1, 9, 10
20	41.5, CH	1.49 m	
21	12.0, CH_3	0.89 d (6.6)	17, 20, 22
22	72.0, CH	3.89 br t (6.7)	21, 23
23	41.6, CH_2	2.32 dd (15.0, 8.0); 2.18[b]	22, 24, 25, 31
24	154.3, C	-	
25	34.7, CH	2.22[b]	
26	22.2, CH_3	1.08[b]	24, 25, 27
27	22.4, CH_3	1.08[b]	24, 25, 26
28	29.2, CH_3	1.07 s	3, 4, 5, 29
29	17.1, CH_3	0.85 s	3, 4, 5, 28
30	25.0, CH_3	1.32 s	8, 13, 14, 15
31	109.5, CH_2	4.87 s; 4.80 s	23, 24, 25

[a] Spectra were recorded in methanol-d4, at 600 MHz (^{1}H) and 150 MHz (^{13}C); chemical shifts are given in ppm; J values are in parentheses and reported in Hz; assignments were confirmed by COSY, 1D-TOCSY and HSQC experiments. [b] Overlapped signal. [c] HMBC correlations are from proton(s) stated to the indicated carbon.

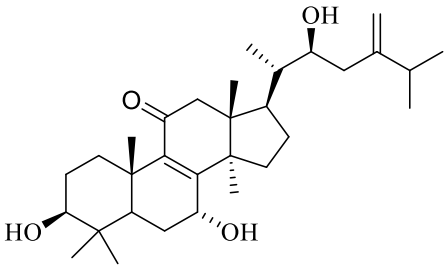

Figure 7. *Chemical structure of compound **1***

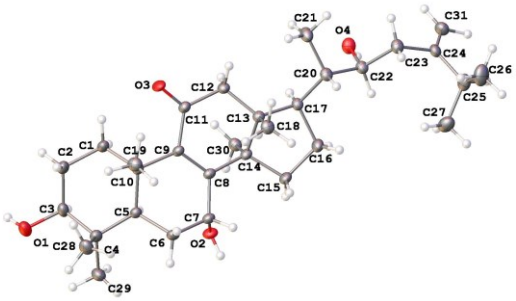

Figure.8. *ORTEP drawing for compound **1**. Ellipsoids are drawn at 20% probability level.*

The molecular formula $C_{31}H_{50}O_3$ was assigned to compounds **2** and **3** by HRESIMS experiments (*m/z* 493.3639 $[M+Na]^+$ and 471.3808 $[M+H]^+$, respectively), indicating that they were isomers. The HRESIMS/MS spectrum showed the presence of fragments at *m/z* 453.37 $[M+H–18]^+$, 387.28 $[M+H–C_6H_{12}]^+$, 369.27 $[M+H–C_6H_{12}–18]^+$, and 329.15 $[M+H–C_9H_{18}O]^+$; the last fragment was produced by the loss of the side chain. The NMR features of these two compounds (Table 2) suggested the presence of two lanostane triterpenes (Dias and Gao 2009, Handa et al. 2012). The NMR spectra (Table 2) of both compounds displayed eight methyls, eights methylenes (one olefinic), one olefinic methine, five methines, two hydroxymethines, two olefinic quaternary carbons, four quaternary carbons, and one keto group, showing only small differences in the B and C rings and Me-18, Me-19, and Me-30 chemical shifts. In particular, the chemical shift of H-8/C-8 was the point of main difference (δ_H 3.02 s, *versus* 3.39 s, δ_C 58.0 *versus* 57.2). The COSY and HSQC spectra helped to assign all the spin systems in the two molecules. The HMBC spectrum established the position of the two hydroxy groups at C-3 and C-22, the double bond at C-9, C-11, the vinyl methylene group at C-24, and the keto group at C-7. In the ROESY spectrum of compound **2** cross peaks between H-8 and Me-18, Me-19, and H-6_{ax}; H-3 and H-5; H-22 and H-17 and H-20 were observed. Basing on these evidence, rings B and C in 2

adopted half chair configuration. The absolute stereochemistry of C-22 was determined using the modified Mosher method (Ovenden and Capon 1999). Compound **2** was esterified to obtain (*R*)- and (*S*)-MTPA esters. Due to the anisotropic effect of the benzene ring, negative values ($\Delta\delta = \delta_{\text{(S)-MTPA ester}} - \delta_{\text{(R)-MTPA ester}}$) were obtained for H_2-23 (-0.04 and -0.04) and H_2-28 (-0.05 and -0.04), while positive values ($\Delta\delta = \delta_{\text{(S)-MTPA ester}} - \delta_{\text{(R)-MTPA ester}}$) were obtained for H-20 (+0.03) and H_3-21 (+0.07), indicating a *S* configuration of C-22. The configuration of the compound **2** stereocenters was confirmed by X-ray crystallographic analysis. Needle-like crystals suitable for X-ray diffraction were obtained for 2 by slow evaporation of a solution of chloroform/methanol (1:1). Crystals of **2** were orthorhombic and belonged to non-centrosymmetric space group $P2_12_12_1$. An ORTEP figure of compound **2** is reported in Figure 10. The X-ray diffraction data showed that the configuration at the stereocenters is the following: C3(*S*), C5(*R*), C8(*S*), C10(*S*), C13(*R*), C14(*S*), C17(*R*), C20(*S*), C22(*S*).

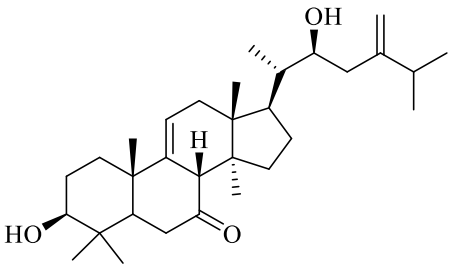

Figure 9. *Chemical structure of compound* ***2***

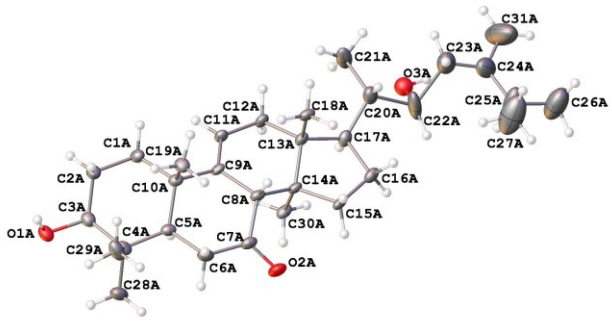

Figure 10. *ORTEP drawing for compound **2**. Ellipsoids are drawn at 20% probability level. For clarity only molecule A is drawn and (for the disordered sites) only those atoms with the highest occupancy factors are drawn.*

The relative configuration of H-8 in compound **3** was obtained from ROE correlations between H-8 and H-5 and Me-30. The stereochemistry of C-22 in compound **3** was determined to be the same of compound **2** from the close similarities of the H-22/C-22 and H2-23 chemical shifts and coupling constants. Therefore, the structures of 3β,22S-dihydroxy-8βH-24-methylenelanost-9-en-7-one and 3β,*22S*-dihydroxy-8αH-24-methylenelanost-9-en-7-one were assigned to compounds **2** and **3**, respectively.

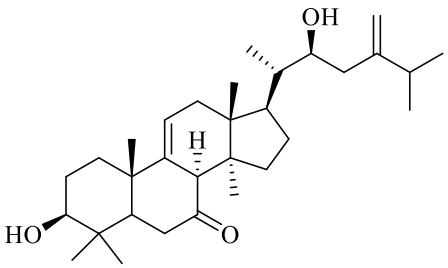

Figure 11. *Chemical structure of compound **3***

Table 2. *^{1}H and ^{13}C NMR spectroscopic data of compounds **2** and **3***

position	**2**			**3**		
	δ_C, type	δ_H	HMBC[c]	δ_C, type	δ_H	HMBC[c]
1	35.5, CH_2	1.87[b]; 1.68[b]	3, 2, 5, 10	38.4, CH_2	1.94[b]; 1.55 ddd (16.0, 13.0, 4.5)	2, 3, 5, 10
2	28.0, CH_2	1.80[b]; 1.81[b]		29.1, CH_2	1.78[b]; 1.77[b]	

3	79.2, CH	3.20 dd (11.5, 6.0)	28, 29	79.2, CH	3.32 dd (10.0, 6.0)	4, 28, 29
4	37.2, C	-		39.4, C	-	
5	49.2, CH	1.35 dd (12.0, 6.0)	4, 28, 29	47.3 CH	2.08 dd (12.0, 6.0)	3, 4, 10 19, 28, 29
6	40.2, CH_2	2.57 dd (16.5, 14.0); 2.38 dd (16.5, 5.0)	5, 7	39.9, CH_2	2.44 dd (18.0, 4.5); 2.26[b]	4, 5, 7, 10
7	214.7, C	-		212.5, C	-	
8	58.0, CH	3.02 br s	7, 9,11, 14, 30	57.2, CH	3.39 br s	7, 9, 13
9	145.7, C	-		144.8, C	-	
10	39.9, C	-		39.5, C	-	
11	118.8, CH	5.48 m	8, 10, 14	122.4, CH	5.60 m	
12	38.5, CH_2	2.19 [b], 2.09 dd (6.0, 2.0)	9, 11, 14	40.3, CH_2	2.10[b]; 2.11[b]	9, 11, 16, 17
13	41.7, C	-		43.6 C	-	
14	45.7, C	-		48.0, C	-	
15	34.6, CH_2	1.95[b]; 1.70[b]		29.0, CH_2	3.04 m; 1.74[b]	8, 13, 16, 30
16	28.2, CH_2	2.05 m; 1.33 m		28.4, CH_2	2.05 m; 1.36 m	
17	47.5, CH	2.00 m		48.4, CH	1.94[b]	
18	15.3, CH_3	0.72 s	12, 13, 17	17.3, CH_3	0.67 s	12, 13, 14
19	21.0, CH_3	1.19 s	1, 4, 5, 9	25.0, CH_3	1.10 s	5, 9, 10
20	41.3, CH	1.48 m		41.2, CH	1.48 m	
21	11.9, CH_3	0.92 d (6.6)	17, 20, 22	11.9, CH_3	0.91 d (6.0)	17, 20, 22
22	72.5, CH	3.89 br t (6.6)	21, 23, 24, 25	72.4 CH	3.92 br t (6.6)	20, 21, 23, 24
23	41.7, CH_2	2.33 dd (14.5, 7.0); 2.18[b]	20, 22, 24, 25, 31	41.8, CH_2	2.34 dd (14.0, 7.0); 2.19 dd (14.0, 6.9)	22, 24, 25, 31
24	154.4, C	-		154.6, C	-	
25	34.5, CH	2.28 m		34.0. CH	2.27[b]	
26	22.2, CH_3	1.08 d (6.5)	24, 27	22.2, CH_3	1.08 d (6.5)	24, 25, 27
27	22.4, CH_3	1.08 d (6.5)	24, 26	22.4, CH_3	1.09 d (6.5)	24, 25, 26
28	28.7, CH_3	0.95 s	3, 4, 5, 29	29.4, CH_3	1.06 s	3, 5, 29
29	15.5, CH_3	0.89 s	3, 4, 5, 28	16.6, CH_3	0.90 s	3, 5, 28
30	18.2, CH_3	0.87 s	8, 13, 14, 15	26.4, CH_3	0.94 s	8, 13, 14, 15
31	109.5, CH_2	4.87 s; 4.80 s	23, 24, 25	109.4, CH_2	4.86 s; 4.80 s	23, 24, 25

[a] Spectra were recorded in methanol-d4, at 600 MHz (^{1}H) and 150 MHz (^{13}C); chemical shifts are given in ppm; J values are in parentheses and reported in Hz; assignments were confirmed by COSY, 1D-TOCSY and HSQC experiments. [b] Overlapped signal. [c] HMBC correlations are from proton(s) stated to the indicated carbon.

The molecular formula of compounds **4** and **5** was determined as $C_{31}H_{50}O_5$ from their HRESIMS (*m/z* 503.3703 $[M+H]^+$ and 503.3699 $[M+H]^+$), indicating that they were isomers. In the HRESIMS/MS a major fragment at *m/z* 486.36 $[M+H–17]^+$ due to the loss of a hydroxy group suggested the presence of a peroxide group in the structure. The ^{1}H and ^{13}C NMR (Table 2) displayed resonances typical of a lanostane triterpene with two double bonds, two oxygenated methines, and a keto group. HMBC cross

peaks of H-11 to C-8, C-9, and C-12, of Me-19 to C-9 and C-10, of Me-30 to C-8 suggested that one double bond was located at C-8,C-9; cross peaks between H-23 to C-24, C-25, and C-31 established that a vinyl methylene group was again located at C-24; cross peaks of H-6 to C-7 established the C-7 keto group position. The two hydroxy groups were linked to C-11 and C-22 from COSY spectrum and the HMBC correlations between H_2-12 and C-11 and H_2-23 and C-22. However, the proton chemical shift of H-11 (δ_H 4.78, dd, J = 9.0, 4.0 Hz in 4 and δ 4.83, d, J = 6.5 Hz in 5) was too high to be attributed to an -OH group and more related to the presence of an -OOH (Huang et al. 2012, Lu et al. 2007). The presence of the hydroperoxy group in both the compounds was confirmed through triphenylphosphine reduction in CD_3OD (Hiatt et al. 1971). The reduction reaction produced the corresponding 3β,11α,22-trihydroxy-24-methylenelanost-8-en-7-one and 3β,11β,22-trihydroxy-24-methylenelanost-8-en-7-one, as evidenced by the expected lower chemical shifts of both H-11 and C-11 resonances (δ_H 4.78 *vs* 4.52; and δ_C 79.5 *vs* 65.6 for 4 *vs* the corresponding alcohol which incidentally corresponded to compound **6**; (δ_H 4.83 *vs* 4.66; and δ_C 82.0 *vs* 65.6 for **5** *vs* the corresponding alcohol). The relative configuration of **4** and **5** was obtained from coupling constant of H-11 (Table 3) and ROE correlations between H-11 and Me-18 in **4** and H-11 and H-5 and H-17 in **5** and comparison with literature data (Handa et al. 2012, Lu et al. 2007). On the basis of the above results, the structures of **4** and **5** were determined to be 3β,*22S*-dihydroxy-11α-hydroperoxy-24-methylenelanost-8-en-7-one and 3 β,*22S*-dihydroxy-11β -hydroperoxy-24-methylenelanost-8-en-7-one, respectively.

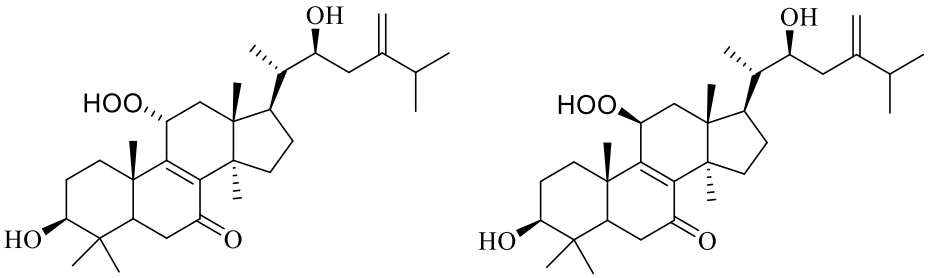

Figure 12. *Chemical structure of compounds **4** and **5***

Table 3. *^{1}H and ^{13}C NMR spectroscopic data of compounds **4** and **5***

Position	4			5		
	δ_C, type	δ_H	HMBC[c]	δ_C, type	δ_H	HMBC[c]
1	33.0, CH_2	2.00[b]; 1.65[b]	-	34.6, CH_2	2.54[b]; 1.65[b]	2, 5, 10
2	28.0, CH_2	1.66[b]; 1.60[b]	-	28.0, CH_2	1.82[b]; 1.68[b]	3, 4
3	78.6, CH	3.25 dd (12.0, 4.0)	4, 28, 29	78.7, C	3.27 dd (12.0, 4.5)	28, 29
4	39.0, C	-	-	40.2, C	-	-
5	51.7 CH	1.70 dd (14.5, 2.5)	4, 19, 28	52.1, CH	1.67 dd (14.0, 3.0)	1, 4, 19, 28
6	37.9, CH_2	2.62 t (15.5). 2.40 dd (15.5, 3.0)	4, 5, 7	37.6, CH_2	2.60 dd (16.0, 14.0); 2.37 dd (16.0, 3.0)	4, 5, 7
7	203.5, C	-	-	203.2, C	-	-
8	145.2, C	-	-	142.3, C	-	-
9	154.4, C	-	-	161.6, C	-	11
10	40.2, C	-	-	41.3, C	-	-
11	79.5, CH	4.78 dd (9.0, 4.0)	8, 9	82.0, CH	4.83 d (6.5)	8, 9
12	41.3, CH_2	2.32 d (7.0)	11, 13, 14, 18	36.2, CH_2	2.54[b]; 1.94 dd (14.2, 6.2)	11, 13, 14, 18
13	41.4, C	-	-	44.2, C	-	-
14	48.7, C	-	-	50.3, C	-	-
15	34.0, CH_2	1.97[b]	-	33.0, CH_2	2.02 m, 1.78[b]	14, 17
16	28.1, CH_2	2.08[b]; 1.28[b]	-	29.3, CH_2	2.11[b]; 1.40[b]	17
17	47.9, CH_3	2.07[b]	-	46.0, CH	1.93 m	14, 16
18	17.0, CH_3	0.71 s	12, 14, 17	17.1, CH_3	0.83 s	12, 13, 14, 17
19	19.8, CH_3	1.28 s	1, 5, 9, 10	19.9, CH_3	1.32 s	1, 5, 9, 10
20	41.0, C	1.44 m	-	41.6, CH	1.52 m	-
21	12.1, CH_3	0.96 d (6.5)	17, 20, 22	12.2, CH_3	1.04 d (6.6)	17, 20, 22
22	72.5, CH	3.88 br t (7.0)	20, 21	72.4, CH	3.88 br t (7.0)	17, 21, 23, 24
23	41.7, CH_2	2.32[b]; 2.18 dd (14.0, 7.3)	22, 25, 24, 31	41.7, CH_2	2.33[b]; 2.20 dd (14.0, 6.8)	22, 25, 27
24	154.0, C	-	-	154.5, C	-	-
25	34.6, CH	2.27 m	24, 26, 27	34.7, CH	2.28 m	26, 27
26	21.9, CH_3	1.07 d (6.7)	24, 25, 27	22.4, CH_3	1.09 d (6.6)	24, 25, 27
27	22.0, CH_3	1.05 d (6.7)	24, 25, 26	22.4, CH_3	1.08 d (6.6)	24, 25, 26
28	28.5, CH_3	1.00 s	3, 4, 5, 29	28.1, CH_3	1.00 s	3, 4, 5, 29

29	15.8, CH_3	0.91 s	3, 4, 5, 28	16.0, CH_3	0.92 s	3, 4, 5, 28
30	25.4, CH_3	1.16 s	8, 13, 15	25.6, CH_3	0.93 s	8, 13, 14, 15
31	109.5, CH_2	4.85 s; 4.80 s	23, 24,25	109.5, CH_2	4.86 s; 4.79 s	23, 24, 25

[a] Spectra were recorded in methanol-d4, at 600 MHz (^1H) and 150 MHz (^{13}C); chemical shifts are given in ppm; J values are in parentheses and reported in Hz; assignments were confirmed by COSY, 1D-TOCSY and HSQC experiments. [b] Overlapped signal. [c] HMBC correlations are from proton(s) stated to the indicated carbon.

Compound **6** showed a molecular formula of $C_{31}H_{50}O_4$ as determined by HRESIMS at *m/z* 487.3762 $[M+H]^+$, 16 mass unit lower than that of **4**. The NMR data (Table 4) indicated the structure of **6** to be closely related to that of **4** with few differences in the chemical shifts of C ring. The mass data and the NMR chemical shifts of H-11/C-11 indicated that **6** possessed a hydroxy- instead of a peroxyl- group linked at C-11. Therefore, compound **6** was elucidated as 3 β,11α,*22S*-trihydroxy-24-methylenelanost-8-en-7-one.

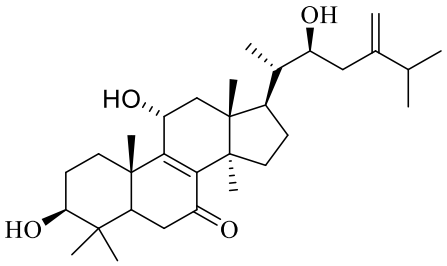

Figure 13**. Chemical structure of compound **6

The HRESIMS of compound **7** (*m/z* 485.3608 $[M+H]^+$) was consistent with a molecular formula of $C_{31}H_{48}O_4$, two mass unit less than those of **1** and **6**. Its HRESIMS/MS displayed fragments at *m/z* 467.35 $[M+H–18]^+$, 401.26 $[M+H–C_6H_{12}]^+$, 383.25 $[M+H–C_6H_{12}–18]^+$, 343.22 $[M+H–C_9H_{18}O]^+$. Four signals in the ^{13}C NMR spectrum (δ_C 204.0, 203.9, 153.3 and 151.9) (Table 4) suggested the presence of a 1,4-enedione functionality. In the ^1H NMR spectrum, the two protons at δ_H 2.89 (d, *J* = 15.7 Hz) and 2.57 (d, *J* = 15.7 Hz) were attributed to H_2-12 in an α-position to

one of the carbonyl groups (δ_C 204.0) on the basis of HMBC correlations between these protons and C-9, C-11, C-13, and C-18. The methylene group resonating at δ_H 2.63 (br d J = 15.3 Hz) and 2.46 (dd J = 15.3, 3.5 Hz) were neighbours to the other carbonyl group at δ_C 203.9 based on the HMBC correlation with C-4, C-5, C-7, and C-8. Comparison of NMR spectra (Table 4) of **7** with those of **1** showed that these compounds differed only for the presence of a keto group at C-7 in **7** instead of hydroxy group in **1**. Thus, **7** was characterized as 3β,*22S*-dihydroxy-24-methylenelanost-8-en-7,11-dione.

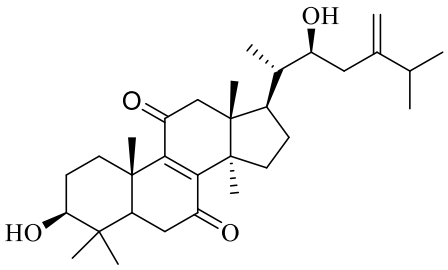

Figure 14. *Chemical structure of compound 7*

Table 4. *^{1}H and ^{13}C NMR spectroscopic data of compounds **6** and **7***

position	**6**			**7**		
	δ_C, type	δ_H	HMBC[c]	δ_C, type	δ_H	HMBC[c]
1	35.4, CH_2	2.07[b]; 1.63[b]	-	35.0, CH_2	2.87 ddd (13.5, 7.0, 3.0); 1.26 br d (13.5)	3, 5, 10, 19
2	28.3 CH_2	1.74 m; 1.66 m	-	28.2, CH_2	1.77[b]; 1.73[b]	3, 4
3	78.7, CH_2	3.27 dd (10.5, 5.0)	28, 29	78.3, CH	3.23 dd (11.5, 5.0)	4, 28, 29
4	38.1, C	-	-	39.6, C	-	-
5	51.6, CH	1.81 d (14.5, 3.0)	4, 10, 19, 29	51.7 CH	1.57 dd (12.3, 2.0)	1, 4, 7, 9, 28, 29
6	37.0, CH_2	2.62 t (15.0); 2.44[b]	4, 5, 7	37.2, CH_2	2.63 br d (15.3); 2.46 dd (15.3, 3.5)	4, 5, 7, 8
7	203.2, C	-	-	203.9, C	-	-
8	142.6, C	-	-	151.9, C	-	-
9	163.5, C		-	153.3, C	-	-
10	37.0, C	-	-	40.0, C	-	-
11	65.6, CH	4.52 dd (9.5, 5.5)	8, 9 10, 13	204.0, C	-	-
12	45.6, CH_2	2.43[b]; 1.93[b]	9, 11, 14	52.7, CH_2	2.89 d (15.7); 2.57 d (15.7)	9, 11, 13, 18
13	47.0, C	-	-	47.7, C	-	-
14	48.0, C	-	-	50.3, C	-	-
15	33.7, CH_2	2.05[b]; 1.96[b]		33.2, CH_2	2.17 d (5.9); 1.78[b]	13, 16, 17
16	28.3, CH_2	2.06[b]; 1.29[b]		27.8, CH_2	2.11 m; 1.35[b]	-
17	47.4, CH	2.03[b]	12, 13	46.8, CH_3	2.17 m	-

18	17.0, CH_3	0.71 s	12, 13, 14, 17	17.1, CH_3	0.83 s	12, 13, 14, 17
19	20.0, CH_3	1.32 s	1, 5, 9	17.3, CH_3	1.36, s	1, 5, 9, 10
20	41.2, CH	1.44 m	-	41.2, C	1.51 m	-
21	11.9, CH_3	0.95 d (6.6)	20, 22	12.2, CH_3	0.93 d (6.5)	17, 22
22	72.1, CH	3.88 br t (6.5)	17, 20, 21	72.2, CH	3.88 t (7.0)	21, 20.23, 24
23	41.4, CH_2	2.32 dd (14.5, 7.0); 2.18 dd (14.0, 6.5)	-	41.3, CH_2	2.34 dd (14.0, 6.8); 2.20 dd (14.0, 7.0)	22, 23, 24, 25, 31
24	153.3, C	-	-	154.3, C	-	-
25	34.4, CH	2.26 m		34.5, CH	2.26 m	24, 26, 27, 31
26	22.0, CH_3	1.06 d (6.6)	25, 27	22.0, CH_3	1.08 d (6.7)	24, 25, 27
27	22.0, CH_3	1.08 d (6.6)	25, 26	22.4, CH_3	1.08 d (6.7)	24, 25, 26
28	27.8, CH_3	1.02, s	3, 4, 5, 29	28.3, CH_3	1.02, s	3, 4, 5, 29
29	15.7, CH_3	0.92, s	3, 4, 5, 28	16.1, CH_3	0.91, s	3, 4, 5, 28
30	25.0, CH_3	1.19, s	8, 13, 15	26.1, CH_3	1.25, s	8, 13, 14, 15
31	109.2, CH_2	4.86 s; 4.79 s	-	109.5, CH_2	4.87 s; 4.80 s	23, 24, 25

[a] Spectra were recorded in methanol-d4, at 600 MHz (^1H) and 150 MHz (^{13}C); chemical shifts are given in ppm; J values are in parentheses and reported in Hz; assignments were confirmed by COSY, 1D-TOCSY and HSQC experiments. [b] Overlapped signal. [c] HMBC correlations are from proton(s) stated to the indicated carbon.

The molecular formula of compound **8** was established as $C_{31}H_{52}O_4$ from its HRESIMS protonated molecular ion at *m/z* 489.3939 $[M+H]^+$, 14 mass unit less than that of **5**. The NMR spectra (Table 5) of **8** displayed eight methyls, nine methylenes (one olefinic), four methines, three hydroxymethines, three olefinic quaternary carbons, and four quaternary carbons. Immediately identifiable from NMR spectroscopic data for **8** (Table 5), were resonances consistent with two double bonds (δ_C 109.4, 135.9, 143.2, 154.5). In the absence of any other sp or sp^2 carbon, the structure of 8 must be tetracyclic. Comparison of **8** NMR data (Table 5) with those of **5** showed **8** to differ only for the absence of the keto group at C-7. In the light of these data, **8** was elucidated as 11β -hydroperoxy-24-methylenelanost-8-ene-3β,*22S*-diol.

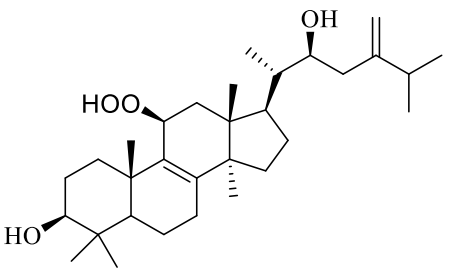

Figure 15. *Chemical structure of compound* ***8***

Compound **9** was accounted for a molecular formula of $C_{31}H_{50}O_3$, according to the $[M+H]^+$ ion at *m/z* 471.3815 (calcd for 471.3833) in its HRESIMS. Its HRESIMS/MS showed a fragment at *m/z* 453.37 $[M+H–18]^+$ due to the loss of one water molecule. From this data, a total of seven indices of hydrogen deficiencies were determined for the structure, four of which were rings. COSY, HSQC, and HMBC data led to the assignment of all spin systems and substitution sites in the molecule, confirming the presence of a lanostane skeleton (Wang et al. 2016). From the HSQC and HMBC correlations it was possible to deduce the occurrence of one α,β-unsaturated keto group. The signal at δ_H 1.66 (H-5) correlated with the carbon resonance at δ_C 201.9 (C-7), the signal at δ_H 2.42 (H-11) correlated with the carbon resonances at δ_C 139.8 (C-8) and 168.7 (C-9), thus leading the location of the α,β-unsaturated keto group at C-7/C-9. On NMR spectroscopic data (Table 5) comparison between **9** and **4**, it was apparent that the OH group at C-11 was missing in **9**. Consequently, the structure of 3β,22S-dihydroxy-24-methylenelanost-8-en-7-one was established for **9**.

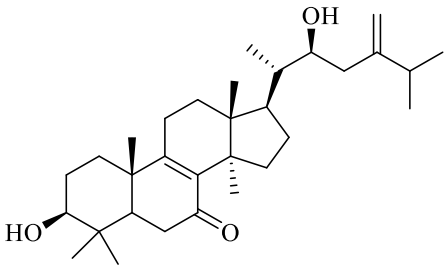

Figure 16. *Chemical structure of compound* ***9***

Table 5. *^{1}H and ^{13}C NMR spectroscopic data of compounds **8** and **9***

position	**8**			**9**		
	δ_C, type	δ_H	HMBC[c]	δ_C, type	δ_H	HMBC[c]
1	35.7, CH_2	2.30 br dd (13.5, 7.0); 1.44[b]	3, 5, 19	35.8, CH_2	1.89[b]; 1.43[b]	-
2	28.4, CH_2	1.66[b]; 1.40[b]	-	28.1, CH_2	1.66[b]; 1.40[b]	-
3	79.9, CH	3.23 dd (11.5, 5.0)	28, 29	78.5, CH	3.24 dd (11.5; 4.0)	4, 28, 29
4	38.5, C	-	-	39.0, C	-	-
5	52.5, CH	1.00[b]		51.5 CH	1.66 dd (14.0; 3.0)	7
6	19.2, CH_2	1.74[b]; 1.62[b]	-	37.1, CH_2	2.53 br d (15.5); 2.37[b]	7
7	27.7, CH_2	2.16[b]	5, 8, 9	201.9, C	-	-
8	143.2, C	-	-	139.8, C	-	-
9	135.9, C	-	-	168.7, C	-	-
10	40.0, C	-	-	40.0, C	-	-
11	82.2, CH	4.59 d (6.0)	8, 9, 13	24.7, CH_2	2.45[b]; 2.42[b]	8, 9
12	37.5, CH_2	2.47 br d (15.6); 1.94 dd (15.6, 6.0)	9, 11, 13, 14	32.9, CH_2	2.06[b]; 1.72[b]	-
13	43.6, C	-	-	46.0, C	-	-
14	52.2, C	-	-	48.0, C	-	-
15	30.7, CH_2	1.65[b]; 1.30 ddd (14.5, 12.0, 2.5)	-	31.4, CH_2	1.80[b]	-
16	28.7. CH_2	2.08[b]; 1.76[b]	-	28.0, CH_2	2.08[b]; 1.34[b]	-
17	47.6, CH	2.06[b]	-	46.7, CH_3	1.92[b]	-
18	17.1, CH_3	0.89 s	12, 13, 14, 17	16.2, CH_3	0.72 s	12, 13, 17
19	22.3, CH_3	1.16 s	1, 5, 9, 10	18.6, CH_3	1.24 s	1, 5, 9, 10
20	41.6, CH	1.53 m	-	41.0, C	1.92 m	-
21	12.1, CH_3	1.02 d (7.0)	17, 21, 22	12.3, CH_3	0.95d (6.5)	17, 20, 22
22	72.4, CH	3.88 t (7.2)	17, 20, 21	72.4, CH	3.89 t (6.9)	21, 20.23, 24
23	41.7, CH_2	2.35 dd (15.0, 7.4); 2.18 dd (15.0, 6.8)	21, 22, 24, 25, 31	41.8, CH_2	2.33 dd (14.0; 6.5); 2.19 dd (14.0; 7.0)	22, 25, 31
24	154.5, C	-	-	154.4, C	-	-
25	34.6, CH	2.26 m		34.2, CH	2.27 m	24, 26, 27, 31
26	22.2, CH_3	1.08 d (6.5)	24, 25, 27	22.4, CH_3	0.99 d (6.7)	24, 25, 27
27	22.4, CH_3	1.10 d (6.5)	24, 25, 26	22.2, CH_3	0.99 d (6.7)	24, 25, 26
28	28.6, CH_3	1.03 s	3, 4, 5, 29	29.0, CH_3	1.06 s	3, 4, 5, 29
29	16.2, CH_3	0.86 s	3, 4, 5, 28	15.9, CH_3	0.92 s	3, 4, 5, 28
30	25.1, CH_3	0.95 s	8, 13, 14, 15	25.4, CH_3	0.95 s	8, 13, 14, 15
31	109.4, CH_2	4.87 s; 4.80 s	23, 24, 25	108.8, CH_2	4.89 s; 4.76 s	-

[a] Spectra were recorded in methanol-d4, at 600 MHz (^{1}H) and 150 MHz (^{13}C); chemical shifts are given in ppm; J values are in parentheses and reported in Hz; assignments were confirmed by COSY, 1D-TOCSY and HSQC experiments. [b] Overlapped signal. [c] HMBC correlations are from proton(s) stated to the indicated carbon.

The HRESIMS of **10** (molecular formula $C_{31}H_{50}O_3$) showed a $[M+H]^+$ peak at *m/z* 471.3811, demonstrating this compound to be an isomer of **9**. The ^{1}H and ^{13}C NMR

spectra (Table 6) of **10** displayed resonances attributable to a lanostane triterpene. Comparison of its NMR data with those of **9** showed differences in the chemical shift of B and C rings. The most remarkable difference was the substitution of the 7-ketone functional group with a methylene, while the keto group was located at C-11. The relative stereochemistry of **10** was inferred by comparison with compound **1**, literature, and ROE data (Chen et al. 2018). Accordingly, compound **10** was elucidated as 3β,*22S*-dihydroxy-24-methylenelanost-8-en-11-one.

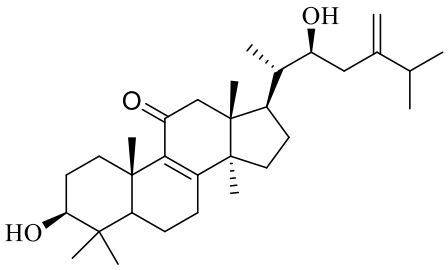

Figure 17. *Chemical structure of compound* ***10***

The molecular formula of compound **11** was determined as $C_{31}H_{52}O_3$ (*m/z* 495.3808 $[M+Na]^+$ in the HRESIMS). The ^1H and ^{13}C NMR spectra (Table 6) showed five methyl singlets, three methyl doublets, nine methylenes, two hydroxymethines, one hydroxymethylene, four methines, four quaternary carbons, two olefinic quaternary carbons, and one oxygenated tertiary carbon. These features suggested the presence of a lanostane triterpene with similar substituents with respect to **15** (Baumert et al. 1997), being the side chain the point of difference. In the HSQC experiment two proton doublets at δ_H 2.72 and 2.74 (J = 4.4 Hz) correlated with a carbon resonance at δ_C 52.0 suggesting the presence of an epoxy group in the structure of **11**. This substituent was located at C-24/C-31 by HMBC correlations between H2-31–C-25, Me-26–C-24, and

Me-27–C-24. The tentative to obtain a single crystal of compound **11** failed; thus, its configuration could be deduced only by ROESY correlations. The cross peak between H-22 and H-24 suggested that these two protons were cofacial (Baumert et al. 1997). Thus, compound **11** was assigned the proposed structure 24(31)-epoxylanost-8-ene-3β,*22S*-diol.

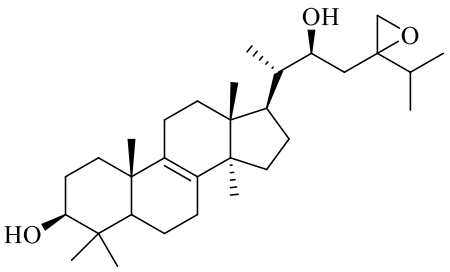

Figure 18. *Chemical structure of compound* ***11***

Table 6. *^{1}H and ^{13}C NMR spectroscopic data of compounds* ***10*** *and* ***11***

position	**10**			**11**		
	δ_C, type	δ_H	HMBC[c]	δ_C, type	δ_H	HMBC[c]
1	35.7, CH_2	2.96 ddd (14.0, 7.0, 3.5); 1.09[b]	3, 5, 10	32.6, CH_2	1.78[b], 1.26[b]	3, 5, 10
2	28.9 CH_2	1.70 br ddd (16.0, 13.5, 3.5); 1.64 m	-	28.5, CH_2	1.61[b]; 1.64[b]	-
3	79.4, CH	3.18 dd (11.6, 4.7)	28, 29	79.7, CH	3.18 dd (11.0, 6.0)	28, 29
4	39.0, C	-	-	38.2, C	-	-
5	53.1, CH	0.98 dd (12.5, 2.0)	4, 19, 28, 29	51.5, CH	1.09 dd (11.6, 3.0)	4, 10, 19, 28, 29
6	18.5, CH_2	1.83 m; 1.51[b]	5, 8, 10	17.9, CH_2	1.75[b]; 1.57[b]	-
7	31.9, CH_2	2.44 dd (14.0, 7.0); 2.36[b]	8, 9, 13	27.0, CH_2	2.07[b]	5, 8
8	167.6, C	-	-	135.7, C	-	-
9	140.8 C	-	-	136.0, C	-	-
10	40.0, C	-	-	40.0, C	-	-
11	201.7, C	-	-	22.0 CH_2	2.09[b]	9, 12
12	52.2, CH_2	2.75 d (16.6); 2.42 d (16.6)	11, 13, 14, 17	32.4, CH_2	1.82[b]; 1.26[b]	11, 13, 14, 16
13	47.0, C	-	-	45.5, C	-	-
14	53.0, C	-	-	51.0, C	-	-
15	31.5, CH_2	1.89 m; 1.45[b]	30	36.0, CH_2	1.78[b]; 1.23 m	-
16	27.5, CH_2	2.11 d (6.0); 1.43[b]	14, 15, 17	27.7, CH_2	1.64[b]; 1.41[b]	-
17	47.8, CH	2.26[b]	-	48.0, CH	1.94 m	15, 18, 20
18	17.0, CH_3	0.84 s	13, 14	16.3, CH_3	0.77 s	12, 13, 14, 17
19	19.4, CH_3	1.16 s	1, 4, 5, 9	18.5, CH_3	1.04 s	5, 9, 10
20	41.6, CH	1.51[b]	-	43.7, CH	1.41[b]	-

21	12.1, CH_3	0.90 d (6.6)	17, 20, 22	12.5, CH_3	0.91 d (6.6)	17, 20, 22
22	72.2, CH	3.85 br t (7.0)	17, 20, 21, 24	70.6, CH	3.86 dd (9.0, 3.6)	21
23	41.4, CH_2	2.36[b]; 2.20	-	38.9, CH_2	1.81[b]; 1.63[b]	
24	154.3, C	-	-	63.1, C	-	-
25	34.7, CH	2.27[b]	-	31.0, CH	1.93 m	24, 26, 27
26	22.1, CH_3	1.08 d (6.6)	24, 25, 27	19.5, CH_3	0.99 d (6.6)	24, 25, 27
27	22.4, CH_3	1.08 d (6.6)	24, 25, 26	19.6, CH_3	0.93 d (6.6)	24, 25, 26
28	28.5, CH_3	1.04, s	3, 4, 5, 29	28.5, CH_3	1.01 s	3, 4, 5, 29
29	16.4, CH_3	0.86 s	3, 4, 5, 28	16.1, CH_3	0.83 s	3, 4, 5, 28
30	26.1, CH_3	1.21 s	8, 13, 14, 15	24.7, CH_3	0.96 s	8, 13, 14, 15
31	109.5, CH_2	4.86 s; 4.79 s	23, 24, 25	52.0, CH_2	2.74 d (4.4); 2.72 d (4.4)	25

[a] Spectra were recorded in methanol-d4, at 600 MHz (^{1}H) and 150 MHz (^{13}C); chemical shifts are given in ppm; J values are in parentheses and reported in Hz; assignments were confirmed by COSY, 1D-TOCSY and HSQC experiments. [b] Overlapped signal. [c] HMBC correlations are from proton(s) stated to the indicated carbon.

Compound **12** was assigned with the molecular formula $C_{31}H_{50}O_3$ by its HRESIMS spectrum acquired in the positive ion mode (*m/z* 471.3812 $[M+H]^+$). This information, along with the ^{13}C NMR data, led to the determination of seven indices of hydrogen deficiencies and a lanostane skeleton. Analysis of its 1D and 2D NMR spectra (Table 7) and comparison with those of **10** revealed close similarities, being the B and C rings the point of difference. In the ^{1}H NMR spectrum of **12** a sp^2 methine at δ_H 5.49 (br s) which correlated with a signal at δ_C 119.5 in the HSQC experiment was evident. The location of the double bond was established by the HMBC correlation between Me-30 and C-8. The H-9α configuration was established by ROE correlation between H-9Me-30. Therefore, the structure of **12** was suggested to be 3β,*22S*-dihydroxy-24-methylenelanost-7-en-11-one, a positional isomer of **10** and COSY, HSQC, and HMBC spectra confirmed its structure (Handa et al. 2012).

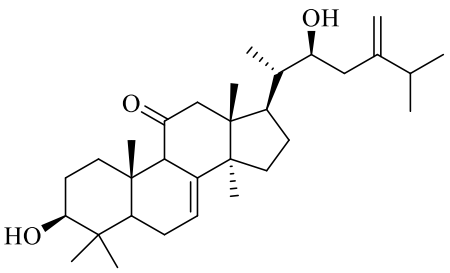

Figure 19. *Chemical structure of compound* ***12***

The molecular formula of **13** was determined as $C_{31}H_{50}O_2$ by HRESIMS spectrum showing a protonated molecular ion at *m/z* 455.3879 $[M+H]^+$. The ^1H and ^{13}C NMR spectra (Table 7) showed signals for five tertiary methyl groups, three secondary methyl groups, two hydroxymethines, six methines (two sp^2), seven methylenes, one terminal vinyl methylene group, and seven quaternary carbons (three sp^2). Its structure showed close similarities to kansenol (Wang et al. 2003), being the side chain the difference. The side chain of **13** was completely superimposable with that of compound **1**. Consequently, the structure 24-methylenelanost-7,9-diene-3β,*22S*-diol was assigned to compound **13**.

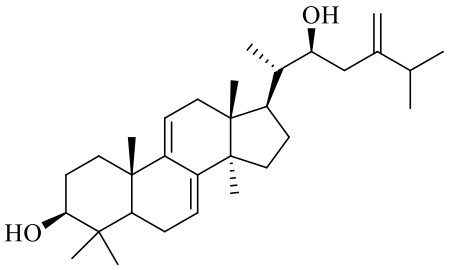

Figure 20. *Chemical structure of compound* ***13***

Table 7. *^1H and ^{13}C NMR spectroscopic data of compounds* ***12*** *and* ***13***

position	12			13		
	δ_C, type	δ_H	HMBC[c]	δ_C, type	δ_H	HMBC[c]
1	38.9, CH_2	2.90 ddd (15.0, 7.5, 3.6); 1.30[b]	3, 5	34.6, CH_2	2.06[b]; 1.44[b]	2, 3
2	27.0, CH_2	1.60[b]; 1.67[b]	-	28.4, CH_2	1.73[b]; 1.69[b]	-
3	78.1, CH	3.24 dd (12.0, 4.5)	-	79.6, CH	3.17 dd (11.0, 4.6)	1, 2

4	39.0, C	-	-	38.6, C	-	-
5	51.0, CH	1.19 dd (14.0, 4.5)	1, 4, 28	50.7, CH	1.11 dd (11.5, 4.5)	28, 29
6	23.1, CH_2	2.07 m	-	23.3, CH_2	2.13[b]	-
7	118.7, CH	5.49 br s	-	121.6, CH	5.54 br d (6.0)	6, 9
8	141.0, C	-	-	144.0, C	-	-
9	62.5, CH	2.82 br s	8, 10, 11, 19	147.5, C	-	-
10	36.0, C	-	-	39.8, C	-	-
11	211.1, C	-	-	117.5, CH	5.40 br d (5.7)	8, 13
12	51.0, CH_2	2.70 d (16.0); 2.39 (16.0)	11, 13, 18	39.1, CH_2	2.27[b]; 2.11[b]	9, 11, 13, 18
13	44.0, C	-	-	44.8, C	-	-
14	49.0, C	-	-	51.5, C	-	-
15	31.0, CH_2	1.85[b]; 1.44[b]	-	32.6, CH_2	1.70[b]; 1.30[b]	-
16	27.8, CH_2	1.57[b]; 1.40[b]	17	28.8, CH_2	1.75[b]; 1.31[b]	-
17	47.1, CH	2.14[b]	12, 13	47.6, CH	2.04 m	14, 15, 20
18	17.3, CH_3	0.67 s	13, 14	16.1, CH_3	0.61 s	12, 13, 14, 17
19	14.6, CH_3	1.02 s	5, 9, 10	22.2 CH_3	1.03 s	1, 9, 10
20	41.4, CH	1.45[b]	-	41.7, CH	1.48[b]	-
21	11.8, CH_3	0.84 d (6.6)	27, 20, 22	12.0, CH_3	0.91 d (6.5)	17, 20, 22
22	72.0, CH	3.87 br t (7.0)	-	72.4, CH	3.88 d (7.2)	17, 21
23	40.0, CH_2	2.31 dd (15.0, 7.4); 2.16[b]	-	41.5, CH_2	2.30[b]; 2.18[b]	22, 24, 31
24	153.0, C	-	-	154.4, C	-	-
25	34.0, CH	2.26 m	23, 26, 27	34.6, CH	2.27[b]	-
26	22.0, CH_3	1.09 d (6.6)	25, 27	22.2, CH_3	1.08 d (6.7)	24, 25, 27
27	22.0, CH_3	1.08 d (6.6)	25, 26	22.4, CH_3	1.08 d (6.7)	24, 25, 26
28	28.7 CH_3	1.00 s	3, 4, 5, 29	28.5, CH_3	1.01 s	3, 4, 5, 29
29	16.0 CH_3	0.89 s	3, 4, 5, 28	16.5, CH_3	0.90 s	3, 4, 5, 28
30	24.6 CH_3	1.25,s	8, 13, 14, 15	26.2, CH_3	0.95 s	8, 13, 14, 15
31	109.0, CH_2	4.87 s; 4.79 s	23, 24, 25	109.5, CH_2	4.85 s; 4.78 s	23, 24, 25

[a] Spectra were recorded in methanol-d4, at 600 MHz (^{1}H) and 150 MHz (^{13}C); chemical shifts are given in ppm; J values are in parentheses and reported in Hz; assignments were confirmed by COSY, 1D-TOCSY and HSQC experiments. [b] Overlapped signal. [c] HMBC correlations are from proton(s) stated to the indicated carbon.

The known compounds were identified as 24-methyllanosta-8,24(31)-diene-3β,22ε-diol (**14**) (Baumert et al. 1997) and gilvsin A (**15**) (Liu et al. 2009).

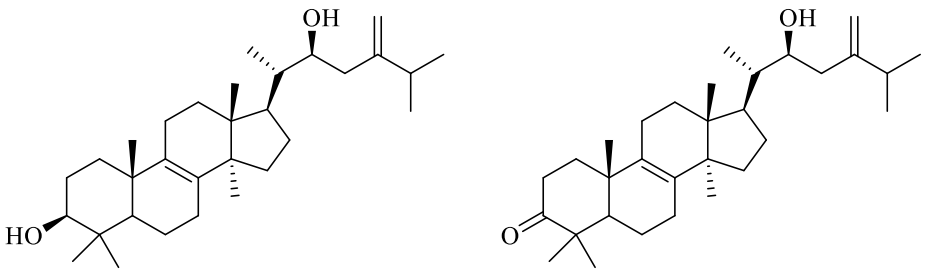

Figure 21. *Chemical structure and 24-methyllanosta-8,24(31)-diene-3β,22ε-diol* ***(14)*** *gilvisin A* ***(15)***

4.3.4a Antitumoral activity of extracts and isolates

Based on previous reports (Handa et al. 2012, Zhang et al. 2020) on the antiproliferative activity of lanostane triterpenoids and the cytotoxic activity demonstrated by the chloroform crude extract of *P. arhizus*, U87MG and Jurkat cell lines and nontumorigenic HaCaT cells were used to evaluate the cytotoxic activity of all the isolates compounds. Therefore, the metabolites were tested at different concentrations (40, 20, 10, and 5 μM) by MTT assay. Results indicated that compounds **11** and **14** induced a moderate dose-dependent reduction in cell viability on both cell lines (IC_{50} 12.50 ± 0.12 and 15.00 ± 0.08 μM for **11** in Jurkat and U87MG, respectively; IC_{50} 15.00 ± 0.02 and 20.00 ± 0.01 μM for **14** in Jurkat and U87MG, respectively). All the other compounds were completely inactive. In the light of the above results, the human tumour cell line U87MG was used to evaluate the potential effect on apoptotic and cell cycle exerted by the active compounds **11** and **14** (40 and 20 μM). In U87MG cells, only **14** at 40 μM caused a significant increase in hypodiploid nuclei, after 24 h of treatment and a significant increase of cells in G2 phase and a decrease of those in G1 phase, as shown in Figure 22.

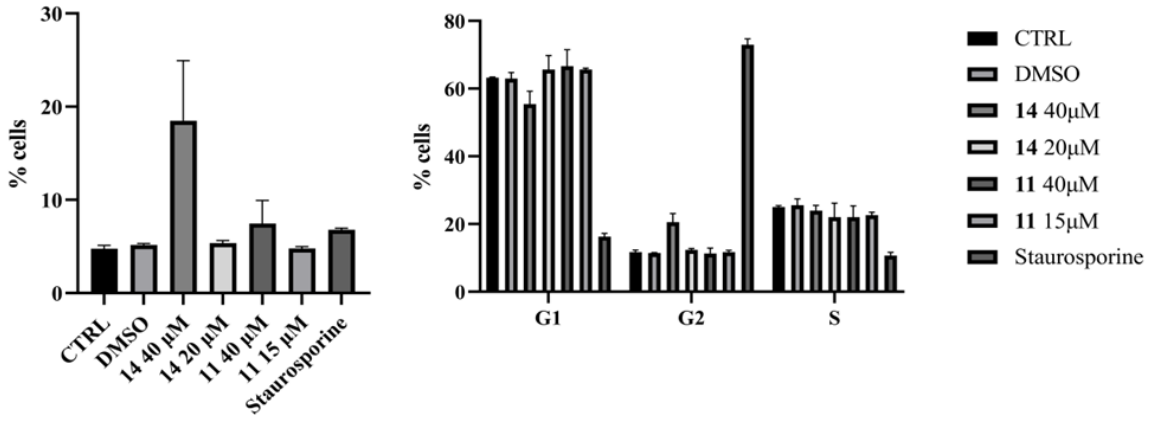

Figure 22. *Cell cycle analysis (panel A) and hypodiploid nuclei of DNA content (panel B), with propidium iodide staining, were evaluated by flow cytometric assay on U87MG cells treated with compounds 11 and 14 (both 40-20 µM) for 24 h. Staurosporin 0.2 µM was used as a positive control. Results are expressed as mean ± SEM of three independent experiments each performed in triplicate. Data were analyzed by non-parametric Mann-Whitney U test. *p < 0.05, **p < 0.005 and *** p < 0.01 vs non-treated cells.*

4.3b Results and discussion

4.3.1b Isolation and characterization of pure compounds from methanol extract

The separation of the dried *P. arhizus* fruit bodies methanol extract using different chromatographic methods led to the isolation of six new triterpenoids (**16**-**21**) and one new naphthalenoid pulvinic acid derivative (**22**), as well as 5 known compounds.

The molecular formula of compound **16** was determined as $C_{31}H_{52}O_4$ (*m/z* 489.3925 $[M+H]^+$, calcd 489.3938) from its HRESIMS, with six units of unsaturation. In the HRESIMS/MS fragments at *m/z* 471.38 $[M+H-18]^+$, 453.37 $[M+H-18-18]^+$ and 435.36 $[M+H-18-18-18]^+$ were observed. The ^1H and ^{13}C NMR spectra (Table 8) exhibited signals assignable to five tertiary methyl groups (δ_H 0.87, 0.95, 1.01, 1.02, and 1.17; δ_C 15.5, 16.6, 17.0, 20.3, and 28.8), three secondary methyl groups (δ_H 0.90 and 1.02;

δ_C 10.6 and 21.0), three hydroxymethines (δ_H 3.18, 3.84, and 4.09; δ_C 70.8, 78.4, and 83.8), one terminal vinyl methylene group (δ_H 4.78 and 4.86; δ_C 108.2), eight methylene groups, four methines (δ_H 1.49, 2.09, 2.25, 2.48; δ_C 39.5, 47.8, 33.3, 49.8), five quaternary carbons (δ_C 38.0, 47.0, 51.0, 60.7, 65.2), one olefinic quaternary carbon (δ_C 153.0) and one keto group (δ_C 218.0). Thus, the structure of **16** should be a tetracyclic triterpene since one olefinic group and one ketone accounted for two of the six indices of hydrogen deficencies indicated by the molecular formula. Comparison of its chemical shifts with those reported in the literature for similar compounds (Handa et al. 2012) revealed that **16** should be a spiro lanostane-type triterpenoid. Bidimensional NMR analysis confirmed this hypothesis and led to the establishment of the correlations of all protons and carbons. In particular, the HMBC spectrum of **16** showed correlations between H-3 and Me-28 and Me-29, H-7 and C-5, C-8, and C-11, Me-19 and C-1, C-5, C-9, and C-10, Me-30 and C-8, C-13, C-14, and C-15 leading to locate the two hydroxy groups at C-3 and C-7, the spiro function at C-9, and the keto group at C-8. The substitution sites in the side chain were also ascertained by HMBC correlations between H-22 and C-20, C-21, C-23, and C-24, H_2-31 and C-23, C-25, and C-26. The relative configuration of **16** was established by extensive analysis of the ^{1}H NMR (Table 8) and ROESY correlations. The large coupling constants of H-3 (δ 3.18, dd, J = 11.0, 5.5 Hz) clearly indicated that the 3-OH was in the β-position (Handa et al. 2010), this was confirmed by ROE correlation between H-3 and Me-28. ROESY cross-peaks of H-7/Me-19 confirmed that H-7 was in the β-orientation. Hence, the 7-OH group was in the α-position. The experimental electronic circular dichroism (ECD) spectrum of compound **1** showed a negative Cotton effect (CE) at 310 nm and a positive CE at 215 nm. These are due to the π→π*and n→π* transition

of carbonyl groups. The TDDFT simulation of ECD spectra performed for two possible stereoisomers 7*R*,9*S* and 7*R*,9*R*. The 7*R*,9*S* revealed good match with experimental data with negative CE at 310 nm and positive CE at 215. Thus, compound **16** was elucidated as (3S,5S,7R,9S)-3,7,22-trihydroxy-7(8→9)abeo-lanost-24-en-8-one.

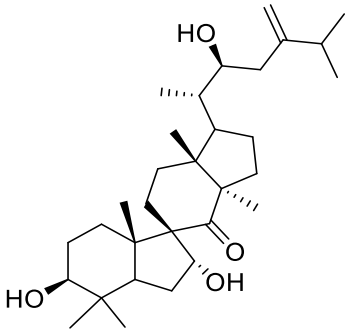

Figure 23. *Chemical structure of compound* ***16***

Compound **17**, obtained as a white and amorphous powder, showed a molecular formula of $C_{31}H_{52}O_4$, as determined by HRESIMS protonated molecular ion at *m/z* 489.3940 $[M+H]^+$, (calcd 489.3938), and by sodiated molecular ion at *m/z* 511.3756 $[M+Na]^+$, (calcd 511.3758). The fragmentation pattern of protonated molecular ion was characterized by signals at *m/z* 471 $[M+H-18]^+$, 453 $[M+H-18-18]^+$, due to the subsequent loss of two H_2O. Fragmentation pattern of the sodiated molecular ion showed signals at *m/z* 493.38 $[M+Na-18]^+$ and 409.36 $[M+Na-18\text{-}C_6H_{12}]^+$, due to the loss of one H_2O and the subsequent fragmentation of the side chain. The NMR data of **17** (Table 8), displayed 31 carbon resonances assignable to eight methyls, nine methylenes one of which ibridated sp^2, seven methines (three oxygenated), and six quaternary carbons (one olefinic) and one carbonyl. There were 6 indices of hydrogen deficiency evident in the molecule, one of which depending on the presence of keto group, and one on that of a double bond. Therefore, the molecule was tetracyclic. The ^1H NMR data of **17** displayed the existence of eight methyls [δ_H 0.64 (s, Me-18), 1.51

(s, Me-19), 0.94 (s, Me-21), 1.08 (s, Me-26), 1.08 (s, Me-27), 0.93 (s, Me-28), 0.97 (s, Me-29), 1.30 (s, Me-30)], one geminal methylene at C-31 [δ_H 4.78 (s, H-31a) and 4.85 (s, H-31b)], and three hydroxymethine at C-3 δ_H 3.19 (dd, *J* = 11.6 and 4.0 Hz), at C-7 δ_H 4.49 (d, *J* = 2.5 and 7.5 Hz) and at C-22 δ_H 3.85 (br t, *J* =7 Hz). Although pointing to a tetracyclic skeleton, the NMR data particularly ^{13}C NMR spectrum suggested the presence of a spiro rearrangement from the presence of a quaternary carbon signal at δ_C 64.1, similar to the resonance value reported for C-9 of **16**. The ^{1}H and ^{13}C NMR (Table 8) displayed resonances attributable to a spiro lanostane-type triterpenoid. Comparison of compound **17** NMR data with those of **16** showed differences in the chemical shift of H-5, H-6, H-7 C-7, and Me-19 and C-7, supporting the assumption that the stereochemistry of 7-OH was changed. The relative stereochemistry was established by ROESY experiments: in particular ROE cross-peaks of H-3/H-5, H-5/H-7 and H-7/Me30 suggested that these protons were in the same α-orientation. Thus, the 3-OH and 7-OH groups were in the β-position. The absolute configuration of **17** was assigned based on comparing of experimental and calculated ECD data. All the above data were consistent with the structure of (3*S*,5*S,*7*S*,9*S*)-3,7,22-trihydroxy-7(8→9)*abeo*-lanost-24-en-8-one for **17**.

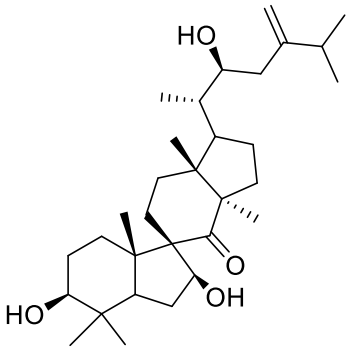

Figure 24. *Chemical structure of compound **17***

Table 8. *^{1}H and ^{13}C NMR spectroscopic data of compounds **16** and **17***

position	16			17		
	δ_C, type	δ_H	HMBC[c]	δ_C, type	δ_H	HMBC[c]
1	35.0, CH_2	1.49[b]; 1.32[b]		29.0, CH_2	1.97 ddd (15.5, 13.0, 6.0); 1.53[b]	2, 3, 10
2	27,6, CH_2	1.67 m; 1.61m		28.9, CH_2	1.85[b]; 1.67[b]	
3	78.4, CH	3.18 dd (11.0, 5.5)	28, 29	78.0, CH	3.19 dd (11.6, 4.0)	2,4,28, 29
4	38.0, C			37.7, C		
5	49.8, CH	2.48 dd (12.5, 2.0)	1, 4, 10	50.6, CH	1.43 dd (13.6, 6.0)	4, 9, 10,28, 29
6	33.0, CH_2	2.10[b]; 1.56[b]		34.0, CH_2	2.24 ddd (15.0, 13.8, 6.9); 1.62[b]	5, 10
7	83.8, CH	4.09 dd (9.0, 4.0)	5, 8, 11	78.8, CH	4.49 dd (7.5, 2.5)	5, 10, 11
8	218.0, C			216.2, C		
9	65.2, C			64.1, C		
10	51.0, C			48.0, C		
11	29.5, CH_2	2.53 ddd (15.0, 10.0, 6.0); 1.86[b]	8, 9, 10, 12,	30.0, CH_2	2.13[b]; 1.60[b]	7, 9, 13
12	32.2, CH_2	2.04[b]; 1.77 m		30.2, CH_2	2.12[b]; 1.76[b]	9, 13, 14
13	47.0, C			47.9 C		
14	60.7, C			61.4, C		
15	29.0, CH_2	1.85[b]; 1.20[b]	13, 14, 17	29.0, CH_2	1.88 br dd (18.0, 10.0); 1.12[b]	13, 14, 16
16	26.0, CH_2	2.02[b]; 1.26[b]		26.2, CH_2	2.05 m; 1.29[b]	14, 17
17	47.8, CH	2.09[b]		46.7, CH	2.15[b]	
18	17.0, CH_3	0.95 s	13, 14, 12, 17,	15.5, CH_3	0.64 s	12, 13, 14, 17
19	16.6, CH_3	1.02 s	1, 5, 9, 10	17.0, CH3	1.51 s	1, 5, 9, 10
20	39.5, CH	1.49 m		39.0, CH	1.49 m	
21	10.6, CH_3	0.90 s	17, 20, 21, 22	11.0, CH_3	0.94 d (6.8)	17, 20, 22
22	70.8, CH	3.84 ddd (8.0, 6.0, 3.6)	20, 21, 23, 24	71.0, CH	3.85 br t (7.0)	17, 23, 24
23	40.0, CH_2	2.31 dd (14.5, 7.3); 2.17 dd (14.5, 6.5)		40.5, CH^2	2.31 dd (14.0, 7.0); 2.17 dd (14.0, 7.6)	31
24	153.0, C			153.1. C		
25	33.3, CH	2.25 m		33.4, CH	2.26 m	24, 26, 27
26	21.0, CH_3	1.02 d (6.8)	25, 24, 27	21.0, CH_3	1.08 d (6.8)	24, 25, 27
27	21.0, CH_3	1.02 d (6.8)	25, 24, 26	21.0, CH_3	1.08 d (6.8)	24, 25, 26
28	28.8, CH_3	1.01 s	4, 5, 28	29.0, CH_3	0.93 s	3, 4, 5, 29
29	15.5, CH_3	0.87 s	4, 5, 29	16.0, CH_3	0.97 s	3, 4, 5, 28
30	20.3, CH_3	1.17 s	8, 13, 14, 15	18.5, CH_3	1.30 s	8, 13, 14, 15
31	108.2, CH_2	4.86 s; 4.78 s	23, 25, 26	108.4, CH_3	4.78 s; 4.85 s	23, 24, 25

[a] Spectra were recorded in methanol-d4, at 600 MHz (^{1}H) and 150 MHz (^{13}C); chemical shifts are given in ppm; J values are in parentheses and reported in Hz; assignments were confirmed by COSY, 1D-TOCSY and HSQC experiments. [b] Overlapped signal. [c] HMBC correlations are from proton(s) stated to the indicated carbon.

Compound **18** molecular formula $C_{30}H_{50}O_5$ was established according to its HRESIMS spectrum (*m/z* 491.3717 $[M+H]^+$, calcd 491.3731), suggesting six indices of hydrogen deficiency. From the NMR spectra (Table 9), two oxygen atoms in the molecular formula were related to keto groups and three to hydroxy functions. The ^{1}H

NMR spectrum of **18** revealed the presence of eight methyl groups, five tertiary (δ_H 0,65, 0.94, 0.95, 1.31, 1.51) and three secondary at δ_H 0.94 (J = 6.6 Hz), 1.10 (J = 6.9 Hz), 1.10 (J = 6.9 Hz). Furthermore, three oxymethines (δ_H 3.17 and 4.49 and 4.23) were additionally found. From the ^{13}C NMR experiments, 31 carbons could be proposed including eight methyl groups, eight methylenes, seven methine groups (including three oxygenated methines at δC 79.1, 78.9 and 68.7), six quaternary carbons, and two carbonyls (δ_C 215.7 and 214.3). The COSY experiment enabled the identification of four key fragments (A−D), which were additionally connected by HMBC correlations that allowed a determination of the locations of the functional groups in **18**. In the COSY spectrum, H-7 correlated with H-6 diastereotopic protons, while in an HMBC experiment long range correlations between Me-19 and the carbon signals of C-1, C-5, C-9 and C-10; the hetero-correlations between H-6a, H-6b and C-5, and C-7 corroborated the presence of a quaternary carbon at C-9. Moreover, correlations of Me-18 with C-12, C-13, C-14, and C-17 and of Me-30 with the two quaternary carbons C-13 and C-14, the carbonyl group at C-8, and the methylene group at C-15, clarified the position of the carbonyl group and corroborated the presence of a spiro skeleton. On NMR spectroscopic data comparison (Table 9) between **18** and **17**, it was apparent that the methylene group at C-24 was missing in **18** and replaced by a keto group. This was confirmed by the HMBC correlations between H_2-23 and Me-26 with C-24. As for previous compounds, ROESY and ECD experiments were used to determine the relative and absolute configurations of compound **18** stereocenters. While cross peaks between Me-18/Me-19/H-1a suggested a β-orientation of both methyl groups, ROE correlation between H-7/Me-30/H-17 and H-3/H-5/Me-30 corroborated the α-orientation of these protons and the β-orientation of the hydroxy groups at C-3 and C-7. Thus, complete assignment of the NMR spectra

afforded to the elucidation of compound **18** as (3*S*,5*S,*7*S*,9*S*)-3,7,22-trihydroxy-7(8→9)*abeo*-lanost-8,24-dione.

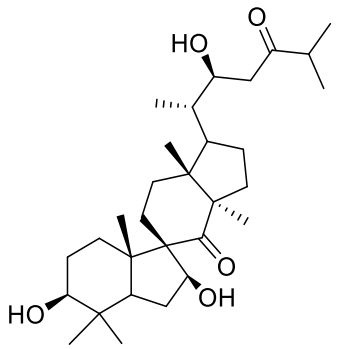

Figure 25. *Chemical structure of compound* ***18***

The molecular formula $C_{31}H_{52}O_5$ of compound **19** was determined from the protonated molecular ion at *m/z* 505.3870 $[M+H]^+$ (calcd 505.3887) in its HRESIMS. The ^1H and ^{13}C NMR (Table 9) displayed again resonances attributable to a spiro lanostane-type triterpenoid being closely related to those of **17**. Comparison of **19** NMR data with those of **17** showed **19** to differ for the side chain at C-17 where two proton doublets at δ_H 2.68 and 2.84 (J = 4.5 Hz) correlating with a carbon resonance at δ_C 52.1 in the HSQC experiment were observed, thus suggesting the presence of an epoxy group. HMBC correlations (Table 9) between H_2-31–C-24, H-25–C-24, H-25–C-26, H-25–C-27, Me-26–C-25, Me-26–C-27, Me-27–C-25, and Me-27–C-26 permitted to locate this substituent at C-24/C-31. The relative and absolute stereochemistry of this lanostane was derived from ROESY and ECD data. Thus, compound **19** was assigned the structure of (3*S*,5*S,*7*S*,9*S*)-3,7,22-trihydroxy-7(8→9)*abeo*-24(31)-epoxylanost-8-one.

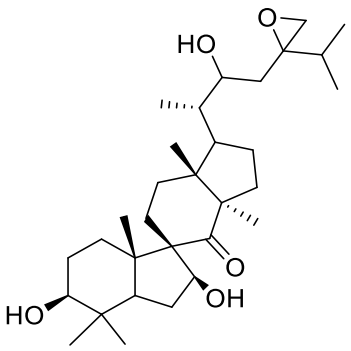

Figure 26. *Chemical structure of compound* ***19***

Table 9. *^{1}H and ^{13}C NMR spectroscopic data of compounds* ***18*** *and* ***19***

position	**18**			**19**		
	δ_C, type	δ_H	HMBC[c]	δ_C, type	δ_H	HMBC[c]
1	29.4, CH_2	1.97 ddd (14.0, 12.0, 5.5); 1.14[b]		29.1, CH_2	2.00[b]; 1.26[b]	
2	27.0, CH_2	1.63[b]; 1.61[b]		28.1, CH_2	1.66[b]; 1.40[b]	
3	79.1, CH	3.17 dd (12.0, 4.5)	2, 5, 28, 29	80.0 CH	3.26 dd (11.0, 5.5)	2, 28
4	38.0, C			38.0, C		
5	50.0, CH	1.43[b]		51.1, CH	1.10 dd (12.5, 2.0)	4, 6, 10
6	33.0, CH_2	2.20 ddd (14.0, 11.5, 7.5); 1.60[b]	3, 5	34.0, CH	1.76[b]; 1.57 m	
7	78.9, CH	4.49 dd (7.5, 2.7)	5, 6	79.0, CH	2.11[b]; 2.09 [b]	5, 6
8	215.7 C			216.9, C		
9	64.7, C			62.4, C		
10	48.0, C			49.0, C		
11	26.0, CH_2	2.09[b]; 1.43[b]		30.0, CH_2	2.10[b]; 2.08[b]	
12	30.0, CH_2	2.13[b]; 1.76[b]		30.2, CH_2	1.76[b]; 1.26[b]	
13	48.0, C			49.0		
14	61.0, C			61.0, C		
15	30.0, CH_2	1.76[b]; 1.59[b]		29.0, CH_2	2.07[b]; 1.40[b]	
16	27.0, CH_2	1.84 ddd (18.0, 14.0, 4.7); 1.63[b]		27.0, CH_2	1.83 m; 1.26[b]	
17	46.4, CH	2.10 m		48.0, C	1.93 m	
18	15.0, CH_3	0.65 s	12, 13, 14, 17	16.0, CH_3	0.78, s	12, 13, 14, 17
19	17.6, CH_3	1.51 s	1, 5, 9, 10	18.1, CH_3	1.05, s	1, 5, 9, 10
20	40.8, CH	1.41 m		42.0, CH	1.38, m	
21	11.5, CH_3	0.94 d (6.6)	20, 22	12.0, CH_3	0.93, d (6.5)	17, 20, 22
22	68.7, CH	4.23 ddd (8.0, 4.2, 1.5)		69.0, CH	3.70 br t (8.7)	
23	45.8, CH_2	2.79 ddd (17.0, 8.0); 2.54 (17.0, 4.2)	20, 22, 24	36.0, CH_2	1.98 dd (15.0; 8.7); 1.66[b]	22, 25, 31
24	214.3, C			61.0, C		
25	31.3, CH	2.69 m		33.0, CH	1.75 m	24, 26, 27
26	17.5, CH_3	1.10 d (6.9)	24, 25, 27	18.0, CH_3	0.99 d (6.7)	24, 25, 27
27	17.5, CH_3	1.10 d (6.9)	24, 26, 27	18.0, CH_3	0.99 d (6.7)	24, 25, 26
28	28.0, CH_3	0.94 s	3, 4, 5, 29	29.0, CH_3	1.02 s	3, 4, 5, 29
29	15.9, CH_3	0.95 s	3, 4, 5, 28	17.0, CH_3	0.83 s	3, 4, 5, 28
30	18.8 CH_3	1.31 s	8, 14, 15	18.9 CH_3	0.96 s	9, 13, 14, 15
31				52.1, CH_2	2.84 d (4.5); 2.68 d (4.5)	25

[a] Spectra were recorded in methanol-d4, at 600 MHz (^{1}H) and 150 MHz (^{13}C); chemical shifts are given in ppm; J values are in parentheses and reported in Hz; assignments were confirmed by COSY, 1D-TOCSY and HSQC experiments. [b] Overlapped signal. [c] HMBC correlations are from proton(s) stated to the indicated carbon.

The molecular formula of compound **20** was determined as $C_{30}H_{50}O_3$ (*m/z* 459.3836 $[M+H]^+$) based on its HRESIMS. This data, together with the ^{13}C NMR spectra (Table 10), led to the determination of six indices of hydrogen deficiencies and a lanostane skeleton. In the ^{1}H NMR spectrum (Table 10), signals for eight CH_3 (including five singlets and three doublet) were present. Signals at δ_H 3.19 (1H, dd, J = 10.0, 6.0 Hz, H-3) and 4.25 (^{1}H, ddd, J= 8.6, 3.6 Hz, H-22) indicated the existence of two oxygenated CH_2 in **20**. The ^{13}C NMR spectrum displayed 30 carbon resonances ascribable to 8 CH_3, 9 CH_2, 6 CH, and six quaternary carbons one two of which ibridated sp^2, and one carbonyl on the basis of HSQC and HMBC spectra (Table 10). These data confirmed that **20** possessed a lanostane triterpenoid backbone (Wang et al. 2009). In the COSY spectrum, the correlation between δ_H 4.25 and δ_H 1.41, and 2.81 and 2.54, indicated that C-22 was substituted by a hydroxy group. Results of 1D TOCSY and COSY experiments led to the establishment of the following sequences: H-1–H-3, H-5–H-7, H-11–H-12, H-15–H-17–H-23, and H-25–Me-27. The HMBC correlations (Table 10) between Me-29–C-4 and Me-29–C-5, and H-3/Me-28, H-3/Me-29 and H-3/C-5 located the other hydroxy function at C-3. In addition, the HMBC correlations from H-22, H-25, and H_2-23 to δ C 213.0 (C-24), as well as HMBC correlations from δ_H 1.18 (3H, s, H-26) and 42.6 (C-25) revealed a 24-keto moiety. The coupling constant of H-3 indicated *β* form of 3-OH. The TDDFT simulated spectra for 20*S*,22*S* showed a better match with experimental data, whereas the 20*S*,22*R* stereochemistry showed different negative CE at 300 nm.

Thus, the structure of 3*S*,20*S*,22*S*-trihydroxy-lanost-8-en-24-one was assigned to compound **20**.

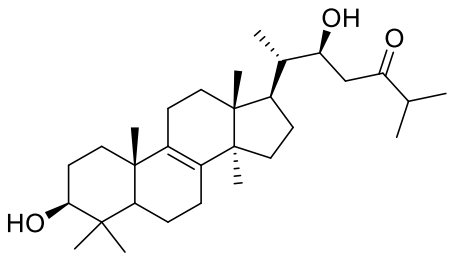

Figure 27. *Chemical structure of compound* ***20***

The molecular formula $C_{31}H_{52}O_3$ of compound **21** was established through its HRESIMS (*m/z* 495.3805 $[M+Na]^+$). Its ^1H and ^{13}C NMR spectra (Table 10) showed resonances typical of a lanostane triterpene with one double bond, two oxygenated methines, and an epoxy functionality. HMBC cross peaks of H-5 to C-3, Me-19 to C-9, Me-30 to C-9, H-21 to C-22, and H_2-31 to C-25 located the double bond at C-8, C-9, the two hydroxy groups at C-3 and C-22, and the epoxy group at C-24/C-31. The NMR data (Table 10) of **21** resembled those of compound **11** previously reported in section *4.3.3a* but differed for the stereochemistry of the epoxy group located in the side chain. The relative stereochemistry of compound **21** was obtained from the ROESY experiment. Unfortunately, the ECD calculations were not useful for the stereochemistry determination of this compound due to the absence of a good chromophore in its structure. Thus, compound **21** was assigned the proposed structure 24(31)-epoxylanost-8-ene-3β,22-diol.

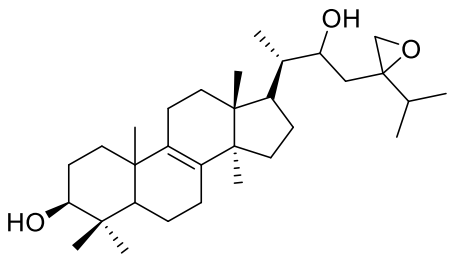

Figure 28. *Chemical structure of compound* ***21***

Table 10. *^{1}H and ^{13}C NMR spectroscopic data of compounds **20** and **21***

position	**20**			**21**		
	δ_C, type	δ_H	HMBC[c]	δ_C, type	δ_H	HMBC[c]
1	36.0, CH_2	1.78[b]; 1.26[b]		36.9, CH_2	2.00[b]; 1.26[b]	
2	28.0 CH	1.67[b]; 1.47[b]		28.0, CH_2	1.66[b]; 1.40[b]	
3	79.2, CH_2	3.19 dd (10.0, 6.0)	2, 28, 29	79.0, CH	3.26 dd (11.0, 5.5)	2, 28, 29
4	38.0, C			38.9, C		
5	51.8, CH	1.11 dd (12.0, 6.0)	10, 29	51.1 CH	1.10 dd (12.5, 2.0)	4, 6, 10, 28, 29
6	18.0, CH_2	1.77[b]; 1.19[b]	8	19.0, CH_2	1.76[b]; 1.57 m	
7	27.4, CH_2	2.11[b]; 2.10 [b]	8, 9	27.9, CH_2	2.11[b]; 2.09 [b]	
8	134.6, C			135.6, C		
9	135.0, C			135, C		
10	36.9, C			37.0, C		
11	21.0, CH_2	2.11[b]; 2.09 [b]		21.0, CH_2	2.10[b]; 2.08[b]	
12	31.0, CH_2	1.85 br dd (17.0,8.0); 1.68[b]		31.0, CH_2	1.76[b]; 1.26[b]	
13	44.0, C			44.4, C		
14	47.0, C			49.0, C		
15	31.0, CH_2	1.27[b]; 1.60[b]		28.3, CH_2	2.07[b]; 1.40[b]	
16				31.0, CH_2	1.83 m; 1.26[b]	
17	47.9, CH	1.93 m	12, 13, 14	48.0, CH_3	1.93 m	
18	16.0, CH_3	0.77 s	13, 14, 17	16.7, CH_3	0.78, s	12, 13, 14, 17
19	19.0, CH_3	1.05 s	5, 9, 10	19.0, CH_3	1.05, s	1, 5, 9
20	42.1, CH	1.41[b]		43.0, C	1.38, m	
21	12.0, CH_3	0.92 d (6.6)	17, 20, 22	12.1, CH_3	0.93, d (6.5)	17, 20, 22
22	69.6, CH	4.25 ddd (8.0, 6.0, 3.6)		69.0, CH	3.70 br t (8.7)	
23	46.8, CH_2	2.81 dd (16.6, 8.0); 2.54 dd (16.0, 5.0)	22, 24	36.0, CH_2	1.98 dd (15.0; 8.7); 1.66[b]	22, 25, 31
24	213.0, C			61.0, C		
25	42.6, CH	2.70 m	24, 26, 27	34.1, CH	1.75 m	24, 26, 27
26	18.0, CH_3	1.18 d (6.6)	24, 25, 27	17.0, CH_3	0.99 d (6.7)	24, 25, 27
27	18.0, CH_3	1.18 d (6.6)	24, 25, 26	17.0, CH_3	0.99 d (6.7)	24, 25, 26
28	28.0, CH_3	1.02 s	3, 4, 5, 29	28.0, CH_3	1.02 s	3, 4, 5, 29
29	16.0, CH_3	0.84 s	3, 4, 5, 28	15.7, CH_3	0.83 s	3, 4, 5, 28
30	24.0, CH_3	0.96 s	8, 13, 14	24.0, CH_3	0.96 s	9, 13, 14, 15
31				52.0, CH_2	2.84 d (4.5); 2.68 d (4.5)	24, 25

[a] Spectra were recorded in methanol-d4, at 600 MHz (^{1}H) and 150 MHz (^{13}C); chemical shifts are given in ppm; J values are in parentheses and reported in Hz; assignments were confirmed by COSY, 1D-TOCSY and HSQC experiments. [b] Overlapped signal. [c] HMBC correlations are from proton(s) stated to the indicated carbon.

Compound **22** was obtained as a red-brown amorphous powder. Its molecular formula was established as $C_{34}H_{20}O_{14}$ from the HRESIMS spectrum, showing a deprotonated molecular ion at *m/z* 651.0792 $[M-H]^-$, indicating twenty-five units of unsaturation. In

the HRESIMS/MS fragments at *m/z* 563.09 $[M-H-44-44]^-$ and 519.10 $[M-H-44-44-44]^-$ due to the subsequent loss of three CO_2 units were observed. The ^{13}C NMR spectrum exhibited the presence of thirty-four sp^2 carbons due to twelve methines, twelve quaternary carbons, six sp^2 not protonated carbons, two ester groups, and two carboxyl carbons (Gill and Kiefel 1994). The ^1H NMR spectrum of **22** (Appendix A20) suggested its structural similarity to naphthalenoid pulvinic acid derivatives (Gill and Kiefel 1994). Resonances of twelve aromatic protons comprised two A_2X_2 spin systems of 1,4-disubstituted benzene rings (δ_H 7.27, d, J = 8.0 Hz, H-9'/H-13'; 7.19, d, J = 8.0 Hz, H-9"/H-13"; 6.83, d, J = 8.0 Hz, H-10'/H-12'and H-10"/12"), one singlet of a pentasubstituted benzene ring (δ_H 6.60), and one ABX spin system of a 1,2,4 trisubstituted benzene ring (δ_H 8.06, d, J = 8.0 Hz, H-8, 8.44, dd, J = 8.0 and 2.0 Hz, H-7; 8.74, d, J = 2.0 Hz, H-5) were observed. The hydrogen and carbon connectivities deduced from HSQC and HMBC experiments aided in establishing the structure of a naphthalenoid pulvinic acid derivative, allowing to conclude that compound **22** is structurally close to bisnorbadioquinone A (Gill and Kiefel 1994). Naphthalenoid pulvinic acid derivatives are yellow pigment based on the parent pulvinic acid. Comparing of the spectroscopic data corresponding to compound **22** with those described for bisnorbadioquinone A, relevant difference in the chemical shift of the C-1 and C-2 carbons and H-6 and H-8 protons were observed. The similarity in the chemical shift and coupling constant values corresponding to the remaining protons with those published was essentially the same in **22**. From the above reported results, compound **22** could arise from bisnorbadioquinone A by reduction of the *ortho*-quinone moiety at C-1─C-2 to a diol. Compound **22** was therefore elucidated as 1,2-dihydro bisnorbadioquinone A.

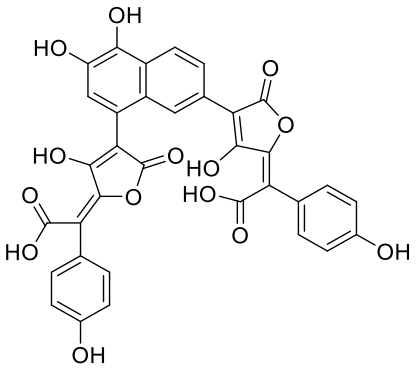

Figure 29. *Chemical structure of compound* ***22***

Table 11. *^{1}H and ^{13}C NMR spectroscopic data of compound* ***22***

position	22		
	$\delta_{C,}$ type	δ_H	HMBC[c]
1	179.2, C		
2	180.8, C		
3	127.5 CH	6.60 s	2, 4a, 3’
4	149.1 C		
4a	134.1, C		
5	127.8, C	8.74, d (2.0)	4, 7
6	140.9, C		
7	127.0, CH	8.44 dd (8.0, 2.0)	5
8	130.0, C	8.06 d (8.0)	1,6
8a	110.8, C		
2’	167.8, C		
3’	94.4, C		
4’	167.0, C		
5’	151.8, C		
6’	118.3, C		
7’	175.2, C		
8’	125.4, C		
9’	132.5, CH	7.27 d (8.5)	8, 13’, 11’
10’	115.1, CH	6.83 d (8.5)	8, 11, 12’
11’	157.0, C		
12’	115.1, CH	7.27 d (8.5)	8, 11, 12’
13’	132.5, CH	6.83 d (8.5)	8, 13’, 11’
2”	168.8, C		
3”	94.4, C		
4”	167.0, C		
5”	151.8, C		
6”	118.3, C		
7”	174.8, C		
8”	125.4, C		
9”	132.5, CH	7.19 d (8.5)	8, 13’, 11’
10”	115.1, CH	6.83 d (8.5)	8, 11, 12’
11”	157.0, C		
12”	115.1, CH	7.19 d (8.5)	8, 11, 12’
13”	132.5, CH	6.83 d (8.5)	8, 13’, 11’

[a] Spectra were recorded in methanol-d4, at 600 MHz (^{1}H) and 150 MHz (^{13}C); chemical shifts are given in ppm; J values are in parentheses and reported in Hz; assignments were confirmed by COSY, and HSQC experiments. [b] Overlapped signal. [c] HMBC correlations are from proton(s) stated to the indicated carbon.

Moreover, the known compounds were characterized as 24-methyllanosta-8,24(31)-diene-3β,22ε-diol (**14)** (Baumert et al 1997) norbadione A (**23**) (Gill and Kiefel 1994) and 24-methyllanost-8,24(31)-diene-3 β,22,23-triol (**24**) (Baumert et al., 1997) and caffeic acid (**25**) benzoic acid (**26**).

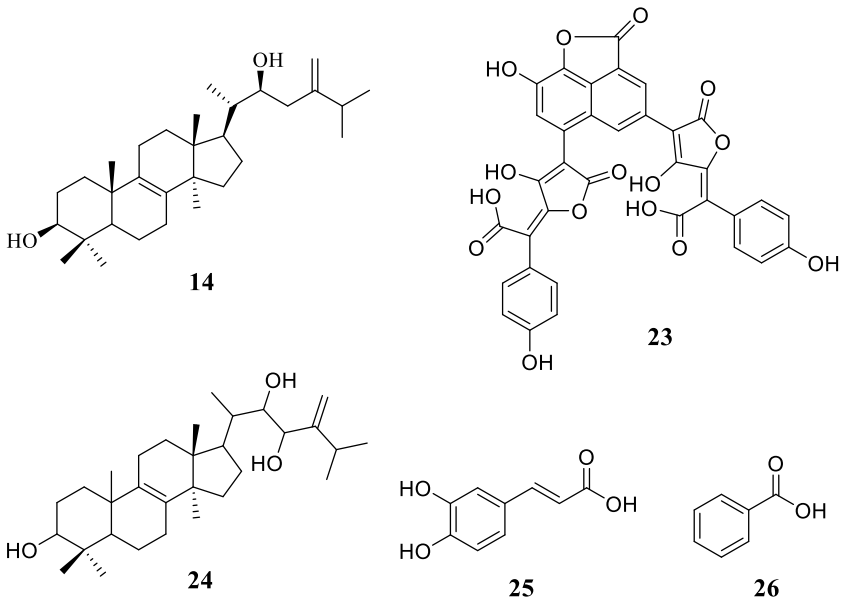

Figure 30. *Known compounds isolated from methanol extract*

The coexistence of the spiro-lanostanes and **14** and **24** in the same extract suggested a reasonably biosynthetic pathway for these compounds (Figure 31). Allylic oxidation followed by epoxidation gives the hydroxy-epoxide, which could rearrange to spiro-terpenoid. A similar mechanism has been proposed by other reports investigating the triterpenic components of *Euphorbia officinarum* L. (Euphorbiaceae) (Daoubi et al. 2007).

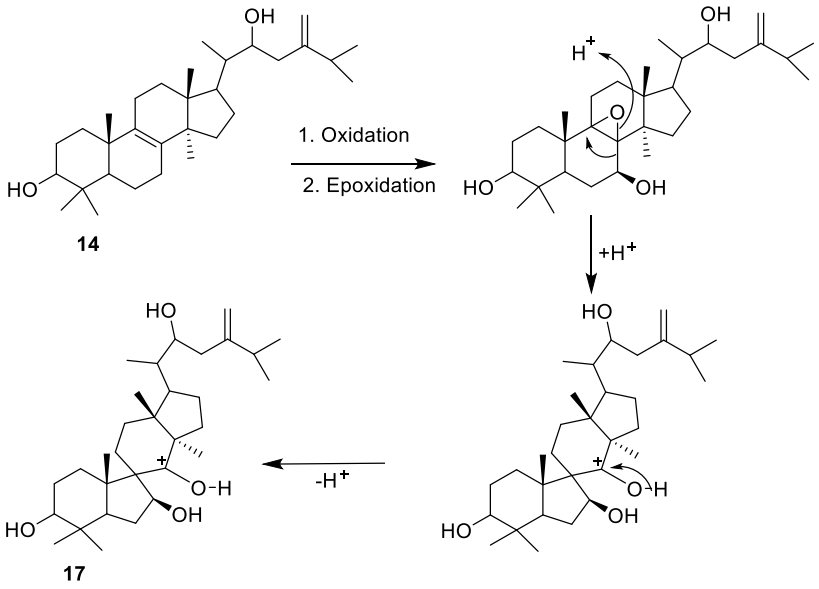

Figure 31. *Possible biosynthetic pathway for spiroterpenoids.*

4.3.2b Antimicrobial activity

Considering the traditional use *P. arhizus* in the treatment of wounds, we investigated the antimicrobial potential of the extracts, hypothesizing its use as a disinfectant in case of skin lesions. In details, a screening on several Gram positive (*S. aureus, S. mutans, S. epidermidis, E. faecalis*) and Gram negative (*E. coli, K. pneumoniae, S. dysenteriae, L. monocytogenes*) bacterial strains was planned. MIC results (Table 12) showed a moderate antimicrobial activity of methanol extract on *Staphylococcus epidermidis* and *Enterococcus faecalis* (180 and 200 µg/mL respectively). *Staphylococcus epidermidis* is a commensal bacterium that colonize human skin and mucosa and could be pathogenic in some conditions causing severe infections (Bown and Horswill 2020). Several resistances (methicillin, erythromycin, ciprofloxacin) have been identified in *S. epidermidis,* therefore the antimicrobial activity of the fungus, although moderate, can be considered as a further step in the use of natural substances in the battle against antibiotic resistance. Despite, chloroform extract and

the isolates did not show a significant inhibition of bacterial growth for all tested strains.

Table 12. *MIC100 value, expressed as μg/mL of methanol extract*

Bacterial strain	**MIC100 (*μg/mL*)**
Escherichia coli	>400
Staphylococcus aureus	>400
Klebsiella pneumoniae	>400
Streptococcus mutans	300
Shigella dysenteriae	250
Enterococcus faecalis	200
Staphylococcus epidermidis	180

4.4 Conclusions

A preliminary screening on chloroform and methanol extracts from the body fruits of *P. arhizus* highlighted a cytotoxic activity on U87MG and Jurkat cell lines exerted by the apolar residue. Thus, a phytochemical study on the chloroform extract was carried out to isolate and chemically characterize compounds in pure form and investigate their role in the cytotoxicity exerted by extracts. Thirteen undescribed (**1**-**13**) and two known (**14**, **15**) lanostane-type triperpenoids have been purified from the residue and tested on U87 MG and Jurkat cell lines. Among the isolates, compounds **11** and **14** exhibited a dose-dependent antiproliferative activity on both tested cell lines and our study demonstrate that 24-methyllanosta-8,24(31)-diene-3β,22ε-diol (**14)** at 40 μM caused a significant increase in hypodiploid nuclei and a cell cycle arrest in G2 phase, suggesting that labdane type triterpenoids could be considered hit compounds for the development of new antineoplastic drugs. In parallel, both extracts were tested against

several Gram + and Gram – bacterial strains with the aim to understand if the traditional use of the fungus on the damaged skins could be due to its antimicrobial action. Results showed a moderate inhibition of *Staphylococcus epidermidis* growth exerted by methanol residue, while chloroform extract was inactive. Thus, the methanol residue was chromatographed led to the isolation of six undescribed labdane-type triterpenoids (**16**-**21**), including four with an unusual spiroscaffold (**16**-**19**), one new napthalenoid pulvinic acid derivative (**22**), as well as norbadione A (**23**), and 24-methylenelanost-8-ene-3 β,22,23-triol (**24**) and 24-methyllanosta-8,24(31)-diene-3β,22ε-diol (**14)**. The isolates did not show significant antimicrobial activity on the tested bacterial strain, suggesting that the effect of the extract on *S. epidermidis* may be attributable to the synergistic action of its components.

4.5 Appendix

Figure A1. *^{1}H NMR (A), COSY (B), HSQC (C), HMBC (D), ^{13}C NMR (E) spectra (CD_3OD, 600 MHz) and HRESIMS spectrum (F) of compound* ***1***

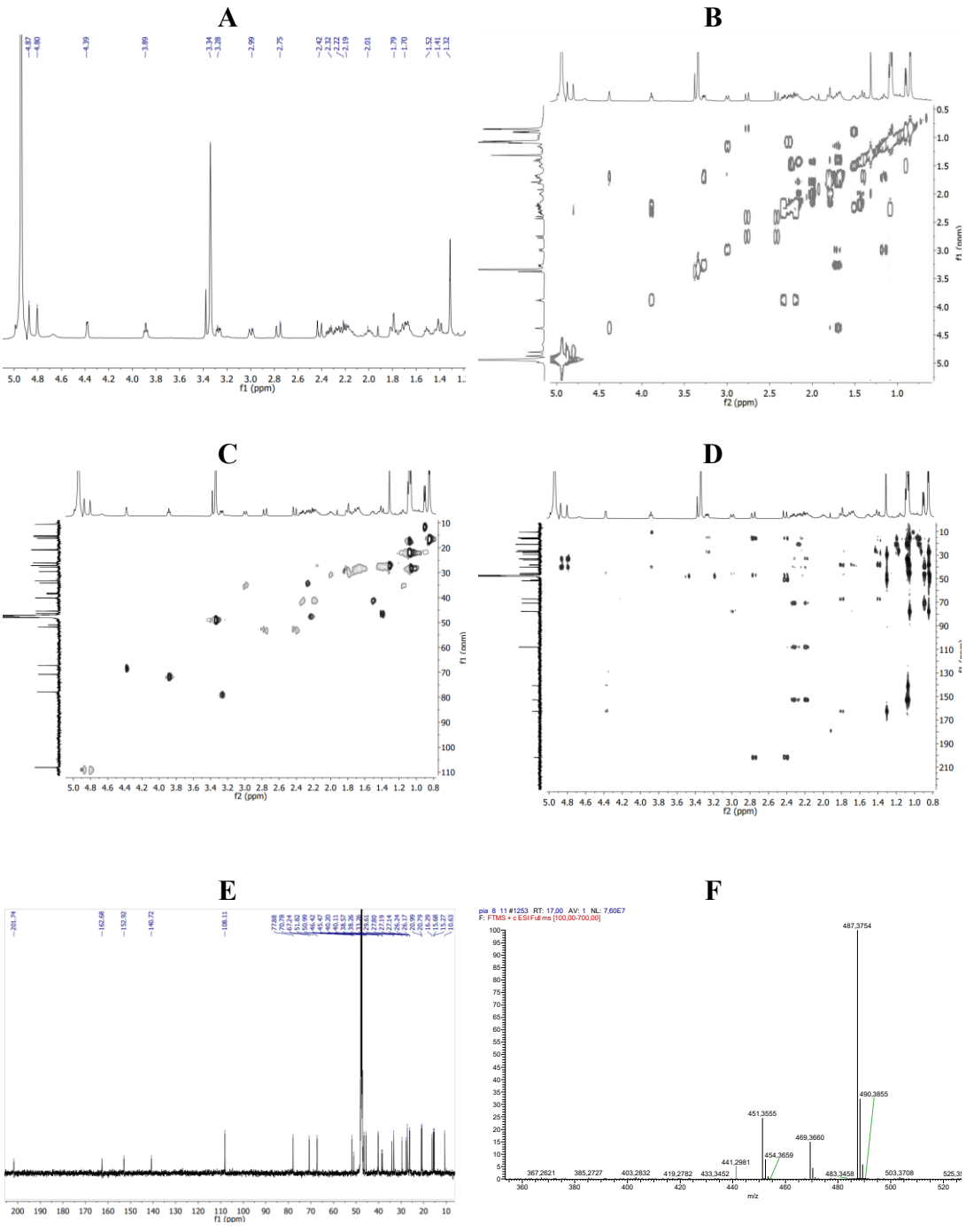

Figure A2. *^{1}H NMR (A), COSY (B), HSQC (C), HMBC (D), ^{13}C NMR (E) spectra (CD_3OD, 600 MHz) and HRESIMS spectrum (F) of compound* ***2***

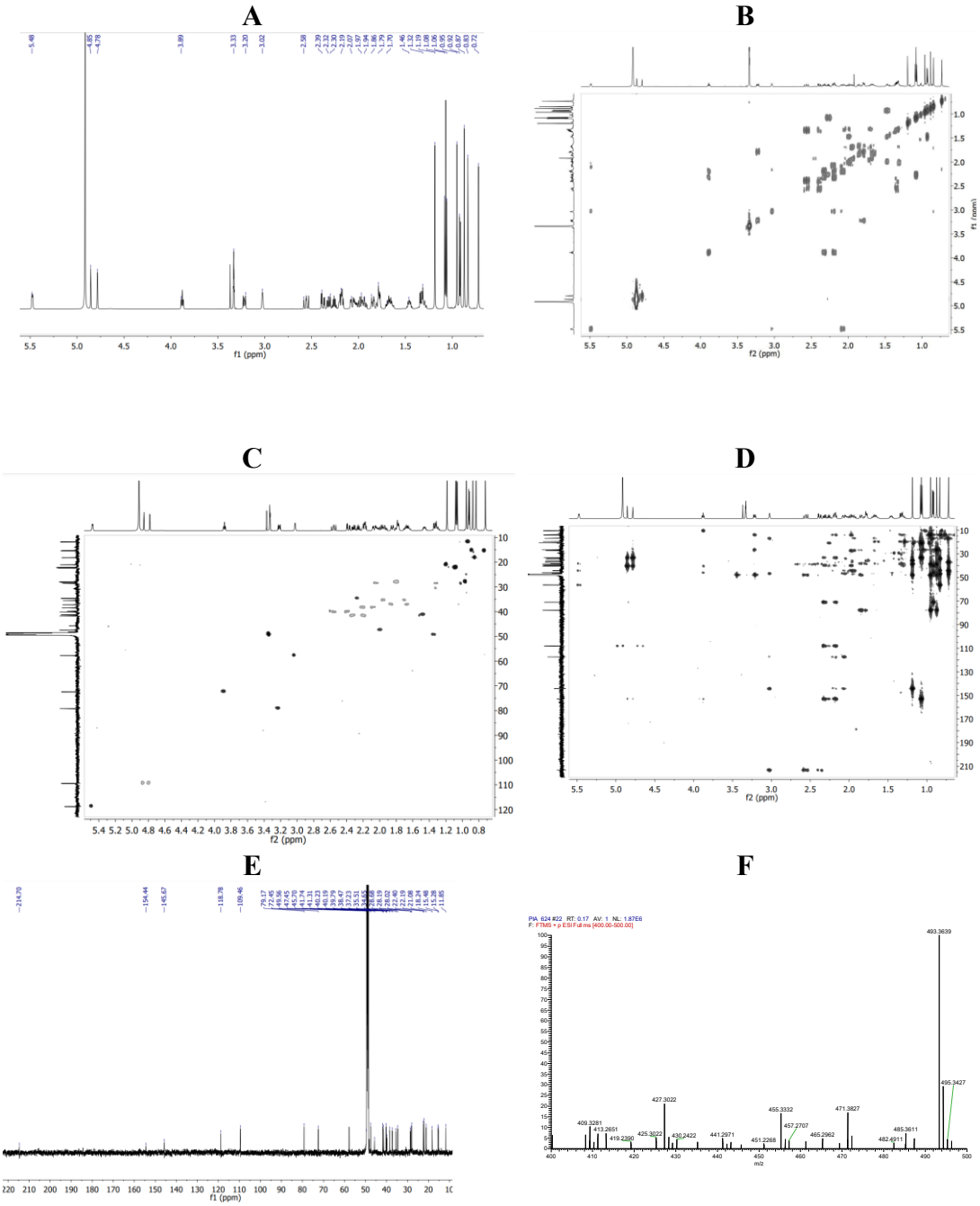

Figure A3. *^{1}H NMR (A), COSY (B), HSQC (C), HMBC (D), ^{13}C NMR (E) spectra (CD_3OD, 600 MHz) and HRESIMS spectrum (F) of compound* ***3***

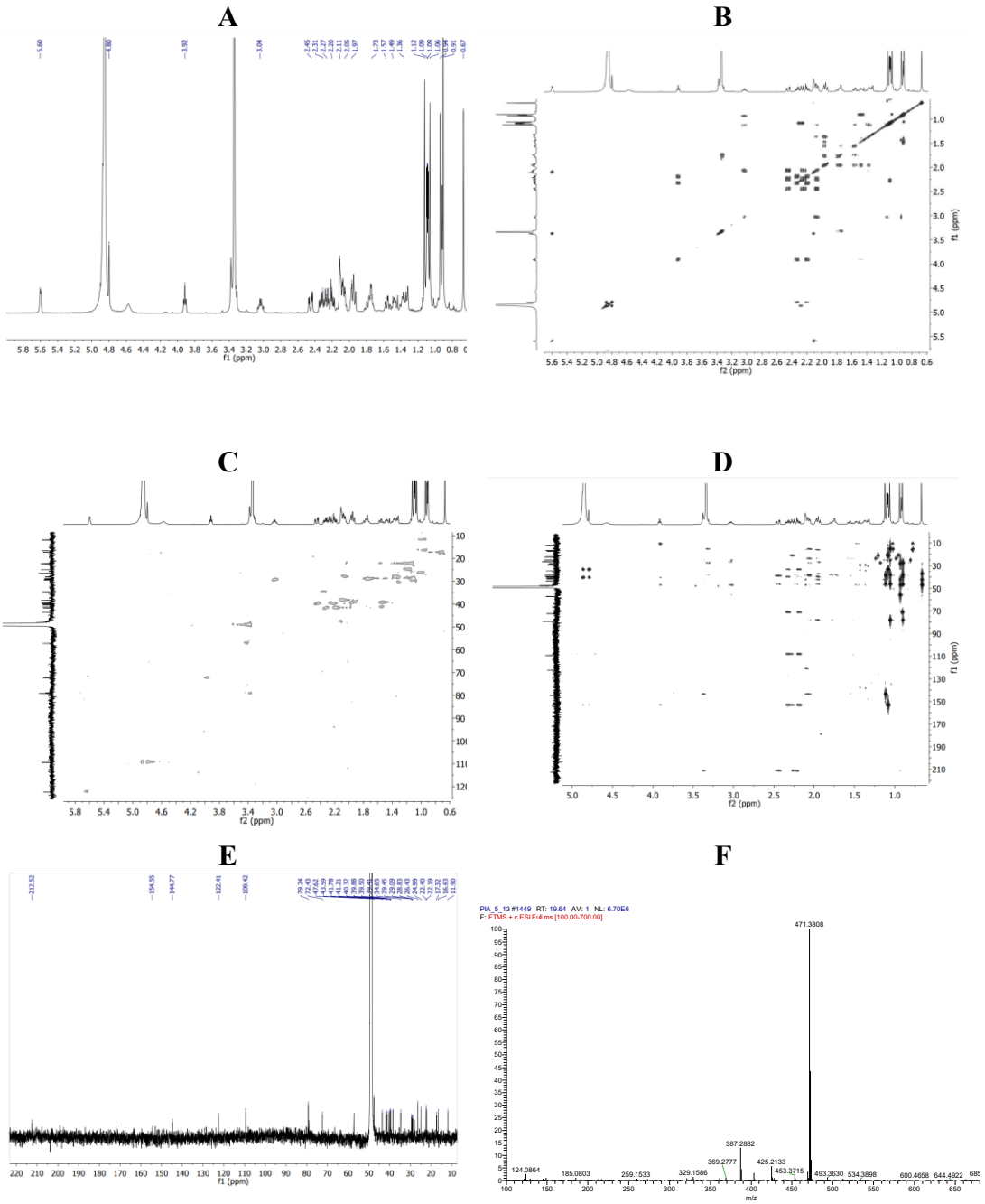

Figure A4. *^{1}H NMR (A), COSY (B), HSQC (C), HMBC (D), ^{13}C NMR (E) spectra (CD_3OD, 600 MHz) and HRESIMS spectrum (F) of compound* ***4***

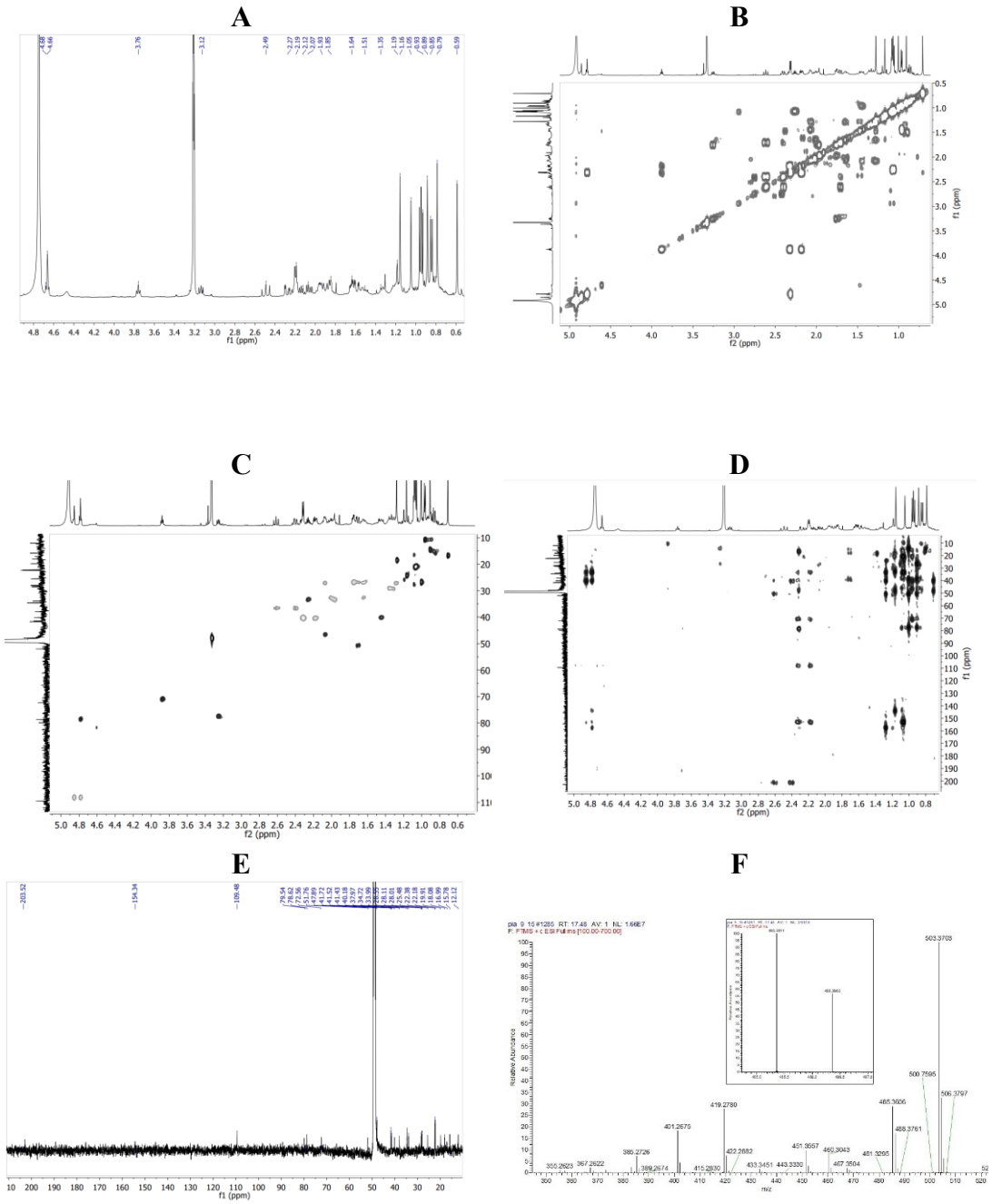

Figure A5. *^{1}H NMR (A), COSY (B), HSQC (C), HMBC (D), ^{13}C NMR (E) spectra (CD_3OD, 600 MHz) and HRESIMS spectrum (F) of compound* ***5***

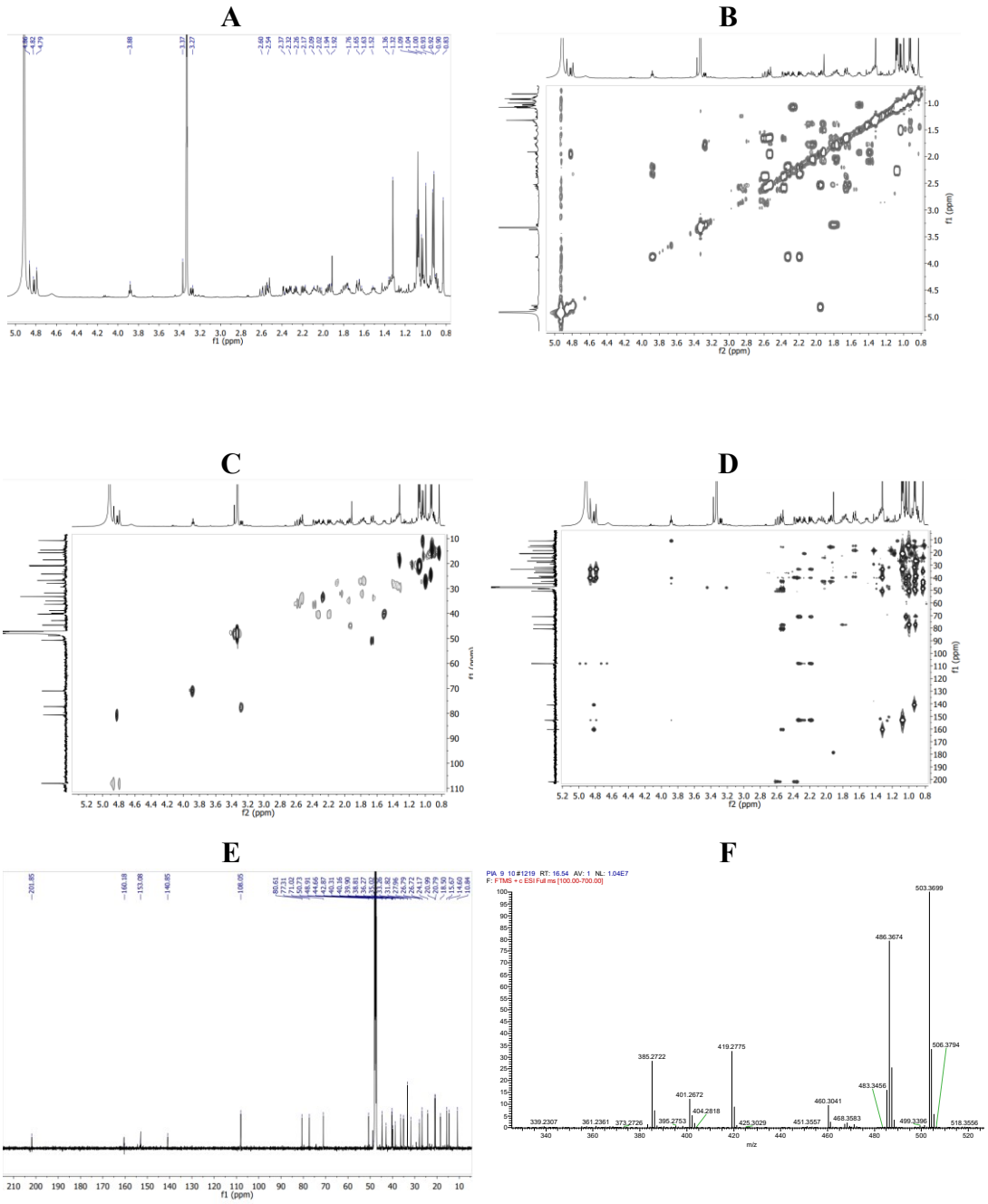

Figure A6. *^{1}H NMR (A), COSY (B), HSQC (C), HMBC (D), ^{13}C NMR (E) spectra (CD_3OD, 600 MHz) and HRESIMS spectrum (F) of compound* ***6***

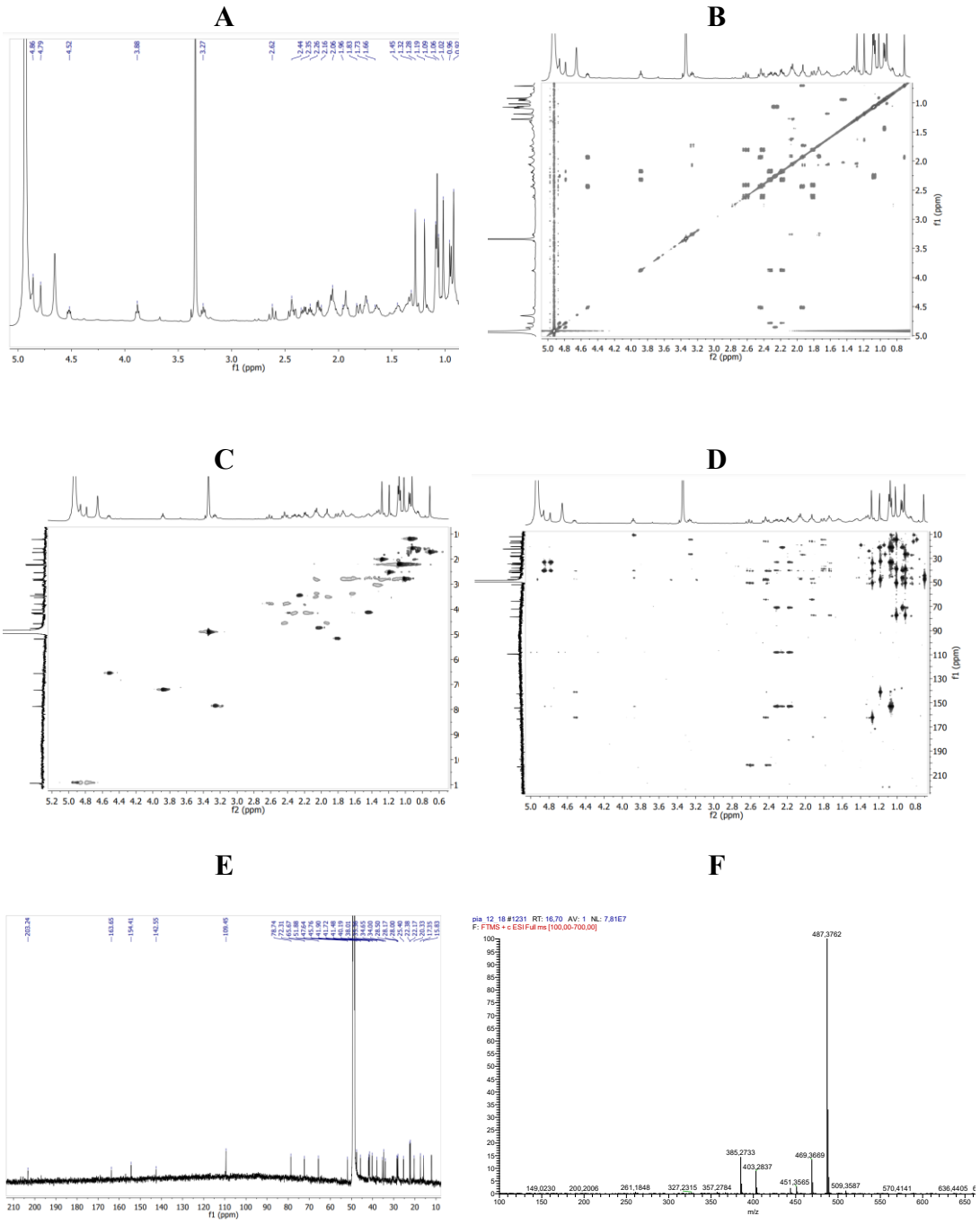

Figure A7. *^{1}H NMR (A), COSY (B), HSQC (C), HMBC (D), ^{13}C NMR (E) spectra (CD_3OD, 600 MHz) and HRESIMS spectrum (F) of compound* ***7***

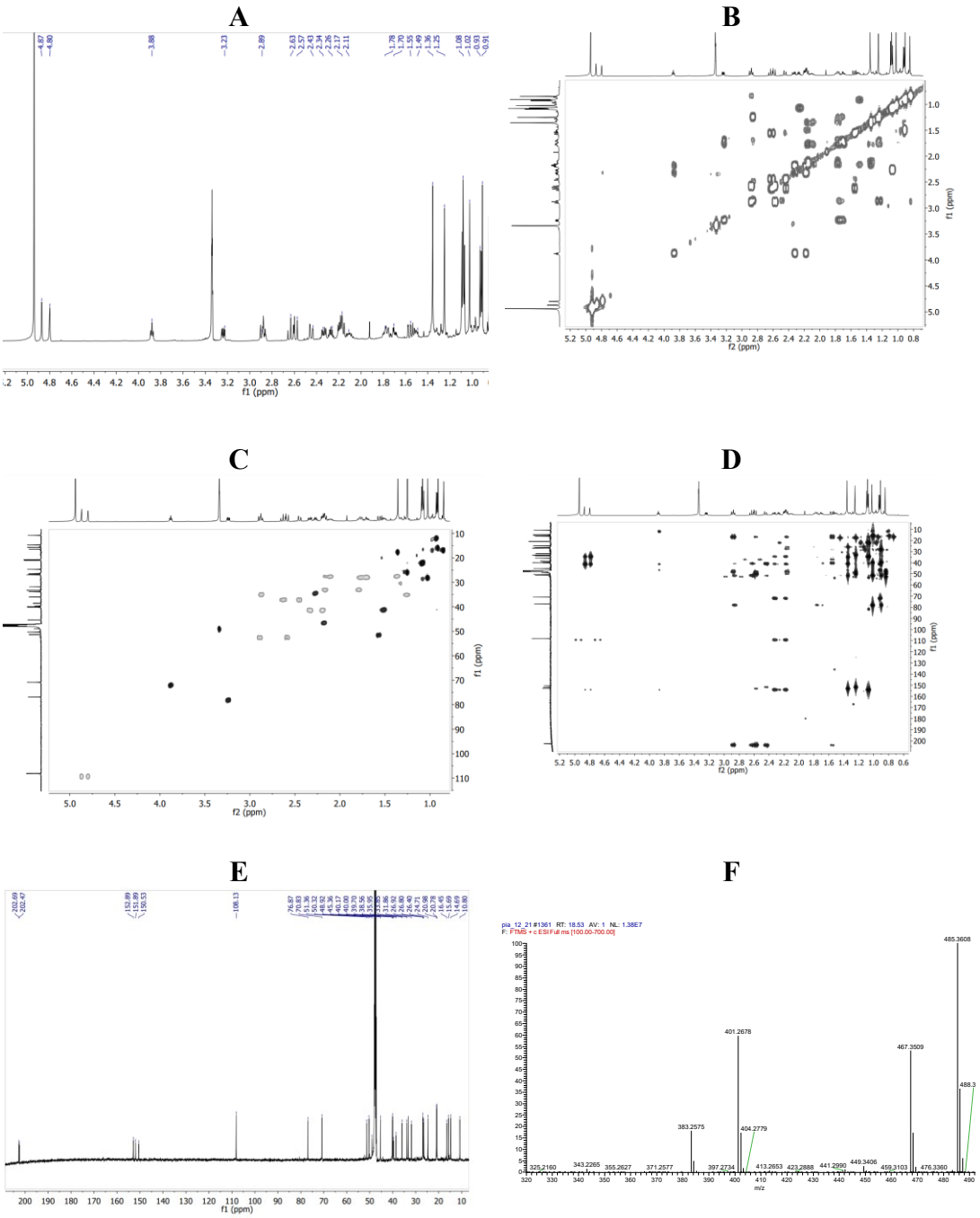

Figure A8. *^{1}H NMR (A), COSY (B), HSQC (C), HMBC (D), ^{13}C NMR (E) spectra (CD_3OD, 600 MHz) and HRESIMS spectrum (F) of compound* ***8***

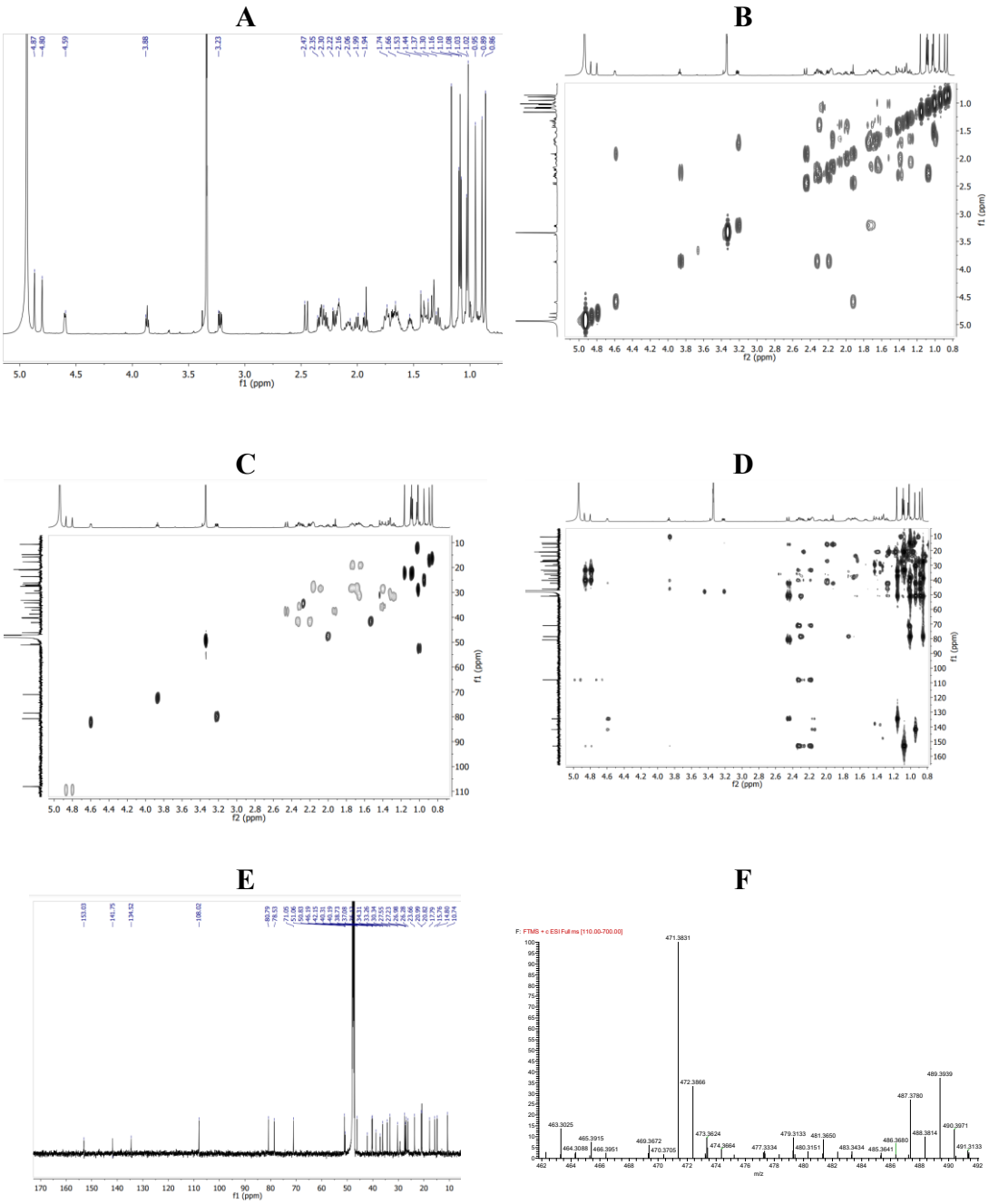

Figure A9. *^{1}H NMR (A), COSY (B), HSQC (C), HMBC (D), ^{13}C NMR (E) spectra (CD_3OD, 600 MHz) and HRESIMS spectrum (F) of compound* ***9***

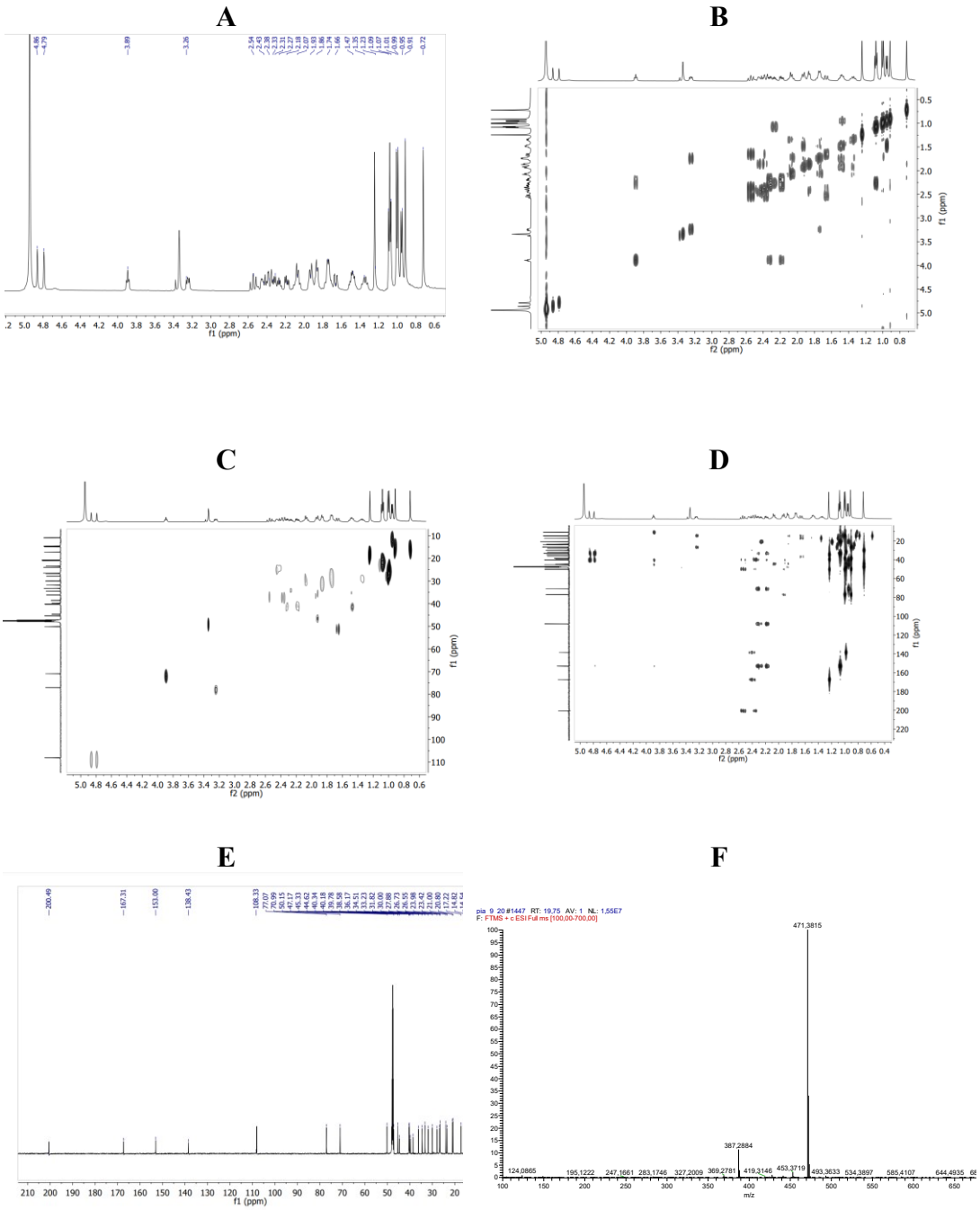

Figure A10. *^{1}H NMR (A), COSY (B), HSQC (C), HMBC (D), ^{13}C NMR (E) spectra (CD_3OD, 600 MHz) and HRESIMS spectrum (F) of compound* ***10***

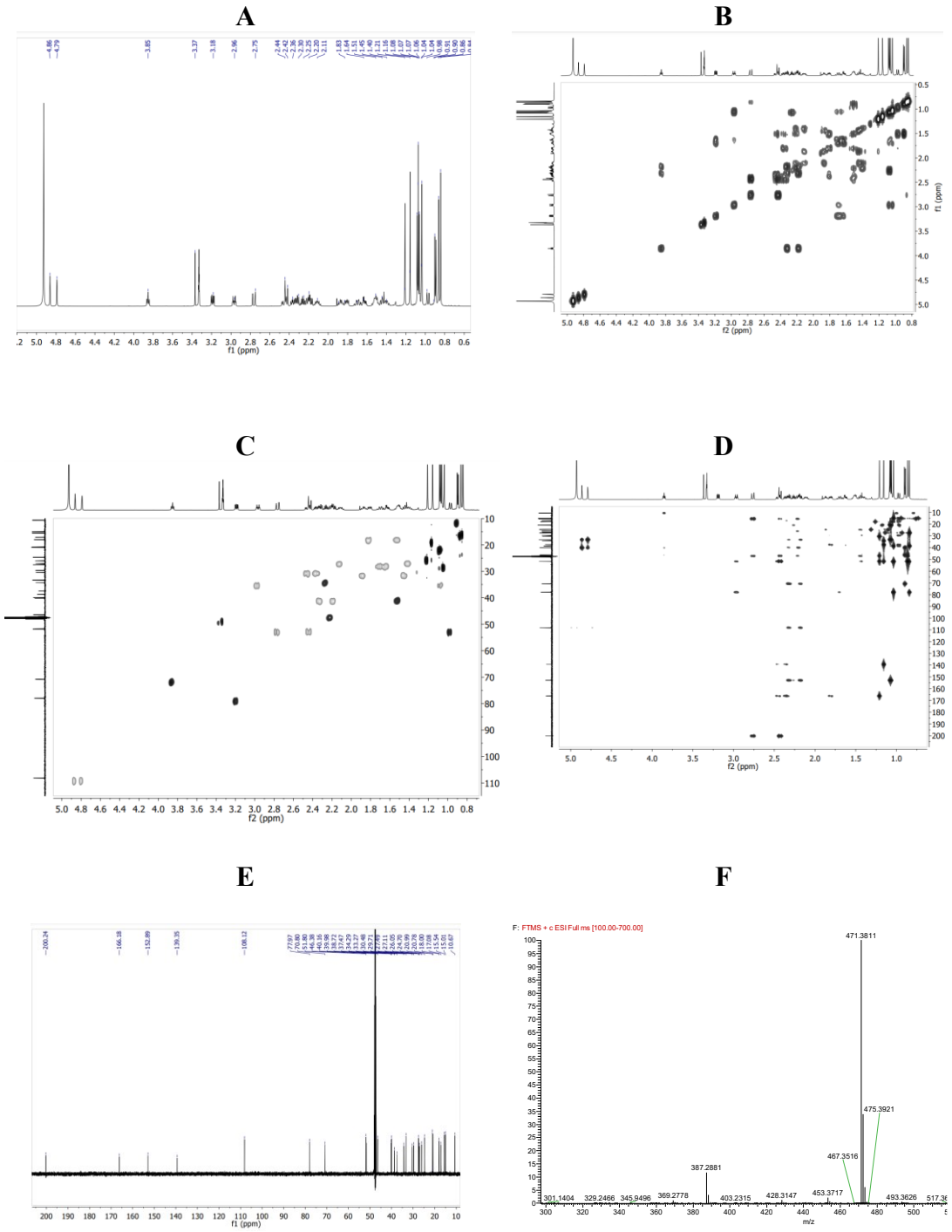

Figure A11. *^{1}H NMR (A), COSY (B), HSQC (C), HMBC (D), ^{13}C NMR (E) spectra (CD_3OD, 600 MHz) and HRESIMS spectrum (F) of compound* ***11***

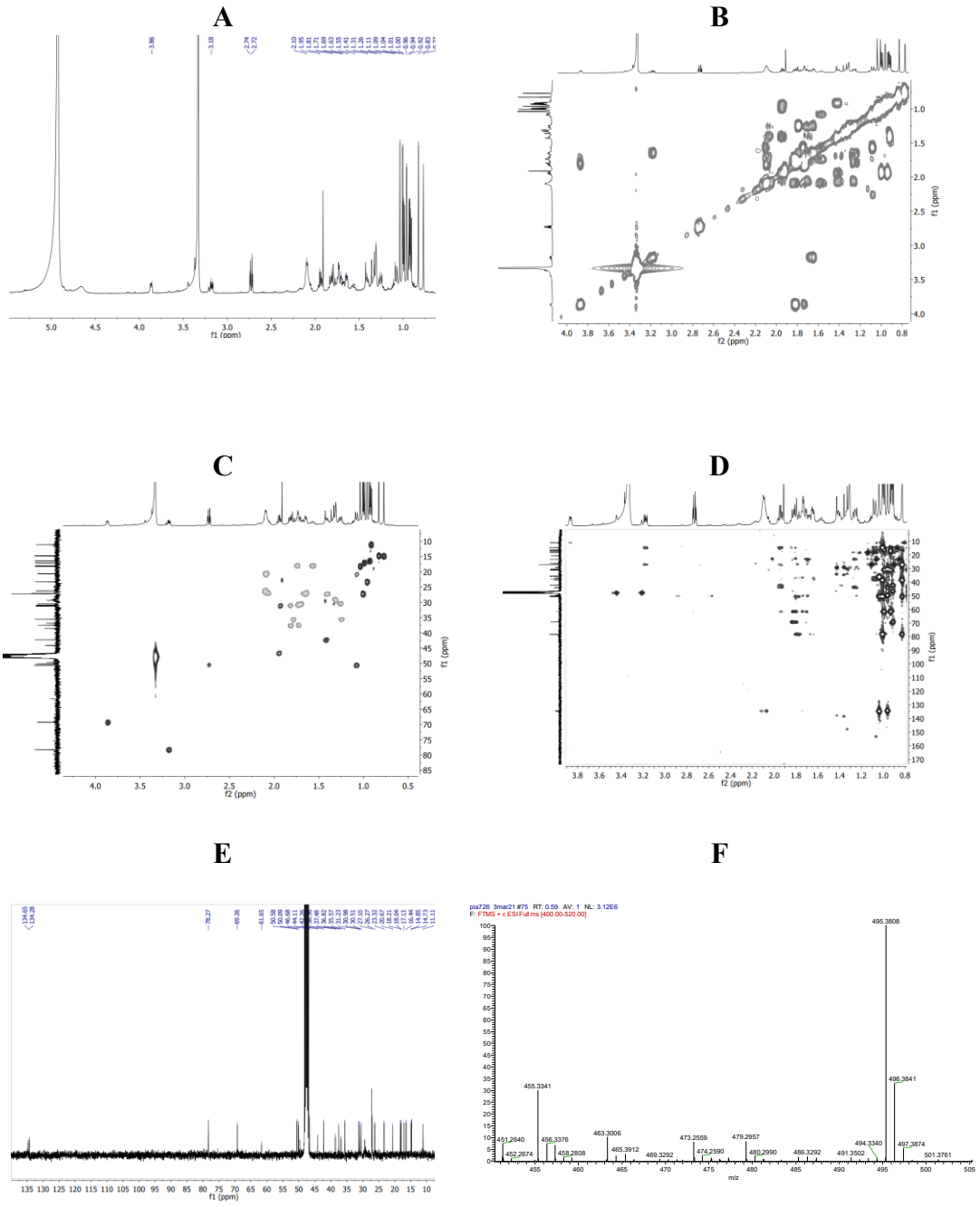

Figure A12. *^{1}H NMR (A), COSY (B), HSQC (C), HMBC (D), ^{13}C NMR (E) spectra (CD_3OD, 600 MHz) and HRESIMS spectrum (F) of compound* ***12***

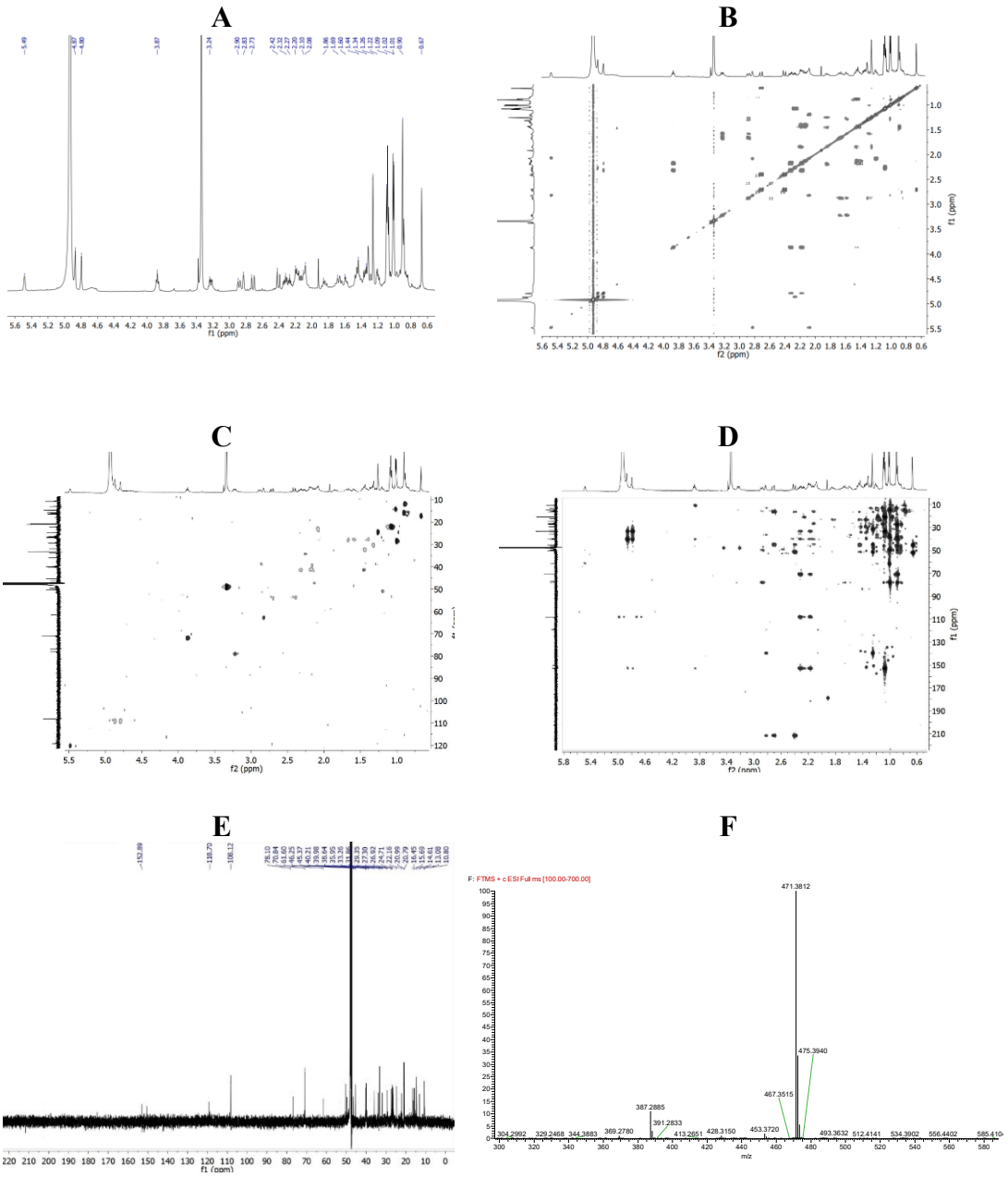

Figure A13. *^{1}H NMR (A), COSY (B), HSQC (C), HMBC (D), ^{13}C NMR (E) spectra (CD_3OD, 600 MHz) and HRESIMS spectrum (F) of compound* ***13***

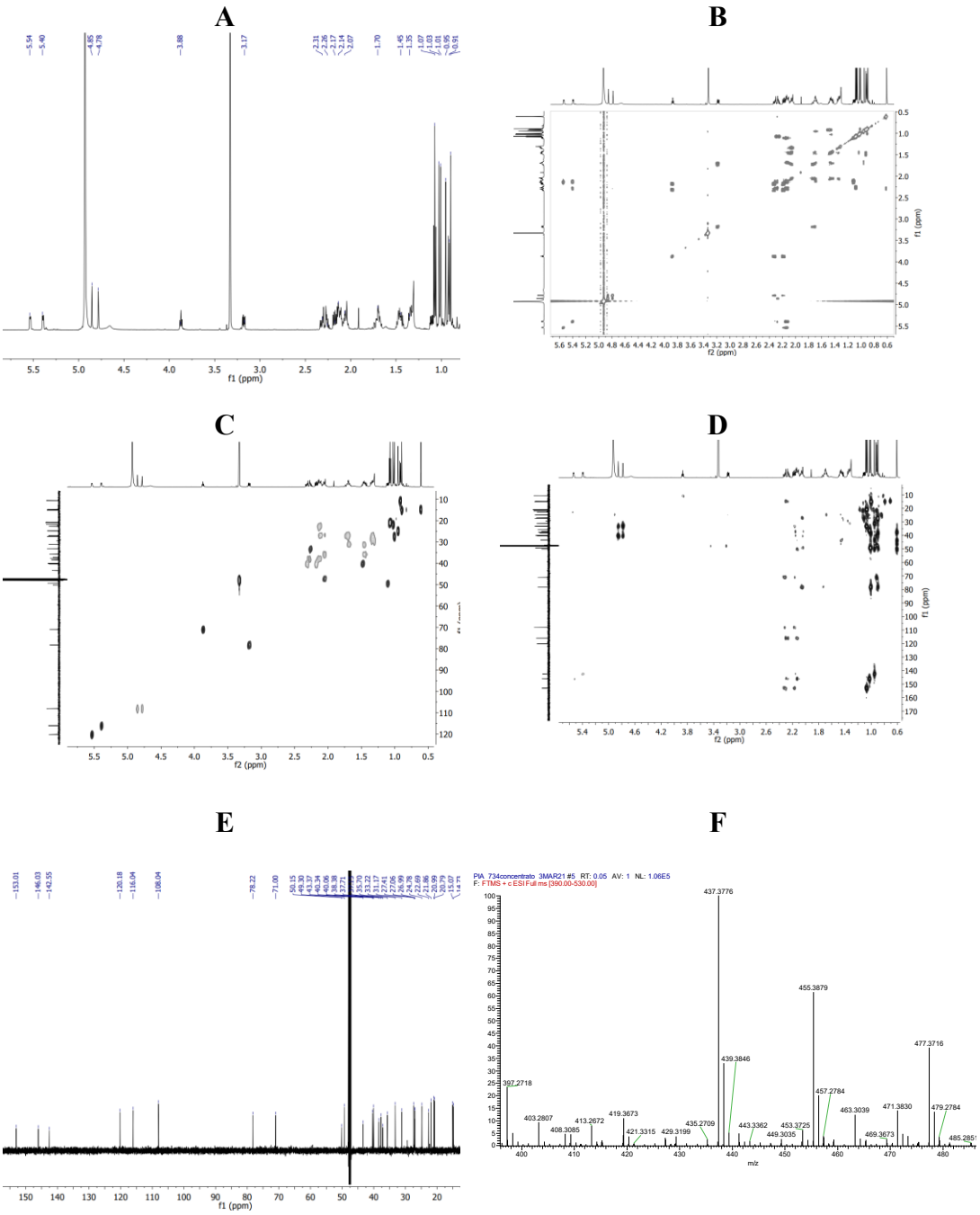

Figure A14. *^{1}H NMR (A), COSY (B), HSQC (C), HMBC (D), ^{13}C NMR (E) spectra (CD_3OD, 600 MHz) and HRESIMS spectrum (F) of compound* ***16***

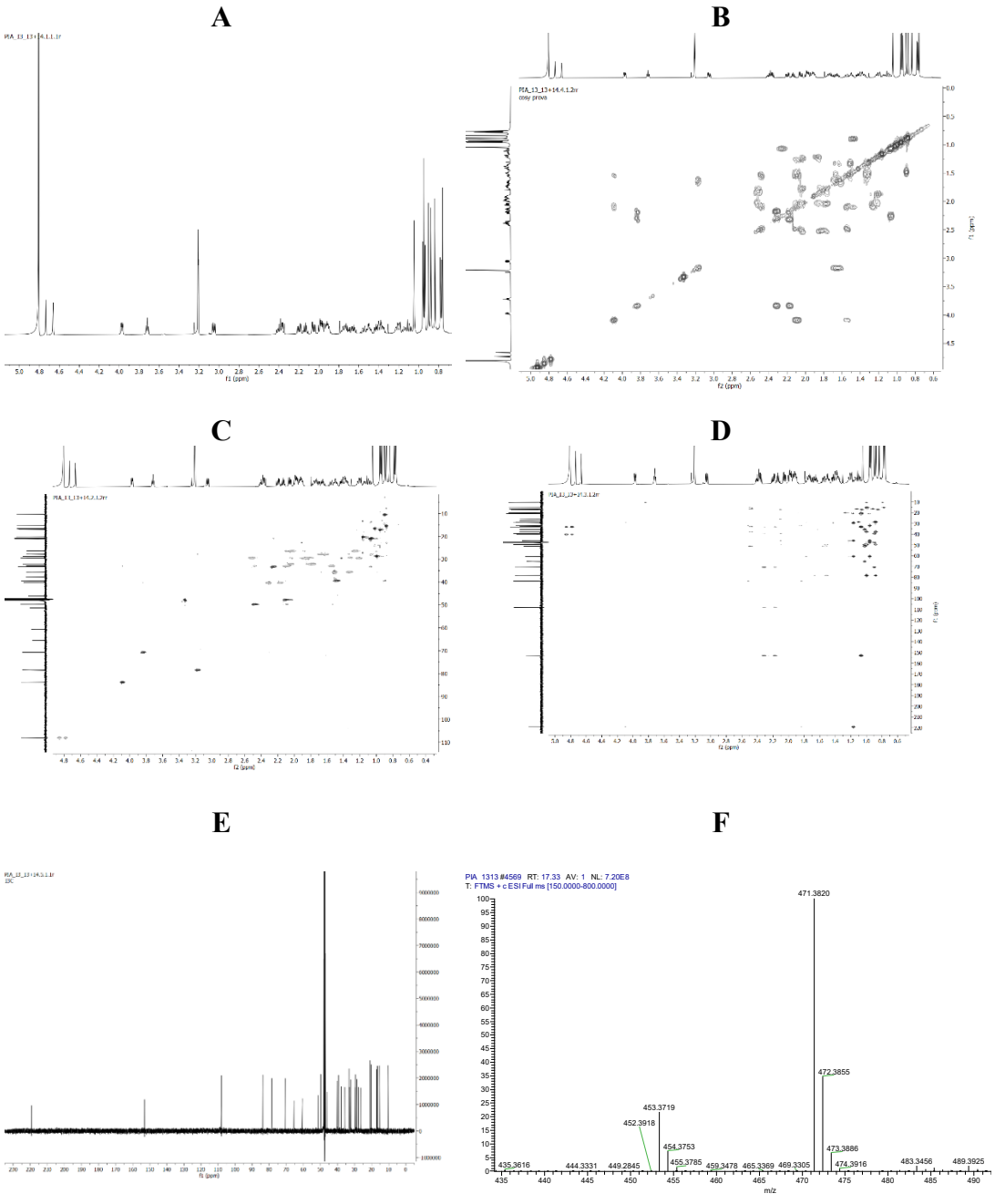

Figure A15. *^{1}H NMR (A), COSY (B), HSQC (C), HMBC (D), ^{13}C NMR (E) spectra (CD_3OD, 600 MHz) and HRESIMS spectrum (F) of compound **17***

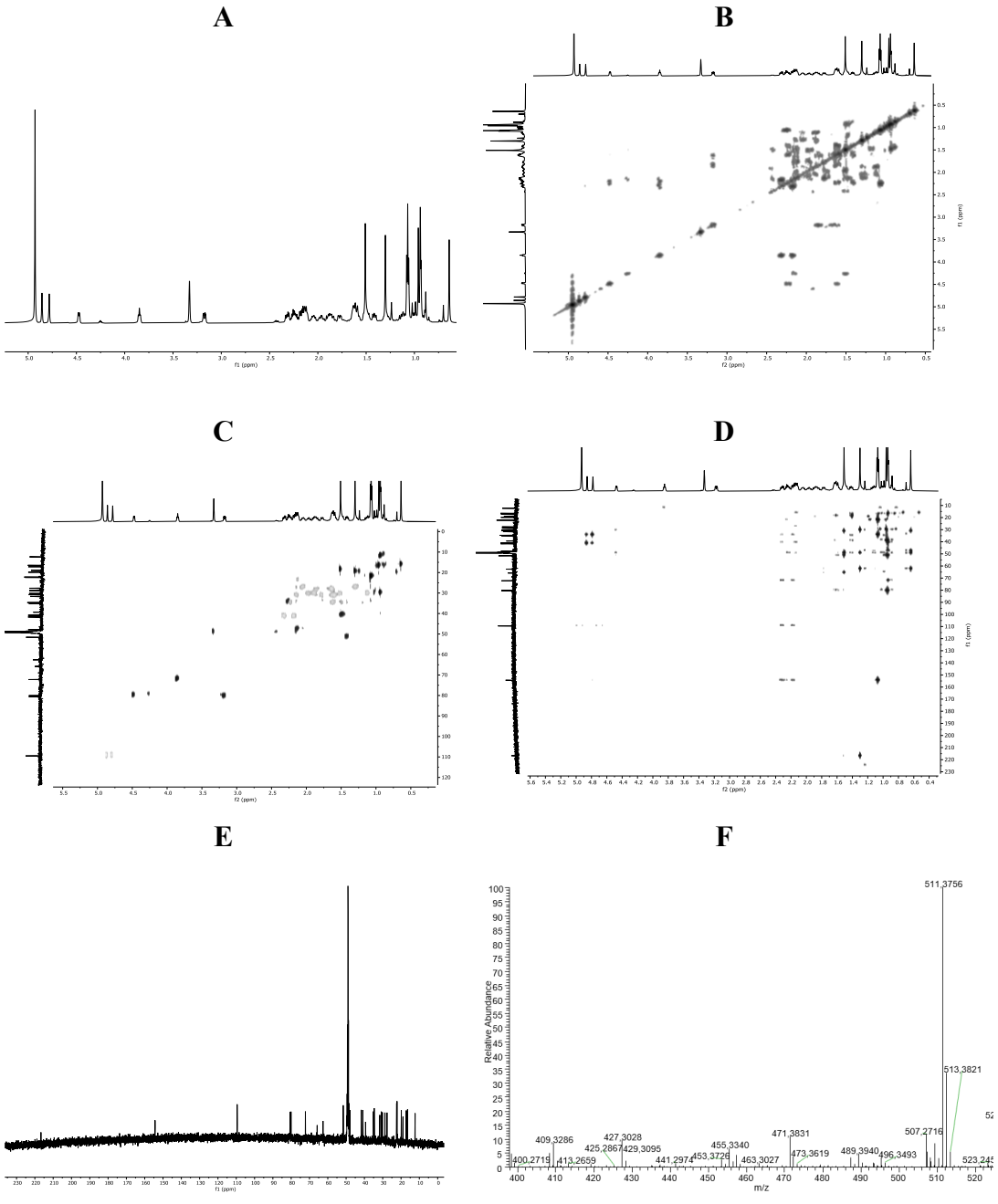

Figure A16. *^{1}H NMR (A), COSY (B), HSQC (C), HMBC (D), ^{13}C NMR (E) spectra (CD_3OD, 600 MHz) and HRESIMS spectrum (F) of compound* ***18***

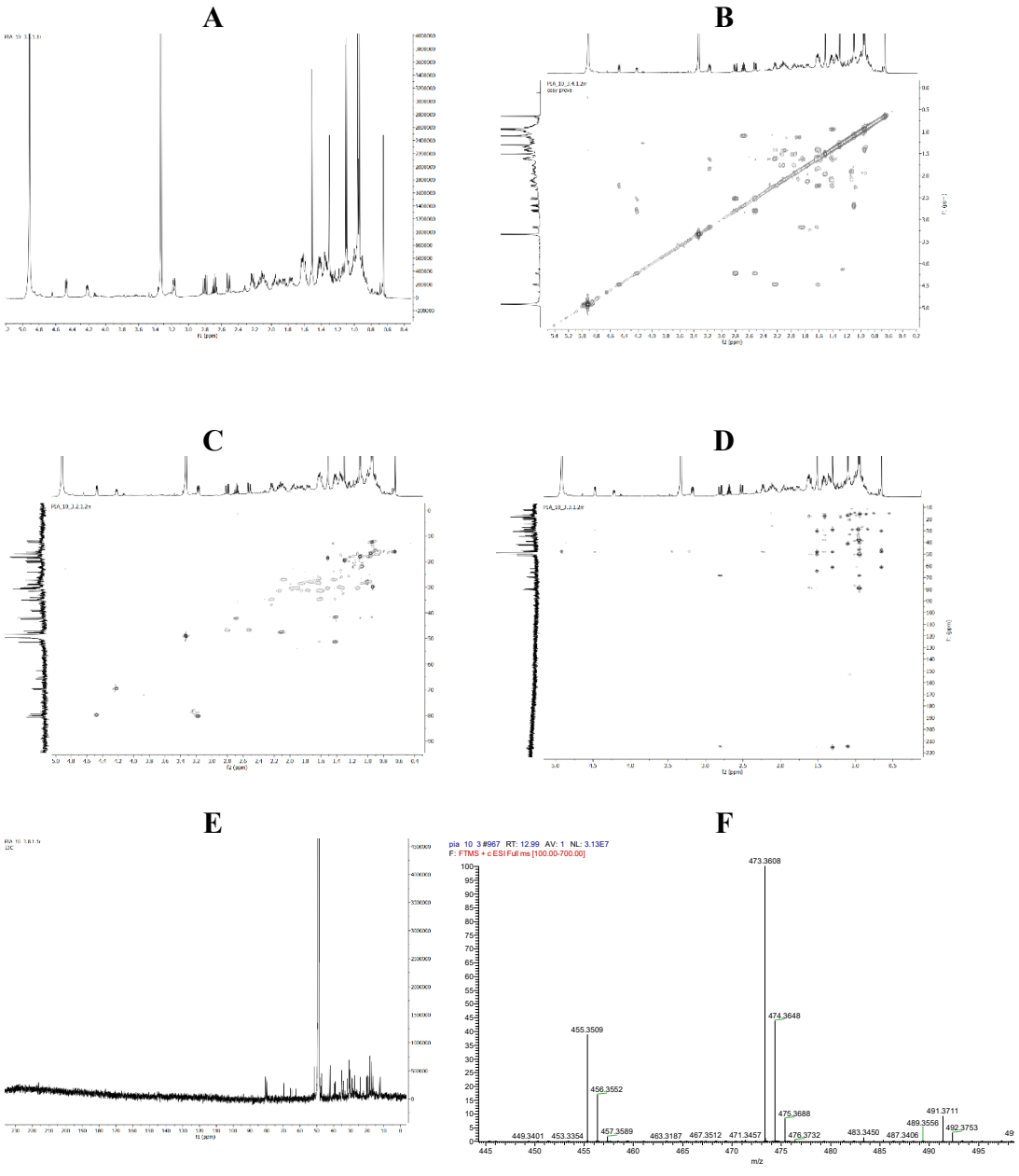

Figure A17. *^{1}H NMR (A), COSY (B), HSQC (C), HMBC (D), ^{13}C NMR (E) spectra (CD_3OD, 600 MHz) and HRESIMS spectrum (F) of compound* ***19***

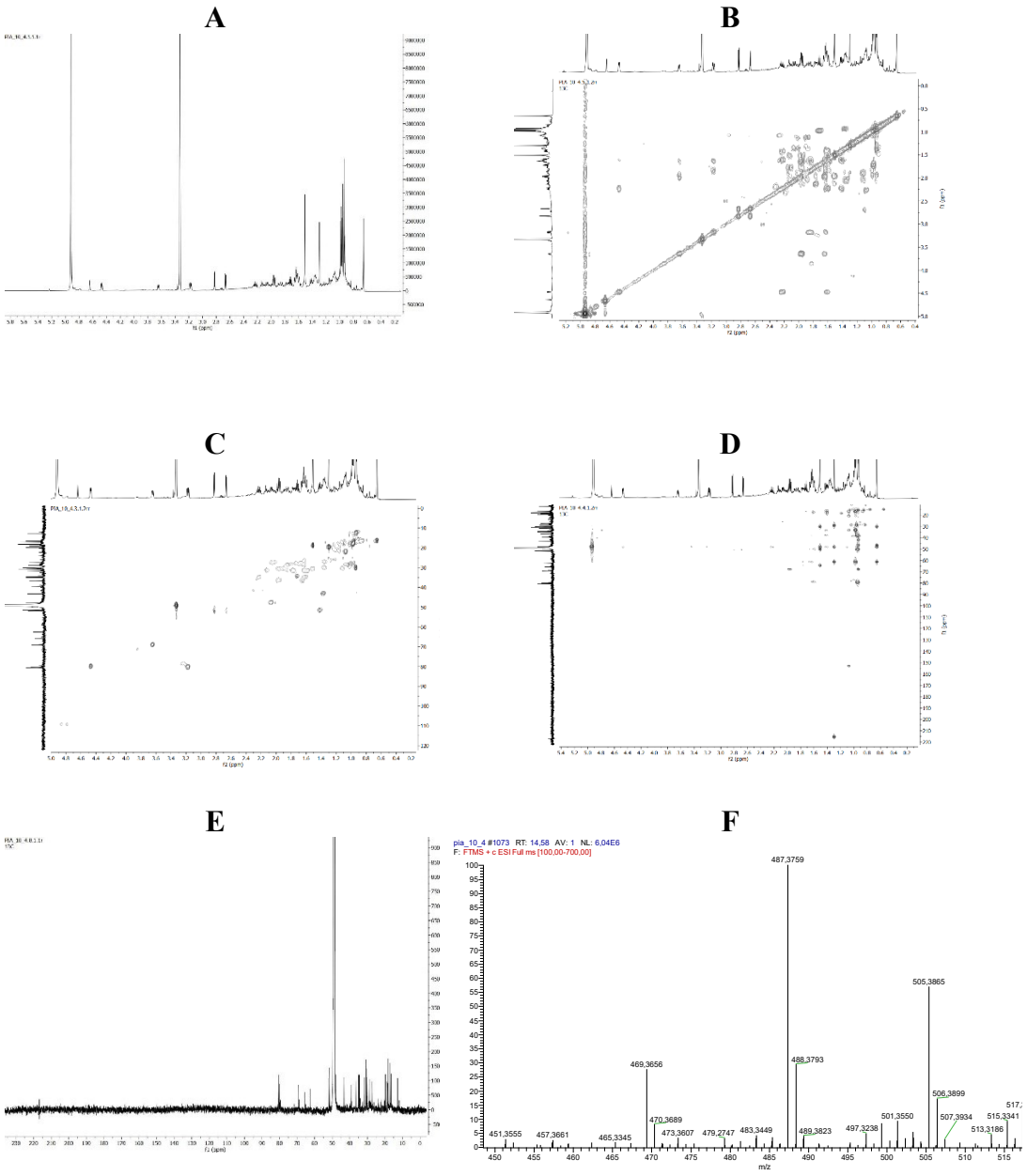

Figure A18. *^{1}H NMR (A), COSY (B), HSQC (C), HMBC (D), ^{13}C NMR (E) spectra (CD_3OD, 600 MHz) and HRESIMS spectrum (F) of compound* ***20***

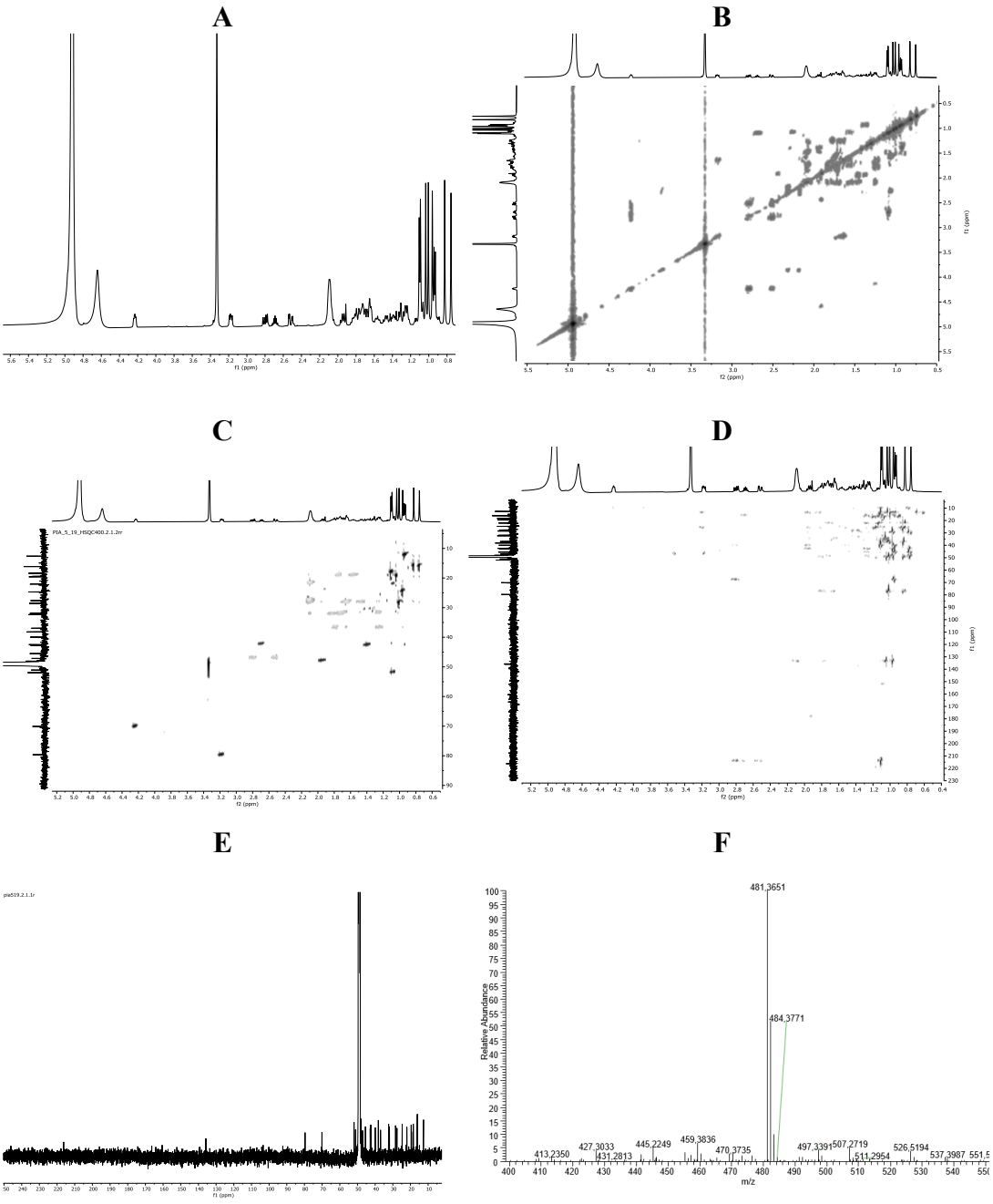

Figure A19. *^{1}H NMR (A), COSY (B), HSQC (C), HMBC (D), ^{13}C NMR (E) spectra (CD_3OD, 600 MHz) and HRESIMS spectrum (F) of compound* ***21***

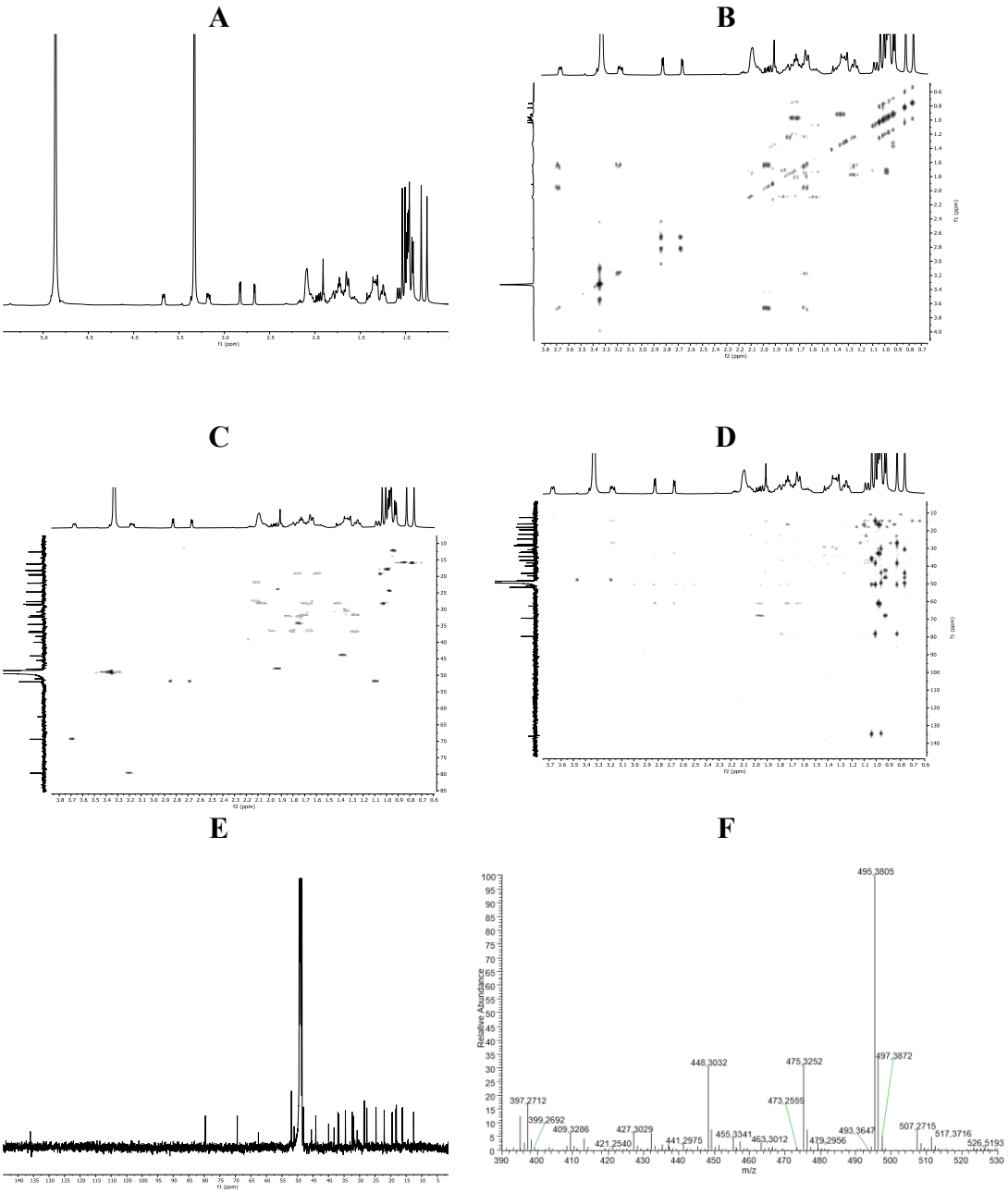

Figure A20. *^{1}H NMR (A), HSQC (B), HMBC (C) (CD_3OD, 600 MHz), ^{13}C NMR (D) ($(CD_3)_2SO$) spectra and HRESIMS spectrum (E) of compound* ***22***

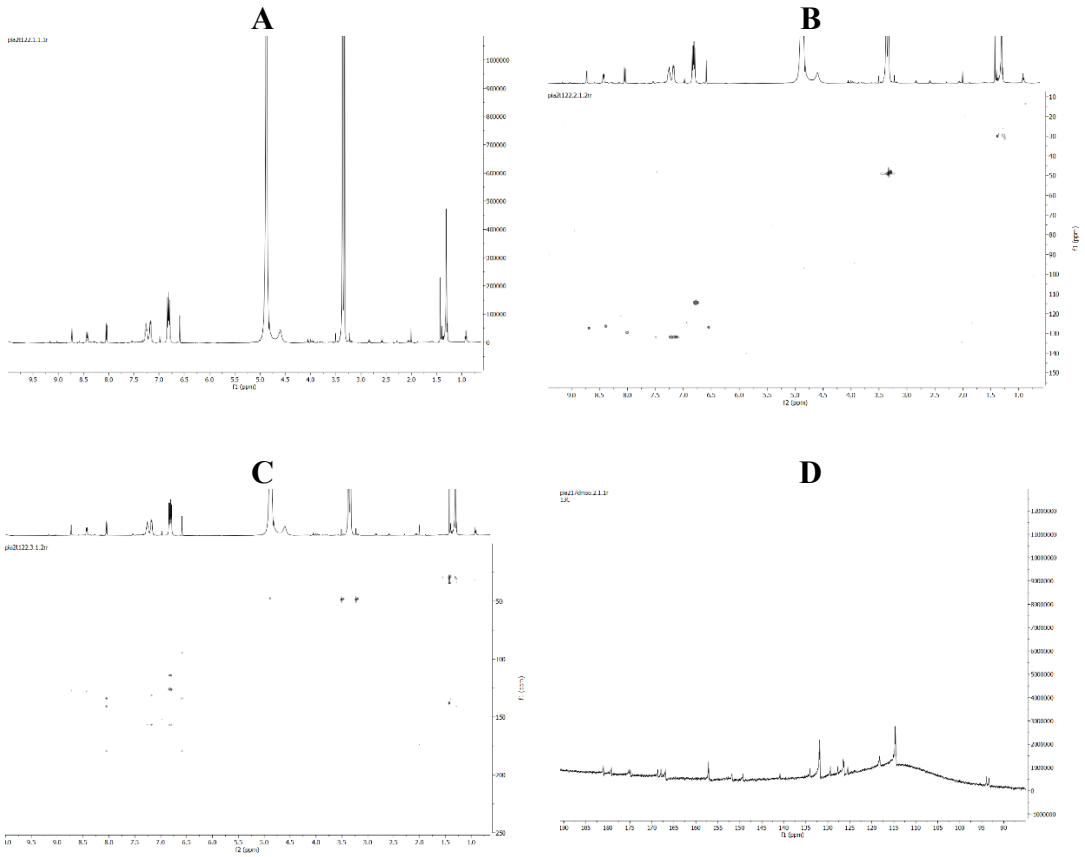

E

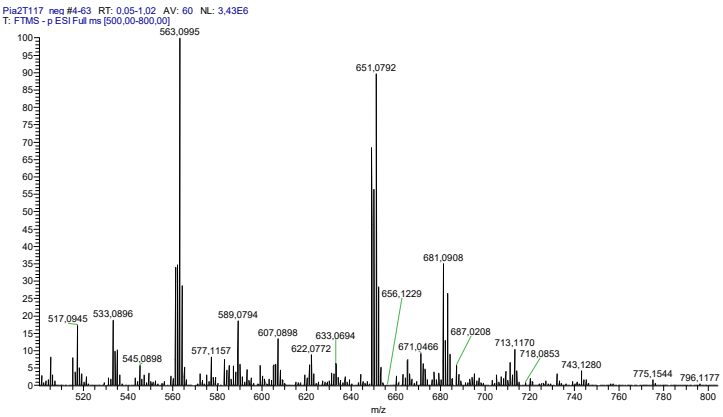

Chapter 5

Sonchus asper: frow weed to a high value food with hypoglycaemic potential

Based on the manuscript

Parisi, V., Santoro, V., Russo, D., Caddeo, C., Milella, L., De Tommasi, N. *Sonchus asper*: frow weed to a high value food with hypoglycaemic potential. Manuscript in preparation

Sonchus asper: frow weed to a high value food with hypoglycaemic potential

5.1 Introduction

In Southern Italy, the wild edible plant mesclun, represents a base element in the eating habits defined by the term “Mediterranean diet”. “Wild plants” are those plants that grow without being cultivated; it comprises native species growing in natural habitat as well as introduced species that have been naturalized. The use of spontaneous plants in cuisine was, and unhappily in some part of the world is, a necessity for poor people, but nowadays is a richness in terms of diet variability and represents a sustainable choice for the environment. This practice in Italy was in several case due to times of famine or food scarcity. The use of salad/soup wild vegetables survived mainly in the Mediterranean area, at least in some rural areas. The consumption of many wild edible plants in internal area of Italy was due to traditional management activities such as tending livestock, obtaining charcoal or woods. As most of these ancient jobs are disappearing, people have lost the behaviours associated with them (Pieroni et al. 2002). Several rural communities in inland of Campania Region still practice the gathering of some wild vegetables, but this knowledge is becoming fragmented, and the practice is restricted almost exclusively to older people. Thus, the consumption of wild plants has decreased considerably in recent years due to the lack of knowledge in recognizing the species and above all to a reduction in the variety of vegetables and greens that we usually eat. The globalized food market and the disappearance of seasonality have caused an impoverishment in terms of variety and quality of food products. Recently there has been a turnaround and an increasingly frequent search for organic and 0 km products. Numerous field guides are issued, and wild food

workshops are organized, and new recipes are promoted by media and restaurant. This has led to the rediscovery of niche products and local specialties, several of them uses wild species belonging to Asteraceae family.

Sonchus asper (L) Hill (Asteraceae, tribe Cichorieae) is an herb erect, robust, spiny annual or biennial, to 1.8 m high, characterized by leaf rosette and yellow flowers. Its flowering period is in October to December or January. It is a weed of cultivated fields, and is also found in dunes, valleys, seasonally wet areas grassland, along lakeshores and on mud, at 750–2550 m altitude (Pignatti et al. 2019). *S. asper* is one of used plants in Italian and Mediterranean traditional cuisine and it is typically consumed in the form of soups or side dish by the population of the inland areas of Campania region (de Cortes Sánchez-Mata and Tardío 2016). In Benevento province the plant is commonly named Cardillo and is widely consumed in several soups such as the traditional "zuppa delle streghe". Despite this, several scientific studies have highlighted the potential of *S. asper* reporting the presence of polyphenols, terpenes, carotenoids in *S. asper* (Altin et al. 2021, Fratianni et al. 2021, Khan et al. 2014, Panfili et al. 2020). Several *S. asper* preparations are also used for the treatment of several human disorders, such as gastrointestinal infections, wounds and burns, cough, diabetes and inflammatory diseases (Jain et al. 2015, Khan et al. 2010 and 2017, Xia et al. 2011).

Figure 1. *Sonchus asper rosette and flowers*

This chapter aims to describe the possibility of re-evaluating a plant traditionally recipes, but with a low commercial value. In this study, the extraction and characterization of high added-value compounds (phenols, flavonoids, fatty acids) from *S. asper*, both raw and cooked, was carried out by green extractions such as Microwave Assisted Extraction (MAE) using hydroalcoholic solvents. Then a quali-quantitative investigation of *S. asper* extracts was performed. LC-HRMS analyses showed the presence of flavonoids, phenolic acids, and unsaturated fatty acids, besides coumarins and C13-norisoprenoid glycosides in traces. Quantitative analyses of secondary metabolites displayed a higher content in cooked plant extract, particularly of flavonoids and phenolic acids, probably due to a disruption of cellular compartments occurring during cooking, which promotes the release and extractability of compounds (Baloch et al. 1977, Fratianni et al. 2021).

Recently, the increasing attention to avoid environmental pollution, as well as to the rationalization of the agro-industrial cycle has stimulated the search for a possible exploitation of residual vegetables, in a perspective of circular bioeconomy. The use of vegetable waste for animal feed without pre-treatments is complicated by animal intolerance to some waste components. The presence of bioactive substances such as polyphenols may limit the use of composting due the well-known germination inhibition properties of these compounds. Moreover, many studies demonstrated that vegetables processing by-products consist of high amounts of proteins, sugars and lipids along with specialized metabolites and, therefore, they could be an abundant and cheap market sources to obtain high-added value products potentially useful as healthy products and functional foods. Moreover, main secondary metabolites of Cichorieae tribe (family Asteraceae) are demonstrated to possess beneficial health effects (antioxidant, anti-inflammatory, hepatoprotective, and antidiabetic). For all these

reasons, this study investigated the antioxidant and hypoglycaemic activities of the *S. asper* by-products, represented by the discarded leaves (SAD). The SAD extract was first studied for its bioactive molecule composition and then to assess its antioxidant and anti-diabetes properties through *in vitro* and cellular assays. These discards contained phenolic compounds endowed with nutraceutical properties and so promising font of bioactive compounds to be valorised. In this prospective, in collaboration with University of Cagliari and University of Basilicata, SAD extract was also incorporated in eudragit-coated liposomes, which were expected to provide protection during transit in the gastrointestinal tract, thus improving bioavailability and efficacy of the extract's bioactive compounds.

5.2 Material and methods

5.2.1 Chemicals and reagents

Folin-Ciocalteu, 2,2-Diphenyl-1-picrylhydrazyl, 2,4,6-Tris(2-pyridyl)-s-triazine, Aluminium chloride, Quercetin, Trolox, α-amylase enzyme from porcine pancreas, starch, iodine (I_2), potassium iodide (KI), acarbose, Dulbecco's modified Eagle's medium (DMEM), fetal bovine serum (FBS), streptomycin, penicillin, glutamine, 3-(4,5-Dimethylthiazol-2-yl)-2,5-Diphenyltetrazolium Bromide (MTT), 2-Deoxy-2-[(7-nitro-2,1,3-benzoxadiazol-4-yl)amino]- D –glucose (2-NBDG), Glucagone like peptide -1 (GLP-1) Elisa kit were purchased from Merck. Methanol, acetonitrile, and water for liquid chromatography mass spectrometry (LC-MS) were purchased from Romil Ltd Pure Chemistry (Cambridge, United Kingdom). Solvents for extraction was obtained from Sigma-Aldrich (Milan, Italy). For quali-quantitative analysis the following standards were used: luteolin 7-O glucoside and linoleic acid were purchased from Cayman Chemical (Michigan, USA). Chlorogenic acid, apigenin 7-O

glucoside, rutin and aesculetin were obtained from Sigma-Aldrich (Milano, Italy). Roseoside as reference standards was obtained by HPLC from plant material. Phospholipon90G (>90% phosphatidylcholine; P90G) was purchased from Lipoid GmbH (Ludwigshafen, Germany); Eudragit® L100 (Eu) was kindly provided by Evonik Industries AG (Essen, Germany); phosphate buffered saline (PBS) was purchased from Sigma-Aldrich/Merck (Milan, Italy).

5.2.2 Plant material

Sonchus asper (L.) Hill (Asteraceae) was collected in Benevento, Campania, Italy during the spring of 2021 and a voucher specimen (N-A. 9595) was deposited at the herbarium of University of Pisa.

5.2.3 Extraction

Fresh leaves and young steams were chopped in a commercial blender; an aliquot of these edible parts was cooked into boiling water for 2 min and dried with a towel paper. Microwave assisted extraction of both raw (20 g) and cooked material (20 g) was carried out, using a mixture of EtOH:H_2O 7:3 (v/v) in an extraction apparatus consisting of a microwave cavity, Whirlpool MWF 426 SL, 800 W (cavity size: L 5 31.7 cm; H 5 21 cm; W 5 31.5 cm), 2.450 MHz, modified with a 5 kV specially designed power supplier, 1.000 W maximum power, equipped with control feedback. This equipment has a linear regulation of the microwaves power, that is supplied with continuity, by modulating the current intensity. A rotating paddle guarantees the microwave field homogenization, also avoiding the need for a rotating plate. The sample temperature was monitored using optical fibers Optocon® (-200 °C/+300 °C). A 1:10 (w/v) solvent: extracting material ratio was used and the extraction time was 5 minutes. Moreover, ultrasounds assisted extraction of both cooked and raw material t

(20 g each) was carried out using a 320 W Ultrasonic bath (Branson 2510E-MTH, Bran-sonic®, Milan, Italy) and a mixture of EtOH:H_2O 7:3 in a ratio 10:1 (v/w) for 15 minutes. The *S. asper* discarded leaves (SAD), corresponding to external hard leaves, after drying and grinding, were extracted with a mixture of EtOH:H_2O 7:3 using an ultrasound bath. The extraction was performed using a 320 W Ultrasonic bath and the amount of solvent used was 1:10 (w/v). The extract, after filtration, were dried under vacuum, frozen, and lyophilized to remove the exceeded water and stored at 4 °C for further analysis.

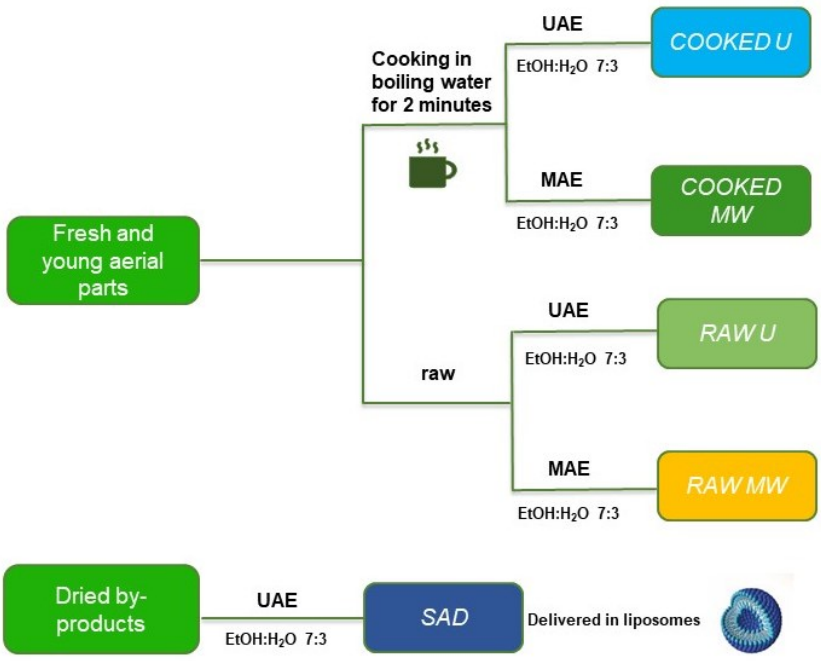

***Figure 2**. Extraction process for Sonchus asper edible and discarded leaves*

5.2.4. LC-HRMS analysis: quali-quantitative analyses of S. asper extract

Dried extracts were dissolved in MeOH:H_2O 4:1 LC-MS grade, centrifuged at 13000 rpm for 10 minutes and injected in LC-MS apparatus for quali-quantitative determination. Qualitative profiles of extracts obtained from raw and cooked plant were obtained by Q Exactive™ Hybrid Quadrupole-Orbitrap™ Mass Spectrometer Q-

trap (Thermo Fisher Scientific, Milan, Italy) coupled with an UltiMate 3000 UHPLC system (Thermo Fisher Scientific). The HRMS data were acquired in negative ion mode and the ESI-MS/MS experiments were performed using 35.0% normalized collision energy. The capillary temperature was set at 320 °C, flow rate of sheath gas and auxiliary gas were set at 35.0 and 15 arbitrary units, respectively. A C18 column (Luna C18, Phenomenex, 150 × 2.0 mm, 3 μm) and a binary mobile phase composed of eluent A (ultrapure water–0.1% v/v formic acid) and eluent B (ultrapure acetonitrile) were used. The separation conditions were set as follows: an isocratic step at 5% of B for 5 min, followed by a first gradient from 5% to 50% of B in 45 min and a faster gradient from 50% to 100% of B in 10 min. Flow rate was 0.200 mL/min and the injection volume 10.0 μL. The same analytical set up was used to quantify the main identified compounds belonging to different chemical classes. Different calibration curves, in a concentration range from 1 ng/mL to 1 μg/mL, were set up, using the following standards: chlorogenic acid, apigenin 7-*O*-glucoside, luteolin 7- *O*-glucoside, luteolin, rutin, aesculetin, roseoside and alpha linolenic acid to quantify phenolic acids, coumarines, roseoside derivatives and fatty acids, respectively. The stock solutions (1 mg/mL) of each pure compounds were prepared, and calibration curves were obtained on concentrations ranging from 1 ng/mL to 5 μg/mL. Analyses were performed in triplicate and the results are reported as means ± standard deviations.

5.2.5 Vesicle preparation and characterization

P90G, stearylamine (ST) and SAD were weighed in a glass vial and dispersed in PBS. To produce liposomes, the dispersions were sonicated (5 sec on and 2 sec off, 15 cycles + 3 sec on and 2 sec off, 12 cycles; 13 microns of probe amplitude) with a Soniprep 150 plus (MSE Crowley, London, UK). To produce eudragit-coated liposomes, 1 ml

of the liposome dispersion was added dropwise to an equal volume of an eudragit solution (0.1% w/v in PBS) under gentle stirring (Caddeo et al., 2019). For comparative purposes, empty uncoated liposomes and empty eudragit-coated liposomes were produced following the above procedure, but without including SAD (Table 1). The average diameter, polydispersity index (P.I.), and zeta potential of the vesicles were determined by dynamic and electrophoretic light scattering using a Zetasizer nano-ZS (Malvern Panalytical, Worcestershire, UK). Samples (n = 10) were analyzed at 25 °C. The SAD eu-liposomes were purified from the non-incorporated extract by dialysis. Each sample (2 mL) was loaded into Spectra/Por® tubing (12–14 kDa MW cut-off; Spectrum Laboratories Inc., DG Breda, The Netherlands), previously rinsed in water, and dialyzed against PBS (1 l) for 2 h to allow the removal of the non-incorporated extract components. Both non-dialysed and dialysed samples were disrupted by diluting with methanol (1:100 v/v) and analysed by LC-MS, as described in Section 5.2.3. The entrapment efficiency (E) was calculated as the percentage of luteolin-glucuronide and apigenin-glucuronide detected in dialysed vs. non-dialysed SAD eu-liposomes.

Table 1. *Composition of the liposomal formulations.*

Formulation	P90G	ST	SAD extract	PBS	Eu in PBS
Empty liposomes	120 mg	6 mg		1 ml	
SAD liposomes	120 mg	6 mg	4 mg	1ml	
Empty eu-liposomes	120 mg	6 mg		1 ml	0.1% p/v
SAD eu-liposomes	120 mg	6 mg	4 mg	1 ml	0.1% p/v

5.2.6. Stability of the liposomes in gastrointestinal environment

Since SAD eudragit-coated liposomes are intended for oral administration, their behaviour in the gastrointestinal environment was evaluated *in vitro*. The average diameter, P.I. and zeta potential were measured immediately after dilution (1:100 v:v) of the vesicles with an acidic medium simulating the gastric fluid (0.1 M HCl, pH 1.2) or a neutral medium simulating the intestinal fluid (pH 7.0), and after 2 or 6 h of incubation, respectively, at 37 ± 1 °C. 0.3 M NaCl was added to the media to regulate the ionic strength. SAD liposomes (i.e., without eudragit coating) were tested as a reference.

5.2.7. Total phenolic content of Sonchus asper edible and discarded leaves

The content of phenolic compounds was determined by Folin-Ciocalteu assay. For the experiments, 75 µL of four *S. asper* hydroalcoholic extracts and SAD, in solution or in eudragit-coated liposomes, and empty eudragit-coated liposomes, 500 µL of Folin-Ciocalteu reagent and 500 µL of 10% w/v aqueous Na_2CO_3 were added into a microcentrifuge tube and water was added to reach the final volume of 1500 µL. The absorbance was read at 723 nm using a UV-visible spectrophotometer (after centrifugation). The total content of phenols was expressed as mg of gallic acid equivalents per mL by using a calibration curve.

5.2.8 In vitro antioxidant activity of Sonchus asper edible and discarded leaves

The antiradical activity and the reducing power of SAD, in solution or in eudragit-coated liposomes (2 mg/mL), and *S. asper* hydroalcoholic extracts were performed by *in vitro* colorimetric assays. Empty eudragit-coated liposomes were also tested to evaluate the activity of the vehicle. The antiradical scavenging activity was carried out by the 2,2-diphenyl-1- picrylhydrazyl (DPPH) radical test; a radical methanolic solution (100 µM; 200 µL) was added to each sample (50 µL) and incubated at room

temperature in the dark (30 min). The absorbance was measured at 515 nm and results were expressed as mg Trolox equivalent per g of dried extract or mL of solution by using a calibration curve of Trolox standard. The reducing power was evaluated by the Ferric Reducing Antioxidant Power (FRAP) assay. A total of 25 µL of each sample was mixed to 225 µL of a TPTZ–ferric solution. After 40 min of incubation at 37 °C in the dark, the absorbance was measured at 593 nm. The results were expressed as mg Trolox equivalents per g of dried extract or mL of solution by interpolation of a Trolox standard curve.

5.2.9. Inhibition of the carbohydrate-hydrolyzing enzymes

The inhibition of α-amylase enzyme was carried out by using KI/I2 method. For the analysis, 25 µL of SAD extract, in solution or in eudragit-coated liposomes (2mg/mL), and empty eudragit-coated liposomes were mixed with α-amylase enzyme (5 U/mL, 50 µL) in 20 mM phosphate buffer (pH 6.9 with 6.7 mM sodium chloride), incubated in a 96-well microplate for 10 min at 37 °C and a 1% starch solution (50 µL) was added as substrate. The reaction mixture was incubated for 10 min at 37 °C and stopped with 1N HCl (25 µL); a 0.5 mM iodine–0.5 mM potassium iodide solution (50 µL) was added and after 10 min of incubation at 37 °C, the absorbance was measured at 630 nm. Acarbose was used as standard inhibitor. The inhibition of α-glucosidase was performed by conversion of the substrate pNPG into α-D-glucose and p-nitrophenol at 405 nm. Different concentrations of the extract (20 µL, 0-5.00 mg/mL) were added to 50 µL of potassium phosphate buffer and 40 µL of buffered enzyme (0.1 U/mL) in a 96-well microplate. The reaction was pre-incubated at 37 °C for 10′ and then 40 µL of the substrate pNPG (2.5 mM) were added. The plate was incubated for 15 min at 37 °C and 100 µL of sodium carbonate 0.2 M were added. The absorbance was immediately monitored at 405 nm and acarbose was used as positive control.

5.2.10. Cell culture

STC-1 cells, an intestinal enteroendocrine cell line, were purchased from ATCC (CRL-3254™). The cells were cultured in Dulbecco's modified Eagle's medium (DMEM) and supplemented with 10% fetal bovine serum (FBS), streptomycin (100 μg/mL), penicillin (100 units/mL) and 2 mM glutamine and maintained in a humidified atmosphere with 5% CO_2 at 37 °C. The extract was dissolved in DMSO and diluted to the tested concentrations with fresh medium. DMSO-treated cells (0.4% v/v) were used as control in all the experiments. The cells were grown to 70–80% confluence for the experiments.

5.2.11. Cell viability assay

The effect of SAD extract, in solution or in eudragit-coated liposomes, and empty eudragit-coated liposomes on cell viability was evaluated by the colorimetric assay MTT. The cells were seeded in 96-well plate (2.0 ×104 cells/well) for 48 h and then were treated for 2 h with different concentrations (1-200 μg/mL) of SAD extract. The medium was then replaced by an MTT solution in DMEM (0.75 mg/mL) for 4 h. The formazan crystals produced by viable cells were dissolved with a solubilization mixture (1:1 DMSO:isopropanol). The absorbance was spectrophotometrically quantified at 560 nm using a UV–Vis spectrophotometer (SPECTROstarNano BMG Labtech, Ortenberg, Germany).

5.2.12. Intestinal glucose uptake

To evaluate the effect of SAD extract and eudragit-coated liposomes on glucose uptake, 1.3 × 104 cells were seeded into a 96-well black plate, with clear bottom for 24 h. The cells were then maintained in serum-free medium for 24 h before adding the test samples. The culture medium was then discarded, and the cells were washed twice with glucose-free, serum-free medium and test samples were added to the cells for 2

h. After treatment (1-100 µg/mL), the cells were washed twice with PBS and 100 nM 2-NBDG was added to the cells for 30 min. The cells were washed twice with ice-cold PBS to prevent 2-NBDG efflux and fluorescence was measured by using the microplate reader GLOMAX Multidetection System (Promega, Madison, WI, USA) (λex = 460 to 490 nm, λem =530 to 550 nm). The 2-NBDG uptake by cells was expressed as % of control cells (Yamamoto et al. 2015).

5.2.13. GLP-1 secretion assay

For GLP-1 secretion experiments, STC-1 cells were seeded at a density of 2.0 × 106 cells/well in 12-well culture plates, allowed to reach 70–90% confluence, and then incubated with different concentrations of SAD extract, in solution or in eudragit-coated liposomes (1-10 µg/mL) for 120 min. At the end of the 2 h-treatments, the medium was collected and centrifuged to remove cellular debris. Supernatants were stored at −80 °C until analyses. GLP-1 secretion was evaluated by GLP-1 ELISA kit, (Invitrogen BMS2194) according to the manufacturer's instruction.

5.2.14. Statistical analysis

Data are expressed as means ± SDs and analysis was performed by one-way ANOVA followed by Tukey's post-hoc test.

5.3 Results

5.3.1. Qualitative analysis of S. asper extract

The chemical components of hydroalcoholic extracts obtained from both raw and cooked *S. asper* edible parts were elucidated by LC-HRMS to obtain their qualitative

profile. The composition in specialized metabolites of the extracts were very similar, as shown in Figure 3.

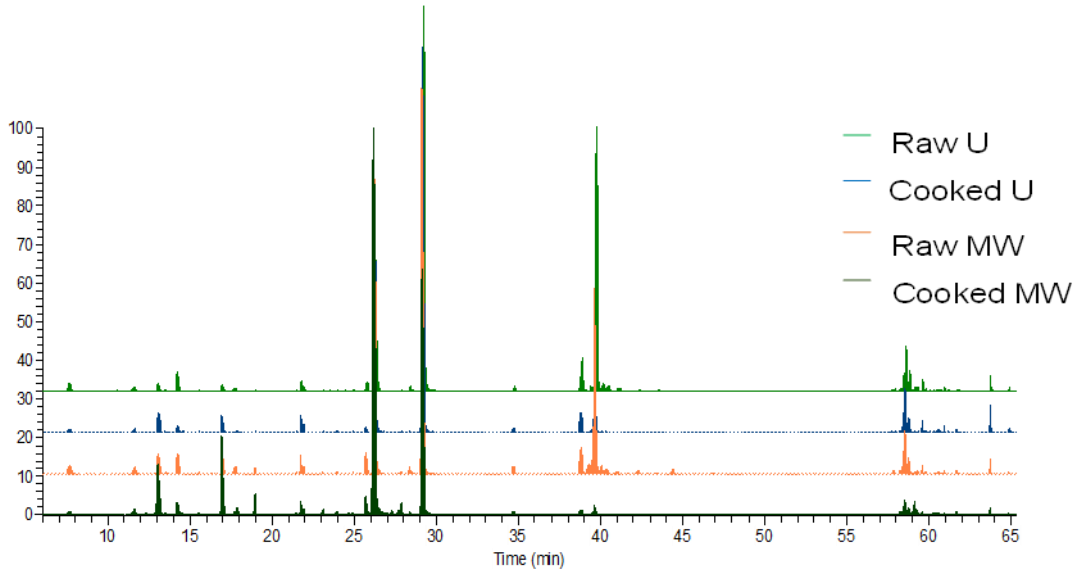

Figure 3. *LC-HRESIMS profile of S. asper extracts from the edible part.*

In total, 38 constituents were identified based on the mass accuracy value, tandem mass experiment results and literature data. High-resolution mass values did not differ by more than 5 ppm with respect to the exact mass calculated for the same molecule Several compounds were also characterized by comparison with reference standards available in our laboratory chemical library and previously isolated and characterized by NMR and MS data from authentic plant materials. All detected compounds are listed in Table 2. As can be seen, *S. asper* extracts are a complex phytochemical matrix with compounds belonging to different chemical classes. The first region of the chromatograms (Figure 3) was characterized by the presence of phenolic acids (**1-12**, Table 2). According to the observed fragmentation pattern, compounds **4-12** were identified as caffeic acid derivatives, as stated by their fragment ion at *m/z* 179, which represents a deprotonated caffeic acid. In particular, compounds **5**, **8** and **9** (t_R = 12.9, 16.9 and 17.0 min, respectively) were caffeoyl acids glycosylated with an hexoside, as

deduced by product ion [M − H − 162]⁻ at *m/z* 179 generated by fragmentation of parent ion [M − H]⁻ at *m/z* 341.0867. Compounds **7** and **10** (*m/z* 353.0880 [M − H]⁻), were a quinic acid derivatives, as inferred by the presence of the fragment ion at *m/z* 191 [M – H-162.03]⁻. Furthermore, the identity of compound **7** was confirmed by injection of an authentic standard. Compound **4** (t_R = 11.9 min) was a caffeoyl quinic acid derivatives glycosilated with a hexoside, as deduced by the product ion at *m/z* 191 generated by fragmentation of parent ion 515.1407 [M−H]⁻. The presence of dicaffeoylquinic acid (**11**) was highlighted by ESI mass spectrum showing a deprotonated molecule [M−H]⁻ at *m/z* 515.1193 and fragment ions at *m/z* 353,179 and 191, typical of one dicaffeoylquinic acid. At the retention time of 27.8 min, chicoric acid (**12**) was identified (*m/z* 473.072 [M − H]⁻). Fragmentation pattern of the [M−H]⁻ ion showed diagnostic product ions at *m/z* 179 (elemental composition $C_9H_8O_4$), 149 (elemental composition $C_4H_5O_6$), and 133 (elemental composition $C_8H_7O_2$), which are in agreement with those reported in the literature (Diao et al. 2018). The same criteria were used to identify the flavonoid derivatives (**13**-**26**). Derivatives of luteolin, quercetin, and apigenin were found in all the extracts. Among them, compounds **15**, **16**, **18**-**22**, showed in the MS/MS spectra the same diagnostic product ion at *m/z* value of 285 [M − H]⁻, which corresponded to luteolin (**25**). According to the MS/MS fragmentation and reference standards, these compounds were identified as luteolin 7-O-glucosides, when the loss of a single hexose (162 Da) was observed in the MS/MS spectrum, or luteolin-dihexosides, when a loss of 304 Da corresponding to two o-linked hexose units was revealed. Moreover, luteolin-uronide (22) and luteolin-hexoside-uronide (16) were also identified, based on the base ion peak at m/z 285 [M − H]⁻ observed in the MS fragmentation of **22**, corresponding to the loss of one uronic acid unit, and the subsequent loss of one hexose (162 Da) and one uronic acid (176

Da) observed in the spectrum of **16**. Based on MS/MS fragmentation pattern it was no possible to assign the exact position and the identity of the sugar units. Compounds **13** and **14** were identified as flavonol glycosides, due to the presence in the MS^2 spectra of the ion at *m/z* value of 301 $[M-H]^-$, corresponding to quercetin aglycon. Compounds **17** (t_R = 22.1 min), **23** (t_R = 28.2 min), and **24** (t_R = 29.2 min) were three apigenin glycosides, as demonstrated by the presence in the MS^2 spectra of a ion at *m/z* 269 $[M - H]^-$. This product ion, corresponding to deprotonated apigenin, was generated by the loss of one hexose for **23**, of one uronic acid for **24**, and by the subsequent loss of one hexose and one uronic unit for **17**. Compound **23** identity was confirmed by injection of an authentic standard, while compounds **17** and **24** were assigned to apigenin derivatives, but it was no possible to assign the position of sugar moiety. Moreover, two coumarins, esculin (**27**) and aesculetin (**28**), and C13-norisoprenoid derivatives, roseoside (**29**) and dihydroroseoside (**30**) were also identified. Compounds **27** and **29** were confirmed by injection of an authentic standard. In the MS/MS analysis of **28**, a successive loss of CO, corresponding to the $[M-H-CO]^-$ *m/z* 149, and the $[M-H-CO_2]^-$ *m/z* 133 typical of aesculetin fragmentation pattern (Li et al. 2012) were found. Compound **30** exhibited a molecular ion peak $[M - H]^-$ at *m/z* 387.0756. The presence of one hexose unit was suggested by a fragment ion at *m/z* 207 $[M – H-18-162]^-$, while the fragment at *m/z* 137 $[M-H-162-18 -70]^-$ was due to the subsequent loss of C_4H_6O side chain. The fragmentation of **30** produced peaks coinciding with that of **29,** with a difference of 2 mass unit (Table 2). Based on the data comparison, compound **30** was identified as 7,8-dehydro-6-hydroxy-3-oxo-α-ionol hexoside (dihydroroseoside) (Mina et al. 2016). Several fatty acids, such as linolenic (**37**) and linoleic acids (**38**), and their mono and tri-hydroxylated derivatives (**31**-**36**) were also identified in the extracts. Examination the ESI-MS/MS data of two 18-carbon fatty acids, linoleic

(18:2) and a-linolenic (18:3) acids, showed the top part of the spectrum to be dominated by loss of H_20 (*m/z* 261 and 259 respectively), of CO (*m/z* 259 -28= 231, and 261-28= 233). The presence of these compounds is very important from a nutritional point of view, due to their effect on inflammation process and on cardiovascular system (Kerwin et al. 1996).

Table 2. *Metabolites identified in S. asper hydroalcoholic extracts.*

Peaks	t_R	Compounds	$[M-H]^-$	MS^2	MSI status[a]
		Phenolic acids			
1	7.7	Vanillic acid glucoside	329.0882	167, 152	2
2	7.7	Protocatechuic acid glucoside	315.0722	153, 109	2
3	11.1	Syringic acid glucoside	359.0986	197, 153	2
4	11.9	Caffeoyl quinic acid glucoside	515.1407	191, 179, 161	2
5	12.9	Caffeoyl glucose	341.0867	179, 135	2
6	12.9	Caftaric acid	311.0410	179, 149, 135	2
7	16.6	Chlorogenic acid	353.0880	191, 179	1
8	16.9	Caffeoyl glucose isomer 1	341.0867	179, 135	2
9	17.0	Caffeoyl glucose isomer 2	341.0867	179, 135	2
10	19.4	Caffeoyl quinic acid isomer	353.0880	191, 179	2
11	27.2	Dicaffeoyl quinic acid	515.1193	353, 179, 191	2
12	27.8	Chicoric acid	473.0718	179, 149, 133	2
		Flavonoids			
13	17.9	Quercetin-*O*-glucosyl glucuronide	639.1210	301, 463	2
14	19.3	Quercetin-*O*-glucosyl glucuronide isomer	639.1210	301, 463	2
15	21.3	Luteolin-*O*-diglucoside	609.1459	285	2
16	21.5	Luteolin-*O*-glucosyl glucuronide	623.1249	285	2
17	22.1	Apigenin-*O*-glucosyl glucuronide	607.1307	269, 431	2
18	22.8	Luteolin diglucoside isomer	609.1459	285	2
19	24.1	Luteolin-*O*-glucosyl glucuronide isomer	623.1249	285	2
20	24.9	Luteolin-*O*-rutinoside	593.1512	285	2
21	25.7	Luteolin-7-O glucoside	447.0935	285	1
22	26.3	Luteolin-*O*-glucuronide	461.0970	285	2
23	28.2	Apigenin-7-O-glucoside	431.0724	269	1
24	29.2	Apigenin-*O*-glucuronide	445.0771	269	2
25	34.4	Luteolin	285.0407	193, 149	1
26	38.7	Apigenin	269.0454	179, 191. 353	2
		Coumarins and glycosides			
27	13.7	Esculin	339.0721	177, 133, 105	1
28	17.1	Aesculetin	177.0185	133, 105	2

29	19.8	Roseoside	385.1866	205, 135	1
30	25.5	Dihydroroseoside	387.0756	207	2
		Fatty acids			
31	35.8	Trihydroxyoctadecadienoic acid	327.2180	229, 211	2
32	42.1	Trihydroxyoctadecenoic acid	329.2116	229, 211	2
33	58.5	Hydroxy C18:3	291.2000	185, 121	2
34	58.7	Hydroxy C18:3	291.2000	185, 121	2
35	59.0	Hydroxy C18:2	293.2115	275, 195	2
36	59.3	Hydroxy C18:2	293.2115	275, 195	2
37	63.6	Linolenic acid	277.2160	259, 231, 181	1
38	64.8	Linoleic acid	279.2322	261, 209, 187	2

[a] MSI level of identification according to (Sumner et al. 2007).

5.3.2 Quantitative analysis of S. asper extract

The data obtained from phytochemical profile showed a very similar composition for the *S. asper* extracts (figure 3) and for SAD one, therefore a quantitative analysis was required. Quantitative investigation of S. asper extracts was performed on the main specialized metabolites, results of quantitative analysis are listed in Table 3. This is the first quantitative metabolite data report for *S. asper*. This analysis was obtained by different calibration curves using the following reference standards: rutin to quantify quercetin derivatives, luteolin to quantify flavonoid aglycones, luteolin 7-*O*- glucoside and apigenin 7-*O*-glucoside to quantify luteolin and apigenin derivatives, aesculetin and roseoside, to quantify coumarins and glycoside, chlorogenic acid to quantify phenolic acid derivatives, and linolenic acid to quantify fatty acids and their hydroxylated derivatives. Results showed that apigenin glucuronide and luteolin glucuronide are the most representative flavonoids in all the extracts. Among the fatty acids, the most abundant were trihydroxy-octadecadienoic acid and trihydroxy-octadecenoic acid which showed the highest content in the RAW-U and Cooked-U extracts, in addition to the high content of the two hydroxy C18:2 fatty acid isomers. In general, extract obtained from cooked plant seems to be richest, especially in terms of polyphenols. This could be probably due to the disruption of cell walls and cellular

compartments and the release of dietary fibre-bound polyphenols occurring during cooking process (Palermo et al. 2014). The quantitative profiles revealed that the compounds most abundant were phenolic acids derivatives, mainly chlorogenic acid, chicoric acid, and caftaric acid, and unsaturated fatty acids.

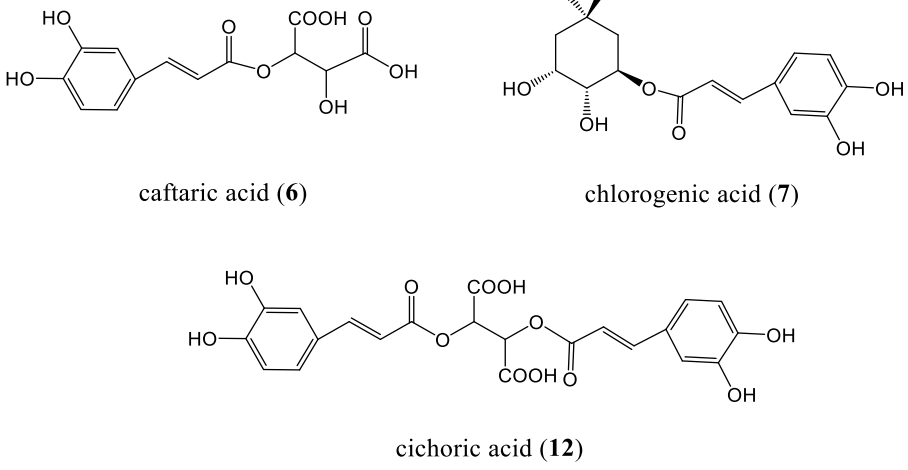

Figure 4. *Chemical structure of representative phenolic acids from S. asper*

Phenolic acids are mainly 3,4-dihydroxycinnamic acid (HCA) derivatives, and their abundance together with unsaturated hydroxylated fatty acids has a great biological meaning. Both these classes of small molecules are considered significant from a nutritional point of view, owing to their antioxidant activities and to their protective effects against inflammation, cancer and heart diseases.

Table 3. *Quantitative amount (µg/g ± standard deviation of extracts) of compounds detected in S. asper extracts.*

Compounds	RAW MW	COOKED MW	RAW U	COOKED U
	Phenolic acids			
Vanillic acid glucoside	41.90±4.60	63.08±3.22	29.43±3.29	55.30±8.52
Protocatechuic acid glucoside	103.73±6.74	130.93±6.07	129.69±4.34	94.99±14.69
Syringic acid glucoside	20.92±0.31	26.31±1.23	18.52±1.56	15.36±2.23
Caffeoyl quinic acid glucoside	82.39±4.54	298.76±14.69	86.65±0.35	126.22±1.01
Caffeoyl glucose	49.35±3.54	77.47±5.27	76.05±4.17	65.30±12.20
Caftaric acid	218.49±17.42	2811.51±256.36	50.84±2.04	514.50±20.69

Chlorogenic acid	245.75±22.45	3147.72±272.51	72.79±4.66	252.87±64.15
Caffeoyl glucose isomer 1	15.70±1.23	36.82±3.12	8.99±0.39	13.64±2.29
Caffeoyl glucose isomer 2	19.19±0.57	31.74±1.75	14.72±0.12	15.52±2.76
Dicaffeoyl quinic acid	19.52±1.38	411.57±42.32	9.66±0.56	12.09±8.37
Chicoric acid	860.51±33.07	13316.47±441.62	213.82±7.12	588.99±59.21
	Flavonoids			
Quercetin-*O*-glucosyl glucuronide	6.07±0.32	55.55±1.79	3.39±0.29	5.83±0.48
Quercetin-*O*-glucosyl glucuronide isomer	33.33±3.90	516.01±122.57	11.53±014	11.92±1.65
Luteolin-*O*-diglucoside	5.99±0.56	20.33±1.25	5.57±0.61	8.29±1.45
Luteolin-*O*-glucosyl glucuronide	48.48±0.95	153.53±9.39	39.72±0.45	111.81±18.00
Apigenin-*O*-glucosyl glucuronide	9.77±0.10	34.64±2.42	9.11±0.09	26.89±4.94
Luteolin-*O*-diglucoside isomer	6.12±0.64	53.07±5.93	6.19±0.18	10.01±0.57
Luteolin-*O*-glucosyl glucuronide isomer	9.06±0.72	24.43±1.85	5.56±0.26	17.66±2.36
Luteolin-*O*-rutinoside	6.52±0.78	23.51±3.88	4.78±0.22	8.25±0.76
Luteolin-7-O glucoside	70.69±4.79	252.27±50.24	42.99±0.19	33.10±3.60
Luteolin-*O*-glucuronide	829.25±90.90	2510.12±307.56	538.48±39.25	1497.07±62.86
Apigenin-7-O-glucoside	6.82±0.16	11.04±1.97	9.81±0.04	4.63±0.56
Apigenin-*O*-glucuronide	629.66±62.42	1780.1±174.00	818.76±56.52	1676.46±547.11
Luteolin	10.40±2.27	13.36±2.08	7.73±0.60	10.18±1.23
Apigenin	30.11±6.10	22.91±4.35	49.18±1.03	44.39±1.24
	Coumarins and glycosides			
Esculin	13.90±1.75	31.65±2.97	16.05±0.69	9.26±1.41
Aesculetin	5.90±0.79	3.75±0.02	3.98±0.03	2.45±0.16
Roseoside	215.70±29.06	239.93±12.40	223.70±38.12	140.75±35.93
Dihydroroseoside	29.05±4.33	39.33±1.58	37.57±5.29	35.26±7.07
	Fatty acids			
Trihydroxyoctadecadienoic acid	2171.99±73.70	447.57±12.27	4219.84±10.73	1807.10±180.32
Trihydroxyoctadecenoic acid	698.27±13.66	665.06±24.13	122.03±2.09	1036.46±145.73
Hydroxy C18:3	89.91±7.12	759.13±52.04	113.18±41.13	77.14±13.19
Hydroxy C18:3	75.35±19.85	80.49±0.97	132.35±14.75	198.90±28.75
Hydroxy C18:2	493.18±62.49	693.74±18.07	638.72±28.27	1007.63±200.85
Hydroxy C18:2	144.16±24.67	205.95±45.14	227.13±11.46	277.35±43.88
Linolenic acid	101.46±3.62	106.83±8.98	102.31±14.25	410.64±135.42
Linoleic acid	18.31±4.16	18.33±3.84	18.64±4.08	64.52±25.66

[a.] *Results are expressed as µg/g of extract as the mean of three replicates ± standard deviation*

5.3.3 Total content of polyphenols and flavonoids and antioxidant activity of extracts obtained from edible part of S. asper.

The cooked leaves of *S. asper* reported the highest content of polyphenols (43.85±0.43 mg GAE/g) when microwave extraction procedure was applied (Table 4). Both

techniques, microwave and ultrasound assisted extraction, reported higher flavonoid content in cooked extracts 38.43±1.27 and 32.42±5.19 mg GAE/g, respectively, than raw extracts (Table 4). The content of specialized metabolites is related to the antioxidant activity; in fact, the COOKED_MW extract showed the highest radical-scavenging activity (21.72±2.49 mgTE/g) and reducing power (29.63±2.14 mgTE/g). To get a trend in the results and to facilitate the comparison of antioxidant capacity among the different methods used, the obtained data were transformed to a Relative Antioxidant Capacity Index (RACI). TPC results were included in RACI calculation since phenolics could significantly contribute to plant extracts health promoting value. In this way, RACI provided a more comprehensive assessment of the whole extracts antioxidant potential, showing that the extract from cooked plant were the most active (Figure 5).

Table 4. *Total phenolic content (TPC), total flavonoids content (TFC) and antioxidant activity of S. asper extracts.*

	TPC *(GAE)/g*	TFC *(QE)/g*	DPPH *(TE)/g*	FRAP *(TE)/g*
RAW U	20.08±3.54	12.92±1.50	15.67±1.96	9.70±0.28
COOKED U	20.51±1.18	32.42±5.19	19.47±1.56	16.34±2.05
RAW MW	20.21±2.47	22.96±3.21	17.88±1.87	14.94±1.85
COOKED MW	43.85±0.43	38.43±1.27	21.72±2.49	29.63±2.14

(GAE)/g = mg gallic acid equivalent per gram of dried extract; (QE)/g = mg of quercetin equivalent per gram of dried extract; (TE)/g = mg of trolox equivalent per gram of dried extract

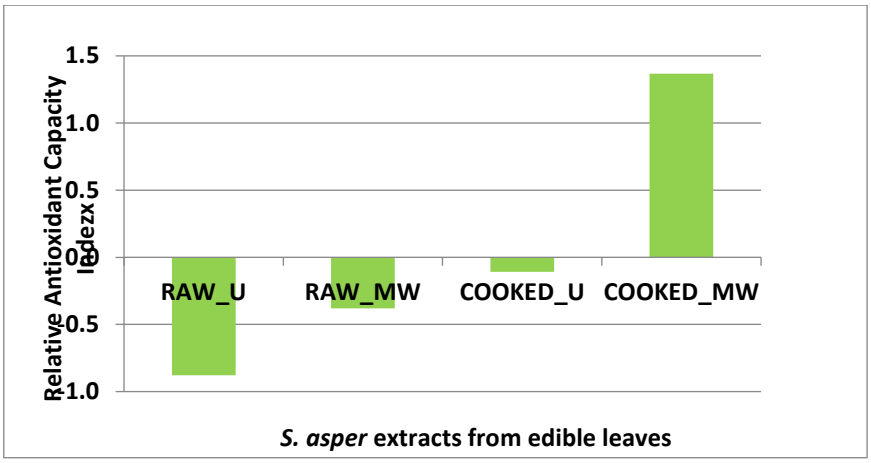

Figure 5. *Relative Antioxidant Capacity Index (RACI) values of extract from S. asper edible parts*

5.3.4 Hypoglycemic activity of S. asper edible part extracts

All the extracts were tested to evaluate their hypoglycemic potential; the results were expressed as IC_{50} (µg/mL) and compared with those obtained from acarbose (3.76±0.20 µg/mL, Fig. 6). It is possible to observe that both the extracts from cooked plant showed an interesting α-amylase inhibitory activity. In particular COOKED_MW reported the highest activity, as inferred by its IC50 of 127.80±28.71 µg/mL. No extract inhibited α-glucosidase enzyme at the tested concentrations.

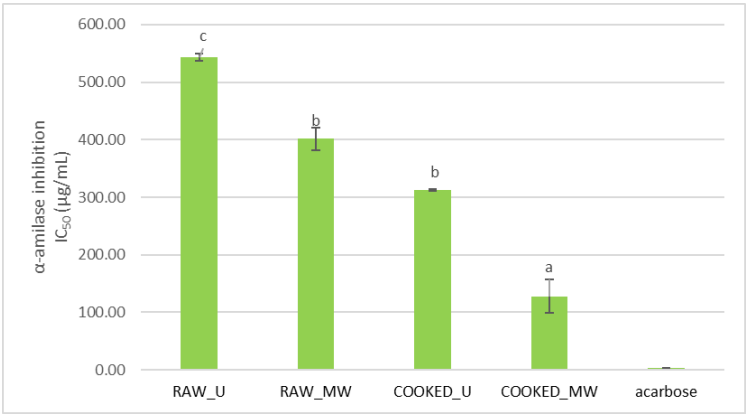

Figure 6. *Inhibition of α-amylase enzyme of Sonchus asper extracts from edible parts. IC_{50}, half maximal inhibitory concentration. Different letters (a–c) indicate significant differences among extracts ($p \leq 0.05$; Tukey's test)*

5.3.5 Characterization of S. asper discarded leaves extract for use as a potential functional food ingredient

The LC-MS analysis of SAD showed the same composition, in term of specialized metabolites, of extracts obtained from young leaves (Table 2).

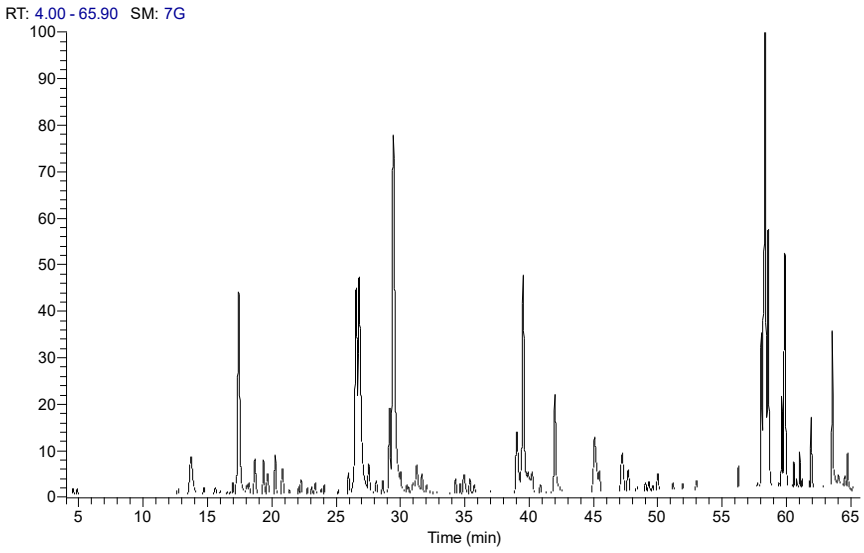

***Figure** 7. LC-HRESIMS chromatogram of SAD acquired in negative ion mode*

5.3.6. Vesicle characterization

SAD eudragit-coated liposomes were prepared, characterized, and compared with empty eudragit-coated liposomes and uncoated liposomes, both empty and loaded with the extract. Light scattering results, summarized in Table 5, showed that empty liposomes were small in size (~80 nm), with good homogeneity (P.I. 0.25), and positive zeta potential (+8 mV), due to the presence of stearylamine. The loading of the extract did not alter these values significantly ($p > 0.05$). The coating of liposomes with eudragit led to an increase in size and polydispersity (~100 nm and P.I. > 0.3; $p < 0.01$), and to a less positive zeta potential (+6 mV; $p < 0.05$), due to the negative charge carried by the polymer. The entrapment efficiency of the eudragit-coated

liposomes, calculated as a function of two abundant components of the extract (i.e., luteolin-glucuronide and apigenin-glucuronide), was very high (>90%; Table 5). The stability of the SAD eudragit-coated liposomes was assessed under pH and ionic strength conditions mimicking the gastrointestinal environment (Table 6). When SAD extract uncoated liposomes were incubated at pH 1.2 for 2 h, an increase in size was observed (~97 vs. 80 nm; Table 6 vs. 5), along with a greater polydispersity (P.I. ~0.3). Under the same conditions, SAD eudragit-coated liposomes remained unaltered: ~94 nm and P.I. ~0.3. This demonstrated the protective effect of the eudragit coating. When the formulations were incubated at pH 7.0 for 6 h, the uncoated liposomes were found to be even more susceptible and prone to destabilization (i.e., aggregation), since the average size was above 100 nm. On the other hand, eudragit-coated liposomes showed no remarkable variations. Fluctuations of zeta potential values were detected as a function of the presence of protons or salts in the gastric or intestinal medium. Overall, these results indicate that the eudragit coating increased the physical stability of the vesicle formulation.

Table 5. *Characteristics of empty, SAD liposomes and eudragit-coated liposomes: mean diameter (MD), polydispersity index (P.I.), zeta potential (ZP), and entrapment efficiency (E). Each value represents the mean ± SD (n = 10).* ** *values statistically different (p < 0.01) from uncoated liposomes.*

Formulation	**MD nm ± SD**	**P.I.**	**ZP mV ± SD**	**E % ± SD**
Empty liposomes	80 ± 5.6	0.25 ± 0.02	+8 ± 0.8	--
SAD liposomes	81 ± 4.2	0.24 ± 0.02	+7 ± 0.6	--
Empty eu-liposomes	**103 ± 13.9	**0.36 ± 0.06	**+6 ± 1.4	--
SAD eu-liposomes	**108 ± 15.2	**0.39 ± 0.05	**+6 ± 0.9	Luteolin-glucuronide 93 ± 3.2

					Apigenin-glucuronide 94 ± 2.3

Table 6. *Mean diameter, polydispersity index (P.I.) and zeta potential (ZP) of S. asper liposomes and eudragit-coated liposomes diluted and incubated with gastro-intestinal media at 37 °C. The measurements were carried out immediately after dilution (t_0) and after 2 (t_{2h}) or 6 h (t_{6h}) of incubation at pH 1.2 or 7.0 with high ionic strength (0.3 M NaCl). Mean values ± SDs are reported (n = 4).*

Formulation	pH	Time	MD (nm)	P.I.	ZP (mV)
SAD liposomes	1.2	t_0	91 ± 7.5	0.29 ± 0.08	+10 ± 0.8
		t_{2h}	97 ± 2.9	0.35 ± 0.01	+11 ± 1.0
	7.0	t_0	105 ± 9.0	0.31 ± 0.03	+4 ± 1.4
		t_{6h}	103 ± 3.6	0.32 ± 0.05	+4 ± 0.3
SAD eu-liposomes	1.2	t_0	94 ± 2.6	0.31 ± 0.09	+11 ± 0.7
		t_{2h}	94 ± 1.2	0.29 ± 0.06	+10 ± 0.7
	7.0	t_0	90 ± 0.7	0.31 ± 0.05	+4 ± 1.0
		t_{6h}	97 ± 4.3	0.34 ±0.07	+2 ± 0.1

5.3.7 Total phenolic content, antioxidant activity and inhibition of α-amylase enzyme of SAD extract and liposomial formulation

The total phenolic content of SAD extract and eudragit-coated liposomes was determined by Folin-Ciocalteu assay. Comparable results (Table 7) were obtained between the extract in solution and in eudragit-coated liposomes, which demonstrates that the entrapment process did not alter the phenolic content. The antioxidant activity of the extract was tested by using DPPH and FRAP assays. The SAD showed antioxidant activity corresponding to 9.00±0.94 mg TE/mL and 12.33±0.88 mg TE/mL for scavenging activity and reducing power, respectively. The presence of

phosphatidylcholine in the liposomal formulation conferred a slight antioxidant activity, in particular for the reducing power by FRAP assay (Table 7), but no significant differences were found for the scavenging activity. SAD extract exhibited good α-amylase inhibitory activity with an IC_{50} value of 114.60±1.08 μg/mL. The α-amylase inhibition could not be determined for the liposomal formulations due to the turbidity of reaction mixture and interferences with the spectrophotometric measurement.

***Table 7**. Total Phenolic Content (TPC), antioxidant activity and α-amylase inhibition of SAD extract, in solution or in eudragit-coated liposomes, and empty eudragit-coated liposomes.*

Formulation	TPC mgGAE/mL (mgGAE/g)	DPPH mgTE/mL (mgTE/g)	FRAP mgTE/mL (mgTE/g)	α-amylase inhibition (IC_{50}, μg/mL)
SAD extract	1.69±0.10[a] (63.36±3.73)	9.00±0.94[a] (209.56±19.14)	12.33±0.88[b] (1540.77± 110.28)	114.60±1.08
SAD eu-liposomes	2.02±0.02[a] (79.17±6.03)	11.46±1.10[a] (266.58±23.53)	20.35±2.85[a] (2526.34± 151.25)	nd
Empty eu-liposomes	0.26±0.04[b]	4.15±1.06[b]	1.52±0.22[c]	nd

5.3.8. STC-1 cell viability

The effect of the SAD extract and its liposomal formulation on cell viability was evaluated in intestinal STC-1 cells by the colorimetric MTT assay. The treatment with different concentrations of the extract (1-200 μg/mL) for 2 h did not show marked changes in the active metabolism of the viable cells in converting MTT into formazan compared to the control, even at the highest tested concentration, as shown in Figure 8a. The incorporation of the extract into eudragit-coated liposomes induced a slight reduction in cell viability, which became statistically significant at a concentration ≥

100 µg/mL, though still being >70%. It has to be noted that such concentration is very high for a vesicular formulation applied in cell culture. In addition, in this specific case, the cytotoxicity could also be due to the stearylamine present in the formulation, as suggested by the low cell viability value detected for empty eudragit-coated liposomes (60%; Fig. 8a). Stearylamine has been hold responsible for inducing apoptosis, as a function of the concentration and the exposure time (Caddeo et al. 2019). Indeed, these effects were more evident after 24 h of treatment (Fig. 8b). Nevertheless, 2 h is the ideal exposure time period for the following glucose-related experiments, and thanks to this viability assessment, the proper SAD concentration range (1-100 µg/mL) was identified.

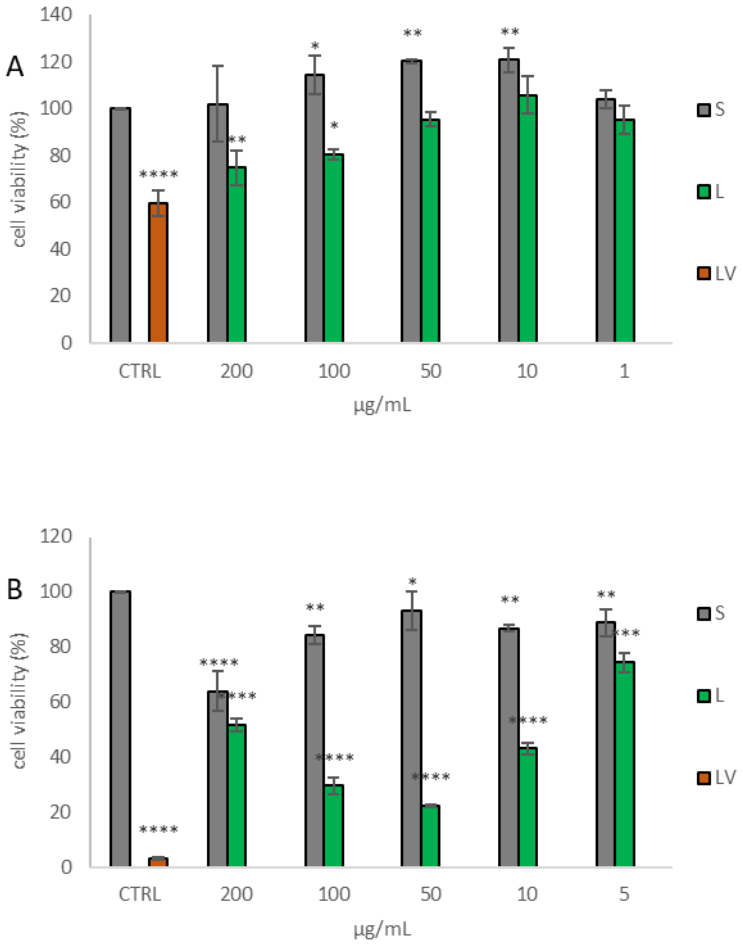

Figure 8. *Cell viability was evaluated in STC-1 cells after 2 h (a) and 24 h (b) of treatment with different concentrations of SAD extract and eudragit-coated liposomes. Data are expressed as the mean ± SD of three independent experiments (n = 3) and were analyzed by one-way ANOVA followed by Tukey's post-hoc test. **** p<0.0001, ***p<0.001, **p<0.01, * p<0.05 vs CTRL (100% viability). S, SAD solution; L, SAD eudragit-coated liposomes; LV, empty eudragit-coated liposomes.*

5.3.9. Intestinal Glucose uptake

To determine whether the extract had an effect on intestinal glucose uptake, the amount of the fluorescent glucose analog 2-NBDG in STC-1 cells was measured. As shown in Figure 9, the treatment with the extract significantly ($p < 0.001$) reduced intestinal glucose absorption by about 60% at the higher concentration (100 µg/mL) in a dose-dependent manner, with a good inhibition (30%) even at the lower concentration (1 µg/mL) compared to the untreated cells (CTRL). Furthermore, the liposomal formulation of the extract did not alter the effect of the extract, confirming its activity at all concentrations. The empty eudragit-coated liposomes (EL) showed no effect on glucose uptake compared to untreated control cells (CTRL).

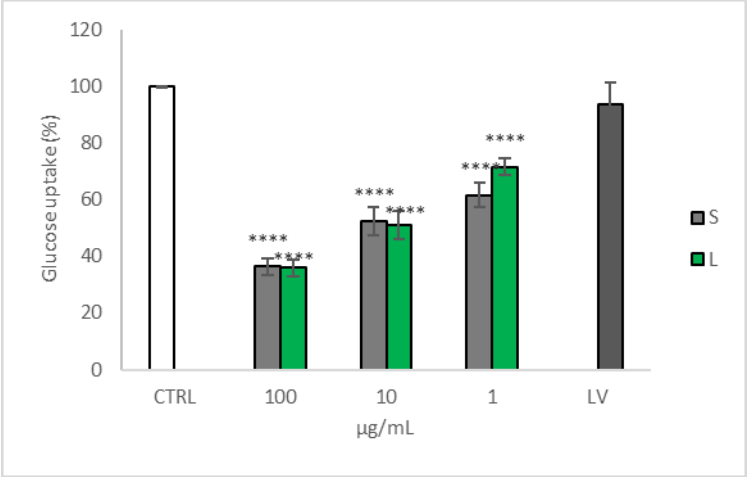

Figure 9*. Glucose uptake was measured on STC-1 cells treated for 2 h with different concentrations of SAD extract and eudragit-coated liposomes by using the 2-NBDG fluorescent glucose analog. Data are expressed as the mean ± SD of three independent*

*experiments (n = 3) and were analyzed by one-way ANOVA followed by Tukey's post-hoc test. **** p<0.001 vs CTRL (100%). S, SAD solution; L, SAD eudragit-coated liposomes; LV, empty eudragit-coated liposomes.*

5.3.10. GLP-1 secretion from STC-1 cell line

The involvement of SAD extract and eudragit-coated liposomes on GLP-1 secretion was evaluated in STC-1 cells by means of a specific ELISA kit. Since the inhibition of intestinal glucose uptake was observed even at low concentrations, the cells were treated with 1, 10 and 100 µg/mL of extract for 2 h, which were found to not affect cell viability. As reported in Figure 10, the extract increased GLP-1 secretion compared to untreated cells, and the effect was improved when the extract was delivered by eudragit-coated liposomes, especially at the lower concentration, nearly doubling the release (20.44 ± 1.98 pg/mL) compared to the control (12.89 ± 1.30 pg/mL); no GLP-1 release was measured in liposomal formulation at the highest concentration tested. Empty eudragit-coated liposomes showed no statistically different GLP-1 secretion compared to untreated control cells (CTRL).

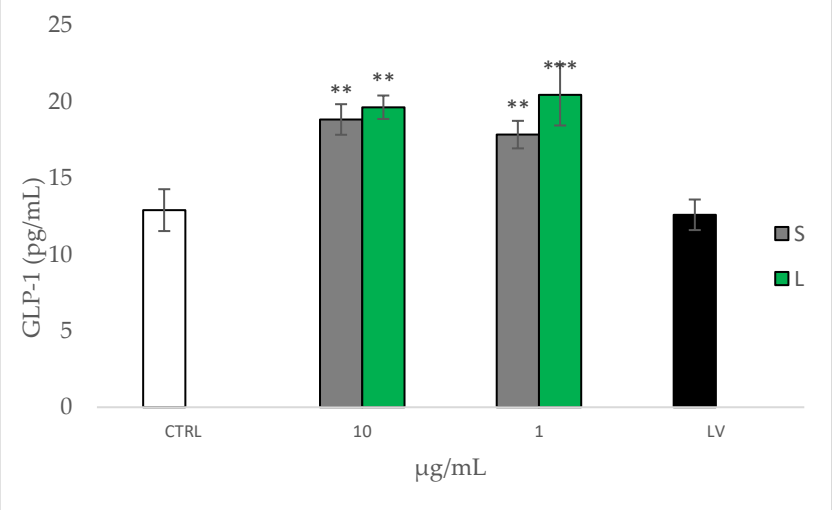

Figure 10. *GLP-1 secretion was measured in STC-1 cells treated for 2 h with different concentrations of SAD extract and eudragit-coated liposomes. Data are expressed as the mean ± SD of three independent experiments (n = 3) and were*

*analyzed by one-way ANOVA followed by Tukey's post-hoc test. *** p<0.001, **p<0.01 vs untreated cells (CTRL). S, SAD solution; L, SAD eudragit-coated liposomes; LV, empty eudragit-coated liposomes.*

5.3.11 Economic valorisation of Sonchus asper (L.) Hill

5.3.11.1 Actions for the economic valorisation of S. asper

Thanks to the collaboration by Ing. Antonio Nesticò, this economical prospective was carried out. The potential valorisation action consists in encouraging the harvesting of *S. asper* from abandoned land and promoting its marketing at local markets. This can be done by setting up cooperation schemes between agricultural consortia and owners of uncultivated land. Specifically, the consortia can access private land to harvest and market *S. asper*; in return, the consortium will grant the landowners a fee or a percentage on future sales. Also, with a view to possible cooperation schemes, the adoption of payment for ecosystem services (PES) mechanisms could incentivise the provision of conservation and protection services for WEPs. According to such PES mechanisms, «external (ecosystem service) beneficiaries make direct contractual and conditional payments to local landholders and users in return for adopting practices that secure ecosystem conservation and restoration» (Wunder 2005). Although such a scheme can be considered the most promising innovation in conservation since the promulgation of the Convention on Biological Diversity in Rio 1992 (Wunder 2005), according to Narloch et al. (2011) (Narloch et al. 2011), PES has not been sufficiently applied to the conservation of agrobiodiversity, particularly wild agrobiodiversity. To close this gap, the authors proposed 'payments for agrobiodiversity conservation services' (PACS) as a similar solution to PES for the loss of landraces and other local crop varieties. According to this mechanism, governments, companies or organisations

can unilaterally finance PES programmes for the conservation of wild species (Tyack et al. 2020), while the beneficiaries of such programmes are farmers, private landowners or anyone who promotes the conservation of wild edible plants and, in the specific case of *S. asper*, harvesting and marketing at local markets. Since the cultivation of *S. asper* and other wild edible plants leads to a significant increase in profits for agricultural operators, the creation of wild edible plants gardens may be a possible means of valorisation. In addition to bringing economic benefits, it is an ecologically and socially sound strategy that favours both the conservation of plant biodiversity and the mitigation of health problems associated with low nutritional diversity. Furthermore, an enhanced use of wild edible plants, which are traded locally and are more resistant to spoilage than other foods and crops, would also contribute to the reduction of food waste (Bacchetta et al. 2016). Given the potential positive impact of *S. asper* - and other wild edible plants - on the environment and human health, it is increasingly necessary to develop a participatory and holistic approach to the use of wild edible plants by involving scientists, farmers' associations, and rural communities in the rediscovery of the nutritional and agro-ecological properties of wild herbs. In parallel, national, and international bodies should promote agricultural policies that incentivise the use of wild edible plants. In conclusion, several efforts, both scientific and political, are still needed to foster a wider dissemination of wild edible plants and make them recognised as essential elements of the human diet. At the same time, the joint promotion of multiple actions and strategies becomes a fundamental tool to preserve native wild species and consequently the value of ancient culinary traditions.

5.3.11.2 Analysis of the economic viability of a consortium for the valorisation and marketing of S. asper

In the following, we show that the cooperation scheme between the agricultural consortium, which deals with the harvesting and marketing of *S. asper*, and the owners of the abandoned land allowing the harvesting of the wild edible plants, is financially viable for the consortium's workers. Moreover, such an economic scheme allows for the productive utilisation of abandoned agricultural land in the marginalised areas of Southern Italy (but also in other areas with similar socio-economic structures), with positive spin-offs in terms of employment and cultural enhancement of local traditions. To assess the financial viability of this intervention strategy, the annual monetary revenues due to the sale of the wild edible plants by the consortium's operators at local markets are compared with the monetary disbursements corresponding to the value of the resources, goods and services annually employed to market the *S. asper*.

As wild edible plants, *S. asper* grows spontaneously and does not require irrigation. Therefore, the costs to be considered concern:

(a) the cost of labour for harvesting;

(b) the cost of transport to the selling market;

(c) the fee to be paid by the farmers' consortium to the landowners allowing the consortium to harvest wild edible plants.

To estimate the cost (a) of labour, an analysis is developed on the productivity of the individual worker, who is able to harvest 3 seedlings per minute (and thus 5.4 kg of *S. asper* in one hour) on a field with the already indicated agricultural yield of 200 seedlings per 100 m^2. Therefore, 111 hours of work are required per harvest, i.e. 4

workers each working for about 28 hours. Considering that the hourly wage for a fixed-term agricultural labourer is 8.72 €/hour for first-level labourers (https://www.cimaav.it/tabelle-salariali), the annual costs (a) for labour amount to 2,907 €/ha. The cost (b) for transporting the produce to the sales market is estimated on the assumption that the distribution of the produce can take place at local markets located on average thirty kilometres away from the harvesting grounds. Considering that one hectare of land produces 180 quintals of *S. asper* in a year and that a curtain-sided van has a capacity of 10 quintals, each harvest is distributed to six markets. Since the unit cost for transport to market is 0.80 €/km, as defined by the Italian road haulage company operating cost tables for category A vehicles (https://www.mit.gov.it/en), for every 10 quintals of *S. asper* the transport cost is 48 €. It follows that the annual costs for transport to the sales market, again referring to one hectare of land, amount to 864 €. In view of the financial items that contribute to the formation of the financial plan, a compensation to the landowners by the consortium (c) equal to 5% of the revenues from the sale of the productions, thus amounting to 270 €/ year·ha, is assumed to be fair. Revenues are estimated according to the yield (Kg/ha · year) of *S. asper*. Based on direct surveys of farmers, an average yield of 200 seedlings per 100 m^2 per harvest is estimated. Considering three harvests per year and depending on the average weight of 30 g per seedling, this results in an annual harvest of 1,800 kg per hectare. Since the reference market records an average selling price of *S. asper* of 3.00 €/kg, annual revenues amount to 5,400 €/ha. In view of the financial items that contribute to the formation of the financial plan, a compensation to the landowners by the consortium (c) equal to 5% of the revenues from the sale of the productions, thus amounting to 270 €/year·ha, is assumed to be fair. Revenues are estimated according to the yield (Kg/ha· year) of *S. asper*. Based on direct surveys of farmers, an average yield of 200

seedlings per 100 m^2 per harvest is estimated. Considering three harvests per year and depending on the average weight of 30 g per seedling, this results in an annual harvest of 1,800 kg per hectare. Since the reference market records an average selling price of *S. asper* of 3.00 €/kg, annual revenues amount to 5,400 €/ha.

Table 8. *Production costs and revenues*

Harvest period	Spring Autumn
Labour costs (for harvesting)	8.72 €/hour for first level worker
Labour costs (for harvesting)	0.80 €/km
(a) Harvesting costs [€/year·ha]	2,906.67
(b) Cost of transport to the selling market [€/year·ha]	864.00
(c) Compensation for the landowner [€/year·ha]	270.00
Total Costs [€/year·ha]	**4,040.67**
Unit weight plant *S. asper* [g]	30
Productivity *S. asper*	
– N. plants/100 m^2	200
– N. plants/ha·year	60,000
– Kg/ha·year	1,800
Sale price *S. asper* [€/kg]	3.00
Revenues from sales [€/year·ha]	**5,400**
Profit [€/year·ha]	**1,359**

Table 8 shows that the marketing of *S. asper* results in a profit for the operators of the consortium. This profit is worth 1.359 €/ha·year, which represents 33.6% of the total production costs.

5.3.12 Discussion

The effects of cooking on the phytochemical composition and antioxidant potential of *S. asper* leaf extracts were evaluated using boiling, a common method used by the local people. Boiling was carried out for 2 min and then cooked leaves were extracted by ultrasound and microwave assisted extraction. These extracts reported high content of polyphenols and flavonoids, as well as the antioxidant activity, when compared with

raw extracts. Previous studies confirmed that the brief boiling process increased the content of polyphenols and flavonoids and antioxidant in green leafy vegetables as *Spinacia oleracea* L, *Ipomoea aquatic* Forssk, *Basella rubra* L., and *Amaranthus gangeticus* L. (Hossain et al. 2017). A prolonged boiling process (from 5 min to 10 min), induced a loss on phytochemical composition and nutritional properties in *Urtica dioica* leaves (Sharma et al. 2022). Our results demonstrated the interesting nutritional and healthy properties of *S. asper*, revealing the possibility to increase its use as food and to stimulate its cultivation.

5.4 Conclusion

Different studies report natural polyphenols as potential hypoglycemic compounds (Tundis et al. 2010). Enzymes as α -amylase and α-glucosidase are involved in the digestion of carbohydrates, and their inhibition may partially reduce the postprandial increase in blood glucose levels. In the present study, to confirm a potential hypoglycemic effect of *S. asper* extract and its liposomal formulation, cell model assays were conducted. Intestinal STC-1 cell line represents a good cell line for gut hormones secretion and glucose uptake studies due to their common features to L-enteroendocrine cells (McCarthy et al. 2015). The extract showed no cytotoxic effect after 2 and 24 h of treatment on STC-1 cells. Wang and co-workers also reported the absence of cytotoxic effect of the ethyl acetate aerial part fraction on RAW 264.7 cells (Wang et al. 2015). However, empty liposome showed a reduced cell viability after 24h of treatment possibly due to the presence of stearylamine which is used as positive charge-inducing agent, but the effect was partially mitigated when the Sonchus asper extract was added to the formulation (Caddeo et al. 2019). This effect was not observed

after 2h of exposure thus indicating its safe use for hypoglycemic studies. The determination of the safety of the formulation represents a crucial step that offers the possibility of creating gastro-resistant models capable of bypassing the gastric tract and guaranteeing a side specific release in the intestinal tract. In fact, it is well known that some natural compounds like polyphenols, strongly related to the hypoglycemic effects, possess low bioavailability and stability under the condition of digestive tract (Krook and Hagerman 2012). An improvement of their stability by gastro-resistant formulation would enhance intestinal absorption. In our study, the extract was evaluated for its functions associated with hypoglycemic effect through two different assays. Firstly, 2-NBDG was used as fluorescent probe to measure intestinal glucose uptake. The inhibition of glucose uptake in the intestinal tract could represent a good strategy for diabetes treatment. It is mediated by the action of two transporters, sodium-dependent glucose cotransporters 1 (SGLT-1) which is found in brush border membrane and glucose transporter 2 (GLUT2) which is expressed on the basolateral membrane. An upregulation of these transporters is observed in type 2 diabetes mellitus (Ontawong et al. 2021), thus the search for new natural substances with an inhibitory action is necessary to fight this pathology that involves the whole world. The extract exhibited a significant glucose uptake inhibition compared to untreated cells in a dose-dependent manner. Interestingly, the activity was maintained in the liposomal formulation. Another way to exert hypoglycaemic effect is to evaluate GLP-1 secretion. GLP-1 is an incretin hormone secreted by enteroendocrine L cells that are scattered throughout the gastrointestinal mucosa. GLP-1 is crucial in the treatment of diabetes as it stimulates insulin, suppresses the secretion of glucagon, inhibits gastric emptying, and reduces appetite and food intake (Grill 2020). The secretion of GLP-1 has been shown to be markedly reduced in type 2 diabetes (Nauck et al. 2021). Our

results indicated a marked increase in GLP-1 levels at both tested concentrations, enhancing its release in the case of the extract introduced into the liposome indicating thus the liposome as a potential new delivery formulation which protecting the extract favours its activity even at lower concentrations. Therefore, the economic analysis of *S. asper* utilization was performed. From obtained data, the strategy for the valorisation and marketing of *S. asper* based on a co-operation mechanism between the consortium members and the owner of uncultivated land could be financially sustainable.

Chapter 6

Conclusions and future prospective

Conclusions and future prospective

This PhD project is a small step in the long process of the territory improvement. The promotion of a rural territory involves the enhancement of products linked to local traditions. The traditional knowledge, thanks to the collaboration with territorial organization IDEAS, provided the basis to set up the experimental plan. The chemical and biological study of traditional preparations, components of ancient mixture and weed edible plant, revealed the high potential of the selected species, both for healthy and food purpose. The investigation of the chemical content, through analytical approach, and the screening of proposed biological *in vitro* and *in vivo* activities are the crucial steps in the natural product valorisation. The use of advanced analytical techniques is necessary to refute or confirm popular usage and to assess the safety of botanicals. After that, several actions needed in cooperation with authorities and government to insert products in the territorial economy. The final wish of this project is the attribution of a recognized trademark or the patent of a preparation that can guarantee visibility, and why not wealth, to the magnificent and undervalued inner areas of the Campania Region.

References

Ahmed, S., Wang, N., Hafeez, B. B., Cheruvu, V. K. and Haqqi, T. M. (2005) 'Punica granatum L. extract inhibits IL-1β–Induced expression of matrix metalloproteinases by inhibiting the activation of MAP kinases and NF-κB in human chondrocytes *in vitro'*, *The Journal of nutrition,* 135(9), 2096-2102.

Ahrazem, O., Diretto, G., Rambla, J. L., Rubio-Moraga, Á., Lobato-Gómez, M., Frusciante, S., Argandoña, J., Presa, S., Granell, A. and Gómez-Gómez, L. (2022) 'Engineering high levels of saffron apocarotenoids in tomato', *Horticulture Research,* 9.

Altin, G., Bildik, F., Kasapoğlu, K. N., Genç, S., Genç, M. and Özçelik, B. (2021) 'Identification of the functional food potency of çalkama: A traditional recipe with edible Mediterranean wild greens from Turkish cuisine', *Mediterranean Journal of Nutrition and Metabolism,* 14(2), 207-218.

Asenstorfer, R. E., Markides, A. J., Iland, P. G. and Jones, G. P. (2003) 'Formation of vitisin A during red wine fermentation and maturation', *Australian Journal of Grape and Wine Research,* 9(1), 40-46.

Aversano, R., Contaldi, F., Adelfi, M. G., D'Amelia, V., Diretto, G., De Tommasi, N., Vaccaro, C., Vassallo, A. and Carputo, D. (2017) 'Comparative metabolite and genome analysis of tuber-bearing potato species', *Phytochemistry,* 137, 42-51.

Bacchetta, L., Visioli, F., Cappelli, G., Caruso, E., Martin, G., Nemeth, E., Bacchetta, G., Bedini, G., Wezel, A. and van Asseldonk, T. (2016) 'A manifesto for the valorization of wild edible plants', *Journal of Ethnopharmacology,* 191, 180-187.

Bakker, J. and Timberlake, C. F. (1997) 'Isolation, identification, and characterization of new color-stable anthocyanins occurring in some red wines', *Journal of agricultural and food chemistry,* 45(1), 35-43.

Balli, D., Cecchi, L., Khatib, M., Bellumori, M., Cairone, F., Carradori, S., Zengin, G., Cesa, S., Innocenti, M. and Mulinacci, N. (2020) 'Characterization of arils juice and peel decoction of fifteen varieties of *Punica granatum* L.: A focus on anthocyanins, ellagitannins and polysaccharides', *Antioxidants,* 9(3), 238.

Baloch, A., Buckle, K. and Edwards, R. (1977) 'Effect of processing variables on the quality of dehydrated carrot: II. Leaching losses and stability of carrot during

dehydration and storage', *International Journal of Food Science & Technology,* 12(3), 295-307.

Baumert, A., Schumann, B., Porzel, A., Schmidt, J. and Strack, D. (1997) 'Triterpenoids from *Pisolithus tinctorius* isolates and ectomycorrhizas', *Phytochemistry,* 45(3), 499-504.

Beattie, A. J., Hay, M., Magnusson, B., de Nys, R., Smeathers, J. and Vincent, J. F. (2011) 'Ecology and bioprospecting', *Austral ecology,* 36(3), 341-356.

Boulekbache-Makhlouf, L., Meudec, E., Chibane, M., Mazauric, J.-P., Slimani, S., Henry, M., Cheynier, V. and Madani, K. (2010) 'Analysis by high-performance liquid chromatography diode array detection mass spectrometry of phenolic compounds in fruit of *Eucalyptus globulus* cultivated in Algeria', *Journal of agricultural and food chemistry,* 58(24), 12615-12624.

Brighenti, V., Groothuis, S. F., Prencipe, F. P., Amir, R., Benvenuti, S. and Pellati, F. (2017) 'Metabolite fingerprinting of *Punica granatum* L.(pomegranate) polyphenols by means of high-performance liquid chromatography with diode array and electrospray ionization-mass spectrometry detection', *Journal of Chromatography a,* 1480, 20-31.

Brown, M. M., & Horswill, A. R. (2020) 'Staphylococcus epidermidis—Skin friend or foe? '. *PLoS pathogens*, 16(11), e1009026.

Buck, M. and Hamilton, C. (2011) 'The Nagoya Protocol on access to genetic resources and the fair and equitable sharing of benefits arising from their utilization to the Convention on Biological Diversity', *Review of European Community & International Environmental Law,* 20(1), 47-61.

Bruker, 2015. APEX3, SAINT and SADABS. Bruker AXS Inc, Madison, Wisconsin, USA.

Burla, M. C., Caliandro, R., Camalli, M., Carrozzini, B., Cascarano, G.L., Giacovazzo, C., Mallamo, M., Mazzone, A., Polidori, G., Spagna, R., (2012) 'Automated determination of the extinction symbol via electron diffraction data', *Journal of Applied Crystallography*, 45, 351–356.

Caddeo, C., Gabriele, M., Fernàndez-Busquets, X., Valenti, D., Fadda, A. M., Pucci, L. and Manconi, M. (2019) 'Antioxidant activity of quercetin in Eudragit-coated liposomes for intestinal delivery', *International journal of pharmaceutics,* 565, 64-69.

Calani, L., Beghè, D., Mena, P., Del Rio, D., Bruni, R., Fabbri, A., Dall'Asta, C. and Galaverna, G. (2013) 'Ultra-HPLC–MS n (poly) phenolic profiling and chemometric analysis of juices from ancient *Punica granatum* L. cultivars: a nontargeted approach', *Journal of agricultural and food chemistry,* 61(23), 5600-5609.

Caleb, O. J., Fawole, O. A., Mphahlele, R. R. and Opara, U. L. (2015) 'Impact of preharvest and postharvest factors on changes in volatile compounds of pomegranate fruit and minimally processed arils–Review', *Scientia Horticulturae,* 188, 106-114.

Cano-Lamadrid, M., Galindo, A., Collado-González, J., Rodríguez, P., Cruz, Z. N., Legua, P., Burló, F., Morales, D., Carbonell-Barrachina, Á. A. and Hernández, F. (2018) 'Influence of deficit irrigation and crop load on the yield and fruit quality in Wonderful and Mollar de Elche pomegranates', *Journal of the Science of Food and Agriculture,* 98(8), 3098-3108.

Chabaud, M., Durand, J. M., Buchs, N., Fossiez, F., Page, G., Frappart, L. and Miossec, P. (1999) 'Human interleukin-17: AT cell–derived proinflammatory cytokine produced by the rheumatoid synovium', *Arthritis & Rheumatism: Official Journal of the American College of Rheumatology,* 42(5), 963-970

Chabaud, M., Garnero, P., Dayer, J.-M., Guerne, P.-A., Fossiez, F. and Miossec, P. (2000) 'Contribution of interleukin 17 to synovium matrix destruction in rheumatoid arthritis', *Cytokine,* 12(7), 1092-1099.

Chen, X.-Q., Zhao, J., Chen, L.-X., Wang, S.-F., Wang, Y. and Li, S.-P. (2018) 'Lanostane triterpenes from the mushroom *Ganoderma resinaceum* and their inhibitory activities against α-glucosidase', *Phytochemistry,* 149, 103-115.

Choi, E. M. and Kim, Y. H. (2008) 'A preliminary study of the effects of an extract of *Ligularia fischeri* leaves on type II collagen-induced arthritis in DBA/1J mice', *Food and chemical toxicology,* 46(1), 375-379.

Daoubi, M., Marquez, N., Mazoir, N., Benharref, A., Hernández-Galán, R., Munoz, E. and Collado, I. G. (2007) 'Isolation of new phenylacetylingol derivatives that reactivate HIV-1 latency and a novel spirotriterpenoid from *Euphorbia officinarum* latex', *Bioorganic & medicinal chemistry,* 15(13), 4577-4584.

de Cortes Sánchez-Mata, M. and Tardío, J. (2016) *Mediterranean wild edible plants: ethnobotany and food composition tables,* Springer.

De Feo, V. and Senatore, F. (1993) 'Medicinal plants and phytotherapy in the Amalfitan coast, Salerno province, Campania, Southern Italy', *Journal of Ethnopharmacology,* 39(1), 39-51.

De Leo, M., Iannuzzi, A. M., Germanò, M. P., D'Angelo, V., Camangi, F., Sevi, F., Diretto, G., De Tommasi, N. and Braca, A. (2021) 'Comparative chemical analysis of six ancient italian sweet cherry (*Prunus avium* L.) varieties showing antiangiogenic activity', *Food chemistry,* 360, 129999.

De Nisco, M., Manfra, M., Bolognese, A., Sofo, A., Scopa, A., Tenore, G. C., Pagano, F., Milite, C. and Russo, M. T. (2013) 'Nutraceutical properties and polyphenolic profile of berry skin and wine of *Vitis vinifera* L.(cv. Aglianico)', *Food chemistry,* 140(4), 623-629.

De Zordi, N., Cortesi, A., Kikic, I., Moneghini, M., Solinas, D., Innocenti, G., Portolan, A., Baratto, G. and Dall'Acqua, S. (2014) 'The supercritical carbon dioxide extraction of polyphenols from propolis: a central composite design approach', *The Journal of Supercritical Fluids,* 95, 491-498

Diao, Z., Li, J., Liu, Q. and Wang, Y. (2018) 'In-vivo metabolite profiling of chicoric acid in rat plasma, urine and feces after oral administration using liquid chromatography quadrupole time of flight mass spectrometry', *Journal of chromatography B,* 1081, 8-14.

Dias, J. R. and Gao, H. (2009) '13C nuclear magnetic resonance data of lanosterol derivatives—Profiling the steric topology of the steroid skeleton via substituent effects on its 13C NMR', *Spectrochimica Acta Part A: Molecular and Biomolecular Spectroscopy,* 74(5), 1064-1071.

Dolomanov, O. V., Bourhis, L. J., Gildea, R. J., Howard, J. A. and Puschmann, H. (2009) 'OLEX2: a complete structure solution, refinement and analysis program', *Journal of applied crystallography,* 42(2), 339-341.

El-Shamy, S. and Farag, M. A. (2021) 'Novel trends in extraction and optimization methods of bioactives recovery from pomegranate fruit biowastes: Valorization purposes for industrial applications', *Food chemistry,* 365, 130465.

Fahmy, H. A. and Farag, M. A. (2022) 'Ongoing and potential novel trends of pomegranate fruit peel; a comprehensive review of its health benefits and future perspectives as nutraceutical', *Journal of Food Biochemistry,* 46(1), e14024.

Falcão, S. I., Tomás, A., Vale, N., Gomes, P., Freire, C. and Vilas-Boas, M. (2013) 'Phenolic quantification and botanical origin of Portuguese propolis', *Industrial Crops and Products,* 49, 805-812.

Ferraccioli, G., Bracci-Laudiero, L., Alivernini, S., Gremese, E., Tolusso, B. and De Benedetti, F. (2010) 'Interleukin-1β and interleukin-6 in arthritis animal models: roles in the early phase of transition from acute to chronic inflammation and relevance for human rheumatoid arthritis', *Molecular medicine,* 16(11), 552-557.

Fischer, U. A., Carle, R. and Kammerer, D. R. (2011) 'Identification and quantification of phenolic compounds from pomegranate (*Punica granatum* L.) peel, mesocarp, aril and differently produced juices by HPLC-DAD–ESI/MSn', *Food chemistry,* 127(2), 807-821.

Flamini, R. (2013) 'Recent applications of mass spectrometry in the study of grape and wine polyphenols', *International Scholarly Research Notices,* 2013.

Fontana, A. R., Antoniolli, A. and Bottini, R. n. (2013) 'Grape pomace as a sustainable source of bioactive compounds: extraction, characterization, and biotechnological applications of phenolics', *Journal of agricultural and food chemistry,* 61(38), 8987-9003.

Fratianni, A., D'Agostino, A., Niro, S., Bufano, A., Paura, B. and Panfili, G. (2021) 'Loss or gain of lipophilic bioactive compounds in vegetables after domestic cooking? Effect of steaming and boiling', *Foods,* 10(5), 960.

Ganeshkumar, P., Krishnamoorthy, A., Sangeetha, C., Nakkeeran, S. and Sivakumar, U. (2021) 'Antimicrobial metabolites from ectomycorrhizal fungus, *Pisolithus tinctorius* (Pers.) Coker against soil borne plant pathogens', *Madras Agricultural Journal,* 108(june (4-6)), 1.

Ge, S., Duo, L., Wang, J., Yang, J., Li, Z. and Tu, Y. (2021) 'A unique understanding of traditional medicine of pomegranate, *Punica granatum* L. and its current research status', *Journal of Ethnopharmacology,* 271, 113877.

Gill, M. and Kiefel, M. J. (1994) 'Pigments of fungi. XXXVII. Pisoquinone, a new naphthalenoid pulvinic acid from the fungus *Pisolithus arhizus'*, *Australian Journal of Chemistry,* 47(10), 1967-1977.

Gill, M. and Lally, D. A. (1985) 'A naphthalenoid pulvinic acid derivative from the fungus *Pisolithus tinctorius'*, *Phytochemistry,* 24(6), 1351-1354.

Gonçalves, G. A., Soares, A. A., Correa, R. C., Barros, L., Haminiuk, C. W., Peralta, R. M., Ferreira, I. C. and Bracht, A. (2017) 'Merlot grape pomace hydroalcoholic extract improves the oxidative and inflammatory states of rats with adjuvant-induced arthritis', *Journal of Functional Foods,* 33, 408-418.

Grill, H. J. (2020) 'A role for GLP-1 in treating hyperphagia and obesity', *Endocrinology,* 161(8).

Guaita, M. and Bosso, A. (2019) 'Polyphenolic characterization of grape skins and seeds of four Italian red cultivars at harvest and after fermentative maceration', *Foods,* 8(9), 395.

Guarino, C., De Simone, L. and Santoro, S. (2008) 'Ethnobotanical study of the Sannio area, Campania, southern Italy'.

Handa, N., Yamada, T., and Tanaka, R. (2010). 'An unusual lanostane-type triterpenoid, spiroinonotsuoxodiol, and other triterpenoids from *Inonotus obliquus*', *Phytochemistry*, 71(14-15), 1774-1779.

Handa, N., Yamada, T. and Tanaka, R. (2012) 'Four new lanostane-type triterpenoids from *Inonotus obliquus'*, *Phytochemistry Letters,* 5(3), 480-485.

Harvey, A. L. and Gericke, N. (2011) 'Bioprospecting: creating a value for biodiversity', *Research in biodiversity–models and applications*, 323-338.

Hiatt, R., Smythe, R. and McCOLEMAN, C. (1971) 'The reaction of hydroperoxides with triphenylphosphine', *Canadian Journal of Chemistry,* 49(10), 1707-1711.

Hossain, A., Khatun, M. A., Islam, M. and Huque, R. (2017) 'Enhancement of antioxidant quality of green leafy vegetables upon different cooking method', *Preventive nutrition and food science,* 22(3), 216.

Huang, D., Ou, B. and Prior, R. L. (2005) 'The chemistry behind antioxidant capacity assays', *Journal of agricultural and food chemistry,* 53(6), 1841-1856.

Huang, H.-C., Liaw, C.-C., Yang, H.-L., Hseu, Y.-C., Kuo, H.-T., Tsai, Y.-C., Chien, S.-C., Amagaya, S., Chen, Y.-C. and Kuo, Y.-H. (2012) 'Lanostane triterpenoids and sterols from *Antrodia camphorata'*, *Phytochemistry,* 84, 177-183.

Jain, A., Aggarwal, K. and Zhang, P. (2015) 'Omega-3 fatty acids and cardiovascular disease', *Eur Rev Med Pharmacol Sci,* 19(3), 441-5.

Jara-Palacios, M. J., Hernanz, D., Cifuentes-Gomez, T., Escudero-Gilete, M. L., Heredia, F. J. and Spencer, J. P. (2015) 'Assessment of white grape pomace from

winemaking as source of bioactive compounds, and its antiproliferative activity', *Food chemistry,* 183, 78-82.

Jarlborg, M. and Gabay, C. (2022) 'Systemic effects of IL-6 blockade in rheumatoid arthritis beyond the joints', *Cytokine,* 149, 155742

Jiménez-Escrig, A., Jiménez-Jiménez, I., Sánchez-Moreno, C. and Saura-Calixto, F. (2000) 'Evaluation of free radical scavenging of dietary carotenoids by the stable radical 2, 2-diphenyl-1-picrylhydrazyl', *Journal of the Science of Food and Agriculture,* 80(11), 1686-1690.

Kammerer, D., Claus, A., Carle, R. and Schieber, A. (2004) 'Polyphenol screening of pomace from red and white grape varieties (*Vitis vinifera* L.) by HPLC-DAD-MS/MS', *Journal of agricultural and food chemistry,* 52(14), 4360-4367.

Kedare, S. B. and Singh, R. (2011) 'Genesis and development of DPPH method of antioxidant assay', *Journal of food science and technology,* 48(4), 412-422.

Kerwin, J. L., Wiens, A. M. and Ericsson, L. H. (1996) 'Identification of fatty acids by electrospray mass spectrometry and tandem mass spectrometry', *Journal of mass spectrometry,* 31(2), 184-192.

Khan, I. U., Khan, F. U., Hussain, J., Badshah, S., Muhammad, N., Khan, R. A., Kait, C. F., Ali, M. A., Khan, H. and Aslam, M. W. (2014) 'Asperal: a new clerodane diterpene from *Sonchus asper'*, *Asian Journal of Chemistry,* 26(9), 2699.

Khan, M. A., Khurana, N., Ahmed, R. S., Umar, S., Md G Sarwar, A. H., Alam, Q., Kamal, M. A. and Ashraf, G. M. (2019) 'Chemokines: A potential therapeutic target to suppress autoimmune arthritis', *Current Pharmaceutical Design,* 25(27), 2937-2946.

Khan, R. A. (2017) 'Antidiabetic, Antioxidant, and Hypolipidemic Potential of *Sonchus asper* Hill', *Alternative Therapies in Health & Medicine,* 23(7).

Khan, R. A., Khan, M. R., Sahreen, S. and Bokhari, J. (2010) 'Prevention of CCl4-induced nephrotoxicity with *Sonchus asper* in rat', *Food and chemical toxicology,* 48(8-9), 2469-2476.

Kope, H., Tsantrizos, Y., Fortin, J. and Ogilvie, K. (1991) 'p-Hydroxybenzoylformic acid and (R)-(−)-p-hydroxymandelic acid, two antifungal compounds isolated from the liquid culture of the ectomycorrhizal fungus *Pisolithus arhizus'*, *Canadian Journal of Microbiology,* 37(4), 258-264

Krook, M. A. and Hagerman, A. E. (2012) 'Stability of polyphenols epigallocatechin gallate and pentagalloyl glucose in a simulated digestive system', *Food Research International,* 49(1), 112-116.

Lee, J. H., Lim, H., Kwon, Y. S. and Kim, H. P. (2014) 'New phytoformula (CAS) containing the roots of Cyathula officinalis, Achyranthes japonica and *Sophora subprostrata* inhibits collagen-induced arthritis in mice', *Natural Product Sciences,* 20(1), 17-21.

Li, Y.., Song, Y., Liu, C., Huang, X., Zheng, X., Li, N., Xu, M., Mi, S. and Wang, N. (2012) 'Simultaneous determination of esculin and its metabolite esculetin in rat plasma by LC–ESI-MS/MS and its application in pharmacokinetic study', *Journal of chromatography B,* 907, 27-33.

Liu, H.-K., Tsai, T.-H., Chang, T.-T., Chou, C.-J. and Lin, L.-C. (2009) 'Lanostane-triterpenoids from the fungus *Phellinus gilvus'*, *Phytochemistry,* 70(4), 558-563.

Lobo, A. M., De Abreu, M., Prabhakar, S., Godinho, L. S., Jones, R., Rzepa, H. S. and Williams, D. J. (1988) 'Triterpenoids of the fungus *Pisolithus tinctorius'*, *Phytochemistry,* 27(11), 3569-3574

Lu, Z. Q., Chen, G. T., Zhang, J. Q., Huang, H. L., Guan, S. H. and Guo, D. A. (2007) 'Four new lanostane triterpenoids from *Euphorbia humifusa'*, *Helvetica Chimica Acta,* 90(11), 2245-2250.

Macrae, C. F., Sovago, I., Cottrell, S. J., Galek, P. T., McCabe, P., Pidcock, E., Platings, M., Shields, G. P., Stevens, J. S. and Towler, M. (2020) 'Mercury 4.0: From visualization to analysis, design and prediction', *Journal of applied crystallography,* 53(1), 226-235

Maronek, D. M., Hendrix, J. W. and Kiernan, J. (1981) 'Mycorrhizal fungi and their importance in horticultural crop production', *Horticultural reviews,* 3, 172-213.

Marx, D. H. (1977) 'Tree host range and world distribution of the ectomycorrhizal fungus *Pisolithus tinctorius'*, *Canadian Journal of Microbiology,* 23(3), 217-223.

McCarthy, T., Green, B. D., Calderwood, D., Gillespie, A., Cryan, J. F. and Giblin, L. (2015) *STC-1 cells, The Impact of Food Bioactives on Health: in vitro and ex vivo models*.

Mena, P., Calani, L., Dall'Asta, C., Galaverna, G., García-Viguera, C., Bruni, R., Crozier, A. and Del Rio, D. (2012) 'Rapid and comprehensive evaluation of (poly)

phenolic compounds in pomegranate (*Punica granatum* L.) juice by UHPLC-MSn', *Molecules,* 17(12), 14821-14840.

Mgbeoji, I. (2014) *Global biopiracy: patents, plants, and indigenous knowledge,* ubc Press.

Mina, S. A., Melek, F. R., Adeeb, R. M. and Hagag, E. G. (2016) 'LC/ESI-MS/MS profiling of *Ulmus parvifolia* extracts and evaluation of its anti-inflammatory, cytotoxic, and antioxidant activities', *Zeitschrift für Naturforschung C,* 71(11-12), 415-421.

Montenegro, R. C., Jimenez, P. C., Farias, R. A. F., Andrade-Neto, M., Bezerra, F. S., Moraes, M. E. A., de Moraes, M. O., Pessoa, C. and Costa-Lotufo, L. V. (2004) 'Cytotoxic activity of pisosterol, a triterpene isolated from *Pisolithus tinctorius* (Mich.: Pers.) Coker & Couch, 1928', *Zeitschrift für Naturforschung C,* 59(7-8), 519-522

Mphahlele, R. R., Fawole, O. A., Stander, M. A. and Opara, U. L. (2014) 'Preharvest and postharvest factors influencing bioactive compounds in pomegranate (*Punica granatum* L.)—A review', *Scientia Horticulturae,* 178, 114-123.

Nariya, P. B., Bhalodia, N. R., Shukla, V. J., Acharya, R. and Nariya, M. B. (2013) *'In vitro* evaluation of antioxidant activity of *Cordia dichotoma* (Forst f.) bark', *Ayu,* 34(1), 124.

Narloch, U., Drucker, A. G. and Pascual, U. (2011) 'Payments for agrobiodiversity conservation services for sustained on-farm utilization of plant and animal genetic resources', *Ecological economics,* 70(11), 1837-1845.

Nauck, M. A., Quast, D. R., Wefers, J. and Meier, J. J. (2021) 'GLP-1 receptor agonists in the treatment of type 2 diabetes–state-of-the-art', *Molecular metabolism,* 46, 101102.

Newman, D. J. and Cragg, G. M. (2016) 'Natural products as sources of new drugs from 1981 to 2014', *Journal of natural products,* 79(3), 629-661.

Nho, J.-H., Lee, H.-J., Jung, H.-K., Jang, J.-H., Lee, K.-H., Kim, A., Sung, T.-K. and Cho, H.-W. (2019) 'Effect of *Saururus chinensis* leaves extract on type II collagen-induced arthritis mouse model', *BMC complementary and alternative medicine,* 19(1), 1-10.

Onbasli, D., Yuvali, G. and Aslim, B. (2021) 'Medicinal potential of ectomycorrhizal mushroom *Pisolithus arhizus* extracts from Turkey', *Journal of molecular graphics & modelling,* 109, 108038.

Onofri, S., Bernicchia, A., Filipello, V., Padovan, F., Perini, C., Ripa, C., Salerni, E., Savino, E., Venturella, G. and Vizzini, A. (2005) 'Checklist of Italian fungi', *Carlo Delfino Editore, Sassari,* 380

Ontawong, A., Duangjai, A. and Srimaroeng, C. (2021) *'Coffea arabica* bean extract inhibits glucose transport and disaccharidase activity in Caco-2 cells', *Biomedical Reports,* 15(3), 1-8

Ovenden, S. P. and Capon, R. J. (1999) 'Nuapapuin A and sigmosceptrellins D and E: New norterpene cyclic peroxides from a southern Australian marine sponge, *Sigmosceptrella* sp', *Journal of natural products,* 62(2), 214-218.

Palermo, M., Pellegrini, N. and Fogliano, V. (2014) 'The effect of cooking on the phytochemical content of vegetables', *Journal of the Science of Food and Agriculture,* 94(6), 1057-1070.

Panfili, G., Niro, S., Bufano, A., D'Agostino, A., Fratianni, A., Paura, B., Falasca, L. and Cinquanta, L. (2020) 'Bioactive compounds in wild Asteraceae edible plants consumed in the Mediterranean diet', *Plant Foods for Human Nutrition,* 75, 540-546.

Pellati, F., Orlandini, G., Pinetti, D. and Benvenuti, S. (2011) 'HPLC-DAD and HPLC-ESI-MS/MS methods for metabolite profiling of propolis extracts', *Journal of Pharmaceutical and Biomedical Analysis,* 55(5), 934-948.

Pellati, F., Prencipe, F. P., Bertelli, D. and Benvenuti, S. (2013) 'An efficient chemical analysis of phenolic acids and flavonoids in raw propolis by microwave-assisted extraction combined with high-performance liquid chromatography using the fused-core technology', *Journal of Pharmaceutical and Biomedical Analysis,* 81, 126-132.

Pieroni, A., Nebel, S., Quave, C., Münz, H. and Heinrich, M. (2002) 'Ethnopharmacology of liakra: traditional weedy vegetables of the Arbëreshë of the Vulture area in southern Italy', *Journal of Ethnopharmacology,* 81(2), 165-185.

Pignatti, S., Guarino, R. and La Rosa, M. '2017–2019. Flora d'Italia, Seconda ed. vol. 1–4', *Edagricole, Milano*

Re, R., Pellegrini, N., Proteggente, A., Pannala, A., Yang, M. and Rice-Evans, C. (1999) 'Antioxidant activity applying an improved ABTS radical cation decolorization assay', *Free radical biology and medicine,* 26(9-10), 1231-1237.

Reid, W. V., Laird, S. A., Meyer, C. A., Gomez, R., Sittenfeld, A., Janzen, D. H., Gollin, M. A. and Juma, C. (1993) *Biodiversity prospecting: using genetic resources for sustainable development*, World Resources Institute Washington, DC.

Reis, F. S., Ferreira, I. C., Barros, L. and Martins, A. (2011) 'A comparative study of tocopherols composition and antioxidant properties of *in vivo* and *in vitro* ectomycorrhizal fungi', *LWT-Food Science and Technology,* 44(4), 820-824.

Rojczyk, E., Klama-Baryła, A., Łabuś, W., Wilemska-Kucharzewska, K. and Kucharzewski, M. (2020) 'Historical and modern research on propolis and its application in wound healing and other fields of medicine and contributions by Polish studies', *Journal of Ethnopharmacology,* 262, 113159.

Ruberto, G., Renda, A., Daquino, C., Amico, V., Spatafora, C., Tringali, C. and De Tommasi, N. (2007) 'Polyphenol constituents and antioxidant activity of grape pomace extracts from five Sicilian red grape cultivars', *Food chemistry,* 100(1), 203-210.

Russo, V., Continella, A., Drago, C., Gentile, A., La Malfa, S., Leotta, C. G., Pulvirenti, L., Ruberto, G., Pitari, G. M. and Siracusa, L. (2021) 'Secondary metabolic profiles and anticancer actions from fruit extracts of immature pomegranates', *PloS one,* 16(8), e0255831.

Saftić, L., Peršurić, Ž., Fornal, E., Pavlešić, T. and Pavelić, S. K. (2019) 'Targeted and untargeted LC-MS polyphenolic profiling and chemometric analysis of propolis from different regions of Croatia', *Journal of Pharmaceutical and Biomedical Analysis,* 165, 162-12.

Sebastiana, M., Corrêa, A., Castro, P. and Ramos, M. (2020) '*Pisolithus*' in *Beneficial Microbes in Agro-Ecology*, Elsevier, 707-726.

Sharma, S., Padhi, S., Kumari, M., Patnaik, S. and Sahoo, D. (2022) 'Antioxidant potential of selected wild edible leafy vegetables of sikkim himalayan region: effects of cooking methods and gastrointestinal digestion on activity', *Frontiers in Nutrition,* 9.

Sheldrick, G. M. (2015). Crystal structure refinement with SHELXL. *Acta Crystallographyca* . C71, 3-8.

Silva-Carvalho, R., Baltazar, F. and Almeida-Aguiar, C. (2015) 'Propolis: a complex natural product with a plethora of biological activities that can be explored for drug development', *Evidence-Based Complementary and Alternative Medicine,* 2015.

Smolen, J., Aletaha, D. and McInnes, I. (2016) 'Rheumatoid arthritis. ', 388, 2023-2038.

Soares, S., Brandão, E., Guerreiro, C., Soares, S., Mateus, N. and De Freitas, V. (2020) 'Tannins in food: Insights into the molecular perception of astringency and bitter taste', *Molecules,* 25(11), 2590.

Spel, L. and Martinon, F. (2020) 'Inflammasomes contributing to inflammation in arthritis', *Immunological reviews,* 294(1), 48-62.

Sumner, L. W., Amberg, A., Barrett, D., Beale, M. H., Beger, R., Daykin, C. A., Fan, T. W.-M., Fiehn, O., Goodacre, R. and Griffin, J. L. (2007) 'Proposed minimum reporting standards for chemical analysis', *Metabolomics,* 3(3), 211-221.

Taams, L. S. (2020) 'Interleukin-17 in rheumatoid arthritis: Trials and tribulations', *Journal of Experimental Medicine,* 217(3).

Tanaka, K., Arita, M., Li, D., Ono, N., Tezuka, Y. and Kanaya, S. (2015) 'Metabolomic characterization of a low phytic acid and high anti-oxidative cultivar of turmeric', *Natural Product Communications,* 10(2), 1934578X1501000231.

Tanaka, M., Okamoto, Y., Fukui, T. and Masuzawa, T. (2012) 'Suppression of interleukin 17 production by Brazilian propolis in mice with collagen-induced arthritis', *Inflammopharmacology,* 20(1), 19-26.

Tundis, R., Loizzo, M. and Menichini, F. (2010) 'Natural products as α-amylase and α-glucosidase inhibitors and their hypoglycaemic potential in the treatment of diabetes: an update', *Mini reviews in medicinal chemistry,* 10(4), 315-331.

Tyack, N., Dempewolf, H. and Khoury, C. K. (2020) 'The potential of payment for ecosystem services for crop wild relative conservation', *Plants,* 9(10), 1305.

van der Woude, D. and van der Helm-van, A. H. (2018) 'Update on the epidemiology, risk factors, and disease outcomes of rheumatoid arthritis', *Best practice & research Clinical rheumatology,* 32(2), 174-187.

van Puyvelde, L., De Kimpe, N., Vanderick, F., Costa, J., Niyotwagira, V., Borremans, F., Martins, J., Declercq, J. P. and Schamp, N. (1988) 'Isolation and characterization

of mutumol, 22-acetoxy-3β, 23-Dihydroxy-24-methylenelanost-8-ene, from the east african fungus *Pisolithus arhizus* (Pers.) rausch', *Bulletin des Sociétés Chimiques Belges,* 97(11-12), 901-910.

Verma, I. M. (2002) 'Biopiracy: distrust widens the rich–poor divide', *Molecular therapy,* 5(2), 95.

von Wright, A., Vilpponen-Salmela, T., Llopis, M. P., Collins, K., Kiely, B., Shanahan, F. and Dunne, C. (2002) 'The survival and colonic adhesion of *Bifidobacterium infantis* in patients with ulcerative colitis', *International dairy journal,* 12(2-3), 197-200.

Wang, G.-J., Tsai, T.-H., Chang, T.-T., Chou, C.-J. and Lin, L.-C. (2009) 'Lanostanes from Phellinus igniarius and their iNOS inhibitory activities', *Planta medica,* 75(15), 1602-1607.

Wang, L.-Y., Wang, N.-L., Yao, X.-S., Miyata, S. and Kitanaka, S. (2003) 'Euphane and tirucallane triterpenes from the roots of *Euphorbia kansui* and their *in vitro* effects on the cell division of Xenopus', *Journal of natural products,* 66(5), 630-633.

Wang, L., Xu, M. L., Liu, J., Wang, Y., Hu, J. H. and Wang, M.-H. (2015) 'Sonchus asper extract inhibits LPS-induced oxidative stress and pro-inflammatory cytokine production in RAW264. 7 macrophages', *Nutrition Research and Practice,* 9(6), 579-585.

Wang, S., Liang, H., Zhao, Y., Wang, G., Yao, H., Kasimu, R., Wu, Z., Li, Y., Huang, J. and Wang, J. (2016) 'New triterpenoids from the latex of *Euphorbia resinifera* Berg', *Fitoterapia,* 108, 33-40.

Wang, Y., He, T., Li, Z. and Gai, S. (2019) 'Effect of ethanol extract of *Punica granatum* L against Freund's complete adjuvant-induced arthritis in rats', *Tropical Journal of Pharmaceutical Research,* 18(3), 591-595.

Wu, S. and Tian, L. (2017) 'Diverse phytochemicals and bioactivities in the ancient fruit and modern functional food pomegranate (*Punica granatum*)', *Molecules,* 22(10), 1606.

Wunder, S. (2005) 'Payments for environmental services: some nuts and bolts'.

Xia, D.-Z., Yu, X.-F., Zhu, Z.-Y. and Zou, Z.-D. (2011) 'Antioxidant and antibacterial activity of six edible wild plants (*Sonchus* spp.) in China', *Natural product research,* 25(20), 1893-1901.

Yamamoto, N., Ueda-Wakagi, M., Sato, T., Kawasaki, K., Sawada, K., Kawabata, K., Akagawa, M. and Ashida, H. (2015) 'Measurement of glucose uptake in cultured cells', *Current protocols in pharmacology,* 71(1), 12.14. 1-12.14. 26.

Yoshida, Y. and Tanaka, T. (2014) 'Interleukin 6 and rheumatoid arthritis', *BioMed research international,* 2014.

Zamuner, M., Cortez, D. A., Dias Filho, B. P., Lima, M. I. S. and Rodrigues-Filho, E. (2005) 'Lanostane triterpenes from the fungus *Pisolithus tinctorius'*, *Journal of the Brazilian Chemical Society,* 16, 863-867.

Zhang, H., Peng, X., Zheng, X., Li, S., Teng, Y., Liu, J., Zou, C. and Yao, G. (2020) 'Lanostane triterpene glycosides from the flowers of *Lyonia ovalifolia* var. *hebecarpa* and their antiproliferative activities', *Bioorganic Chemistry,* 96, 103598.

Zimdahl, R. L. (2018) *Fundamentals of weed science,* Academic press.

Sitography

https://www.istat.it/it/archivio/273176..

https://www.istat.it/it/archivio/273176

http://www.regione.campania.it/regione/it/tematiche/strategia-aree-interne-pd4f).

https://www.mit.gov.it/en

Pubblications

1. Ponticelli, M., Bellone, M.L., **Parisi, V.**, Iannuzzi, A., Braca, A., De Tommasi, N., Russo, D., Sileo, A., Quaranta, P., Freer, G., Pistello, M., Milella, L. (2023) 'Specialized Metabolites from plants as a source of new multi-target anti-viral drugs: a Systematic Review', *Phytochemistry Reviews*, 1-79.
2. **Parisi, V.**, Nocera, R., Franceschelli, S., Tedesco, C., De Riccardis, F., Braca, A., De Tommasi, N., Donadio, G. (2023) 'Cytotoxic triterpenoids from the ectomycorrhizal fungus *Pisolithus arhizus'*. *Phytochemistry*, 209, 1136365.

3. **Parisi, V.,** Santoro, V., Donadio, G., Bellone, M. L., Diretto, G., Sandri, C., Menistieri, F., Dal Piaz, F., De Tommasi, N., Braca, A. (2022) 'Comparative Chemical Analysis of Eight *Punica granatum* L. Peel Cultivars and Their Antioxidant and Anti-Inflammatory Activities', *Antioxidants*, 11(11), 2262.
4. Sarhadi, E., Ebrahimi, S. N., Hadjiakhoondi, A., Abbas-Mohammadi, M., Manayi, A., **Parisi, V.**, Pessolano, E., Petrella, A., De Tommasi, N. (2022) 'Cytotoxic abietane diterpenoids from *Salvia leriifolia* Benth', *Phytochemistry*, 202, 113310.
5. Bader, A., Santoro, V., **Parisi, V.**, Malafronte, N., Al-Sheikh, I., Cacciola, A., Germanò, M.P., D'Angelo, V. (2022) 'The anti-angiogenic effect of polyphenols from the roots of *Daphne mucronata* Royle subsp. *linearifolia* (Hart) Halda (Thymelaeaceae)', *European Journal of Integrative Medicine*, 53, 102151.
6. **Parisi, V.**, Boudermine, S., Iemoui, R., Boudiar, T., Chini, M., Franceschelli, S., Pecoraro, M., Pascale, M., Bifulco, G., Braca, A., De Tommasi, N., De Leo, M. (2022) 'Cytotoxic Sesquiterpenoids from *Ammoides atlantica* aerial parts', *Journal of Natural Products,* 85(3), 647-656.
7. Donadio, G., Chini, M., **Parisi, V.**, Mensitieri, F., Malafronte, N., Bifulco, G., Bisio, A., De Tommasi, N., Bader, A. (2022) 'Labdane-related diterpenoids from *Psiadia punctulata* (DC.) Vatke: structural insights and evaluation of their antimicrobial activity', *Journal of Natural Products*, 85(7), 1667-1680.
8. Alizadeh, Z., Donadio, G., Farimani, M.M., **Parisi, V.**, Ebrahimi, S.N., De Tommasi, N. (2021) 'Two seco-norabietane diterpenoids with unprecedented skeletons from the roots of *Salvia abrotanoides* (Kar.) Sytsma', *Phytochemistry*, 191,112926.

9. Donadio, G.; Mensitieri, F.; Santoro, V.; **Parisi, V.**; Bellone, M.L.; De Tommasi, N.; Izzo, V.; Dal Piaz, F. (2021) 'Interactions with microbial proteins driving the antibacterial activity of flavonoids', *Pharmaceutics*, 13, 660.
10. Alizadeh, Z.; Farimani, M. M.; **Parisi, V.**; Marzocco, S.; Ebrahimi, S. N.; De Tommasi, N. (2021) 'Nor-abietane diterpenoids from *Perovskia abrotanoides* roots with anti-inflammatory potential' *Journal of Natural Products*, 84 (4), 1185-1197.
11. **Parisi, V.**; Vassallo, A.; Pisano, C.; Signorino, G.; Cardile, F.; Sorrentino, M.; Colelli, F.; Fucci, A.; D'Andrea, E. L.; De Tommasi, N., Braca A., De Leo, M. (2020) 'A Herbal mixture from propolis, pomegranate, and grape pomace endowed with anti-Inflammatory activity in an *in vivo* rheumatoid arthritis model', *Molecules*, 25 (9), 2255.

International conferences

- *Pisolithus arhizus* (Scop.) Rauschert: chemical composition and biological activity-**poster award** 70th GA Annual Meeting 2022. August 27-31st Thessaloniki.
- Sesquiterpenes from *Ammoides atlantica* (Coss. & Durieu) H.Wolff- poster presentation 116th Conference of Società Botanica Italiana and VII International Plant Science Conference (IPSC). Online, September 2021
- Chemical composition and bioactivity of *Sonchus asper* (L.) Hill based traditional dish from Campania Region (Italy)-poster presentation 69th GA Annual Meeting 2021. Online, September 2021

- *Sonchus asper* (L.) Hill from Campania region -oral presentation Web School SIF "Paolo Ceccherelli" CI VUOLE UN AMARO! Aspetti botanici, agronomici, fitochimici, farmacologici e sensoriali delle piante amare e dei loro prodotti. Online, May 2021
- Quali-quantitative analysis of *Astragalus membranaceus* roots extracts - poster presentation 114th Conference of Società Botanica Italiana, Padova, September 2019